



**HAL**  
open science

# Peripheral and intestinal microbiota alterations in Autism Spectrum Disorders: The specific role of p-Cresol

Patricia Bermudez-Martin

► **To cite this version:**

Patricia Bermudez-Martin. Peripheral and intestinal microbiota alterations in Autism Spectrum Disorders: The specific role of p-Cresol. Molecular biology. Université Côte d'Azur, 2020. English. NNT: 2020COAZ6011 . tel-03122688

**HAL Id: tel-03122688**

**<https://theses.hal.science/tel-03122688>**

Submitted on 27 Jan 2021

**HAL** is a multi-disciplinary open access archive for the deposit and dissemination of scientific research documents, whether they are published or not. The documents may come from teaching and research institutions in France or abroad, or from public or private research centers.

L'archive ouverte pluridisciplinaire **HAL**, est destinée au dépôt et à la diffusion de documents scientifiques de niveau recherche, publiés ou non, émanant des établissements d'enseignement et de recherche français ou étrangers, des laboratoires publics ou privés.

# THÈSE DE DOCTORAT

## Perturbations de la Périphérie et du Microbiote Intestinal dans les Troubles du Spectre Autistique

Le Rôle Spécifique du *p*-Crésol

**Patricia BERMUDEZ MARTIN**

Institut de Pharmacologie Moléculaire et Cellulaire, Valbonne, France

Présentée en vue de l'obtention  
du grade de docteur en  
Sciences de la Vie et de la Santé – mention :  
Interactions Moléculaires et Cellulaires  
d'Université Côte d'Azur  
Dirigée par : Laetitia DAVIDOVIC  
Soutenue le : 9 Septembre 2020

Devant le jury, composé de :  
**Dr. Joëlle CHABRY**,  
D.R. INSERM, Université Côte d'Azur  
**Dr. Hélène BOUDIN**,  
C.R. INSERM, Université de Nantes  
**Dr. Sylvie RABOT**,  
C.R. INRAE, Université Paris-Saclay  
**Dr. Julie Le MERRER**  
D.R. CNRS, Université de Tours  
**Pr. Nicolas GLAICHENHAUS**,  
P.U. Université Côte d'Azur  
**Dr. Pierre-Yves MOUSSET**,  
D.R. NovoBiome SAS



# Perturbations de la Périphérie et du Microbiote Intestinal dans les Troubles du Spectre Autistique

## Le Rôle Spécifique du *p*-Crésol

Devant le jury composé de :

Présidente du jury :

**Jöelle CHABRY**, Directeur de Recherche INSERM, Université Côte d'Azur

Rapporteurs :

**Hélène BOUDIN**, Chargée de Recherche INSERM, Université de Nantes

**Sylvie RABOT**, Chargée de Recherche INRAE, Université Paris-Saclay

Examineurs :

**Julie LE MERRER**, Directeur de Recherche CNRS, Université de Tours

**Nicolas GLAICHENHAUS**, Professeur d'Université, Université Côte d'Azur

Invités :

**Pierre-Yves MOUSSET**, Directeur Général, NovoBiome, Latresne

Directrice de thèse :

**Laetitia DAVIDOVIC**, Chargée de Recherche CNRS, Université Côte d'Azur

## **En Français**

Titre de la thèse : Perturbations de la Périphérie et du Microbiote Intestinal dans les Troubles du Spectre Autistique  
Sous-titre de la thèse : Le Rôle Spécifique du *p*-Crésol  
Mots-clés : Autisme, comportement, *p*-Crésol, microbiote, dysbiose, circuit de la récompense

## **Résumé**

Ce travail de thèse porte principalement sur les anomalies périphériques associées aux Troubles du Spectre Autistique (TSA), un groupe de pathologies du neurodéveloppement fréquentes.

La première section est consacrée au travail principal de ma thèse et porte sur l'influence du microbiote et des métabolites bactériens dans les TSA. Chez les patients autistes, les déficits d'interaction sociale et les comportements répétitifs ou stéréotypés sont fréquemment associés à des symptômes gastro-intestinaux, des anomalies de composition de la flore intestinale et des niveaux anormaux de métabolites produits par le microbiote. Ceci laisse suggérer que des perturbations de l'axe microbiote-intestin-cerveau pourraient contribuer au développement des TSA. Néanmoins, le lien de causalité entre dysbiose, métabolites microbiens et comportements autistiques reste à démontrer. Notre hypothèse de travail est que certains métabolites microbiens sont les médiateurs des effets délétères de la flore intestinale sur les comportements impactés dans les TSA. Nous avons étudié le *para*-Crésol (*p*-Crésol), un métabolite microbien anormalement élevé chez les patients TSA et notamment produit par les *Clostridies*, des bactéries surabondantes chez ces patients. Nous avons exploré chez la souris le lien de causalité entre l'exposition au *p*-Crésol et le développement de comportements autistiques. Nous avons ainsi montré que les souris exposées au *p*-Crésol pendant 4 semaines présentent des stéréotypies et des déficits d'interaction sociale. Ces symptômes comportementaux propres aux TSA sont accompagnés d'une diminution de l'excitabilité des neurones dopaminergiques dans l'aire tegmentaire ventrale (ATV), une région du cerveau clé pour la récompense sociale, connue pour être dérégulée chez les patients TSA. Nous observons également des anomalies de la composition du microbiote, avec les abondances de certains taxa microbiens corrélées aux déficits d'interactions sociales. Enfin, la restauration d'un microbiote sain par un transfert de microbiote de souris normales à des souris exposées au *p*-Crésol nous a permis de restaurer les déficits d'interaction sociale et l'activité dopaminergique. Cette étude démontre, d'une part, un lien de cause à effet entre l'exposition à un métabolite microbien et le développement des comportements autistiques, et d'autre part, que la manipulation du microbiote est une voie thérapeutique possible pour les TSA.

La seconde section de la thèse se compose de trois articles, auxquels j'ai contribué, et qui portent sur l'exploration des phénotypes périphériques dans le Syndrome de l'X Fragile (FXS), la première cause génétique de TSA. Le premier article porte sur l'étude de la dérégulation du métabolisme du glucose et des lipides dans le FXS et repose sur la souris *Fmr1*-KO, le modèle murin du FXS, ainsi que des échantillons de patients FXS. Dans le second article, nous avons analysé l'impact de l'inactivation du gène *Fmr1* sur la composition corporelle et la structure osseuse dans le modèle murin du FXS. Dans le troisième article, nous avons mis en évidence des anomalies des profils de chimiokines dans le sérum de patients FXS, laissant supposer des dysfonctions immunitaires.

Dans l'ensemble, mon travail de thèse a permis de mettre en évidence une contribution périphérique dans les TSA, et en particulier le rôle clé de métabolite microbien *p*-Crésol dans le développement des comportements autistiques.

## **In English**

Thesis title: Peripheral and Intestinal Microbiota Alterations in Autism Spectrum Disorders  
Thesis sub-title: The Specific Role of *p*-Cresol  
Keywords: Autism, behaviour, *p*-Cresol, microbiota, dysbiosis, reward circuit

## **Abstract**

This thesis mainly focuses on the peripheral anomalies associated with Autism Spectrum Disorders (ASD), a group of frequent neurodevelopmental pathologies.

The first section is devoted to my main thesis work and focuses on the influence of the microbiota and bacterial metabolites in ASD. In autistic patients, deficits in social interaction and repetitive behaviours (stereotypies) are frequently associated with gastrointestinal symptoms, abnormal composition of the intestinal flora and abnormal levels of metabolites produced by the microbiota. This suggests that disturbances in the microbiota-gut-brain axis could contribute to the development of ASD. However, the causal link between dysbiosis, microbial metabolites and autistic behaviour remains to be demonstrated. Our working hypothesis is that certain microbial metabolites are mediators of the deleterious effects of the intestinal flora on the behaviours impacted in ASD. We have studied the microbial metabolite *para*-Cresol (*p*-Cresol) that is abnormally elevated in ASD patients and produced in particular by *Clostridia* bacteria that are overabundant in these patients. We have explored in mice the causal relationship between exposure to *p*-Cresol and the development of autistic behaviours. We have thus shown that mice exposed to *p*-Cresol for 4 weeks display social interaction deficits and stereotypies. These behavioural symptoms specific to ASD are accompanied by a decrease in the excitability of dopaminergic neurons in the Ventral Tegmental Area (VTA), a brain region key to social reward and known to be deregulated in ASD patients. We also highlighted anomalies in the composition of the microbiota upon *p*-Cresol exposure, with the abundances of specific microbial taxa correlated with social behaviour deficits. Finally, the restoration of a healthy microbiota by a transfer of microbiota from normal mice to mice exposed to *p*-Cresol allowed us to restore social behaviour deficits and VTA dopaminergic activity. This study demonstrates a causal relationship between exposure to the microbial metabolite *p*-Cresol and the development of ASD core behaviours and also a possible therapeutic avenue for ASD through the manipulation of microbiota.

The second section of the thesis consists of three articles, to which I have contributed, that explore peripheral phenotypes in Fragile X Syndrome (FXS), the leading genetic cause of ASD. The first article addresses the deregulation of glucose and lipid metabolism in FXS relying on the *Fmr1*-KO mouse, the mouse model of FXS, as well as on samples from FXS

patients. In the second article, we analysed the impact of *Fmr1* gene inactivation on body composition and bone structure in the mouse model of FXS. In the third article, we highlighted anomalies in the profiles of chemokines in the serum of FXS patients, suggesting immune dysfunctions.

Overall, my thesis work highlighted peripheral contributions in ASD, and in particular the key role of the microbial metabolite *p*-Cresol in the development of autistic behaviour.

## **Acknowledgements**

I would particularly like to thank my supervisor Laetitia for teaching me everything I know as a scientist, and helping me both professionally and personally. For trusting me to start this project 5 years ago and encouraging me when things didn't go as we expected. I also want to thank Nicolas for accepting me in his team. Thanks to both of you for this opportunity, I will always be grateful to you.

I also wanted to thank Antoine, for being a great lab partner. I have missed working with you during these years. Thank you for your help and for teaching me what it means to work as a team. Thank to Cristina for those long conversations and for encouraging me.

I also wanted to thank Julie and Jerome, for making me feel at home when I talk to them, for their sympathy, for teaching me everything I know about behavior, for their advice in the experiments, for their sympathy, help, thank you very much. Thank you for being part of my follow-up committee. Thank Xavi for his participation in my follow-up committee, his sympathy and thank you for your support. I also want to thank Jacques and Sebastian for all their support, their conversations and advices, their great help in the project and always welcome me in their lab with a smile.

Special thanks to Helene Boudin for her extraordinary welcome in Nantes and her sympathy. Thank you very much for agreeing to be part of my thesis committee.

I want to thank Joëlle Chabry for helping me in the beginning with the behaviour and always greeting me with a big smile. Thank you for accepting to be the president of the jury for my thesis.

I would also like to thank Sylvie Rabot and Pierre-Yves Mousset for accepting to be part of my thesis jury.

I also want to thank Thomas Lorivel for his enormous help in Animex and always being reactive and helping me. Thanks to Lucien for taking care of my animals and the long conversations during the long days in Animex.

I want to thank my family for always supporting and encouraging me over the years. Thanks to my mother Marimar for all her help and encouragement. I wouldn't be here without all your help, patience and dedication. Gracias Mama, no estaría hoy aquí si no fuese por ti, toda tú ayuda, tú apoyo y toda tú dedicación. Thanks to my father Teo for encouraging me in difficult times and supporting me. Thank to my sister and brother Cristina and Diego for bringing a smile to my face on the bad days and for listening to me and giving me good advice. Thanks to Luca, because if it wasn't for you, this would never have started, thanks for supporting me and giving me advice.

I want to thanks Ester for always being there since our adventure began in Nice 7 years ago, thanks for supporting me and always encouraging me. Thanks to Nathaly for teaching me to see things differently and for our long infinite talks on the promenade.

# Table of Contents

<b>LIST OF ABBREVIATIONS</b> .....	<b>8</b>
<b>LIST OF FIGURES</b> .....	<b>11</b>
<b>LIST OF TABLES</b> .....	<b>11</b>
<b>CHAPTER 1: INTRODUCTION</b> .....	<b>12</b>
NEURODEVELOPMENTAL DISORDERS.....	12
AUTISM SPECTRUM DISORDERS .....	13
A. <i>Generalities</i> .....	13
1. Prevalence, Core Symptoms of ASD and Diagnosis.....	13
2. Associated Peripheral Symptoms.....	14
a. Immune Dysfunction .....	14
b. Gastrointestinal Symptoms .....	15
B. <i>ASD Causes</i> .....	16
1. Genetic Causes.....	16
a. Genes Linked to ASD.....	16
b. Functions of the Genes Involved .....	17
c. One Example of a Syndromic Form of ASD: Fragile X Syndrome .....	17
2. Environmental Factors .....	19
a. <i>In utero</i> Exposure to Drugs Consumed by the Mother .....	19
b. <i>In utero</i> Exposure to Maternal Immune Activation .....	20
c. Mode of Delivery .....	21
C. <i>Disturbed Neuronal Circuits in ASD</i> .....	21
D. <i>ASD Animal Models</i> .....	23
1. Introduction .....	23
2. Genetic and Environmental Animal Models in ASD .....	24
a. Genetic Models.....	24
i. Fmr1-knockout (KO) mice.....	24
ii. Shank3b-KO mice .....	25
iii. BTBR T+ Itpr3tf/J (BTBR) mice .....	26
b. Environmentally-Induced ASD Models .....	26
i. <i>In utero</i> Exposure to Valproic Acid .....	26
ii. <i>In utero</i> Exposure to MIA.....	27
iii. <i>In utero</i> Exposure to Diet-Induced Maternal Obesity (DIO) .....	28
THE MICROBIOTA-GUT-BRAIN AXIS IN ASD .....	29
A. <i>The Microbiota-Gut-Brain Axis: a Bidirectional Communication Axis</i> .....	29
1. Introduction .....	29
2. The Microbiota-Gut-Brain-Axis .....	30
a. Involvement of the Peripheral Nervous System .....	30
i. Enteric Nervous System (ENS) .....	30
ii. Vagus Nerve (Parasympathetic System).....	31
b. Involvement of Neuroendocrine Signals.....	32
i. Involvement of the Hypothalamus-Pituitary-Adrenocortical Axis (HPA).....	32
ii. Involvement of Intestinal Epithelial Cells .....	33
c. Involvement of Immune Signals .....	34
d. Involvement of Microbial Metabolites .....	34
3. Microbiota Can Impact Brain Function and Behaviour .....	36
a. GF Animals Exhibit Neurobiological and Behavioural Impairments.....	36
b. Developmental Windows for the Brain and the Microbiota.....	37
B. <i>Evidences for a Disruption of the Microbiota-Gut-Brain Axis in ASD</i> .....	39
1. Microbiota Dysbiosis in ASD .....	39
a. ASD Risk Factors Can Target the Microbiota .....	39
b. Microbiota Dysbiosis in ASD Patients and ASD Models .....	40
c. Manipulations of the Microbiota Can Improve ASD Symptoms .....	42
i. Faecal Microbiota Transplantation (FMT) .....	42
ii. Probiotic .....	42
2. Abnormal Microbial Metabolites Patterns in ASD Patients and ASD Models .....	43
a. SCFAs Altered in ASD .....	43
b. Tryptophan-Derived Microbial Metabolites Altered in ASD .....	45

c.	Phenylalanine-Tyrosine-Derived Metabolites Altered in ASD .....	46
3.	The Specific Case of <i>p</i> -Cresol in ASD .....	46
a.	General Introduction .....	47
b.	<i>p</i> -Cresol Metabolism in the Host .....	47
c.	Clinical Evidence Connecting <i>p</i> -Cresol to ASD .....	48
i.	Increased Excretion of <i>p</i> -Cresol in ASD.....	48
ii.	Correlation with ASD GI Symptoms and ASD Core Behaviours .....	48
iii.	Increased Abundances of Bacterial Taxa Synthetizing <i>p</i> -Cresol in ASD .....	49
d.	<i>p</i> -Cresol and Behaviour in Mice .....	49
<b>CHAPTER 2: ROLE OF THE MICROBIAL METABOLITE <i>P</i>-CRESOL IN ASD .....</b>		<b>50</b>
I.	CONTEXT.....	50
II.	RESEARCH HYPOTHESIS AND OBJECTIVES OF THE STUDY .....	51
III.	RESULTS.....	52
IV.	MANUSCRIPT .....	53
CONCLUSIONS AND PERSPECTIVES .....		114
A.	<i>Conclusions</i> .....	114
B.	<i>Perspectives in the p-Cresol Mouse Model</i> .....	114
1.	Understanding the Cellular and Molecular Pathways Impacted by <i>p</i> -Cresol .....	114
2.	Possible Therapeutic Strategies to Explore in the <i>p</i> -Cresol Model .....	116
3.	Possible Therapeutic Intervention Strategies Targeting the Microbiota in ASD .....	117
a.	FMT.....	117
b.	Probiotic and Prebiotic Treatment .....	118
<b>CHAPTER 3: PERIPHERAL PHENOTYPES IN FRAGILE X SYNDROME .....</b>		<b>120</b>
I.	CONTEXT.....	120
METABOLIC ANOMALIES IN FXS: PUBLICATION #1 .....		120
A.	<i>Research Hypothesis and Objectives of the Study</i> .....	120
B.	<i>Results</i> .....	121
C.	<i>Manuscript</i> .....	122
SKELETAL ANOMALIES IN FXS: PUBLICATION #2 .....		172
A.	<i>Research Hypothesis and Objectives of the Study</i> .....	172
B.	<i>Results</i> .....	172
C.	<i>Manuscript</i> .....	173
IMMUNE ANOMALIES IN FXS: PUBLICATION #3 .....		187
A.	<i>Research Hypothesis and Objectives of the Study</i> .....	187
B.	<i>Results</i> .....	187
C.	<i>Manuscript</i> .....	188
CONCLUSIONS ON FXS WORK .....		201
<b>TAKE-HOME MESSAGE .....</b>		<b>202</b>
<b>BIBLIOGRAPHY .....</b>		<b>203</b>

# List of Abbreviations

3,4-Dihydroxyphenylacetic Acid	DOPAC
4-Ethylphenylsulfate	4-EPS
5-Aminovaleric Acid	5AV
5-Hidroxi-Triptamina	5-HT
Acyl-CoA Dehydrogenase	AcdA
Attention-Deficit/Hyperactivity Disorder	ADHD
Autism Spectrum Disorder	ASD
Blood-Brain Barrier	BBB
Body Mass Index	BMI
Brain-Derived Neurotrophic Factor	BDNF
Cadherin-1	<i>CDH1</i>
Caesarean Section	CS
Calcium voltage-gated channel	<i>CACN</i>
Central Nervous System	CNS
Choline Acetyltransferase	ChAT
Cluster of Differentiation 3	CD3
Coeliac Disease	CD
Complement 4B	<i>C4B</i>
Corticotrophin-Releasing Hormone	CRH
Dendritic Cells	DC
Diagnostic and Statistical Manual of Mental Disorders	DSM-V
Diet-Induced Maternal Obesity	DIO
Dorsal Raphe Nucleus	dRN
Dorsal Vagal Complex	DVC
Enteric Nervous System	ENS
Enterocromaffin Cells	EC
Eotaxin-1	CCL11
Faecal Microbiota Transplantation	FMT
Fragile X Mental Retardation 1 gene	<i>FMR1</i>
Fragile X Mental Retardation Protein	FMRP
Fragile X Related 2	<i>Fxr2</i>
Fragile X Syndrome	FXS
Free Fatty Acid Receptor 1-2	FFAR1-2
Functional Magnetic Resonance Imaging	fMRI
G Protein-Coupled Receptor 142	GPR142
G Protein-Coupled Receptor 35	GPR35
G Protein-Coupled Receptor 41	GPR41
G Protein-Coupled Receptor 43	GPR43
Gamma-Aminobutyric Acid type A Receptor	<i>GABR</i>
Gastro-Intestinal	GI
Gestational Diabetes Mellitus	GDM
Glial Fibrillary Acidic Protein	GFAP
Glutamate Ionotropic Receptor AMPA type subunit 1	<i>GRIA1</i>
Glutamate Ionotropic Receptor NMDA type subunit 1	<i>GRIN1</i>
Granulocyte-Macrophage Colony Stimulating Factor	GM-CSF
Gut-Associated Lymphoid Tissue	GALT
Human Leukocyte Antigen Complex	<i>HLA</i>

Hydroxycarboxylic acid receptor 2	<i>Hca2</i>
Hydroxyphenylacetate Decarboxylase	Hpd
Hypothalamus-Pituitary-Adrenocortical	HPA
Indole-3-Lactic Acid	ILA
Innate Lymphoid Cells	ILC
Innate Lymphoid Cells	ILCs
Intellectual Disability	ID
InterFeron- $\gamma$	IFN- $\gamma$
InterLeukin-1 Receptor Antagonist	IL-1R $\alpha$
InterLeukin-10	IL-10
InterLeukin-6	IL-6
InterLeukin-8	IL-8
InterLeukine 1 Receptor Accessory Protein Like 1	<i>IL1RAPL1</i>
Intraepithelial Lymphocytes	IEC
Intraepithelial Lymphocytes	IECs
kiloDalton	kDa
Lipopolysaccharides	LPS
Long-Term Depression	LTD
Long-Term Potentiation	LTP
Macrophage Migration Inhibitory Factor	<i>MIF</i>
Major Histocompatibility Complex	MHC
Maternal Immune Activation	MIA
Medium Spiny Neurons	MSN
Methyl-CpG Binding Protein 2	<i>MECP2</i>
Microfold Epithelial Cells	M
Miniature Excitatory Postsynaptic Currents	mEPSC
Modified Checklist for Autism in Toddlers – Revised	M-CHAT-R
Monocyte Chemoattractant Protein-1	MCP-1
Neurexins	<i>NRXN</i>
NeuroDevelopmental Disorders	NDD
Neuroigin 3	<i>NLGN3</i>
Neuroigin 4	<i>NLGN4</i>
Nitric Oxide Synthase	nNOS
NonObese Diabetic	NOD
Nuclear factor- $\kappa$ B	NF- $\kappa$ B
Nucleus Accumbens	NAc
Nucleus of Solitary Tract	NTS
Olfactory Receptor 78	OLFR78
ParaVentricular Nucleus	PVN
Pathogen-Associated Molecular Patterns	PAMP
Phenyllactate Dehydratase	FldBC
Phenyllactate Dehydrogenase	FldH
Polyinosinic-Polycytidylic Acid poly	Poly (I:C)
Postsynaptic Density Protein 95	PSD95
Potassium voltage-gated channel	<i>KCN</i>
PreFrontal Cortex	PFC
Propionic Acid	PPA
Protein Kinase C Beta	<i>PRKCB</i>
Psoriasis	PS
Pyruvate:Ferredoxin Oxidoreductase A	PorA

Quantitative – Checklist for Autism in Toddlers	Q-CHAT
Restricted Repetitive Behaviour	RRB
Rheumatoid Arthritis	RA
SH3/Ankyrin Domain gene 3	<i>SHANK3</i>
Short Chain Fatty Acid	SCFA
Single Nucleotide Polymorphisms	SNP
Sodium voltage-gated Channel	<i>SCN</i>
Synapsin-1 and -2	<i>SYN1-2</i>
Thiazole Synthase H	ThiH
Transforming Growth Factor Beta 1	TGF-β1
Tryptophan Hydroxylase 1	Tph1
Tuberous Sclerosis Complex 2	<i>TSC2</i>
Tumor Necrosis Factor-α	TNF-α
Type-1 Diabetes	TD1
Tyrosine Aminotransferase B	TyrB
Ubiquitin Protein Ligase E3A	<i>UBE3A</i>
Vaginal Delivery	VD
Valproic Acid	VPA
Ventral Tegmental Area	VTA
α-Amino-3-Hydroxy-5-Methyl-4-Isoxazolepropionic Acid	AMPA
γ-AminoButyric Acid	GABA

# List of Figures

Figure 1: <i>In utero</i> exposure to maternal environmental factors increases the risk of ASD in offspring. ....	19
Figure 2: Maternal immune activation risk factor for ASD in offspring (Estes and McAllister, 2016).....	21
Figure 3: Brain regions involved in the Mesolimbic Reward Circuit. ....	22
Figure 4: Mesolimbic reward pathway: white matter tracts connecting the NAc and the VTA (Supekar et al., 2018). ....	23
Figure 5: Communication pathways from the gut to the brain.....	30
Figure 6: Microbiota and neurodevelopmental windows: implications for brain disorders by (Borre et al., 2014) . ....	38
Figure 7: Factors shaping the neonatal microbiome (Tamburini et al., 2016).....	39
Figure 8: Direct (A) and Indirect (B) pathway for <i>p</i> -Cresol synthesis using tyrosine as a precursor by gut bacteria (Saito et al., 2018). ....	47

# List of Tables

Table 1: Epithelial cells of the GI system. ....	33
Table 2: Effects of bacterial metabolites on the host's immune and GI function. ....	36
Table 3: Behavioural phenotypes and biological processes in GF rodents.....	37

# Chapter 1: Introduction

## Neurodevelopmental Disorders

Central Nervous System (CNS) disorders with early onset are commonly termed Neurodevelopmental Disorders (NDD). NDD include a large number of pathologies in which abnormal neurodevelopment leads to neurological and/or behavioural impairments. These pathologies affect four times more males than females (Rutter et al., 2003). Intellectual Disability (ID), Autism Spectrum Disorders (ASD), Attention-Deficit/Hyperactivity Disorder (ADHD), motor disorders and epilepsy are common NDD (Thapar et al., 2017). NDD are frequently associated with communication and social behaviour deficits, sensory disorders, learning disabilities, hyperactivity, anxiety, depression, mood instability, sleep problems, stereotypies, self-injurious behaviours, etc. The prevalence and intensity of the different symptoms will determine the diagnosis class and the specific needs for each NDD patient (Hansen et al., 2018). The symptomatology and severity of symptoms vary greatly among patients, even within a specific diagnosis class, and the frequent comorbidities among NDD underline the great heterogeneity in the clinical spectrum of NDD.

The differential manifestations of NDD can be explained by complex interactions between genetic predisposition and exposure to different environmental NDD risk factors (Jones and Szatmari, 2002). Several environmental factors -such as nutrition, pollution, immune changes, stress, environmental enrichment- are known to influence neurodevelopment (Hertz-Picciotto et al., 2018). In addition, the existence of critical time-windows in neurodevelopment, as well as the limited time-window for recovery or compensation of abnormal neurodevelopment modulates the risk to later develop NDD (Krol and Feng, 2018). One important neurodevelopmental time-window is the prenatal period. *In utero*, the foetus can be exposed to large number of factors that can compromise neurodevelopment at various stages. NDD environmental risk factors include *in utero* exposure to drugs consumed during pregnancy, maternal immune activation, maternal obesity or pollution (Hertz-Picciotto et al., 2018). Even the birth delivery mode can affect the child's behavioural outcome during childhood (Hertz-Picciotto et al., 2018).

This Thesis focuses on a specific class of NDD, ASD, and encompasses studies related to i) the role played by the environment, and more specifically the microbiota in the development of ASD and ii) a genetic form of ASD, Fragile X Syndrome.

# Autism Spectrum Disorders

## A. Generalities

### 1. Prevalence, Core Symptoms of ASD and Diagnosis

ASD are characterized by impairment in communication and social behaviour, as well as the presence of restricted repetitive behaviours and atypical sensory processing (Green et al., 2016; Lai et al., 2013). ASD are often accompanied by comorbidities such as ADHD, ID, anxiety and depressive disorders (Cremone-Caira et al., 2019; Mazurek et al., 2013). Epidemiological studies report an incidence of 1 in 68 children with ASD in 2012 in the United States, with an estimated male: female sex ratio of 4:1 (Christensen et al., 2019). In recent years, the prevalence of ASD has increased. This may be due to a higher exposure to environmental factors that increase the risk of the onset of ASD (Lai et al., 2013). In fact, recent improvements in ASD diagnosis criteria also allow reducing the diagnosis bias of ASD in women, which used to be under-recognised based on anterior diagnostic criteria (Lai et al., 2013).

Most of ASD cases are detected from 24 to 36 months of age (Bejarano-Martín et al., 2019). ASD screening and diagnosis is performed when family members, paediatrician or caregivers suggest that the infant has developmental difficulties. These infants are screened using either of these two questionnaires: Modified Checklist for Autism in Toddlers, Revised (M-CHAT-R) (Robins and Casagrande, 2014) or the Quantitative Checklist for Autism in Toddlers (Q-CHAT) (Allison et al., 2008). These screening tools are designed to identify difficulties in young children and determine whether the toddler should be referred for full ASD diagnosis evaluation (Baird et al., 2000). ASD clinical diagnosis relies on the Diagnostic and Statistical Manual of Mental Disorders (DSM-V) criteria (Doernberg and Hollander, 2016). DSM-V diagnostic criteria for ASD rely on the evaluation of two behavioural domains: social communication impairments and restricted repetitive behaviours (RRBs) (Lord and Bishop, 2015). Social and communication problems encountered in ASD include deficits in social-emotional reciprocity and non-verbal behaviours involved in social interaction, and maladaptive social behaviour. The restricted/repetitive behaviours associated with ASD include repetitive movements or stereotypies, perseverative behaviours, inflexible routines, restrictive interests and hypo- or hyper-reactivity to sensory stimuli (Lord and Bishop, 2015). Once diagnosed with ASD, the child will be redirected to specialized mental health services.

Professionals will inform families of the child's specific needs, highlighting the educational needs (Bejarano-Martín et al., 2019).

## 2. Associated Peripheral Symptoms

### a. Immune Dysfunction

In addition to behavioural symptoms, ASD patients frequently present immune dysfunction. ASD patients are at increased risk of developing immune disorders such as asthma, food allergies or autoimmune disorders (e.g. coeliac disease, Crohn's disease, type 1 diabetes, rheumatoid arthritis, psoriasis...) (Ashwood et al., 2006; Atladóttir et al., 2009). Furthermore, peripheral alterations in cytokine levels are also observed in the blood of ASD patients. Recent meta-analysis show that increased plasma levels of Interferon (IFN)- $\gamma$ , Interleukin (IL)-1 $\beta$ , IL-6, Tumor Necrosis Factor (TNF)- $\alpha$ , Monocyte Chemoattractant Protein-1 (MCP-1), Eotaxin-1 (CCL11), IL-8 and reduced levels of Transforming Growth Factor Beta 1 (TGF- $\beta$ 1), IL-10, Interleukin-1 Receptor Antagonist (IL-1R $\alpha$ ) are associated with ASD (Masi et al., 2015; Saghazadeh et al., 2019).

Furthermore, some studies suggest that some ASD patients exhibit neuroinflammation. Neuroinflammation is an inflammatory process that occurs within the CNS (DiSabato et al., 2016) which involves resident cells in the brain -such as astrocytes, microglia, endothelial cells- and immune cells migrating from the periphery. Neuroinflammation is accompanied by an increased production of cytokine, chemokines and second messengers driving the inflammatory process (DiSabato et al., 2016). Several studies conducted on *post mortem* brains of ASD patients revealed microglial and astroglial activation, which is a hallmark of neuroinflammation. The expression of the astrocyte marker Glial Fibrillary Acidic Protein (GFAP) was increased in the cortex of ASD patients (Laurence and Fatemi, 2005). Also, the cortex of ASD patients exhibit an increased microglial density and signs of microglial activation such as increases in microglial somatic volume, retraction, thickening and extension of prolongations (Morgan et al., 2010; Tetreault et al., 2012). One study showed increased cytokine levels including TNF- $\alpha$ , IL-6, Granulocyte-Macrophage Colony Stimulating Factor (GM-CSF), IFN- $\gamma$  and chemokine Interleukin-8 (IL-8) in *post mortem* ASD brain tissues (Li et al., 2009).

In addition, signs of inflammation have been detected in the gastrointestinal (GI) tract of ASD patients. Some studies have shown abnormalities in the proinflammatory cytokines levels expressed by CD3<sup>+</sup> lymphocytes (e.g. increased level of TNF- $\alpha$  and INF- $\gamma$ , IL-4 and IL-5 with reduction of IL-10) in intestinal biopsies from ASD children (Ashwood and Wakefield, 2006; Jyonouchi, 2009; Luna et al., 2017).

### b. Gastrointestinal Symptoms

A considerable number of studies have shown that ASD patients are more prone to GI functional disorders (McElhanon et al., 2014). Further, ASD patients are 4.4 times more likely to exhibit GI symptoms than neurotypical individuals (McElhanon et al., 2014). The most common symptoms are abdominal pain, diarrhoea, constipation and abdominal bloating (Chaidez et al., 2014). Furthermore, ASD children are 5 times more susceptible to develop feeding problems as compared to neurotypical children (Sharp et al., 2013), and often present anorexia and anhedonia (Mazefsky et al., 2014). In ASD patients, the GI problems are associated with increased severity of social/affective problem, social withdrawal, repetitive behaviours, irritability, hyperactivity, anxiety and aggressiveness (Adams et al., 2011; Buie et al., 2010; Gorrindo et al., 2012; Mazefsky et al., 2014; Nikolov et al., 2009).

Moreover, some ASD patients also present alterations of intestinal permeability (D'Eufemia et al., 1996; Esnafoglu et al., 2017; De Magistris et al., 2010). In physiological conditions, the intestinal epithelium strictly controls the passage of particles, toxins and microorganism. In pathological conditions, the intestinal epithelium can become more permeable or “leaky” and allow passage of potentially harmful molecules and microorganisms (Camilleri et al., 2012). This can also be accompanied by intestinal inflammation, that may eventually become systemic (Mu et al., 2017). This inflammation can also contribute to exacerbate the intestinal damages and allow the translocation of intestinal bacteria and other harmful substances (Mu et al., 2017). Studies in subsets of ASD patients have highlighted a reduction in the expression of tight junctions proteins, which regulate the permeability of the intestinal barrier (Fiorentino et al., 2016; Luna et al., 2017).

Both GI problems and immune system dysfunction in ASD patients may be closely related to anomalies of microbiota composition, or dysbiosis, found in ASD patients (Fung et al., 2017). This topic will be further developed in section 3 of the Thesis, which addresses the possible contribution of perturbations of the microbiota-gut-brain axis in ASD.

## B. ASD Causes

The causes for ASD are complex and multifactorial. As most NDD, ASD likely result from strong interaction between genetic susceptibility and exposure to environmental factors which perturb neurodevelopment. The genetic contribution in ASD appears to be approximately 45% for monozygotic twins and 16% for dizygotic twins (Bourgeron, 2016). Twin studies have also revealed that genetics and environmental factors share equal influence on ASD risk (Bourgeron, 2016).

### 1. Genetic Causes

#### a. Genes Linked to ASD

Approximately 10-25% of ASD cases can be explained by mutation in specific genetic *loci*. ASD is associated with more than 913 genes, as summarized in the SFARI database (<https://www.sfari.org/resource/sfari-gene/>). We can distinguish non-syndromic and syndromic forms of ASD.

Non-syndromic forms are generally of unknown genetic aetiology and accounts for the majority of ASD cases. Non-syndromic forms are usually related to the presence of several allelic variants corresponding to single nucleotide polymorphisms (SNP). These variants usually have slight effects and can be found in the general population (Bourgeron, 2016). Allelic variants play an important role in the susceptibility to ASD. In some individuals, a specific genetic background will be able to buffer or compensate the impact of the rare genetic variations. In contrast, in some individuals, the buffering capacity of the genetic background will not be sufficient to compensate the impact of the deleterious mutations and they will develop ASD.

Syndromic forms of ASD account for a small percentage of ASD cases and are linked to the deletion, duplication or silencing of a specific genetic *locus* (Rylaarsdam and Guemez-Gamboa, 2019). Usually, syndromic forms of ASD are accompanied with a clinically defined pattern of somatic abnormalities (such as dysmorphic features, gastrointestinal problems) and a neurobehavioral phenotype that include ASD and often learning and ID.

## b. Functions of the Genes Involved

The genes associated with ASD operate multiple functions. However, there is a high incidence of genes with synaptic function or immune function.

Among the genes affecting synaptic function and plasticity lie genes encoding adhesion proteins (e.g. neuroligin3, 4 (*NLGN3/4*), neurexins (*NRXN*), and cadherins (*CDHI*)), synaptic vesicles proteins (e.g. synapsin-1 and -2 (*SYN1-2*)), channels (e.g. sodium, calcium and potassium voltage-gated channel (*SCN*, *CACN* and *KCN*) and receptors (e.g. glutamate and GABA receptors (*GRIAI*, *GRINI* and *GABR*)) that are critical for synaptic functions (Rylaarsdam and Guemez-Gamboa, 2019). Genes involved in signal transduction such as *Tuberous sclerosis complex 2* (*TSC2*), and protein degradation such as *Ubiquitin protein ligase E3A* (*UBE3A*) are also associated with ASD (Rylaarsdam and Guemez-Gamboa, 2019). Finally, genes encoding regulators of mRNA translation -such as the *Fragile X Mental Retardation 1* gene encoding the RNA-binding protein FMRP linked to Fragile X Syndrome- or transcription -such as the *Methyl-CpG binding protein 2* encoding the transcription factor MECP2 linked to Rett Syndrome- are also associated with ASD (Rylaarsdam and Guemez-Gamboa, 2019). Loss-of-function of these genes was shown to impact synaptic development and function in animal models and these are thought to contribute to the behavioural impairments in ASD patients.

Another class of genes associated with ASD is related to immune components such as: Macrophage Migration Inhibitory Factor (*MIF*), Human Leukocyte Antigen Complex (*HLA-A2*, *HLA-DRB1*), Major Histocompatibility Complex (MHC class I and MHC class II), elements involved in complement cascade (*C4B*) and Interleukin 1 Receptor Accessory Protein Like 1 (*IL1RAPL1*) (Estes and McAllister, 2015). In patients bearing mutations in these genes, perturbations of immune processes could impair neurodevelopment and contribute to behavioural alterations (Estes and McAllister, 2015).

## c. One Example of a Syndromic Form of ASD: Fragile X Syndrome

**Clinical features of FXS.** Fragile X syndrome (FXS) is the first genetic cause of ASD diagnosis, with up to 50% of Fragile X patients diagnosed with ASD (Penagarikano et al., 2007). FXS is also the most common form of inherited ID mainly associated with mild to strong cognitive impairments, attention deficits and hyperactivity. Besides presenting behavioural alterations, FXS is also accompanied by physical abnormalities (Kidd et al.,

2014). In subsets of FXS patients, morphometric studies have highlighted increased stature and height (Butler et al., 1993) and a general overgrowth in prepubertal boys affected by FXS (Kidd et al., 2014; De Vries et al., 1995). FXS patients present connective tissue dysplasia (Hagerman et al., 1984), dental and mandibular anomalies (Sabbagh-Haddad et al., 2016), orthopedic anomalies such as scoliosis (Davids et al., 1990), and abnormal metacarpophalangeal pattern profile (Butler et al., 1988). In addition, FXS patients display specific craniofacial abnormalities with reduced facial depth, hypoplasticity of the nasal bone–cartilage interface and narrow mid-facial width exaggerating ear prominence (Heulens et al., 2013). Also, subtle craniofacial anomalies with morphometric changes in the mandible and skull are observed in FXS patients (Heulens et al., 2013).

***Functions of the gene mutated in FXS.*** FXS is caused by the silencing of the *FMRI* gene, located in a “fragile” site on the X chromosome in the 27q3 region (Harrison et al., 1983). Given that the *FMRI* gene is X-linked, random inactivation of the mutated allele in females yields a biased sex-ratio of 2 males (1:4000 males) for 1 female affected (1:8000 females), with a global incidence rate of 1:6000 in the general population. In FXS patients, abnormal expansions of CGG trinucleotide repeats in the 5' untranslated region of the *FMRI* gene lead to a hypermethylation of the CpG island upstream to the gene promotor. As a result, the *FMRI* gene is silenced and the encoded protein, FMRP is absent (Penagarikano et al., 2007). FMRP is an RNA binding protein involved in the regulation of mRNA translation, transport and stability (Penagarikano et al., 2007). The *FMRI* gene is expressed in the CNS and in all peripheral tissues, to the exception of adult skeletal and cardiac muscle (Davidovic et al., 2006; Khandjian et al., 1998). Loss of FMRP in the brain induces anomalies in the formation of synapses, with an increased density of immature dendritic spines thought to be at the basis of the ID (Hinton et al., 1991).

As a reflection of the expression of FMRP in the periphery, some FXS patients exhibit changes in metabolic or immune markers with decreased cholesterol levels, increase of triacylglycerols levels and changes in the levels of cytokines and chemokines (Ashwood et al., 2006; Berry-Kravis et al., 2015; Lisik et al., 2016), although these changes cannot be considered a patient-specific trait. These findings suggest that the effect of *FMRI*-deficiency generates physiological dysfunction in the CNS and in the periphery.

In the 4<sup>th</sup> sections of this Thesis, we will present three studies carried out on Fragile X patients and the mouse model of FXS addressing the peripheral consequences of *FMRI*-deficiency.

## 2. Environmental Factors

Environmental influences in combination with individual genetic susceptibility modulate the risk of developing ASD. In recent years, the importance of environmental factors during pregnancy has been pointed out as possible triggers for the development of ASD in the offspring. The nature of the environmental factors and the time-window of exposure during gestation are important elements that can modulate the genetic predisposition of an individual to NDD (Hertz-Picciotto et al., 2018). Following the “multiple hit” model for ASD, the repeated exposure to detrimental environmental factors can result in the appearance of ASD in genetically predisposed individuals (Miles, 2011). Some of the factors that increase the risk of the appearance of ASD in the offspring are summarized in **Figure 1**.

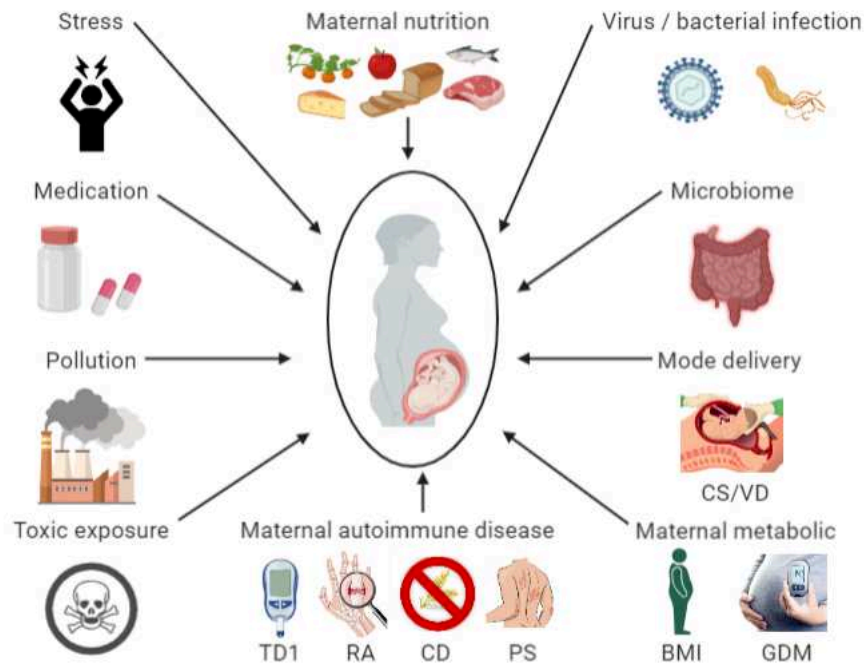


**Figure 1:** *In utero* exposure to maternal environmental factors increases the risk of ASD in offspring.

*Abbreviations:* TD1, Type-1 Diabetes; RA, Rheumatoid Arthritis; CD, Coeliac Disease; PS, Psoriasis; BMI, obesity based in Body Mass Index; GDM, Gestational Diabetes Mellitus; CS, Caesarean Section; VD, Vaginal Delivery.

### a. *In utero* Exposure to Drugs Consumed by the Mother

Epidemiological studies have shown that exposure to teratogens substances such as valproic acid -an anticonvulsant drug and mood stabilizer, used to treat migraines, epilepsy and bipolar

disorder- (Cotariu and Zaidman, 1991; Veroniki et al., 2017), thalidomine -an anti-emetic medication- (Jones and Szatmari, 2002) or misoprostol -used to treat gastric ulcers- (Ornoy et al., 2015) during the prenatal and early postnatal periods can alter neurodevelopment and lead to ASD in the offspring (Dufour-Rainfray et al., 2011).

### b. *In utero* Exposure to Maternal Immune Activation

There are three important risk factors for ASD linked to maternal immune activation (MIA). First, diagnosis of maternal autoimmune diseases (e.g. TD1, RA, CD, PS and Crohn's disease...) increases the risk of developing ASD in the offspring (Atladóttir et al., 2009). Second, the presence of maternal antibodies against foetal brain proteins (IgG antibodies) also increases the risk of ASD in the offspring (Hsiao, 2013). These antibodies would access the foetal brain at a developmental stage at which the blood-brain barrier (BBB) is still immature. This could contribute to generate brain abnormalities that may favour the emergence of later neurological problems in the offspring. Third, maternal infections and notably viral infection during the first trimester of pregnancy or unspecific infections during the second trimester are associated with an increased ASD risk in the offspring (Atladóttir et al., 2010). Frequent episodes of fever during pregnancy, linked to an infectious state, are also associated with increased ASD risk in the offspring (Hornig et al., 2018). Studies in mouse models have highlighted that the gestational period of exposure, the type of MIA (viral, bacterial or chronic) and the duration and intensity of the MIA will determine the appearance of neurodevelopmental and behavioural problems in the progeny (Estes and McAllister, 2015). It is hypothesised that maternal pro-inflammatory cytokines released upon MIA reach the foetal brain and perturb neurodevelopmental processes, increasing the susceptibility to later develop ASD (**Figure 2**).

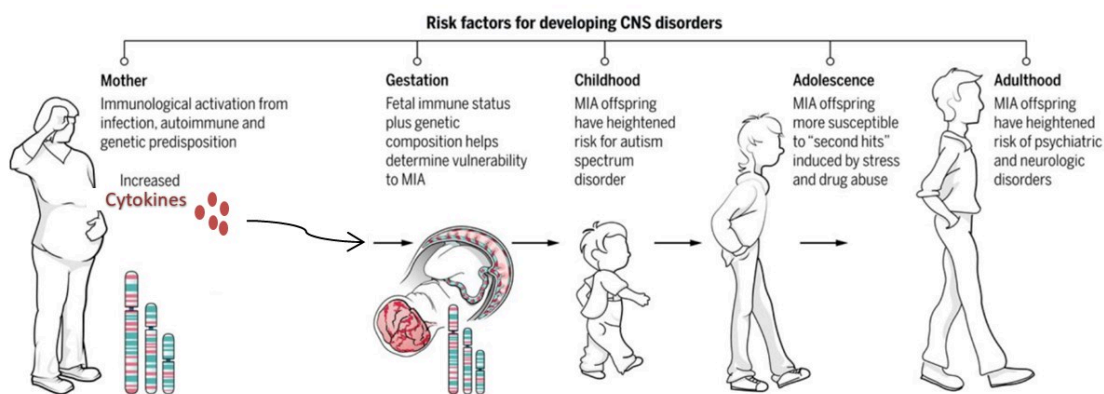


**Figure 2:** Maternal immune activation risk factor for ASD in offspring (Estes and McAllister, 2016)

### c. Mode of Delivery

The birth delivery mode can also modulate ASD risk. Several studies suggest that delivery by caesarean section increases the risk of the offspring to develop ASD (Curran et al., 2015; Yip et al., 2017). Meta-analyses have also identified other environmental risk factors for ASD such as advanced parental age, birth complications (e.g. trauma, ischemia, hypoxia), pregnancy-related risk factors (e.g. foetal distress, multiple births), deficiencies in essential nutrients (e.g. fatty acids, vitamin D and folate) and prenatal exposure to environmental toxins (e.g. heavy metals, pesticides, endocrine-disrupting chemicals) (Modabbernia et al., 2017; Wang et al., 2016).

## C. Disturbed Neuronal Circuits in ASD

The connection between behavioural abnormalities and deregulation in neural circuits and synaptic function in ASD is the subject of active research to understand the neurobiological correlates of ASD behavioural impairments. Several brain circuits have been identified as altered in ASD patients. Notably, the reward circuit could be involved in ASD-related social behaviour deficits (Supekar et al., 2018).

Social interactions are pleasurable events for humans and animals, as shown notably by the activation of the reward circuit by social stimuli – activation that is blunted in ASD patients (Pellissier et al., 2018). The mesolimbic dopamine reward circuit controls notably the social reward and the literature suggests that ASD patients experience a lower social reward as compared to neurotypical subjects (Chevallier et al., 2012). The interconnection between brain regions involved in the reward circuit have been mostly described in rodents and encompass: the Ventral Tegmental Area (VTA), Nucleus Accumbens (NAc), Paraventricular Nucleus (PVN) and Prefrontal Cortex (PFC) (**Figure 3**). To dissect out the connections between the main brain areas involved in the reward system, animal models have been used.

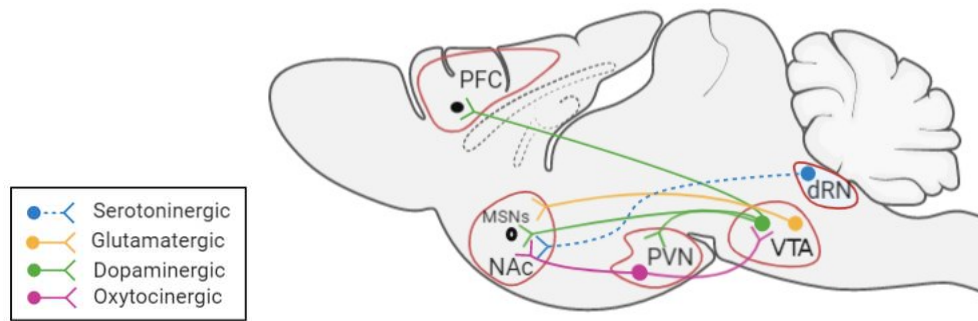


**Figure 3:** Brain regions involved in the Mesolimbic Reward Circuit.

*Abbreviations:* PFC, Prefrontal Cortex; MSNs, Medium Spiny Neurons; NAc, Nucleus Accumbens; PVN, Paraventricular Nucleus; VTA, Ventral Tegmental Area; dRN, dorsal Raphe Nucleus.

The VTA is a critical region for the mesolimbic reward circuit and is involved in the modulation of responses to reward stimuli. The VTA is localised in the brainstem and is composed mainly of GABA, dopaminergic and glutamatergic neurons (Morales and Margolis, 2017). VTA glutamate neurons are important for the socialisation of mice (Krishnan et al., 2017). The reduction of VTA glutamatergic transmission to Medium Spiny Neurons (MSNs) in the NAc, decreased the sniffing time in mice (Krishnan et al., 2017). On the other hand, VTA dopamine neurons project notably towards the NAc and the PFC. VTA dopamine neurons are regulated by oxytocinergic projection from the PVN (Hung et al., 2017). Oxytocin enhances the excitability of VTA dopamine neurons projecting to the NAc, which reinforces social interactions (Hung et al., 2017). In the NAc, MSNs express the D1 and D2 dopamine receptors (Dölen et al., 2013). At the same time oxytocinergic neurons of the PVN and serotonergic neurons of the dRN project to the NAc and both are important for the synaptic plasticity in the NAc that is essential for the social reward process (Dölen et al., 2013).

Functional neuroimaging, a non-invasive technique to monitor the activity and connectivity of brain regions in the resting state or during a task, was used to analyse the social reward system in ASD patients. A functional magnetic resonance imaging (fMRI) study reported a decrease in the density of the fibres which originate in the VTA and project to the NAc in young ASD patients (**Figure 4**) (Supekar et al., 2018). Another study has also shown a decreased activity in the NAc in ASD patients during reward-related motivation (Assaf et al., 2013).

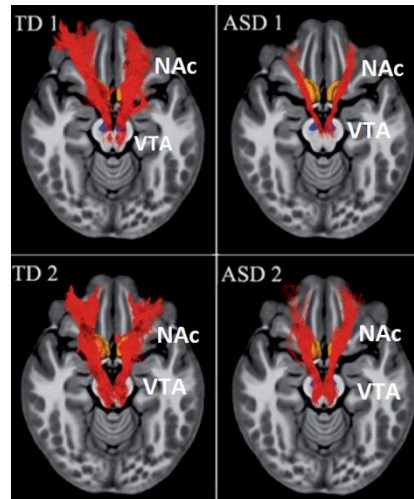


**Figure 4:** Mesolimbic reward pathway: white matter tracts connecting the NAc and the VTA (Supekar et al., 2018).

Finally, one study combined electroencephalography and high-resolution eye-tracking and reported that ASD patients present decreased activation of the PFC and the anterior cingulate cortex during neural processing of dynamic cartoons related to human-like social interactions (Jan et al., 2019). Also, using positron emission tomographic scanning, one study highlighted that ASD patients displayed a decreased dopaminergic activity in the anterior medial PFC during a story comprehension paradigm (Ernst et al., 1997).

Altogether, these studies suggest that social behaviour deficits in ASD patients could result from dysfunctions in the circuitry processing social reward, which modulate notably social cognition, perception and motivation (Mundy, 2003).

## D. ASD Animal Models

### 1. Introduction

ASD animal models have been developed to better understand the pathophysiological processes leading to ASD in human. There are three criteria established by Willner in 1984 that an animal model must fulfil in order to be considered a good model for neuropsychiatric disorders (Belzung and Lemoine, 2011). First, the construct validity criterion is met when the behavioural phenotypes of the model and the symptoms and manifestation of the disease in human are homologous (Belzung and Lemoine, 2011). Second, the face validity criterion is reached when the biological dysfunctions observed in the animal model reflects the currently understood disease aetiology and the identified biomarkers in humans (similarity of mechanisms and neurobiological substrates). Third, predictive validity is achieved when there

are similarities in the response of the animal model to therapies and notably pharmacological interventions used in human to treat the disease.

The mouse is an adequate organism to model neuropsychiatric diseases such as ASD (Crawley, 2012; Silverman et al., 2010). In mice, behavioural testing enables to analyse the behavioural dimensions related to ASD core symptoms (social behaviour, repetitive movements/stereotypies, behavioural flexibility and sensory processing) and comorbidities (cognition, emotional processing with anxiety/depression features...). Similarly, neurodevelopmental, neurobiological and physiological processes are very similar between mice and human, enabling to evaluate the construct validity of the models. Finally, mice can be treated with drugs or subjected to different interventional strategies as it is done in humans to treat ASD, enabling to assess their predictive validity.

Along these criteria, a large number of mouse models have been validated to study ASD. The SFARI base (<https://gene.sfari.org/database/animal-models/genetic-animal-models/>) recapitulates the available models, classified along 3 categories: 1) 277 genetic models are associated with mutation in a gene or a genetic region that is known to be associated with ASD, 2) 45 induced environmental models are obtained by *in utero* exposure to environmental factors known to increase the risk of the onset of ASD in the offspring, and 3) 8 inbred models of idiopathic ASD are described.

## 2. Genetic and Environmental Animal Models in ASD

### a. Genetic Models

There are several genetic models in mice, that are usually generated by the deletion, duplication, mutation or loss of function of a gene or a genetic *locus* that is known to be associated with ASD in humans (Carmichael and Lockhart, 2012; Patel et al., 2018). Hereafter, we review several commonly used models of ASD.

#### *i. Fmr1-knockout (KO) mice*

Two mouse models for FXS have been developed (Dutch Belgium consortium 1991, (Mientjes et al., 2006)). *Fmr1*-KO mice recapitulate a number of the behavioural abnormalities observed in Fragile X patients: cognitive impairments, autistic-like features, such as social interaction deficits and stereotypies, and hyperactivity (Bakker and Oostra, 2003). On the neurobiological level, it has been observed that there is an increase in the

number of immature dendritic spines and an abnormal increase in local protein synthesis at the synapse (Bakker and Oostra, 2003; Nimchinsky et al., 2001). Furthermore, several studies have described alterations of various forms of synaptic plasticity in *Fmr1*-KO mice, which could explain the behavioural defects observed (Bakker and Oostra, 2003). In particular, the *Fmr1*-KO mice display deficits in long-term depression (LTD) and long-term potentiation (LTP) in the hippocampus and cortex (Bagni and Zukin, 2019; Huber et al., 2002; Li et al., 2002). In addition, abnormalities in cortical-cerebellar circuits have also been described, which perturb VTA dopamine release in the PFC (Rogers et al., 2013).

*Fmr1* gene is widely expressed not only in the CNS but also in peripheral tissues (liver, adipose tissue, skin) (Davidovic et al., 2006; Khandjian et al., 1998). When I started my PhD, very few studies had addressed the peripheral effects of *Fmr1* gene silencing. The double *Fmr1/Fxr2* KO mouse obtained by double inactivation of the *Fmr1* and *Fxr2* gene (*Fxr2* being an autosomal homolog 2 of *Fmr1* gene) displayed an increase in glucose tolerance and insulin sensitivity, a reduction in adiposity and circulating glucose (Lumaban and Nelson, 2015). In addition, cranioencephalic abnormalities have been described in *Fmr1*-KO mice, such as an increase in the size of the mandible-skull complex similar, to what was observed in Fragile X patients (Heulens et al., 2013).

I contributed to two studies which identified metabolic and body composition anomalies in *Fmr1*-KO mice. These studies are presented in the 4<sup>th</sup> section of this Thesis.

## *ii. Shank3b-KO mice*

Mutations in the SH3/ankyrin domain gene 3 (*SHANK3*) are typically associated with Phelan-McDermid syndrome, a syndromic form of ASD (Balaan et al., 2019).

*Shank3b*-KO mice present social interactions impairments with reduced number of nose contacts and an increase in self-injurious repetitive grooming (Peça et al., 2011). At the neurobiological level, the *Shank3b* gene encodes the PostSynaptic Density protein of 95 kDa (PSD95) expressed at glutamatergic synapses. This protein regulates the trafficking and localization of glutamate receptors. The deletion of the *Shank3b* gene in mice alters postsynaptic molecular composition in the striatum with consequences on the glutamatergic system (Peça et al., 2011). *Shank3b*-KO mice also display anomalies in the oxytocinergic and dopaminergic system. More specifically, *Shank3b*-KO mice present a decrease of dopamine neurons excitability in the VTA, an important region involved in the social reward circuit (Bariselli et al., 2016). As a consequence, *Shank3b*-KO mice present social interaction

impairments and notably deficits in the social preference for a novel congener (Bariselli et al., 2016). These effects are accompanied by an increase in the expression of  $\alpha$ -amino-3-hydroxy-5-methyl-4-isoxazolepropionic acid (AMPA) receptors and the consequent disturbance in VTA synaptic plasticity (Bariselli et al., 2016, 2018). Furthermore, *Shank3b*-KO GABAergic MSNs, which receive dopaminergic inputs from the VTA, present an increase in dendritic arborisation while dendritic spines density is reduced. This is accompanied by a decrease in the frequency and amplitude of their spontaneous activity or miniature Excitatory Postsynaptic Currents (mEPSC). The deletion of the *Shank3b* gene in mice alters glutamatergic (Peça et al., 2011) as well as dopaminergic transmission (Bariselli et al., 2016).

### *iii. BTBR T+ Itpr3tf/J (BTBR) mice*

The BTBR mouse is considered as an idiopathic model of ASD. BTBR mice exhibit impaired social interactions, increased repetitive behaviours, compulsive cleaning, alterations in behavioural flexibility and learning deficits, compared to C57BL6/J control mice (Amodeo et al., 2012). The BTBR model is also characterized by the complete absence of the *corpus callosum*, and a significant reduction of the hippocampal commissure. A reduction in the *corpus callosum* volume is also observed in some ASD patients (Pagnozzi et al., 2018). Moreover, cerebral ventricles are reduced and this is accompanied by a decrease in neurogenesis (Meyza and Blanchard, 2017). Alterations in the dopaminergic system are also observed, contributing to an hypoactivation of the reward system (Squillace et al., 2014). Finally, this model also presents an increase of proinflammatory cytokines such as IL-33, IL-18 and IL-1 $\beta$  (Meyza and Blanchard, 2017) and an increase of autoantibodies (IgG) directed against brain proteins in the cortex, hippocampus, striatum and cerebellum (Kim et al., 2016). Finally, BTBR mice display increased intestinal permeability (Golubeva et al., 2017).

## **b. Environmentally-Induced ASD Models**

In this section we will describe the different environmental models of ASD. All of them are developed during the prenatal period.

### *i. In utero Exposure to Valproic Acid*

Valproic acid (VPA) has been associated with an increased risk of developing ASD in the offspring (Christensen et al., 2014). An animal model has been developed in which pregnant dams are injected intraperitoneally with VPA at embryonic day 12.5. The progeny of these

dams, exposed *in utero* to VPA, display social interaction impairments, repetitive/compulsive movements, anxiety-like behaviour and memory deficits (Kataoka et al., 2013; Wagner et al., 2006). VPA mice also exhibit signs of neuroinflammation in the brain and the male offspring displays decreased levels of serotonin in the PFC and amygdala (De Theije et al., 2014). In addition, VPA mice display increased intestinal permeability and decreased serotonin production in the gut (De Theije et al., 2014).

### *ii. In utero Exposure to MIA*

Another risk factor for ASD in the offspring is *in utero* exposure to MIA (Estes and McAllister, 2016). An animal model has been generated in which MIA is triggered by either exposure to the *Influenza* virus or to pathogen-associated molecular patterns (PAMPs) via injection of lipopolysaccharides (LPS), which mimic bacterial infection or the synthetic double-stranded RNA polyinosinic-polycytidylic acid poly (I:C), which mimic viral infection. The most commonly used model is obtained by intraperitoneal injection of poly (I:C) at E12.5 (Hsiao et al., 2013; Zuckerman et al., 2003). However, in this model, the dose and developmental window targeted, i.e. the precise timing of poly (I:C) is a critical element for the appearance of behavioural abnormalities in the offspring.

The behavioural features of MIA offspring are social behaviour impairments, decrease in ultrasonic vocalizations, repetitive movements and deficits in sensorimotor gating, highlighting reduced behavioural flexibility, resembling the core symptoms of ASD (Hsiao et al., 2013; Smith et al., 2007). MIA offspring also display enhanced anxiety and short-term memory impairment (Luchicchi et al., 2016), resembling the frequent comorbidities in ASD of anxiety disorder and ID. At the molecular level, the MIA offspring present alterations in the reward circuit, notably due to reduced activity of dopamine neurons in the VTA (Luchicchi et al., 2016).

At the systemic level, this model also has GI disturbances, with an increase in intestinal permeability (Hsiao et al, 2013). The integrity of the intestinal barrier is compromised in this model, with a decrease in tight junction proteins expression and an increase in inflammatory markers expression (cytokines).

### *iii. In utero Exposure to Diet-Induced Maternal Obesity (DIO)*

Maternal obesity during pregnancy is a risk in the development of neurological disorders in the offspring (Connolly et al., 2016). Thus, an animal model has been developed, where pregnant dams are fed on a high-fat diet (Buffington et al., 2016). Mice born from DIO mothers display social behaviour impairments, increased repetitive behaviours and anxiety (Buffington et al., 2016). These animals also present anomalies in the reward circuit (Buffington et al., 2016). Concretely, the DIO offspring exhibit impairments in the synaptic plasticity of dopamine neurons (long term potentiation, LTP) in the VTA (Buffington et al., 2016).

In conclusion, all these genetic and environmental models of ASD exhibit behavioural abnormalities similar to those observed in ASD patients, and notably social interactions impairments and stereotypies. This is accompanied by alterations in dopaminergic neurotransmission, and deficits in the social reward circuit appear as one of the neurobiological features correlates for the behavioural alterations. Finally, some ASD models display neuroinflammation and increased intestinal permeability revealing that immune and gut dysfunctions could also be linked to microbiota dysbiosis, as developed in the next section.

In this Thesis, we will present a new environmental mouse model of ASD obtained by the manipulation of its microbiota.

# The Microbiota-Gut-Brain Axis in ASD

## A. The Microbiota-Gut-Brain Axis: a Bidirectional Communication Axis

### 1. Introduction

The term microbiota refers to the ecological communities of commensal, symbiotic and pathogenic microorganisms that live in symbiosis with the human body. Microbiota reside in a number of tissues and biofluids: skin, mammary glands, placenta, saliva, oral mucosa, vagina, uterus and GI tract (Cho and Blaser, 2012). The microbiota includes bacteria, bacteriophages, fungi, protozoa and viruses that live inside and on the human body (Fattorusso et al., 2019). The human gut hosts more than 100 trillion organisms. Microorganisms outnumber by 1.3-fold the average number of somatic and germ cells of an adult human, according to recent revised estimates (Sender et al., 2016). Strikingly, the collective genome of the microbiota, termed the microbiome, contains 100 times more genes than the human genome. This gene richness confers unique functional properties to the microbiota, notably in terms of metabolic and enzymatic reactions which cannot be performed by the host (Stilling et al., 2014).

In a way, the gut microbiota can be assimilated to a human organ that can be transplanted and accomplishes specific functions, notably digestion and metabolism of food (David et al., 2014), regulations of intestinal barrier functions (Hooper et al., 2001), gut immune maturation and homeostasis (Chung et al., 2012), regulation of hormonal and neurotransmitters secretion and of host's brain function and behaviour (Goulet et al., 2019).

Specific alterations in microbiota composition, notably in terms of microbial abundances and diversity or metabolic output are termed dysbiosis. Microbiota dysbiosis influences health outcomes and when microbiota homeostasis is compromised, several pathological conditions may arise and notably ASD. In this Section, we will review the evidence in the literature supporting the hypothesis that dysregulation of the Microbiota-Gut-Brain axis contributes to the development of ASD symptoms.

## 2. The Microbiota-Gut-Brain-Axis

The Microbiota-Gut-Brain axis refers to the bidirectional communication between the microbiota and the brain. The main routes of communication involve the peripheral nervous system (mainly the enteric nervous system and parasympathetic system), the neuroendocrine system and the immune system (Carabotti et al., 2015; Fülling et al., 2019; Sherwin et al., 2019; Vuong and Hsiao, 2017). All these systems are interconnected and can mutually influence each other. Also, these systems are modulated by environmental factors and neuroendocrine systems such as the hypothalamus-pituitary axis and the limbic system (Carabotti et al., 2015).

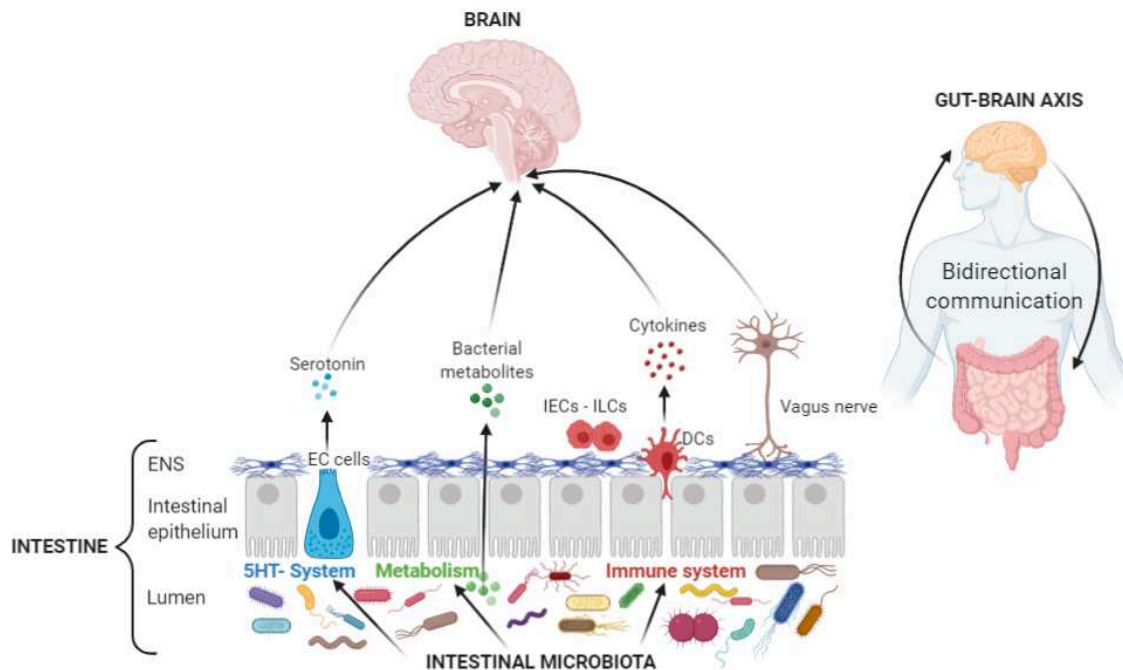


**Figure 5:** Communication pathways from the gut to the brain.

*Abbreviations:* ENS, Enteric nervous system; EC, Enterocromaffin cells; IECs, Intraepithelial lymphocytes; ILCs, Innate lymphoid cells; DC, Dendritic cells.

### a. Involvement of the Peripheral Nervous System

#### i. Enteric Nervous System (ENS)

The ENS is a part of the autonomous nervous system. The ENS is composed of enteric neurons and glial cells that form two plexus (i.e. myenteric and submucosal plexus), located between the circular and longitudinal muscle layers of the of GI tract (Nagy and Goldstein,

2017). The ENS is mostly composed of two neuronal types: cholinergic neurons (which account for 60% of the neurons in the GI tract), sensory and excitatory neurons and nitrinergic inhibitory interneurons and motoneurons (Rao and Gershon, 2016). Enteric neurons express cell-surface G-protein-coupled receptors (GPCRs) which can detect microbial metabolites, such as GPR41-43 for SCFAs and GPR142-35 for aromatic amino acids (L-Tryptophan, L-Phenylalanine and Kynurenic acid) (Husted et al., 2017). The ENS operates independently of the CNS even if it connected to the spinal cord and brain (Carabotti et al., 2015). Also, the ENS also has close connections with epithelial cells and immune cells in the intestinal barrier and integrates their signals (Carabotti et al., 2015). The function of the ENS is to regulate the neuroendocrine secretion and motility of the digestive tract as well as the maintenance of the mucosa and the regulation of intestinal immunity (Rao and Gershon, 2016).

#### *ii. Vagus Nerve (Parasympathetic System)*

The vagus nerve connects the ENS to the CNS. Sensory information coming from the GI tract is relayed by vagal afferent fibres to the nucleus of the solitary tract (NTS). The NTS is an integrative centre of sensory information in the CNS. Via efferent projections, the NTS is connected to several regions of the brain, including the limbic system (Browning and Travagli, 2014). The vagus nerve can detect microbial signals and relay information from the GI tract to the CNS (Cryan and Dinan, 2012). Vagal afferent fibres do not cross the epithelial layer and are therefore not in direct contact with the gut luminal microbiota. Therefore, these fibres can detect signals from the microbiota either by directly sensing bacterial compounds which have diffused through the epithelium or by integrating signals communicated by epithelial cells (Bonaz et al., 2018). Recent studies suggest that the vagus nerve is an important route by which the gut microbiota can send signals to the brain and induce behavioural changes. There is some evidence on how the microbiota can use this pathway to mediate behavioural and physiological changes in the brain (Bonaz et al., 2018). There are three examples of how different probiotics produce changes in behaviour using the vagus nerve as a pathway and the effects are suppressed after vagotomy, a surgical procedure in which a sub-diaphragmatic section of the vagus nerve is performed. The first example is the administration of *Lactobacillus reuteri* increases oxytocin release from the hypothalamus and improves social behaviour (Sgritta et al., 2019). This behavioural effects are blocked in vagotomized animals (Poutahidis et al., 2013; Sgritta et al., 2019). The second example is the administration of *Bifidobacterium longum* NCC3001 which decreases anxiety levels in mice

and whose effects are blocked in vagotomized mice (Bercik et al., 2011a). And finally, the administration of *Lactobacillus rhamnosus* reduces anxiety and depressed behaviours and these behavioural effects are abolished in vagotomized mice (Bravo et al., 2011). In addition, some microbiota-derived metabolites, such as butyrate (Stilling et al., 2016) and indole (Jaglin et al., 2018) can activate the vagus nerve.

Further, several articles have described the different components linking the vagus nerve and the brain, *via* the NTS and the brain structures involved in the social reward circuit. Bellono and colleagues describe the capacity of enterochromaffin cells (EC) to transduce specific intestinal signals in action potentials. EC cells are in close contact with the vagus nerve (Bellono et al., 2017). Han and colleagues explain that the information come from the right nodose ganglia. Its projections arrive at the NTS and trigger activation of the dorsolateral region of the parabrachial nucleus in the brainstem. From this nucleus, glutamatergic projections activate the *substantia nigra pars compacta*. From this region, dopaminergic projections release dopamine in the dorsal striatum, reinforcing the reward (Han et al., 2018). Another alternative on the circuit is described by Sgritta and colleagues. This study suggests that the fibers of the vagus nerve project to the PVN in the hypothalamus. Oxytocinergic neurons of the PVN project to the VTA region, enhancing the dopamine neurons activity. This would produce a release of dopamine in the NAc, promoting social behaviour reward (Buffington et al., 2016; Sgritta et al., 2019).

## b. Involvement of Neuroendocrine Signals

### i. *Involvement of the Hypothalamus-Pituitary-Adrenocortical Axis (HPA)*

The HPA axis is a key system that modulates response to stress. The hypothalamus is composed of several nuclei, but the most important one for the stress response is the PVN (Farzi et al., 2018). The PVN presents two types of neurons, magnocellular neurons that release oxytocin and vasopressin and parvocellular neurons that release corticotrophin-releasing hormone (CRH) (Browning and Travagli, 2014). The PVN receives inputs from the nucleus of the solitary tract (NTS) and other brain regions such as the PFC and amygdala (Browning and Travagli, 2014). In response to the CRH, the anterior pituitary gland synthesises and releases the adrenocorticotrophic hormone (ACTH). The activation of ACTH receptor in the adrenal glands activates the synthesis and secretion of glucocorticoids and they are released into the systemic circulation.

The HPA axis is in close connection with components of the gut-brain axis, sending oxytocinergic projections to the Dorsal Vagal Complex (DVC) in the NTS (Llewellyn-Smith et al., 2012) and limbic regions of the brain (e.g. VTA and amygdala) (Browning and Travagli, 2014; Hung et al., 2017). These connections modulate the information exchanged between the gut and the CNS (Browning and Travagli, 2014).

### *ii. Involvement of Intestinal Epithelial Cells*

The GI system is made up of a layer of epithelial cells that are completely renewed every week (Pastuła et al., 2015). This layer is formed by a great variety of cells with different functions:

CELL TYPE	FUNCTION	REFERENCES
<b>Goblet cell</b>	Mucus secretion	(Knoop and Newberry, 2018)
<b>Tuft cells</b>	Mediator of epithelial-immune signalling (cytokine release)	(Ting and von Moltke, 2019)
<b>Paneth cells</b>	Antimicrobial peptides secretion Modulate factors secretion to epithelial stem and progenitor cells	(Clevers and Bevins, 2013)
<b>M cells</b>	Sampling and presentation of antigens to the immune cells	(Mabbott et al., 2013)
<b>EC</b>	Chemosensory cells to bacterial metabolites (e.g. SCFA) 90% of serotonin production Electrical properties	(Bellono et al., 2017; Lund et al., 2018; Sharkey et al., 2018)

**Table 1:** Epithelial cells of the GI system.

*Abbreviations:* M cells, Microfold epithelial cells; EC, Enteroendocrine cells; SCFA, short chain fatty acid.

Epithelial cells are in close contact with bacteria located in the gut lumen and they integrate environmental luminal signals to maintain gut homeostasis (Sharkey et al., 2018; Viggiano et al., 2015). The gut microbiota can regulate EC functions, impacting notably serotonin synthesis (Yano et al., 2015). EC cells also display electrical properties. They are located in

the vicinity of nerve terminals and have an important function in the signals transmission from the intestinal lumen to the nervous system (Bellono et al., 2017). Some studies have shown the existence of receptors to bacterial metabolites in EC cells. Similarly to enteric neurons, EC cells express receptors for SCFA (i.e. FFAR1-2, HCA2, OLF78, GPR41, GPR43) and aromatic amino acids such as L-Tryptophan, L-Phenylalanine and Kynurenic acid (i.e. GPR142, GPR35) among others (Lund et al., 2018).

### c. Involvement of Immune Signals

In the GI tract, there are three main components involved in intestinal immune response: the gut epithelial layer, the *lamina propria* and the gut-associated lymphoid tissue (GALT). These components constitute the largest lymphatic organ of the body and their main function is to protect the organism against potential pathogens while providing tolerance to commensal bacteria (Ahluwalia et al., 2017). Immune cells (i.e. intraepithelial lymphocytes and innate lymphoid cells) in the GI tract interact with the intestinal microbiota and provide a protective or tolerant response depending on the microorganism (Montalban-Arques et al., 2018). This phenomenon is very important for the maintenance of homeostasis in the gut. Tolerance prevents the activation of an inappropriate immune response against food antigens or beneficial symbiotic bacteria (da Silva Menezes et al., 2003). Alterations in immune tolerance processes can lead to the development of food allergies or inflammatory diseases.

Both protective and tolerant responses involve the secretion of cytokines by immune cells. Disruption of the balance between circulating pro-inflammatory and anti-inflammatory cytokines can directly impact CNS functions (Cryan and Dinan, 2012). Cytokines have the ability to influence behavioural responses via their action on neuronal circuits and neurotransmitter pathways such as monoaminergic, glutamatergic and BDNF signalling pathways (Felger and Lotrich, 2013).

### d. Involvement of Microbial Metabolites

Small molecules with a molecular weight < 10kDa are commonly termed metabolites. They are usually produced by enzymatic reactions performed by the host and by the intestinal bacteria or both. Microbial-derived metabolites have received considerable attention in the recent years given their ability to modulate many physiological processes of the host. Microbial metabolites are produced from the diet by intestinal bacteria using enzymes of which the host is deprived. One study show that at least 10% of the detected serum

metabolites vary in concentration of at least 50% between conventionally colonized and germ-free (GF) mice (Wikoff et al., 2009). GF animals are usually obtained by caesarean section and maintained in sterile isolators enabling to raise them in an environment free from detectable viruses, bacteria and other organisms (Luczynski et al., 2016). Importantly, several microbial metabolites are either largely reduced or absent in the serum of GF mice: indoles derivatives (indoxylsulfate, indolepropionate), phenyl derivatives (phenylsulfate, *p*-cresolsulfate, phenylpropionylglycine, cinnamoylglycine, hippurate, phenylacetyl-glycine) or flavones (equol sulfate, methyl equol sulfate). This demonstrates that the presence of the microbiota is required for their synthesis. SCFA are another class of metabolites essentially produced by the gut microbiota (Sherwin et al., 2019; Wikoff et al., 2009).

Several bacterial metabolites have been identified in rodent models as mediators of the microbiota's effects on the host. Indoles, SFCAs and secondary bile acids notably regulate the development and function of DCs, IECs and ILCs in the GI tract (Wang et al., 2019). SCFA can affect the development and gene expression of intestinal epithelial cells (Willemsen et al., 2003). Bacteria can also release neuroactive metabolites such as GABA, serotonin, dopamine and influence the ENS or peripheral nerve terminals (Sarkar et al., 2016). Metabolites exclusively synthesized by the microbiota are involved in different biological processes in the host, as listed in **Table 2**.

<b>METABOLITES</b>	<b>BIOLOGICAL IMPACT</b>	<b>REFERENCE</b>
<b><i>p</i>-Cresol</b>	*Impaired <i>in vitro</i> development of oligodendrocyte	(Gacias et al., 2016)
<b>SCFA</b>	*Controls hormone secretion in EC cells	(Bonaz et al., 2018)
	*Activates vagal afferent fibers	(Reigstad et al., 2015)
	*Increase levels of <i>Tph1</i> mRNA in EC cells and intestinal 5-HT levels	
<b>Butyrate</b>	*Modulate energy metabolism in IECs	(Donohoe et al., 2011;
	*Modulate cytokine production in DCs	Liu et al., 2012)
<b>Secondary bile acids</b>	*Promotes epithelial barrier function	(Inagaki et al., 2006;

	*Regulates the response of DCs *Inhibition of NF-κB activity	Wang et al., 2019)
<b>Indole</b>	*Reinforces tight junctions	(Thaiss et al., 2016)
<b>Indoxyl-3-sulfate</b>	*Suppression of CNS inflammation	(Rothhammer et al.,
<b>Indole-3-propionic acid</b>	via astrocytes	2016)
<b>Indole-3-aldehyde</b>		
<b>Indole-3-lactic acid</b>	*Inhibits mouse polarization of TH17 cells <i>in vitro</i>	(Wilck et al., 2017)
<b>Polyamines</b>	*Increases production of tight junctions proteins *Favour maturation of T lymphocytes	(Chen et al., 2007) (Wang et al., 2019)

**Table 2:** Effects of bacterial metabolites on the host's immune and GI function.

*Abbreviations:* SCFAs, short chain fatty acids; *Tph1*, tryptophan hydroxylase 1; 5-HT, serotonin; EC, enterocromaffin cells; IECs, intraepithelial lymphocytes; DCs, Dendritic cells; CNS, Central nervous system.

Importantly, a recent study has shown that bacterial metabolites, including indoles, amines and phenolic compounds can be detected in the brain and their levels change at various postnatal ages in the mice's brains (Swann et al., 2020). This suggests that at least bacterial metabolites synthesized in the intestine by the microbiota can cross the BBB and could possibly influence the neurodevelopment in the offspring. Finally, microbial metabolites, such as 4-EPS, indoles and propionate, can modulate anxiety, cognitive and social abilities when administered to wild-type rodents (Hsiao et al., 2013; Jaglin et al., 2018; MacFabe et al., 2011).

### 3. Microbiota Can Impact Brain Function and Behaviour

#### a. GF Animals Exhibit Neurobiological and Behavioural Impairments

Behavioural studies in GF-free rodents strongly support that gut microbiota influences the host's nervous system and behaviour. **Table 3** summarizes some of the neurobiological and behavioural characteristics of GF rodents.

BIOLOGICAL DYSFUNCTIONS IN GF RODENTS	REFERENCE
Reduced anxiety behaviours	(Neufeld et al., 2011)
Increased locomotor activity	(Heijtz et al., 2011)
Social interaction deficits	(Crumeyrole-Arias et al., 2014; Desbonnet et al., 2014)
Functional abnormalities of the ENS	(De Vadder et al., 2018)
Slowed intestinal transit	
Decreased peripheral serotonin levels	(Wikoff et al., 2009)
Decrease of 5-HT synthesis and <i>Tph1</i> expression (rate-limiting enzyme for 5-HT synthesis)	(De Vadder et al., 2018)
Enhanced level and turn-over rate of brain serotonin	(Clarke et al., 2013) (Crumeyrole-Arias et al., 2014)
Increased monoamine turnover in striatum	(Heijtz et al., 2011)
Altered synaptic plasticity	
Reduced BDNF expression in cortex and hippocampus	(Sudo et al., 2004)
Decreased kynurenin/tryptophan plasma ratio	(Clarke et al., 2013)
Exacerbated reactivity of the HPA axis	(Clarke et al., 2013; Crumeyrole-Arias et al., 2014; Huo et al., 2017; Sudo et al., 2004)

**Table 3:** Behavioural phenotypes and biological processes in GF rodents.

*Abbreviations:* 5-HT, serotonin; *Tph1*, tryptophan hydroxylase 1; ENS, enteric nervous system; BDNF, brain-derived neurotrophic factor; HPA, hypothalamo-pituitary-adrenocortical axis.

#### b. Developmental Windows for the Brain and the Microbiota

The prenatal period is an important time window for neurodevelopment. It is characterized by fast changes at the neuronal level and birth is marked by early colonization of the gut microbiota. This period is highly sensitive to environmental changes.

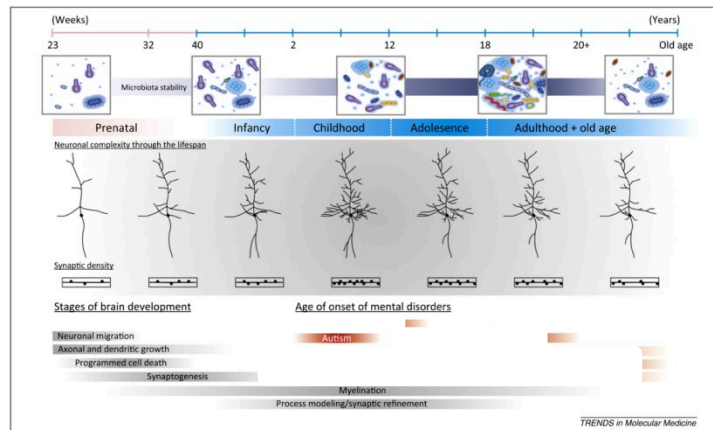


**Figure 6:** Microbiota and neurodevelopmental windows: implications for brain disorders by (Borre et al., 2014) .

The microbiota can influence neurodevelopment during the early postnatal period. GF mice exhibit an increase in hippocampal neurogenesis and microbiota recolonization does not prevent abnormal neurogenesis in adults (Ogbonnaya et al., 2015). Microbiota also participates in the development and maturation of the microglia, the brain-resident immune cells. GF mice have a greater number of immature microglia (increase in the number of branches and terminal points), which do not respond adequately to infection (Erny et al., 2015). In contrast, the recolonization with a normal microbiota partially restores the microglia defects (Erny et al., 2015). Another study showed that the microbiota influences the permeability of the BBB. In GF animals, the BBB is more permeable, allowing the passage of a greater number of substances, which can affect the neurological level by reducing the neuron viability (Braniste et al., 2014). In the same manner, microbiota colonization of GF mice restores BBB permeability, notably by increasing the expression of tight junction proteins (Braniste et al., 2014).

All these findings demonstrate that the microbiota could influence numerous neurodevelopmental and neurobiological processes with final consequences on behaviour.

## B. Evidences for a Disruption of the Microbiota-Gut-Brain Axis in ASD

### 1. Microbiota Dysbiosis in ASD

#### a. ASD Risk Factors Can Target the Microbiota

As previously discussed in the ASD risk factors section, several environmental factors increase the risk of ASD, such as *in utero* exposure to MIA, drug exposure (VPA) or maternal obesity (DIO), nutritional deficiencies and delivery mode. Exposure to these environmental factors occurs during the prenatal period contributes to influence future development of the offspring microbiota (**Figure 7**) (Tamburini et al., 2016). There are also other factors that can modify the microbiota in the offspring such as: breastfeeding and antibiotic exposure (Tamburini et al., 2016).

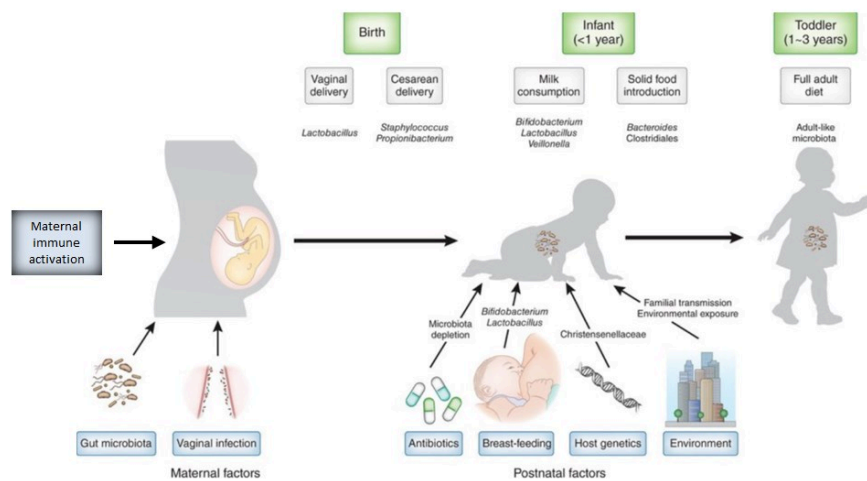


**Figure 7:** Factors shaping the neonatal microbiome (Tamburini et al., 2016)

Breast-feeding contributes to the establishment of the new bacteria flora in the infant's intestine. Breast milk present millions of live cells including immune cells and bacteria such as *Bifidobacterium* and *Lactobacillus* species accompanied with proteins, amino acids, oligosaccharides (with possible prebiotic activity), enzymes, growth factors, hormones, vitamins, minerals and antibodies (Goulet et al., 2019). All of these components can influence the composition of the infant gut microbiome. Caesarean delivery is associated with increased risk of breast-feeding problems like delay in breast-feeding, short duration of breast-feeding and reduced milk consumption by the newborn (Dewey et al., 2003; Evans et al., 2003).

Antibiotic exposure of newborn and infants is another important factor which can influence the establishment of the intestinal flora. Antibiotics are powerful medicines to treat or prevent bacterial infections. After delivery, it is common to administer an intrapartum antimicrobial prophylaxis cocktail of antibiotics to the mother to avoid possible infections. This treatment induces a microbiota dysbiosis in the newborn and significant decreases in the SCFAs productions in early life (Nogacka et al., 2017). These perturbations can have a negative influence on later health outcome such as increased susceptibility to allergies, increased risk of colic and diarrhoea in the newborn (Stinson et al., 2018). Yet, whether these factors modulate ASD risk remain to be demonstrated by adequate epidemiological studies.

#### b. Microbiota Dysbiosis in ASD Patients and ASD Models

Clinical studies. Several studies suggest that ASD patients present anomalies in microbiota composition (known as dysbiosis), characterized by an imbalance of intestinal microbial community. Notably, some studies have shown a reduction of bacterial diversity in the faecal microbiota of ASD patients (De Angelis et al., 2013; Kang et al., 2018). Some report increased abundances and diversity of *Clostridioides* species, (Parracho et al., 2005; Srikantha and Mohajeri, 2019) from the *Firmicutes* phylum and others report a decreased abundance of the *Bacteroidetes* phylum (Williams et al., 2011). Moreover, the relative abundance of *Bifidobacterium* are reduced (Adams et al., 2011; De Angelis et al., 2013) and *Lactobacillus* are increased (Adams et al., 2011) in children with ASD. In contrast, there are discrepancies in the findings regarding certain bacterial taxa. For example, *Akkermansia* abundances can be higher (De Angelis et al., 2013) or lower (Wang et al., 2011) according to two independent studies in ASD patients. Due to inconsistent results regarding microbial dysbiosis in ASD patients, we still lack a specific microbiota signature for ASD. The discrepancies among studies can be due to differences in study design (choice of controls: unrelated neurotypical individuals or siblings), sample size, the methods for quantification of bacterial abundances (quantitative RT-PCR vs. 16S rRNA sequencing), statistical handling of the data and variables which are sometimes not accounted for such as ASD symptoms heterogeneity, geographical localization, lifestyle or diet.

In an attempt to identify common microbiota variations in ASD patients, three meta-analyses were performed. The first study analysed 16 studies that include a total of 381 ASD patients and 283 neurotypical individuals of which 107 were healthy siblings (Liu et al., 2019). The result obtained were a decrease in *Bifidobacterium*, *Blautia*, *Dialister*, *Prevotella*, *Veillonella*,

and *Turicibacter*, with an increase in *Lactobacillus*, *Bacteroides*, *Desulfovibrio*, and *Clostridioides* in ASD patients compared to controls (Liu et al., 2019). The second study analysed 9 studies that included a total of 254 ASD patients and 167 age-matched neurotypical individuals (Xu et al., 2019). The results obtained were a decrease in the abundance of *Akkermansia*, *Bacteroides*, *Bifidobacterium*, *E. coli*, and *Enterococcus*, with an increase in the abundance of *Faecalibacterium* and *Lactobacillus*, and a moderate increase in the abundance of *Ruminococcus* and *Clostridioides* (Xu et al., 2019). The third study analysed 18 studies that included a total of 500 ASD children and 400 neurotypical individuals (Iglesias-vázquez et al., 2020). The results obtained were an increase in the abundance of *Bacteroidetes* (*Bacteroides* and *Parabacteroides*) and some *Firmicutes* genera (specifically *Clostridioides*, *Faecalibacterium* and *Phascolarctobacterium*). They also observed a decrease in the abundance of *Coprococcus* and *Bifidobacteria* (Iglesias-vázquez et al., 2020).

These 3 meta-analyses converge towards a decreased bacterial  $\beta$ -diversity associated with an increase in the abundance of *Clostridioides* genus and a decrease in *Bifidobacterium* genus in ASD patients, supporting the existence of microbiota dysbiosis in at least subsets of ASD patients.

*Studies in ASD models.* As described previously in the Section on ASD models, some of them display compromised intestinal permeability and intestinal inflammation which could possibly be due to microbiota dysbiosis in genetic (e.g. *Shank3b*-KO), idiopathic (e.g. BTBR) and environmental (e.g. VPA, MIA and DIO) mouse models.

*Shank3b*-KO mice display microbiota dysbiosis, with a decrease in the abundance of the commensal bacteria *Lactobacillus reuteri* (*L. reuteri*) (Sgritta et al., 2019). BTBR mice exhibit reduced bacterial diversity, with increased and decreased abundances of the *Bacteroidetes* and *Firmicutes* phyla, respectively (Coretti et al., 2017; Golubeva et al., 2017), similar to what is observed in ASD patients. Moreover, BTBR mice have a decrease of *L. reuteri* abundance (Sgritta et al., 2019). The VPA model displays microbiota dysbiosis (De Theije et al., 2014), including a decrease in *L. reuteri* abundance (Sgritta et al., 2019). The MIA model displays microbiota dysbiosis mainly affecting *Bacteroidetes* and *Firmicutes* phyla, with increased abundances of *Clostridioides* and reduced abundances of *Bacteroidia* species (Hsiao et al., 2013). And finally, DIO offspring present microbiota dysbiosis with reduced bacterial diversity and lower abundances of *L. reuteri* (Buffington et al., 2016).

## c. Manipulations of the Microbiota Can Improve ASD Symptoms

### i. *Faecal Microbiota Transplantation (FMT)*

Clinical studies. A recent clinical pilot study assessed the beneficial effects of FMT of a healthy microbiota to 18 ASD children presenting GI symptoms. FMT promoted microbial diversity, increasing the levels of *Bifidobacterium*, *Prevotella*, and *Desulfovibrio*. This was accompanied by an improvement in GI symptoms, with a reduction of constipation, diarrhoea, abdominal pain and indigestion symptoms. It also improved behavioural abnormalities, with notable decreases in the severity of ASD symptoms and self-injurious behaviours and improvements in social and cognitive skills (Kang et al., 2017). In addition, the beneficial effects of the microbial transfer persisted up to 2 years after the initial FMT (Kang et al., 2019).

Studies in ASD models. Recolonization of GF mice with microbiota restored social behaviour deficits (Desbonnet et al., 2014). The abnormalities in social behaviour of the DIO mouse model were also restored after a transfer of normal microbiota from control animals (Buffington et al., 2016).

Another study performed faecal microbiota transplantation using stool from ASD and neurotypical patient to recipient GF mice (r-mice). Then, the offspring of these recipient mice (o-mice) were analysed (Sharon et al., 2019). ASD o-mice presented a microbiota profile similar to human ASD donors and the differences of microbiota composition between ASD and neurotypical controls were maintained between ASD o-mice and control-o-mice. ASD o-mice exhibited decreased microbial  $\beta$ -diversity, with decreased abundances of *Bacteroidetes*, *Bacteroides*, and *Parabacteroides* and increased abundances of *Akkermansia*, *Sutterella*, and *Lachnospiraceae*. ASD o-mice displayed behavioural abnormalities, with social interaction impairments, an increase in stereotypies and a decrease in locomotor activity. These behavioural outcomes were correlated with the abundances of several bacterial taxa.

These studies clearly show that FMT can influence ASD-related behaviours in ASD models.

### ii. *Probiotic*

Clinical studies. A meta-analysis using 5 articles analysed the gastrointestinal and behavioural effects of probiotic supplements in ASD patients. A total of 117 ASD children were supplemented with probiotic therapy (Patusco and Ziegler, 2018). The administration of

probiotics such as *Lactobacillus casei* and *Bifidobacterium longum* normalized the *Bacteroidetes/Firmicutes* ratio and reduced the levels of TNF- $\alpha$  in the stool of ASD children (Tomova et al., 2015). Probiotic treatment with *Lactobacillus acidophilus*, *Lactobacillus rhamnosus* and *Bifidobacterium longum* improved some of gastrointestinal problems such as flatulence, abdominal pain, constipation and stool consistency in ASD children. In the same way the severity of the ASD symptoms were also reduced, with improvements in communication and sociability abilities (Shaaban et al., 2018). Probiotic treatment with *Lactobacillus delbruecki*, *L. acidophilus*, *L. casei*, *Bifidobacterium longum*, and *B. bifidum* improves the constipation and diarrhoea in ASD children. Similarly, ASD symptoms were reduced, with improvements in communication, sociability and cognition (Patusco and Ziegler, 2018).

Despite these studies, the results on whether probiotics improve GI or behavioural symptoms in autistic patients deserve further investigation.

Studies in ASD models. The abundance of *L. reuteri* is reduced in several ASD models. As a consequence, probiotic supplementation of *L. reuteri* has been tested. In the *Shank3b*-KO model, *L. reuteri* treatment restores social behaviour deficits, oxytocin secretion and VTA dopamine neurones excitability (Sgritta et al., 2019). In the BTBR and VPA models, *L. reuteri* improves social interaction deficits (Sgritta et al., 2019). In the DIO model, *L. reuteri* restores the activity of dopamine neurons in the VTA (Buffington et al., 2016). This phenomenon is due to the fact that *L. reuteri* increases the activity of oxytocinergic neurons located in PVN that project to the VTA and corrects synaptic plasticity anomalies in dopamine neurons (Buffington et al., 2016). Finally, in the MIA model, probiotic treatment with *Bacteroides fragilis* restores specific behavioural abnormalities such as repetitive movements and anxiety. In contrast, social interaction impairments, such as sociability and social preference, are not restored (Hsiao et al., 2013).

## 2. Abnormal Microbial Metabolites Patterns in ASD Patients and ASD Models

### a. SCFAs Altered in ASD

Clinical studies. SCFA are produced by bacterial fermentation of dietary fibre or carbohydrates in the gut (Dalile et al., 2019). SCFA mainly include acetic acid (AA), propionic acid (PPA), butyrate (BTA) and valeric acid (VA). The role of SCFA in ASD is

controversial. One study has reported an increase in the total production of SCFA in the stool of ASD patients (Wang et al., 2012), while another has shown that ASD patients treated with probiotics present a decrease in the total production of SCFA (Adams et al., 2011). SCFA can cross the BBB and influence early brain development by modulating the production of neurotransmitters, such as serotonin and dopamine (Dalile et al., 2019). SCFA levels were positively correlated with the abundances of the *Faecalibacterium*, *Ruminococcus* and *Bifidobacterium* genera, while the abundances of *Bacteroides* species were correlated with PPA levels in ASD individuals (De Angelis et al., 2013). Poor digestion of carbohydrates has been observed in ASD patients, that is possibly due to a decrease in the *Bacteroidetes* phylum (Williams et al., 2011).

Studies in ASD models. The BTBR model displays altered levels of microbial metabolites and notably a decrease in SCFA (Golubeva et al., 2017). Behavioural effects produced by the administration of SCFA have been described in rodent models. Adult rats injected intracerebroventricularly with PPA exhibited social interaction deficits, stereotypies, perseverative behaviours, deficits in spatial memory, and elevated anxiety (Macfabe, 2012; MacFabe et al., 2011; Mepham et al., 2019). The effects of PPA are reversible, since behavioural abnormalities are normalized when treatment is discontinued (Mepham et al., 2019). In addition, PPA has broad effects affecting the release and synthesis of neurotransmitters, mitochondrial metabolism and gene expression (MacFabe et al., 2011). In another model obtained by studying the offspring of mice colonized by microbiota transplantation from stool of ASD (ASD o-mice) and neurotypical patient (Sharon et al., 2019). In the ASD o-mice, microbiota compositions changes were accompanied by changes in the levels of 27 metabolites in the colonic content and 21 metabolites levels in the serum of ASD o-mice. One metabolite, the SCFA 5-aminovaleric acid (5AV) whose synthesis is microbiota-dependent was notably decreased in ASD o-mice. To study the potential beneficial effect of 5AV supplementation on the offspring, BTBR mice were treated with 5AV dispensed in drinking water from conception until weaning and the behaviour of the progeny was analysed. 5AV supplementation improved the stereotypies, locomotor activity and sociability of BTBR mice (Sharon et al., 2019). They further show that the prenatal and weaning period are critical windows for 5AV administration, since the administration of 5AV after these periods no longer rescues the behavioural abnormalities in BTBR mice.

## b. Tryptophan-Derived Microbial Metabolites Altered in ASD

Clinical studies. Tryptophan is an essential amino acid involved in two metabolic pathways. On one hand, tryptophan will give rise to serotonin, melatonin and Nicotinamide Adenine Dinucleotide (NAD<sup>+</sup>). On the other hand, an alternative oxidative pathway has been described, known as the kynurenine pathway (Bender, 2003). Tryptophan availability is influenced by the microbiota and affected in ASD patients presenting intestinal dysbiosis (De Theije et al., 2011). Kynurenic acid has an important role in the balance for immune tolerance and the maintenance of commensal intestinal bacteria. As a consequence, low levels of kynurenic acid are associated with GI problems (Ormstad et al., 2018).

In addition, tryptophan can be used by intestinal bacteria to produce indoles and their derivatives. The levels of indole and 3-methylindole are increased in the stool of ASD patients (De Angelis et al., 2013). Similarly, the levels of indoxyl sulfate, indole-3-acetate and indole-3-lactate are elevated in the urine of ASD patients (Gevi et al., 2016). Another study has shown that the levels of indole-3-acetate were decreased in urine of ASD patients (Emond et al., 2013). Indoles are important precursor for the synthesis of tryptophane which in turn is a precursor for serotonin and melatonin, all these compounds are disturbed in ASD patients (De Angelis et al., 2013).

Studies in ASD models. The BTBR model display impaired intestinal serotonin production, possibly due to microbiota dysbiosis (Golubeva et al., 2017). In the MIA model, a significant increase in the levels of indole-3-pyruvate was observed in the serum (Hsiao et al., 2013).

Behavioural effects produced by the administration of indoles have been described in rodent models. Acute intraperitoneal injection of the indole derivatives isatin and oxindole in control rats produces a decrease in locomotor activity and rearings frequency (Jaglin et al., 2018). The intra-caecal administrations of indole in control rats increase the levels of isatin and oxindole in the brain. Further, it increases in the eye blinking frequency, a proxy for vagal activation and c-Fos reactivity in the DVC located in the NTS, the entry point of vagal afferences in the CNS. This suggests that exposure to indoles induces vagus nerve activation (Jaglin et al., 2018). These findings result from acute treatment with indoles and it is unknown if the effects can persist over longer times of exposure. In addition, GF rats were monocolonized either with a bacterial strain of *Escherichia coli* (*E.coli*) producing (i<sup>+</sup>) or not-producing (i<sup>-</sup>) indoles. When compared to rats colonized by *E.coli*-i<sup>-</sup> non-producer of indole, rats colonized with *E.coli* -i<sup>+</sup> displayed increased social interaction time and anxiety levels,

decreased latency to explore novel object, increased level of helplessness (immobility) (Jaglin et al., 2018).

### c. Phenylalanine-Tyrosine-Derived Metabolites Altered in ASD

Clinical studies. ASD patients display a perturbation of the phenylalanine metabolism, which has been related to an overabundance of *Clostridioides* species (Li and Zhou, 2016; Xiong et al., 2016). Some studies show an increase in the levels of dimethylamine (Yap et al., 2010), *para*-cresol, *para*-cresylsulfate (Altieri et al., 2011; Gabriele et al., 2014), and a decrease in the levels of hippurate, phenylacetylglutamine (Yap et al., 2010), 3-hydroxyphenylacetate, 3-hydroxy-hippurate (Emond et al., 2013) in the urine of ASD patients. Another study have shown an increase in the levels of phenolic compounds (e.g., phenol, 4-(1,1-dimethylethyl)-phenol, 3,7-dimethyl-2,6-octadien-1-ol, phenol, 4-(1,1,3,3- tetramethylbutyl)-phenol) in the stool of ASD patients (De Angelis et al., 2013).

The next section will detail the evidence supporting the link between the tyrosine-derived microbial metabolite *para*-cresol and ASD, which has been the focus of my Thesis.

Studies in ASD models. The MIA presents altered serum profiles of bacterial metabolites. Notably, the microbial metabolite 4-EPS displayed a 40-fold increase in its serum levels in the MIA offspring (Hsiao et al., 2013). Wild-type animals were treated with the 4-EPS metabolite, and after 3 weeks of administration, the animals showed an increase in anxiety levels compared to control mice (Hsiao et al., 2013), however social behaviour was unaffected. This result suggests that this 4-EPS may be contributing to anxiety behaviours, which are ASD comorbid symptoms.

## 3. The Specific Case of *p*-Cresol in ASD

Among the different microbial metabolites which are more abundant in ASD patients compared to sex- and age-matched neurotypical controls, the small aromatic metabolite *p*-Cresol is one of those for which the results are the more consistent across studies. This section will detail the connections between *p*-Cresol and ASD.

### a. General Introduction

The metabolite *p*-Cresol is an aromatic organic compound [CH<sub>3</sub>C<sub>6</sub>H<sub>4</sub>(OH)] -also known as *para*-Cresol, 4-methylphenol or 4-Cresol- that can be found in nature as a result of the photo-oxidation of toluene. This compound can also be produced by the gut microbiota. Some bacteria have specific enzymes such as *p*-hydroxyphenylacetate decarboxylase and thiazole synthase enabling them to synthesize *p*-Cresol using L-tyrosine as a precursor following two pathways (Persico and Napolioni, 2013; Saito et al., 2018).

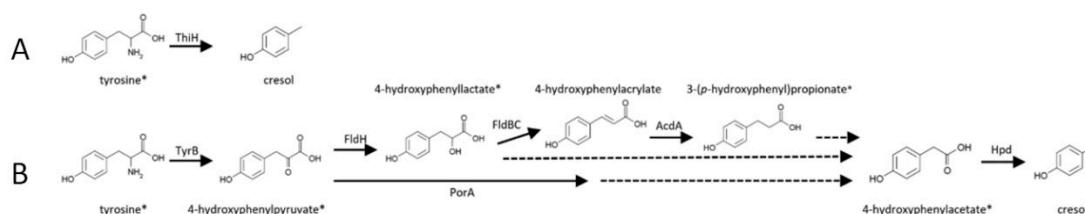


**Figure 8:** Direct (A) and Indirect (B) pathway for *p*-Cresol synthesis using tyrosine as a precursor by gut bacteria (Saito et al., 2018).

**Abbreviations:** ThiH, Thiazole synthase H; TyrB, Tyrosine aminotransferase B; FldH, phenyllactate dehydrogenase; FldBC, phenyllactate dehydratase; AcdA, acyl-CoA dehydrogenase; PorA, pyruvate:ferredoxin oxidoreductase A; Hpd, hydroxyphenylacetate decarboxylase.

Approximately, 51 bacterial strains present in the human microbiota have been identified as capable of producing *p*-Cresol (Persico and Napolioni, 2013; Saito et al., 2018). Among *p*-Cresol bacterial producers, four species are classified as major producers : *Blautia hydrogenotrophica*, *Clostridioides difficile*, *Olsenella uli*, and *Romboutsia lituseburensis* (Saito et al., 2018). *p*-Cresol was shown to have bacteriostatic properties and to inhibit the growth of some bacterial species, affecting more drastically Gram-negative bacteria (Passmore et al., 2018). Further, it confers a selective advantage to strains tolerant to a *p*-Cresol-rich environment, such as *Clostridioides difficile* (Passmore et al., 2018).

### b. *p*-Cresol Metabolism in the Host

*p*-Cresol can be detected in plasma, urine and stool. A very small percentage (0.5% - 1%) of free *p*-Cresol binds to albumin and can be detected in plasma (Persico and Napolioni, 2013). Free *p*-Cresol is metabolized by the host into *p*-cresylsulfate and *p*-cresylglucuronide, by means of sulfation (95% of total *p*-Cresol) or glucuronidation (3%-4% of total *p*-Cresol)

(Persico and Napolioni, 2013). These processes improve the solubility of phenolic compounds to facilitate their detoxification (Shangari et al., 2005), filtration by renal glomeruli and elimination in urine (Persico and Napolioni, 2013). Several studies have shown that *p*-cresylsulfate is the most abundant *p*-Cresol derivative circulating in the organism (Gabriele et al., 2014).

### c. Clinical Evidence Connecting *p*-Cresol to ASD

#### i. *Increased Excretion of p-Cresol in ASD*

Several studies have pointed out the increased urinary (Altieri et al., 2011; De Angelis et al., 2013; Gabriele et al., 2014, 2015; Persico and Napolioni, 2013) and faecal excretion of *p*-Cresol (De Angelis et al., 2013; Kang et al., 2018) in ASD patients as compared to neurotypical age- and sex-matched controls.

Two independent cohorts were conducted with ASD children from France and Italy. One initial study included 59 ASD patients with 59 sex- and age-matched neurotypical individuals (Altieri et al., 2011). ASD children under 7 years of age exhibited a 2.5-fold increase in urinary levels of *p*-Cresol. A replication study conducted on 33 ASD patients and 33 sex- and age-matched neurotypical individuals showed a similar increase in the urinary levels of *p*-Cresol in ASD children (Gabriele et al., 2014). Increased levels of *p*-Cresol were also observed in the stool of ASD patients when compared to neurotypical individuals in two independent studies. However, their sample size was relatively small as one study enrolled 21 ASD children and 23 neurotypical children between 4-17 years of age and with mixed sex (Kang et al., 2018) and the other 10 ASD children and 10 neurotypical children between 4-10 years of age and with mixed sex (De Angelis et al., 2013).

#### ii. *Correlation with ASD GI Symptoms and ASD Core Behaviours*

Urinary *p*-Cresol levels correlated with the intensity of ASD behavioural impairments, in particular stereotypies and compulsive-repetitive behaviours (Altieri et al., 2011; Gabriele et al., 2014). The ASD behavioural were assessed using the Autism Diagnostic Observation Schedule (ADOS), the Autism Diagnostic Interview – Revised (ADI-R), the Children Autism Rating Scales (CARS) and the Vineland Adaptive Behavior Scales (VABS). Urinary *p*-Cresol levels are also correlated with slow intestinal transit and chronic constipation in young ASD children (Gabriele et al., 2015).

### iii. *Increased Abundances of Bacterial Taxa Synthetizing p-Cresol in ASD*

Importantly, *p*-Cresol is the product of tyrosine degradation by the intestinal microbiota and mainly by *Clostridioides difficile* and other species from the *Clostridioides* genus (Passmore et al., 2018; Saito et al., 2018). Some studies show increased of *Clostridioides* species in ASD such as *C. perfringens* (Srikantha and Mohajeri, 2019; Tomova et al., 2015), *C. histolyticum* and *C. boltae* (Adams et al., 2011; Jyonouchi, 2009). Finally, three meta-analyses (Iglesias-vázquez et al., 2020; Liu et al., 2019; Xu et al., 2019) converge on consistent increased abundance of the *Clostridioides* genus in ASD patients. Therefore, increased abundances of the *Clostridioides* genus could explain increased urinary excretion of *p*-Cresol in ASD patients.

### d. *p*-Cresol and Behaviour in Mice

Two recent studies have linked *p*-Cresol to behavioural alterations in mouse models. In the first study, nonobese diabetic (NOD) mice which exhibit social behaviour deficits were used (Gacias et al., 2016). The authors performed an FMT from NOD donor mice to recipient wild-type mice. Post FMT, recipient mice exhibited social impairments and increased intestinal levels of microbial metabolites, and notably of *p*-Cresol. They performed *in vitro* experiments and showed that *p*-Cresol treatment of oligodendrocyte cultures affected the differentiation of oligodendrocytes and decreased myelin gene expression. They concluded that the gut microbiota of NOD mice influences social behaviour and that *p*-Cresol could be responsible for the behavioural changes by impacting the myelin expression in prefrontal cortex. However, this study did not investigate the causal link between the *p*-Cresol and social behaviour impairments.

The second study focussed on the effect of an acute intravenous injection of *p*-Cresol in the BTBR ASD model (cf. D. Animal model section). Fifteen minutes after injection, BTBR mice treated with *p*-Cresol exhibited an increase in anxiety, hyperactivity, accompanied with an increase in the time spent in self-grooming and a loss of social preference (Pascucci et al., 2020). Further, the levels of dopamine and DOPAC, a catabolite of dopamine were increased in the amygdala, caudate putamen and NAc of *p*-Cresol-treated mice. The intravenous injection and the fact that the behavioural tests were performed 15 min post injection suggest that the observed effect could result from acute activity of *p*-Cresol.

The metabolite *p*-Cresol appears consistently upregulated in ASD patients as compared to neurotypical controls. However, the causal relationship between elevated *p*-Cresol and ASD behaviours remained to be elucidated. This was the main focus of this Thesis.

# Chapter 2: Role of the Microbial Metabolite *p*-Cresol in ASD

## I. Context

The intestine hosts to billions of intestinal bacteria and is in constant communication with the brain. As noted in the Introduction, perturbations of this axis have been observed in ASD. The main symptoms of ASDs are social communication and interaction deficits, as well as the presence of repetitive movements (stereotypies), perseverative behaviours and restricted interests (Vuong and Hsiao, 2017). Brain imaging studies of ASD patients have also shown decreased connections between the VTA and the NAc, which are important regions for the social reward circuit (Supekar et al., 2018). In addition, ASD are also associated with gastrointestinal symptoms (abdominal pain, diarrhoea, constipation) (Vuong and Hsiao, 2017). Several studies have shown an association between gastrointestinal problems and behavioural symptoms in patients with ASD (Adams et al., 2011). The stools of patients with ASD show a lower bacterial diversity and an increase in bacterial species belonging to the *Clostridioides* genus (Iglesias-vázquez et al., 2020; Liu et al., 2019; Xu et al., 2019), among which some are producers of the microbial metabolite *p*-Cresol (Saito et al., 2018). In addition, several studies have shown that ASD patients have increased urinary excretion of *p*-Cresol (Altieri et al., 2011; Gabriele et al., 2014). Finally, a recent study has shown that transplanting a healthy microbiota to ASD patients improves their gastrointestinal and behavioural symptoms, including social interactions deficits (Kang et al., 2017). These findings suggest that the microbiota may play a key role in ASD and that targeting the microbiota could be a therapeutic avenue for the future.

Studies in animal models support this hypothesis. Indeed, mice lacking a microbiota show deficits in social interaction, which are restored by colonization with a healthy microbiota (Desbonnet et al., 2014). Also, in some genetic or environmental models of ASD, social interaction deficits are associated with alterations in the composition of the microbiota and the levels of microbial metabolites (Buffington et al., 2016; Golubeva et al., 2017; Hsiao et al., 2013; Sgritta et al., 2019; Sharon et al., 2019; De Theije et al., 2014).

Yet, the causal relationship between microbiota dysbiosis, altered levels of microbial metabolites and behavioural impairments in ASD remains to be demonstrated.

## II. Research Hypothesis and Objectives of the Study

Our working hypothesis is that *p*-Cresol synthesised by the microbiota is involved in the development or the maintenance of behavioural symptoms of ASD.

To test this hypothesis, I used wild-type mice and my objectives were:

1. To elucidate whether *p*-Cresol treatment in mice induced ASD-like symptoms
2. To elucidate whether *p*-Cresol effects were mediated by gut microbiota remodelling

To achieve my first objective, I used 4-week old wild-type male C57/BL6J mice that were treated chronically for 4 weeks with *p*-Cresol in drinking water. We reasoned that this mode of administration would mimic intestinal exposure to *p*-Cresol through the microbiota. Then, I subjected *p*-Cresol-treated and control mice to a battery of behavioural tests to assess behaviours related to core ASD symptoms (social behaviour deficits, stereotypic/perseverative behaviours) and ASD common comorbidities (hyperactivity, anxiety and cognitive deficits). Our collaborators Jérôme Becker and Julie Le Merrer (INRAe, PRC, Nouzilly, France), specialised in ethology and behavioural characterization of ASD models trained us to behavioural phenotyping and I was able to implement these tests in our animal facility. I also collected serum and urine samples in which *p*-Cresol levels were measured by our collaborators, Dr. M.-E. Dumas and colleagues (Imperial College, London, UK). Finally, I generated *p*-Cresol and control animals and our collaborators, Dr. J. Barik and colleagues (IPMC, Valbonne, France) performed *ex vivo* electrophysiological recording of VTA dopamine neurons in brain sections of these animals.

To achieve my second objective, I collected faecal pellets samples from *p*-Cresol-treated and control mice to evaluate the effects of *p*-Cresol on the microbiota composition. Our collaborators, Dr. Philippe Langella and colleagues (Institut Micalis, Jouy-en-Josas, France) performed microbial 16S rDNA sequencing in these samples to determine changes in bacterial diversity and the relative abundances of bacterial taxa induced by *p*-Cresol exposure. We then correlated the relative abundances of dysregulated bacterial taxa with behavioural scores related to social behaviour and stereotypies. Finally, I performed faecal microbiota transplantations to study whether manipulation of the gut microbiota of wild-type mice or mice previously exposed to *p*-Cresol could respectively induce or normalise behavioural

impairments induced by *p*-Cresol exposure. Three weeks after FMT, both the behaviour and the activity VTA dopamine neurons were assessed.

### III. Results

The results are presented in the following manuscript (Manuscript #1)

*Manuscript #1:*

The microbial metabolite *p*-Cresol induces autistic-like behaviours in mice by remodelling the gut microbiota

**P. Bermudez-Martin**, J. A. J. Becker, S. P. Fernandez, R. Costa-Campos, S. Barbosa, L. Martinez-Gili, A. Myridakis, M.-E. Dumas, A. Bruneau, C. Cherbuy, P. Langella, J. Chabry, J. Barik, J. Le Merrer, N. Glaichenhaus, L. Davidovic

doi: <https://doi.org/10.1101/2020.05.18.101147>

deposited on the BioRxiv server

(<https://www.biorxiv.org/content/10.1101/2020.05.18.101147v2>)

To summarise, in this study, we show that chronic intestinal exposure to *p*-Cresol in mice induces the core symptoms of ASD: stereotypies and social interaction deficits, without impacting anxiety, locomotor activity and cognition. These behavioural symptoms specific to ASD are accompanied by a decrease in the excitability of dopamine neurons in the VTA, a key brain region for social reward, known to be deregulated in ASD patients. We have also shown that *p*-Cresol exposure induced changes in microbiota composition. Furthermore, the abundances of the deregulated taxa correlated with deficits in social interaction in *p*-Cresol mice. Also, we induced social interaction deficits in mice that received a microbiota from *p*-Cresol-treated mice. Finally, the restoration of a healthy microbiota by transferring microbiota from normal mice to *p*-Cresol-exposed mice normalised social interaction deficits and dopamine neurones excitability in the VTA.

Our data support the construct, face and predictive validity of the *p*-Cresol-induced environmental ASD model. Also, we demonstrate a causal link between a deregulated microbial metabolite in ASD and ASD core behavioural symptoms. Also, we show that *p*-Cresol effects on social behaviour are mediated by a remodelling of the microbiota. Finally, our data suggest that microbiota manipulation is a therapeutic target to be explored for the treatment of ASD.

## IV. Manuscript

### **The microbial metabolite *p*-Cresol induces autistic-like behaviors in mice by remodeling the gut microbiota**

Microbial *p*-Cresol induces autistic-like behaviors in mice

Bermudez-Martin, P.<sup>1, 2</sup>, Becker, J. A. J.<sup>3,#</sup>, Fernandez, S. P.<sup>1, 2</sup>, Costa-Campos, R.<sup>1, 2</sup>, Barbosa, S.<sup>1,2</sup>, Martinez-Gili, L.<sup>4</sup>, Myridakis, A.<sup>4</sup>, Dumas, M.-E.<sup>4</sup>, Bruneau, A.<sup>5</sup>, Cherbuy, C.<sup>5</sup>, Langella, P.<sup>5</sup>, Chabry, J.<sup>1,2</sup>, Barik, J.<sup>1,2</sup>, Le Merrer, J.<sup>3,#</sup>, Glaichenhaus, N.<sup>1,2</sup>, Davidovic, L.<sup>1, 2\*</sup>

<sup>1</sup> Centre National de la Recherche Scientifique, Institut de Pharmacologie Moléculaire et Cellulaire, Valbonne, France

<sup>2</sup> Université Côte d'Azur, Nice, France

<sup>3</sup> Physiologie de la Reproduction et des Comportements, INRAE UMR-0085, CNRS UMR-7247, Inserm, Université François Rabelais, IFCE, 37380, Nouzilly, France

<sup>4</sup> Division of Computational and Systems Medicine, Department of Surgery and Cancer, Imperial College London, Exhibition Road, South Kensington, London SW7 2AZ, United Kingdom

<sup>5</sup> Institut Micalis, INRAE, AgroParisTech, Université Paris-Saclay, 78350 Jouy-en-Josas, France

# Current address: UMR-1253 iBrain, Inserm, Université de Tours, CNRS, Faculté des Sciences et Techniques, Parc de Grandmont, F 37200 Tours, France

**Corresponding author:**

\*Mailing address: Institut de Pharmacologie Moléculaire et Cellulaire UMR7275, 660 route des Lucioles 06560 Valbonne, France; E-mail: [davidovic@ipmc.cnrs.fr](mailto:davidovic@ipmc.cnrs.fr); Phone: +33(0)493 957 763

**Keywords:** microbiota, autism, behavior, reward system, metabolite, *p*-Cresol, 4-Cresol

## ABSTRACT

Brain development and behavioral responses are influenced by gut microbiota. Perturbations of the microbiota-gut-brain axis have been identified in autism spectrum disorders (ASD), suggesting that the microbiota could be involved in abnormal social and stereotyped behaviors in ASD patients. Notably, changes in microbiota composition and fecal, serum or urine levels of microbial metabolites are associated with ASD. Yet, a causal relationship between abnormal microbiota composition, altered microbial metabolite production, and ASD remains to be demonstrated. We hypothesized that *p*-Cresol (also known as 4-Cresol), a microbial metabolite that was described as more abundant in ASD patients, contributes to ASD core behavioral symptoms. Here we show that mice exposed to *p*-Cresol for 4 weeks in drinking water presented social behavior deficits, stereotypies, and perseverative behaviors, but no changes in anxiety, locomotion, or cognition. Abnormal social behavior induced by *p*-Cresol was associated with decreased activity of central dopamine neurons involved in the social reward circuit. Further, *p*-Cresol modified the relative abundance of specific bacterial taxa which correlated with social behavior. In addition, social behavior deficits were transferrable from *p*-Cresol-treated mice to control mice by fecal matter transplantation. In contrast, the microbiota from control mice restored both social interactions and dopamine neurons excitability when transplanted to *p*-Cresol-treated mice. Altogether, our results suggest that microbial metabolites *p*-Cresol could be involved in the development of core autistic behaviors via a gut microbiota-dependent mechanism. Further, this study paves the way for therapeutic interventions targeting the production of *p*-Cresol by gut bacteria to treat patients with ASD.

## INTRODUCTION

Autism spectrum disorders (ASD) are frequent (1:100) neurodevelopmental pathologies characterized by social interaction and communication deficits, perseverative/stereotyped behaviors and restricted interests, as well as abnormal sensory processing<sup>1</sup>. Also, ASD often co-occur with anxiety, hyperactivity and intellectual disability<sup>1</sup>. ASD is also associated with gastrointestinal (GI) dysfunction and increased intestinal permeability<sup>2</sup>. Children with ASD and concurrent GI symptoms exhibit more pronounced social impairments, sensory over-responsivity and anxiety compared to ASD peers without GI symptoms<sup>3-5</sup>. In addition, ASD patients exhibit gut microbiota dysbiosis characterized by reduced bacterial  $\beta$ -diversity and changes in the relative abundances of several bacterial taxa<sup>6-8</sup>. Dysbiosis in ASD patients is associated with altered urinary, plasmatic or fecal levels of microbial metabolites such as short-chain fatty acids (SCFA), indoles and tyrosine-derived metabolites<sup>9-16</sup>. In a pilot study, fecal microbiota transplantation (FMT) from healthy individuals to ASD patients durably alleviated both GI symptoms and ASD core symptoms<sup>17</sup>. Dysbiosis<sup>18-22</sup> and altered levels of microbial metabolites<sup>18, 21, 22</sup> have also been observed in rodent models of ASD : the maternal immune activation (MIA), the diet-induced obesity (DIO) and the valproate environmental models, the BTBR T+tf/J idiopathic model, and the *Shank3b*-KO genetic model. Furthermore, changes in microbiota composition induced by FMT or probiotic treatment alleviated behavioral alterations in several of these ASD models<sup>18-20</sup>. Finally, mice born from mothers transplanted with feces from ASD patients exhibited social behavior deficits, dysbiosis and abnormal patterns of microbial metabolites<sup>23</sup>.

The link between altered levels of microbial metabolites and behavioral impairments in ASD remains mostly unknown. However, several microbial metabolites can induce behavioral changes when administered to rodents. Treatment with the SCFA propionate induced social interaction deficits, stereotypies, cognitive deficits and anxiety in rats<sup>14</sup>. The tyrosine derivative 4-ethylphenylsulfate (4-EPS) induced anxiety in mice<sup>18</sup>. Finally, indoles impacted

socioemotional behavior in rats<sup>24</sup>. Altogether, these data suggested that dysbiosis could contribute to ASD core and associated symptoms via the production of microbial metabolites. Among the microbial metabolites linked to ASD, the small aromatic metabolite *p*-Cresol (*para*-Cresol, 4-Cresol, 4-methylphenol) is one of those for which the results are the more consistent across studies. Urinary<sup>11, 12</sup> and fecal<sup>15, 16</sup> levels of *p*-Cresol were found to be increased ASD patients in four independent studies. Also, *p*-Cresol urinary levels correlated with the severity of ASD behavioral alterations<sup>11, 12</sup>. *p*-Cresol is the product of tyrosine degradation by the intestinal microbiota and mainly by *Clostridioides difficile* and other species from the *Clostridioides* genus<sup>25, 26</sup>, which is more abundant in ASD patients<sup>6-8</sup>. Based on these findings, we hypothesized that increased *p*-Cresol levels contribute to the induction or maintenance of ASD core symptoms. To test this hypothesis, we investigated in mice the impact of *p*-Cresol exposure on behavior, dopamine neurons electrophysiology and microbiota composition.

## METHODS AND MATERIALS

*Extended methods and materials are available in Supplementary Information.*

**Ethics.** Animal housing and experimentation were conducted in facilities certified by local authorities (Direction Départementale de Protection des Populations des Alpes-Maritimes, accreditation #EC-06-152-5) and performed according to policies on the care and use of laboratory animals of European Communities Council Directive (2010/63EU) and under the agreement from the French Ministry of Research.

**Animals treatment.** Weaned C57BL/6J mice (21 to 28 day-old) were ordered to Charles Rivers (France). This developmental stage was chosen to avoid confounding effects of maternal exposure to *p*-Cresol, while still being in the time window for late neurodevelopment during which the microbiota-gut-brain axis can intervene<sup>27</sup>. Since the sex ratio for ASD is biased towards 3 males diagnosed for 1 female suggesting a higher susceptibility of males<sup>28</sup>, only males were considered in this study. Mice were randomly assigned to experimental groups. After 6 days of acclimation to the animal facility, mice were treated for at least 4 weeks with *p*-Cresol (Sigma-Aldrich) dispensed in drinking water at a concentration of 0.25g/l for a target dose of 50 mg/Kg/24 h. This dose per day corresponded to 7 times less the reported LD50 dose of 350 mg/Kg for acute oral administration of *p*-Cresol by gavage in mice, based on available toxicity data<sup>29</sup>.

**Quantification of *p*-Cresol in urine and serum.** Urine (20  $\mu$ L) and serum (100  $\mu$ L) samples were spiked with 10  $\mu$ L internal standard solution (myristic acid-d<sub>27</sub> in isopropanol, 750 mg/mL), subjected to methanol extraction and analyzed using gas chromatography-mass spectrometry (GC-MS)<sup>30</sup>.

**Behavioral testing.** Standard behavioral tests that have extensively been used to characterize genetic and environmental models of ASD<sup>31-34</sup> were implemented to assess: social behavior (three-chamber sociability test, dyadic social interactions), repetitive behaviors (motor stereotypies, marble burying test, Y-maze exploration), locomotor activity (actimetry), anxiety (open-field, novelty suppressed feeding) and cognition (novel object recognition test).

**Ex vivo patch-clamp electrophysiological recordings.** Spontaneous excitatory post-synaptic currents (sEPSCs) or excitability were measured in 250  $\mu\text{m}$  brain sections encompassing the ventral tegmented area (VTA) using visualized whole-cell voltage-clamp and current-clamp recordings, respectively, as described<sup>35</sup>. Depolarizing (0-300 pA) or hyperpolarizing (0- 450 pA) 800 ms current steps were used to assess excitability and membrane properties of VTA dopamine neurons. sEPSCs were assessed in voltage-clamp mode at a voltage of -65mV in the presence of picrotoxin (50  $\mu\text{M}$ ) using the same internal solution. Offline analyzes were performed using Clampfit 10.2 (Axon Instruments, USA).

**Fecal microbiota analysis by 16S rRNA gene sequencing.** Genomic DNA was obtained from fecal samples using the QIAamp power fecal DNA kit (Qiagen). The V3-V4 hypervariable region of the 16S rRNA gene were amplified by PCR and sequenced (Illumina Miseq technology). High-quality filtered reads were assembled and processed using FROGS pipeline to obtain operational taxonomic units (OTU) and their respective taxonomic assignment<sup>36</sup>, yielding 591 final clusters. Clusters were then affiliated to OTU by using a Silva123 16S reference database and the RDP (Ribosomal Database Project) classifier taxonomic assignment procedure. Richness and diversity indexes of bacterial community were computed using the Phyloseq package (v 1.19.1) in RStudio software<sup>37</sup>. Statistical differences in the microbial communities between groups were evaluated using constrained analysis of principal coordinates and permutational multivariate ANOVA. To identify

discriminating taxa and OTU associated with the control or *p*-Cresol class and estimate their effect size, we used the linear discriminant analysis (LDA) effect size (LEfSe) method<sup>38</sup>.

**Fecal microbiota transplantation (FMT).** Mice were gavaged with omeprazole (50mg/Kg/24 h, Day 1-3) each morning. On Day 4, mice received 5 consecutive gavages of 200 $\mu$ L of Moviprep (Norgine) at 90 min intervals. On Day 5, recipient mice received 1 omeprazole gavage and 3 consecutive gavages of 200  $\mu$ L of a fecal slurry at 2 h intervals. The fecal slurry consisted of pools of individual fecal pellets from donor mice homogenized in ice-cold ddH<sub>2</sub>O (w:v=1:50). Behavioral phenotyping or electrophysiological recordings were performed three weeks post FMT.

**Statistics.** Two-group comparisons were performed using 2-tailed Mann-Whitney's U-test. Multiple group comparisons were performed using two-way ANOVA. *Post hoc* comparisons were performed using Šidák's correction for multiple comparison. For comparison analysis of frequency distributions, Kolmogorov-Smirnov's test was used. Statistical analysis was performed using GraphPad Prism version 6.00 for iOS (GraphPad Software, USA). Principal Component Analysis (PCA) of behavioral data was performed for each dataset consisting of scores from the dyadic social interaction test and scores from the direct monitoring of motor stereotypies. Correlations were performed using Spearman's  $\rho$  correlation coefficient rank test with Benjamini-Hochberg's multiple testing correction. Statistical significance was set at an adjusted *p*-value below 0.05. Only significant differences are displayed.

## RESULTS

### ***p*-Cresol induces ASD core symptoms in mice**

To mimic exposure to *p*-Cresol through the GI tract, we treated C57BL/6J male mice with *p*-Cresol in drinking water starting at 4.5 weeks of age (Supplementary Figure 1A). A 4-week treatment with *p*-Cresol did not induce changes in body weight, drink or food intake

(Supplementary Figure 1B-D), suggesting that it did not have overt toxicity effects. Compared to control animals, *p*-Cresol-treated mice exhibited a 4-fold increase in levels of *p*-Cresol in urine, but not in serum (Supplementary Figure 1E, F).

We then analyzed *p*-Cresol-treated mice for social interaction deficits and repetitive/perseverative behaviors (as proxies for ASD core symptoms) as well as anxiety, hyperactivity and cognitive deficits (as proxies of ASD comorbidities). In the 3-chamber test, *p*-Cresol-treated mice presented reduced sociability (Figure 1B) and no preference for the mouse interactor towards the toy mouse (Figure 1C) compared to control mice. Although the number of close contacts with the mouse interactor was higher than with the toy mouse (Supplementary Figure 2G), their mean duration was reduced (Figure 1D). During dyadic social interactions, *p*-Cresol-treated mice displayed a decrease in time spent in social contact compared to control mice (Figure 1E). The time, number and mean duration of both nose and paw contacts as well as the number of followings were also reduced (Figure 1F-J, Supplementary Figure 2H, I). This indicates that *p*-Cresol treatment reduces social interactions and deteriorates the quality of social contacts.

As for repetitive/perseverative behaviors, *p*-Cresol-treated mice displayed more frequent head shakes and circling events (Figure 1K, L), but similar numbers of rearing episodes and time spent in digging or self-grooming as compared to control mice (Supplementary Figure 2J-L). Thus, the occurrence of stereotyped behaviors was increased in *p*-Cresol-treated mice, as confirmed in the marble burying test (Figure 1M). Consistently, *p*-Cresol treatment increased the frequency of perseverative same arm returns in the Y-maze spontaneous alternation task (Figure 1N). Finally, *p*-Cresol-treated mice were clearly separated from control mice along the PC1 axis in a PCA analysis of scores recorded in the dyadic social interaction and stereotypies tests (Figure 1O).

As for other behaviors, *p*-Cresol-treated and control mice displayed similar nocturnal and diurnal locomotor activity as assessed in actimetry chambers, and travelled the same distance in the open-field (Supplementary Figure 2M-O). This indicated that *p*-Cresol did not induce hyperactivity. Also, the number of entries and time spent in the open-field center, as

well as the latency to feed in the novelty-suppressed feeding test were not impacted (Supplementary Figure 2P-R), suggesting that *p*-Cresol did not alter anxiety levels. Finally, *p*-Cresol-treated mice explored objects similarly to control mice and displayed a similar recognition index for the novel object in the novel object recognition task, indicating that their exploratory behavior and cognitive ability were preserved (Supplementary Figure 2S, T).

We then investigated whether *p*-Cresol-induced behaviors were abolished when treatment was discontinued (Supplementary Figure 3A). We observed that the effect of *p*-Cresol on social interactions and stereotyped/perseverative behaviors persisted and were of similar magnitude, even after a 4-week washout (Supplementary Figure 3B-O). Control and *p*-Cresol-treated mice were clearly separated along the PC1 axis, and before and after washout along the PC2 axis in a PCA analysis of social behavior and stereotypies scores (Supplementary Figure 3P).

Altogether, these results suggest that *p*-Cresol selectively induces ASD core symptoms which persist in the absence of *p*-Cresol, but does not impact the other behavioral dimensions investigated here.

### ***p*-Cresol impairs dopamine neurons excitability in the VTA and induces long-lasting autistic-like behaviors that persist after washout**

We then sought to identify the neuronal circuits that were impacted by *p*-Cresol. We focused on dopamine neurons from the VTA that are part of a 'socially engaged reward circuit'<sup>39</sup>. Altered VTA connectivity and impaired VTA dopamine neurons activity were demonstrated in ASD patients<sup>40</sup> and in ASD models<sup>19, 20, 41-44</sup> respectively. We used whole-cell patch-clamp to record VTA dopamine neurons in acute brain slices from control and *p*-Cresol-treated animals (Figure 1P-W). First, *p*-Cresol-treated animals displayed reduced excitability of VTA dopamine neurons, with a reduction in the number of evoked action potentials (Figure 1P-R). Second, both the amplitude and frequencies of miniature spontaneous excitatory postsynaptic currents (sEPSC) were reduced in VTA dopamine neurons of *p*-Cresol-treated

animals compared to controls (Figure 1S-W). Therefore, *p*-Cresol treatment results in a decreased activity of dopamine neurons in the VTA.

### ***p*-Cresol induces microbiota dysbiosis**

Previous studies suggested that *p*-Cresol could have bacteriostatic properties<sup>26</sup>. We reasoned that irreversible changes in microbiota composition could explain the persistence of *p*-Cresol behavioral effects after a 4-week washout. We therefore analyzed the bacterial composition and community structure of the fecal microbiota from *p*-Cresol-treated and control mice using bacterial 16S ribosomal RNA sequencing. *Bacteroidia* and *Clostridia* were the dominant classes in both groups (Supplementary Figure 4A). Bacterial  $\alpha$ -diversity indices did not reveal differences in richness or evenness between groups (Supplementary Figure 4B-E). However, the  $\beta$ -diversity index based on Jaccard's distances revealed changes in microbial taxonomic abundance profiles upon *p*-Cresol treatment (Supplementary Figure 4F). We then sought to identify the bacterial taxa and OTU that discriminated *p*-Cresol-treated and control mice. Among the 91 OTU identified, 70 were discriminant ( $|\text{Log}_{10}\text{LDA score}| > 2$ ;  $p < 0.05$ ) and the largest effect sizes ( $|\text{Log}_{10}\text{LDA score}| > 3$ ) were observed for OTU related to the *Bacteroidales* and *Clostridiales* orders (Supplementary Table 1). We identified 29 OTU associated with *p*-Cresol exposure, mostly from the *Lachnospiraceae* and *Muribaculaceae* families. We also identified 41 OTUs associated with the control group, mostly from the *Lachnospiraceae*, *Ruminococcaceae* and *Muribaculaceae* families.

We then analyzed the association between the relative abundance of the 70 discriminant bacterial OTU (Supplementary Table 1) and social behavior and stereotypies scores impacted by *p*-Cresol (Figure 1E-L). Correlation analyzes revealed moderate to strong associations ( $0.38 < |\rho| < 0.74$ ) between bacterial abundances and behavior, in particular social behavior (Table 1, Supplementary Table 2). Among the OTU that were associated with *p*-Cresol treatment, the abundance of 4 OTU from the *Bacteroidales* and the *Clostridiales*

orders correlated with social interaction deficits. Among the OTU that were associated with the control group, the abundance of 20 OTU from the *Clostridiales* order (*Ruminococaceae* and *Lachnospiraceae* families) correlated with higher sociability. The abundance of two OTU correlated with reduced numbers of head shakes. All these OTU were differentially impacted by *p*-Cresol treatment, either downregulated if they correlated positively with behavioral outcome or upregulated if they were correlated with the severity of behavioral impairments (Figure 2A-C). This supports a tight link between microbiota dysbiosis induced by *p*-Cresol and behavioral impairments relative to core ASD symptoms.

### **The microbiota from *p*-Cresol-treated mice induces social behavior deficits when transplanted to normal recipients**

Having shown that *p*-Cresol remodeled the intestinal microbiota, we investigated whether these changes were responsible for *p*-Cresol-induced behavioral alterations. To this aim, we transplanted the fecal microbiota from *p*-Cresol-treated mice to normal recipients (Figure 3A). Compared to control mice transplanted with a normal microbiota, mice transplanted with microbiota of *p*-Cresol-treated mice spent less time in social contact, exhibited decreased time, number and mean duration of nose and paw contacts (Figure 3B-F, Supplementary Figure 5A, B). In contrast, the number of followings was not impacted (Figure 3G). Social behavior deficits were accompanied by stereotypies with increased number of head shakes (Figure 3H), while circling episodes, grooming and digging time were not impacted (Figure 3I, Supplementary Figure 5C, D). Mice transplanted with the microbiota from *p*-Cresol-treated and control mice were clearly separated along the PC1 axis using PCA analysis of social interaction and stereotypies scores (Figure 3J). In conclusion, the microbiota from *p*-Cresol-treated mice transfers social behavior deficits and to some extent stereotypies when transplanted to recipient mice.

### **Transfer of a normal microbiota to *p*-Cresol-treated recipient mice restores social behavior deficits and VTA dopamine neurons excitability**

Having shown that the microbiota from *p*-Cresol-treated mice induced social behavior deficits when transplanted into normal recipients, we investigated whether *p*-Cresol-induced behavioral alterations could be restored by a normal microbiota. We therefore transplanted a normal microbiota to either control mice or mice that had been treated for 4 weeks with *p*-Cresol (Figure 4A). Before FMT, *p*-Cresol-treated mice displayed social behavior deficits and stereotypies (Figure 4B-K) consistent with our previous results (Figures 1, 2). Recolonization of *p*-Cresol-treated mice with a normal microbiota restored all parameters to control levels in the dyadic social interaction test (Figure 4B, C, E, G, Supplementary Figure 6I, J). The quality of social contacts was also restored as the mean duration of both nose and paw contacts were rescued (Figure 4D, F). In the three-chamber test, the sociability index was also normalized (Figure 4H, Supplementary Figure 6F), as well as the preference for the interactor mouse (Supplementary Figure 6G, H). The quality of social interactions was also rescued as assessed by normalization of contact mean duration (Figure 4I). In contrast, reversal of stereotyped behaviors was incomplete, since head shakes were only modestly reduced and circling episodes were still present after FMT in recipient mice that had been treated with *p*-Cresol (Figure 4J, K). Normalization of *p*-Cresol-induced behaviors by the microbiota of untreated mice was confirmed by PCA analysis which showed that control mice prior FMT and control and *p*-Cresol-treated mice transplanted with a normal microbiota clustered on the right side of the PC1 axis, while *p*-Cresol-treated mice prior FMT stood alone on the left side (Figure 4L). Importantly, besides normalizing *p*-Cresol-induced social behavior deficits, transplantation of a normal microbiota also restored the excitability of dopamine neurons in the VTA (Figure 4M, N).

## DISCUSSION

### ***p-Cresol induces ASD core behavioral deficits***

ASD result from interactions between genes and environment. While 10-25% of ASD cases are explained by mutations in specific genetic *loci*, twin studies have revealed that genetic and environmental factors share equal influence on ASD risk<sup>45</sup>. The identification of environmental factors, including microbiota-linked factors, contributing to ASD is therefore critical to better understand the etiology of these multi-factorial pathologies.

Here we show that *p*-Cresol-treated mice exhibit social behavior deficits and stereotypies, demonstrating a possible causal relationship between elevated *p*-Cresol levels and ASD core symptoms. Like *p*-Cresol, other microbial metabolites are possibly linked to ASD. While several of these metabolites were demonstrated to modify behavior when administered to rodents, none of them selectively induced ASD core symptoms. For example, the microbial SCFA propionate did not only induce social interaction deficits and stereotypies, but also anxiety and hyperlocomotion<sup>14</sup>. Indoles increased social contact and anxiety but reduced locomotor activity in rats<sup>24</sup>. Lastly, 4-EPS increased anxiety and startle reflex in mice but had no impact on social behavior or stereotypies<sup>18</sup>. Therefore, in contrast to mice treated with other microbial metabolites, *p*-Cresol has selective effects on ASD core behaviors by inducing social behavior deficits and repetitive/perseverative behaviors, while not impacting behaviors related to frequent ASD comorbidities (stress, anxiety, hyperactivity, cognition).

Mice displaying social avoidance exhibited an increase in *p*-Cresol levels measured in gut tissue<sup>46</sup>. However, the causal relationship between social behavior and *p*-Cresol levels was not investigated. Also, a recent study showed that a single acute intravenous injection of *p*-Cresol exacerbated anxiety and reduced social preference in the BTBR idiopathic model of ASD<sup>47</sup>. Nonetheless, the intravenous administration of *p*-Cresol did not recapitulate chronic intestinal exposure and the broad observed effects may have resulted from acute activity of the compound. The specific induction of ASD core symptoms upon *p*-Cresol intestinal exposure supports the face validity of our environmental ASD model.

### ***p-Cresol-induced dysbiosis modulates the social behavior of the host***

How microbial metabolites linked to ASD such as propionate, indoles or 4-EPS impact the brain remains unknown. Some of these metabolites are ligands to the host's receptors: 3-indoxylsulfate and indole-3-propionate are ligands to the aryl-hydrocarbon receptor<sup>48</sup> and the xenobiotic sensor pregnane X receptor<sup>49</sup> respectively, while propionate binds to GPR41 and GPR43<sup>50</sup>. Yet, their signaling role has been mostly investigated in the context of metabolic, GI or autoimmune disorders<sup>48-50</sup>, and not in the context of neuropsychiatric disorders. It appears unlikely that *p*-Cresol exerts *per se* a direct systemic or even central effect on a receptor in our experimental paradigm. In support of this, its circulating serum levels are not increased in *p*-Cresol-treated mice, making it unlikely to reach bioactive levels in the brain. Also, *p*-Cresol effects on behavior persist even in its absence after a 4-week washout period. Rather, we propose that GI exposure to *p*-Cresol triggers ASD behaviors by inducing a selective microbiota dysbiosis, which is sufficient to fully induce social behavior deficits and partially stereotypies upon transplantation to control mice. We indeed show that a *p*-Cresol-rich environment reduces bacterial  $\beta$ -diversity, as described in ASD patients<sup>6-8</sup>, and provides a selective growth advantage for several taxa, in line with a previous *in vitro* study<sup>26</sup>. The correlation between the abundances of 26 OTU and social behavior argues for a clear link between certain bacterial taxa and social abilities. Notably, members of the *Blautia* genus are reduced both in ASD patients<sup>8</sup> and in *p*-Cresol-treated animals and their abundances correlate positively with social abilities in our model. Conversely, OTU from the *Muribaculaceae* and *Peptococcaceae* families are overabundant in *p*-Cresol-treated animals and their abundances correlate negatively with social behavior abilities. We anticipate that the selective overgrowth of yet-to-be-identified bacterial species in a *p*-Cresol rich environment could contribute to social behavior deficits in our model. Finally, our model displays a 4-fold increase in *p*-Cresol urinary excretion, within the 2.5-fold increase range identified in ASD patients<sup>11, 12</sup>. Elevated urinary *p*-Cresol<sup>11, 12</sup> and dysbiosis<sup>6-8</sup> are observed both in ASD patients and in our model, underpinning its construct validity. Furthermore, its

predictive validity is supported by our findings that FMT of a normal microbiota normalizes behavior in *p*-Cresol-treated mice, as already shown in a pilot study in ASD patients<sup>17</sup>.

### ***p*-Cresol-induced dysbiosis dysregulates central dopamine pathways and the social reward system**

Social interactions are pleasurable events for humans and animals, as shown by the activation of the reward circuit by social stimuli – activation that is blunted in ASD patients<sup>51</sup>. The VTA is a key subcortical node of the mesolimbic reward pathway<sup>52</sup> and ASD patients display defects in VTA connectivity<sup>40</sup>. Moreover, blocking VTA dopamine neurons that are part of a ‘socially engaged reward circuit’ is sufficient to diminish social interactions in rodents<sup>39, 53</sup>. Further, impaired dopamine neurons activity in the VTA has been previously described in models targeting the ASD genes *Shank3b*, *Nlgn3* and *Ube3a*<sup>20, 41-43</sup> and in the MIA and DIO environmental models of ASD<sup>19, 44</sup>. The disruption of the social reward pathway both in ASD patients and in our model also argues for its construct validity. Dopaminergic circuits are sensitive to changes in gut microbiota composition<sup>54</sup> and gut-innervating vagal sensory neurons control striatal dopamine release<sup>55</sup>. Further, normalization of microbiota composition by FMT abolished social interaction deficits and restored VTA dopamine neurons excitability in *p*-Cresol-treated mice. Taken together, these results support a model in which *p*-Cresol-induced dysbiosis results in impaired VTA dopamine neurons activity which eventually disrupts the social reward pathway and causes social behavior deficits.

### **Conclusions and perspectives**

We found that *p*-Cresol-treated mice exhibited social interaction deficits and stereotypies reminiscent of ASD core symptoms in humans. These behaviors were dependent on changes in microbiota composition and were associated with a reduced activity of dopamine neurons in the VTA. This environmental model of ASD exhibited face, construct and predictive validity. Because *p*-Cresol levels are elevated in ASD patients, our study suggests that increased *p*-Cresol levels could contribute to ASD core symptoms in humans. Further,

the ability of a normal microbiota to normalize social interaction deficits when transplanted into *p*-Cresol-treated mice supports the rationale for the ongoing clinical trials aiming at ascertaining the beneficial impact of FMT in ASD, as highlighted in a pilot study<sup>17</sup>. Finally, prebiotic treatment with oligofructose-enriched inulin or probiotic treatment with *Lactobacillus casei* decreased *p*-Cresol urinary excretion in healthy volunteers<sup>56</sup>. Future clinical studies could evaluate the benefits of such interventions to reduce the microbial production of *p*-Cresol and alleviate the core symptoms of ASD.

## **ACKNOWLEDGEMENTS**

We thank Lucien Relmy for expert technical assistance with animal care and Thomas Lorivel for help with behavioral tests set-up. We are grateful to Dominique Gauguier (Centre de Recherche des Cordeliers, Paris) for helpful discussions regarding the procedure for fecal microbiota transplantations. LD and MED are grateful to the European Community 7<sup>th</sup> Framework Program under Coordinated Action NEURON-ERANET (grant agreement 291840), ANR and MRC (MR/M501797/1). JAJB and JLM thank Region Centre-Val de Loire (ARD2020 Biomedicaments GPCRAb) and the Labex MabImprove for financial support.

## **CONFLICT OF INTEREST**

None to declare.

## **SUPPLEMENTARY INFORMATION**

Supplementary information is available at MP's website

## REFERENCES

1. Lai MC, Lombardo MV, Baron-Cohen S. Autism. *Lancet* 2014; **383**(9920): 896-910.
2. Vuong HE, Hsiao EY. Emerging Roles for the Gut Microbiome in Autism Spectrum Disorder. *Biol Psychiatry* 2017; **81**(5): 411-423.
3. Mazurek MO, Vasa RA, Kalb LG, Kanne SM, Rosenberg D, Keefer A *et al.* Anxiety, sensory over-responsivity, and gastrointestinal problems in children with autism spectrum disorders. *J Abnorm Child Psychol* 2013; **41**(1): 165-176.
4. Nikolov RN, Bearss KE, Lettinga J, Erickson C, Rodowski M, Aman MG *et al.* Gastrointestinal symptoms in a sample of children with pervasive developmental disorders. *J Autism Dev Disord* 2009; **39**(3): 405-413.
5. Gorrindo P, Williams KC, Lee EB, Walker LS, McGrew SG, Levitt P. Gastrointestinal dysfunction in autism: parental report, clinical evaluation, and associated factors. *Autism Res* 2012; **5**(2): 101-108.
6. Xu M, Xu X, Li J, Li F. Association Between Gut Microbiota and Autism Spectrum Disorder: A Systematic Review and Meta-Analysis. *Front Psychiatry* 2019; **10**: 473.
7. Iglesias-Vazquez L, Van Ginkel Riba G, Arija V, Canals J. Composition of Gut Microbiota in Children with Autism Spectrum Disorder: A Systematic Review and Meta-Analysis. *Nutrients* 2020; **12**(3).
8. Liu F, Li J, Wu F, Zheng H, Peng Q, Zhou H. Altered composition and function of intestinal microbiota in autism spectrum disorders: a systematic review. *Transl Psychiatry* 2019; **9**(1): 43.
9. Emond P, Mavel S, Aidoud N, Nadal-Desbarats L, Montigny F, Bonnet-Brilhault F *et al.* GC-MS-based urine metabolic profiling of autism spectrum disorders. *Analytical and bioanalytical chemistry* 2013; **405**(15): 5291-5300.
10. Yap IK, Angley M, Veselkov KA, Holmes E, Lindon JC, Nicholson JK. Urinary metabolic phenotyping differentiates children with autism from their unaffected siblings and age-matched controls. *J Proteome Res* 2010; **9**(6): 2996-3004.

11. Altieri L, Neri C, Sacco R, Curatolo P, Benvenuto A, Muratori F *et al.* Urinary p-cresol is elevated in small children with severe autism spectrum disorder. *Biomarkers* 2011; **16**(3): 252-260.
12. Gabriele S, Sacco R, Cerullo S, Neri C, Urbani A, Tripi G *et al.* Urinary p-cresol is elevated in young French children with autism spectrum disorder: a replication study. *Biomarkers* 2014; **19**(6): 463-470.
13. Dieme B, Mavel S, Blasco H, Tripi G, Bonnet-Brilhault F, Malvy J *et al.* Metabolomics Study of Urine in Autism Spectrum Disorders Using a Multiplatform Analytical Methodology. *J Proteome Res* 2015; **14**(12): 5273-5282.
14. Macfabe DF. Short-chain fatty acid fermentation products of the gut microbiome: implications in autism spectrum disorders. *Microbial ecology in health and disease* 2012; **23**.
15. De Angelis M, Piccolo M, Vannini L, Siragusa S, De Giacomo A, Serrazzanetti DI *et al.* Fecal microbiota and metabolome of children with autism and pervasive developmental disorder not otherwise specified. *PLoS One* 2013; **8**(10): e76993.
16. Kang DW, Ilhan ZE, Isern NG, Hoyt DW, Howsmon DP, Shaffer M *et al.* Differences in fecal microbial metabolites and microbiota of children with autism spectrum disorders. *Anaerobe* 2017; **49**: 121-131.
17. Kang DW, Adams JB, Coleman DM, Pollard EL, Maldonado J, McDonough-Means S *et al.* Long-term benefit of Microbiota Transfer Therapy on autism symptoms and gut microbiota. *Sci Rep* 2019; **9**(1): 5821.
18. Hsiao EY, McBride SW, Hsien S, Sharon G, Hyde ER, McCue T *et al.* Microbiota modulate behavioral and physiological abnormalities associated with neurodevelopmental disorders. *Cell* 2013; **155**(7): 1451-1463.
19. Buffington SA, Di Prisco GV, Auchtung TA, Ajami NJ, Petrosino JF, Costa-Mattioli M. Microbial Reconstitution Reverses Maternal Diet-Induced Social and Synaptic Deficits in Offspring. *Cell* 2016; **165**(7): 1762-1775.

20. Sgritta M, Dooling SW, Buffington SA, Momin EN, Francis MB, Britton RA *et al.* Mechanisms Underlying Microbial-Mediated Changes in Social Behavior in Mouse Models of Autism Spectrum Disorder. *Neuron* 2019; **101**(2): 246-259 e246.
21. Golubeva AV, Joyce SA, Moloney G, Burokas A, Sherwin E, Arboleya S *et al.* Microbiota-related Changes in Bile Acid & Tryptophan Metabolism are Associated with Gastrointestinal Dysfunction in a Mouse Model of Autism. *EBioMedicine* 2017; **24**: 166-178.
22. de Theije CG, Wopereis H, Ramadan M, van Eijndthoven T, Lambert J, Knol J *et al.* Altered gut microbiota and activity in a murine model of autism spectrum disorders. *Brain Behav Immun* 2014; **37**: 197-206.
23. Sharon G, Cruz NJ, Kang DW, Gandal MJ, Wang B, Kim YM *et al.* Human Gut Microbiota from Autism Spectrum Disorder Promote Behavioral Symptoms in Mice. *Cell* 2019; **177**(6): 1600-1618 e1617.
24. Jaglin M, Rhimi M, Philippe C, Pons N, Bruneau A, Goustard B *et al.* Indole, a Signaling Molecule Produced by the Gut Microbiota, Negatively Impacts Emotional Behaviors in Rats. *Front Neurosci* 2018; **12**: 216.
25. Saito Y, Sato T, Nomoto K, Tsuji H. Identification of phenol- and p-cresol-producing intestinal bacteria by using media supplemented with tyrosine and its metabolites. *FEMS Microbiol Ecol* 2018; **94**(9).
26. Passmore IJ, Letertre MPM, Preston MD, Bianconi I, Harrison MA, Nasher F *et al.* Para-cresol production by *Clostridium difficile* affects microbial diversity and membrane integrity of Gram-negative bacteria. *PLoS Pathog* 2018; **14**(9): e1007191.
27. Borre YE, O'Keeffe GW, Clarke G, Stanton C, Dinan TG, Cryan JF. Microbiota and neurodevelopmental windows: implications for brain disorders. *Trends Mol Med* 2014; **20**(9): 509-518.
28. Loomes R, Hull L, Mandy WPL. What Is the Male-to-Female Ratio in Autism Spectrum Disorder? A Systematic Review and Meta-Analysis. *J Am Acad Child Adolesc Psychiatry* 2017; **56**(6): 466-474.

29. Lewis RJ, Sax NI. Sax's Dangerous Properties of Industrial Materials. 11th Edition edn. Hoboken, N.J.; J. Wiley & Sons: Hoboken, NJ, USA, 2004, p 1004.
30. Fiehn O. Metabolomics by Gas Chromatography-Mass Spectrometry: Combined Targeted and Untargeted Profiling. *Curr Protoc Mol Biol* 2016; **114**: 30 34 31-30 34 32.
31. Becker JA, Clesse D, Spiegelhalter C, Schwab Y, Le Merrer J, Kieffer BL. Autistic-like syndrome in mu opioid receptor null mice is relieved by facilitated mGluR4 activity. *Neuropsychopharmacology* 2014; **39**(9): 2049-2060.
32. Pujol CN, Pellissier LP, Clement C, Becker JAJ, Le Merrer J. Back-translating behavioral intervention for autism spectrum disorders to mice with blunted reward restores social abilities. *Transl Psychiatry* 2018; **8**(1): 197.
33. Leboucher A, Bermudez-Martin P, Mouska X, Amri EZ, Pisani DF, Davidovic L. Fmr1-Deficiency Impacts Body Composition, Skeleton, and Bone Microstructure in a Mouse Model of Fragile X Syndrome. *Front Endocrinol (Lausanne)* 2019; **10**: 678.
34. Silverman JL, Yang M, Lord C, Crawley JN. Behavioural phenotyping assays for mouse models of autism. *Nature reviews Neuroscience* 2010; **11**(7): 490-502.
35. Fernandez SP, Broussot L, Marti F, Contesse T, Mouska X, Soiza-Reilly M *et al.* Mesopontine cholinergic inputs to midbrain dopamine neurons drive stress-induced depressive-like behaviors. *Nat Commun* 2018; **9**(1): 4449.
36. Escudie F, Auer L, Bernard M, Mariadassou M, Cauquil L, Vidal K *et al.* FROGS: Find, Rapidly, OTUs with Galaxy Solution. *Bioinformatics* 2018; **34**(8): 1287-1294.
37. McMurdie PJ, Holmes S. Phyloseq: a bioconductor package for handling and analysis of high-throughput phylogenetic sequence data. *Pac Symp Biocomput* 2012: 235-246.
38. Segata N, Izard J, Waldron L, Gevers D, Miropolsky L, Garrett WS *et al.* Metagenomic biomarker discovery and explanation. *Genome Biol* 2011; **12**(6): R60.
39. Hung LW, Neuner S, Polepalli JS, Beier KT, Wright M, Walsh JJ *et al.* Gating of social reward by oxytocin in the ventral tegmental area. *Science* 2017; **357**(6358): 1406-1411.

40. Supekar K, Kochalka J, Schaer M, Wakeman H, Qin S, Padmanabhan A *et al.* Deficits in mesolimbic reward pathway underlie social interaction impairments in children with autism. *Brain* 2018; **141**(9): 2795-2805.
41. Krishnan V, Stoppel DC, Nong Y, Johnson MA, Nadler MJ, Ozkaynak E *et al.* Autism gene Ube3a and seizures impair sociability by repressing VTA Cbln1. *Nature* 2017; **543**(7646): 507-512.
42. Bariselli S, Hornberg H, Prevost-Solie C, Musardo S, Hatstatt-Burkle L, Scheiffele P *et al.* Role of VTA dopamine neurons and neuroligin 3 in sociability traits related to nonfamiliar conspecific interaction. *Nat Commun* 2018; **9**(1): 3173.
43. Bariselli S, Tzanoulinou S, Glangetas C, Prevost-Solie C, Pucci L, Viguie J *et al.* SHANK3 controls maturation of social reward circuits in the VTA. *Nat Neurosci* 2016; **19**(7): 926-934.
44. Lecca S, Luchicchi A, Scherma M, Fadda P, Muntoni AL, Pistis M. Delta(9)-Tetrahydrocannabinol During Adolescence Attenuates Disruption of Dopamine Function Induced in Rats by Maternal Immune Activation. *Front Behav Neurosci* 2019; **13**: 202.
45. Bourgeron T. Current knowledge on the genetics of autism and propositions for future research. *C R Biol* 2016; **339**(7-8): 300-307.
46. Gacias M, Gaspari S, Santos PM, Tamburini S, Andrade M, Zhang F *et al.* Microbiota-driven transcriptional changes in prefrontal cortex override genetic differences in social behavior. *Elife* 2016; **5**.
47. Pascucci T, Colamartino M, Fiori E, Sacco R, Coviello A, Ventura R *et al.* P-cresol Alters Brain Dopamine Metabolism and Exacerbates Autism-Like Behaviors in the BTBR Mouse. *Brain Sci* 2020; **10**(4).
48. Kim CH. Immune regulation by microbiome metabolites. *Immunology* 2018; **154**(2): 220-229.
49. Venkatesh M, Mukherjee S, Wang H, Li H, Sun K, Benechet AP *et al.* Symbiotic bacterial metabolites regulate gastrointestinal barrier function via the xenobiotic sensor PXR and Toll-like receptor 4. *Immunity* 2014; **41**(2): 296-310.

50. Bolognini D, Tobin AB, Milligan G, Moss CE. The Pharmacology and Function of Receptors for Short-Chain Fatty Acids. *Mol Pharmacol* 2016; **89**(3): 388-398.
51. Pellissier LP, Gandia J, Laboute T, Becker JAJ, Le Merrer J. mu opioid receptor, social behaviour and autism spectrum disorder: reward matters. *Br J Pharmacol* 2018; **175**(14): 2750-2769.
52. Rinaldi R. Dopamine and reward seeking: the role of ventral tegmental area. *Rev Neurosci* 2014; **25**(5): 621-630.
53. Gunaydin LA, Grosenick L, Finkelstein JC, Kauvar IV, Fenno LE, Adhikari A *et al.* Natural neural projection dynamics underlying social behavior. *Cell* 2014; **157**(7): 1535-1551.
54. Gonzalez-Arancibia C, Urrutia-Pinones J, Illanes-Gonzalez J, Martinez-Pinto J, Sotomayor-Zarate R, Julio-Pieper M *et al.* Do your gut microbes affect your brain dopamine? *Psychopharmacology (Berl)* 2019; **236**(5): 1611-1622.
55. Han W, Tellez LA, Perkins MH, Perez IO, Qu T, Ferreira J *et al.* A Neural Circuit for Gut-Induced Reward. *Cell* 2018; **175**(3): 887-888.
56. De Preter V, Vanhoutte T, Huys G, Swings J, De Vuyst L, Rutgeerts P *et al.* Effects of *Lactobacillus casei* Shirota, *Bifidobacterium breve*, and oligofructose-enriched inulin on colonic nitrogen-protein metabolism in healthy humans. *Am J Physiol Gastrointest Liver Physiol* 2007; **292**(1): G358-368.

# FIGURES & TABLES

## Figure 1

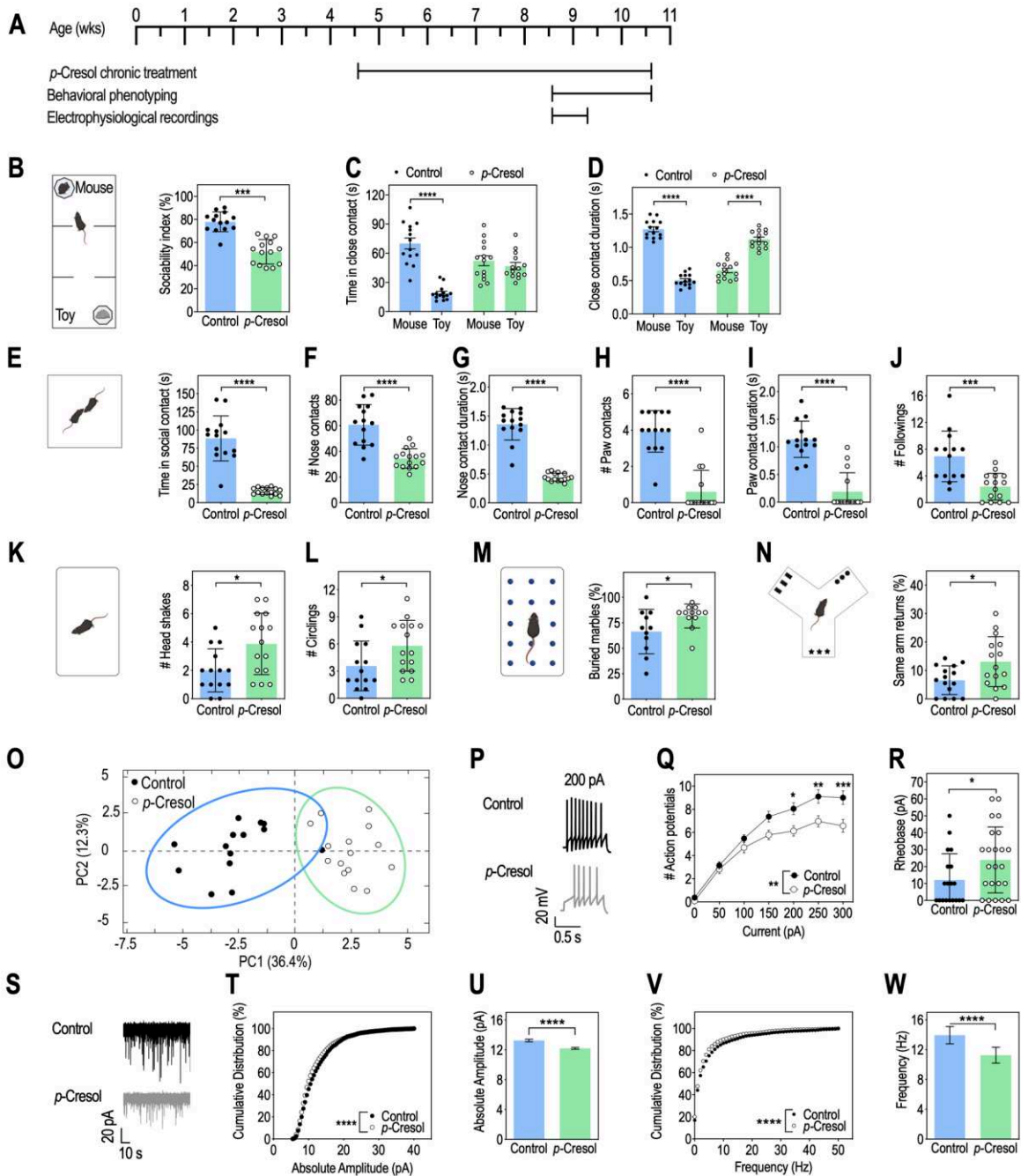


**Figure 1. *p*-Cresol treatment induces autistic-like behaviors and alters VTA dopamine neurons excitability**

(A) Timeline of the experiments

(B-D) Three-chamber test (n=14/group):

(B) Sociability index (ratio of the time spent in close contact with the mouse interactor normalized to the sum of the time in close contact with both mouse interactor and toy mouse); Mann-Whitney U-test: \*\*\*p<0.001.

(C) Time spent in close contact with the mouse interactor or the toy mouse; 2-way ANOVA:  $p(\text{Treatment})=0.2601$ ,  $p(\text{Preference})=p<0.0001$ ,  $p(\text{Treatment} \times \text{Mouse-Toy})=p<0.0001$ ; Šidák's post hoc tests for treatment effect: \*\*\*\* $p<0.0001$ .

(D) Mean duration of each close contact with the mouse interactor or the toy mouse; 2-way ANOVA:  $p(\text{Treatment})=0.9416$ ,  $p(\text{Preference})=p<0.0001$ ,  $p(\text{Treatment} \times \text{Mouse-Toy})=p<0.0001$ , Šidák's post hoc tests for treatment effect: \*\*\*\* $p<0.0001$ .

(E-J) Dyadic social interaction test (n=14 Control, n=15 *p*-Cresol): (E) total time spent, (F) number of events and (G) mean duration of nose contacts, (H) number of events and (I) mean duration of paw contacts, (J) number of following events; Mann-Whitney U-test: \*\*\*\* $p<0.0001$ , \*\*\* $p<0.0001$ .

(K-L) Motor stereotypies (n=14 Control, n=15 *p*-Cresol): (K) number of head shakes and (L) circling events; Mann-Whitney U-test: \* $p<0.05$ .

(M) Marble burying test (n=11 Control, n=12 *p*-Cresol): percentage of buried marbles; Mann-Whitney U-test: \* $p<0.05$ .

(N) Y-maze spontaneous alternations (n=15/group): % of same arm returns; n=15/group; Mann-Whitney U-test: \* $p<0.05$ .

(O) PCA plot of behavioral scores recorded in the dyadic social interaction and direct monitoring of motor stereotypies (Figure 1 E-L and Supplementary Figure 2H-L); ellipses of the 95% confidence intervals are indicated for each group (n=14 Control, n=15 *p*-Cresol); PC, principal component.

(P-W) Electrophysiological recordings of dopamine neurons activity in the VTA:

(P) Representative traces of dopamine neuron activity in patch-clamp experiments after a 200pA current injection

(Q) Number of action potentials evoked by current injection in current-clamp experiments; n=5 animals/group, 19 cells recorded for Control, 23 cells recorded for *p*-Cresol; 2-way ANOVA:  $p(\text{Treatment})=0.0066$ ,  $p(\text{Current})<0.0001$ ,  $p(\text{Treatment} \times \text{Current})=0.0006$ ; Šidák's post hoc tests for treatment effect, \* $p<0.05$ , \*\* $p<0.01$ , \*\*\* $p<0.001$ .

(R) Rheobase, minimal electric current required to evoke an action potential; n=5 animals/group, 19 cells recorded for Control, n=23 cells recorded for *p*-Cresol; Mann-Whitney U-test: \* $p<0.05$ ,

(S) Representative traces of spontaneous miniature excitatory postsynaptic currents (sEPSC)

(T) Cumulative frequencies of sEPSC absolute amplitude; n=5 animals/group, >2500 events/group; Kolmogorov-Smirnov test: \*\*\*\* $p<0.0001$ .

(U) Mean absolute amplitude of sEPSC; Mann-Whitney U-test: \*\*\*\* $p<0.0001$ .

(V) Cumulative frequencies of sEPSC frequency; n=5 animals/group, >2500 events/group; Kolmogorov-Smirnov test: \*\*\*\* $p<0.0001$ .

(W) Mean frequency of sEPSC; Mann-Whitney U-test: \*\*\*\* $p<0.0001$ .

(B-N, R) Data are shown as means  $\pm$  SD. (Q, U, W) Data are shown as means  $\pm$  SEM.

**Figure 2**

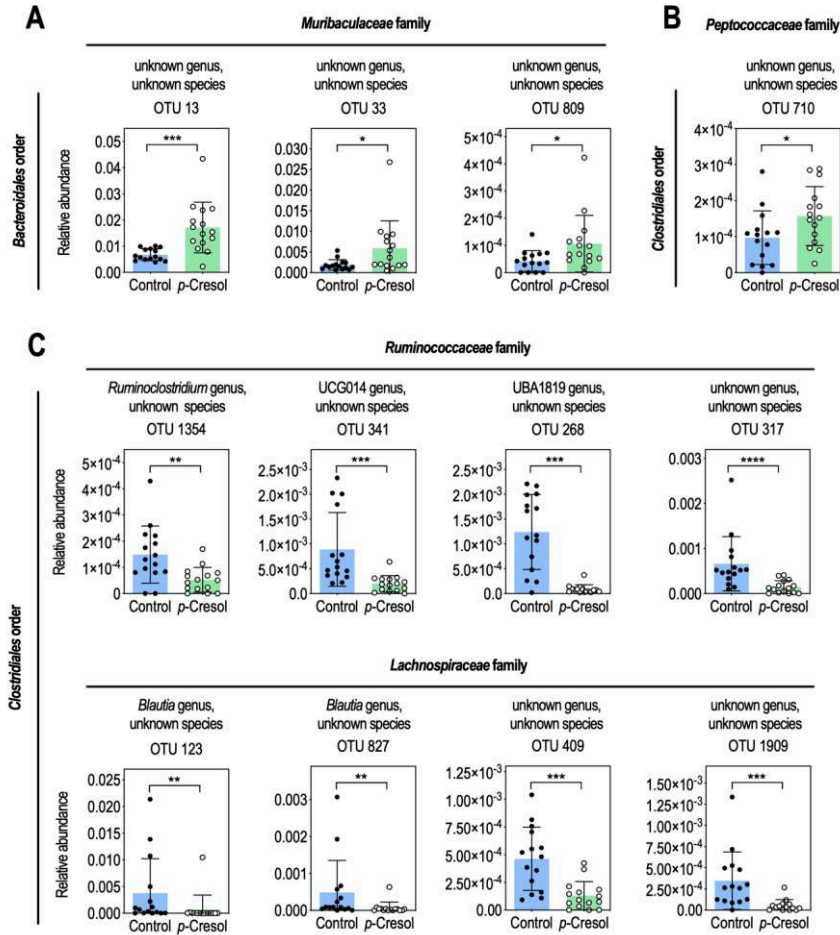


**Figure 2. The abundances of microbial OTU correlating with social behavior are impacted by *p*-Cresol**

(A, B) OTU associated with the *p*-Cresol class in LEfSE analysis and negatively correlated with social behavior abilities (n=15/group): abundances for members of the *Muribaculaceae* (A) and *Peptococcaceae* family (B) from the *Bacteroidales* and *Clostridiales* orders respectively; Mann-Whitney U-test: \*p<0.05, \*\*p<0.01, \*\*\*p<0.001.

(C) OTU associated with the Control class in LEfSE analysis and positively correlated with social behavior abilities (n=15/group): abundances for members of the *Ruminococcaceae* and *Lachnospiraceae* families from the *Clostridiales* order; Mann-Whitney U-test: \*\*p<0.01, \*\*\*p<0.001, \*\*\*\*p<0.0001.

Data are presented as dot-plots featuring means  $\pm$  SD.

**Figure 3**

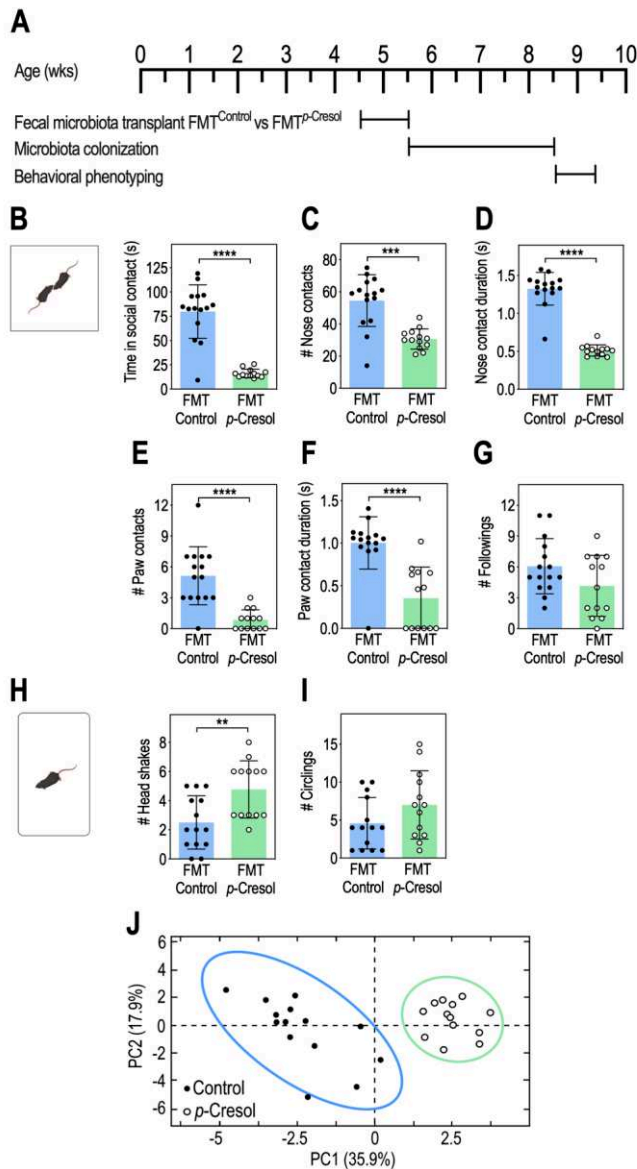


**Figure 3. Microbiota remodeling following *p*-Cresol treatment induces social behavior deficits**

(A) Timeline of the fecal microbiota transplant (FMT) experiment of fecal slurry from control or *p*-Cresol-treated donor animals to recipient wildtype mice.

(B-G) Dyadic social interaction test (n=15 Control, n=13 *p*-Cresol):

(B) Total time spent in social contact; Mann-Whitney U-test: \*\*\*\*p<0.0001.

(C) Number of nose contacts; Mann-Whitney U-test: \*\*\*p<0.001.

(D) Mean duration of nose contact; Mann-Whitney U-test: \*\*\*\*p<0.0001.

(E) Number of paw contacts; Mann-Whitney U-test: \*\*\*\*p<0.0001.

(F) Mean duration of each paw contact; Mann-Whitney U-test: \*\*\*\* $p < 0.0001$ .

(G) Number of followings; Mann-Whitney U-test:  $p = 0.1563$ .

(H, I) Motor stereotypies: (n=14 Control, n=13 p-Cresol):

(H) Number of head shakes; Mann-Whitney U-test: \*\* $p < 0.001$ .

(I) Number of circling events; Mann-Whitney U-test:  $p = 0.1762$ .

(J) PCA plots of behavioral scores recorded in the dyadic social interaction and direct monitoring of motor stereotypies (Figure 3B-I, Supplementary Figure 5A-D); ellipses of the 95% confidence intervals are indicated for each group (n=15 Control, n=13 p-Cresol).

(B-I) Data are presented as dot-plots featuring means  $\pm$  SD.

**Figure 4**

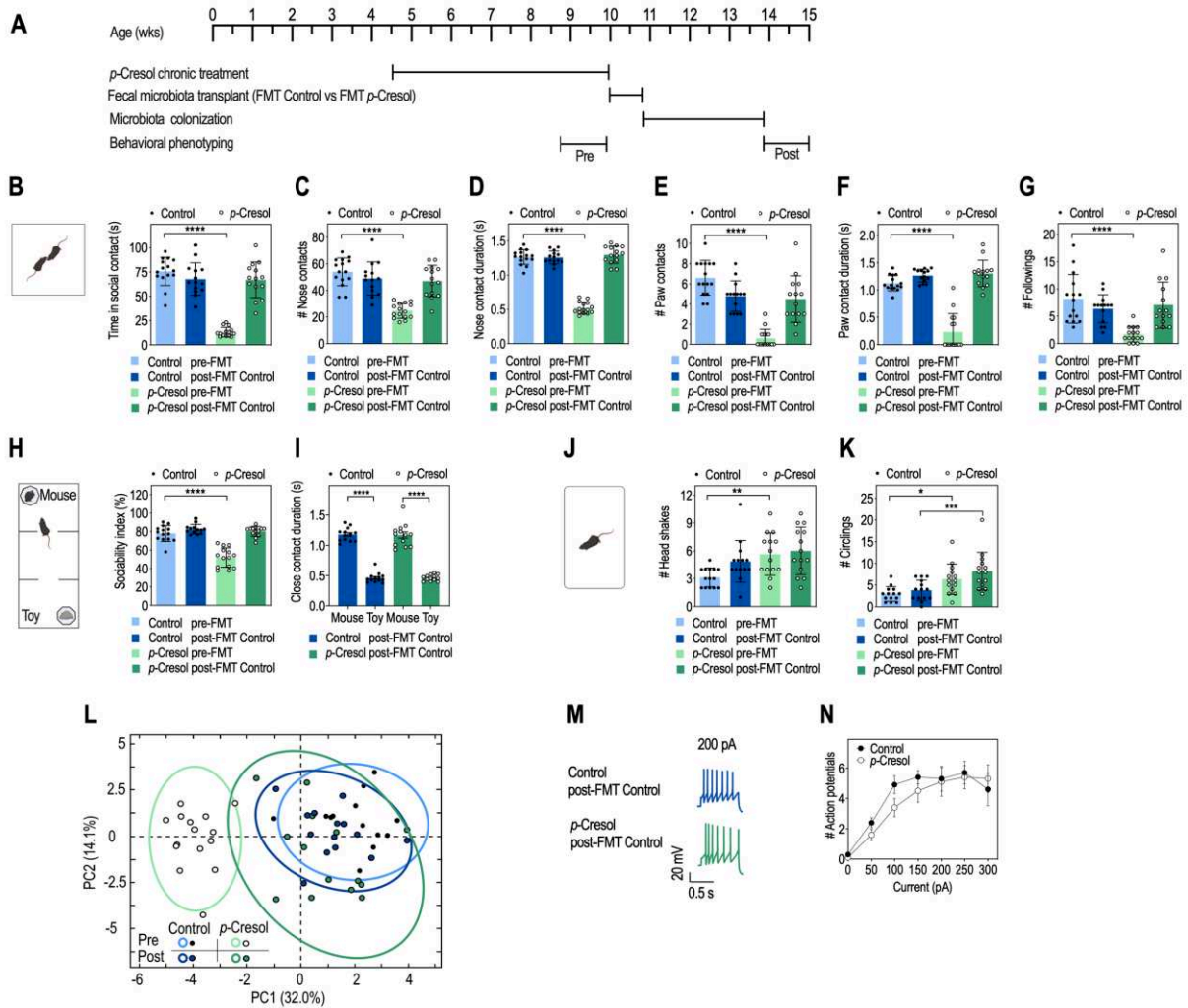


**Figure 4. Transfer of microbiota from control mice to *p*-Cresol-treated mice restores social behavior deficits and VTA dopamine neurons excitability**

(A) Timeline of the fecal microbiota transplant (FMT) experiment of fecal slurry from control donor mice to control or *p*-Cresol-treated recipient mice.

(B-G) Dyadic social interaction test (n=15/group pre-FMT, n=14/group post-FMT)

(B) Total time spent in social contact; 2-way ANOVA:  $p(\text{Treatment}) < 0.0001$ ,  $p(\text{FMT Control}) < 0.0001$ ,  $p(\text{Treatment} \times \text{FMT Control}) < 0.0001$ ; Šidák's post-hoc tests for treatment effect: \*\*\*\* $p < 0.0001$  for pre-FMT Control groups,  $p > 0.05$  for post-FMT Control groups

(C) Number of nose contacts; 2-way ANOVA:  $p(\text{Treatment}) < 0.0001$ ,  $p(\text{FMT Control}) = 0.0022$ ,  $p(\text{Treatment} \times \text{FMT Control}) < 0.0001$ ; Šidák's post-hoc tests for treatment effect: \*\*\*\* $p < 0.0001$  for pre-FMT Control groups,  $p > 0.05$  for post-FMT Control groups

(D) Mean duration of each nose contact; 2-way ANOVA:  $p(\text{Treatment}) < 0.0001$ ,  $p(\text{FMT Control}) < 0.0001$ ,  $p(\text{Treatment} \times \text{FMT Control}) < 0.0001$ ; Šidák's post-hoc tests for treatment effect: \*\*\*\* $p < 0.0001$  for pre-FMT Control groups,  $p > 0.05$  for post-FMT Control groups

(E) Number of paw contacts; 2-way ANOVA:  $p(\text{Treatment}) < 0.0001$ ,  $p(\text{FMT Control}) = 0.0221$ ,  $p(\text{Treatment} \times \text{FMT Control}) < 0.0001$ ; Šidák's post-hoc tests for treatment effect: \*\*\*\* $p < 0.0001$  for pre-FMT Control groups,  $p > 0.05$  for post-FMT Control groups

(F) Mean duration of each paw contact; 2-way ANOVA:  $p(\text{Treatment}) < 0.0001$ ,  $p(\text{FMT Control}) < 0.0001$ ,  $p(\text{Treatment} \times \text{FMT Control}) < 0.0001$ ; Šidák's post-hoc tests for treatment effect: \*\*\*\* $p < 0.0001$  for pre-FMT Control groups,  $p > 0.05$  for post-FMT Control groups

(G) Number of followings; 2-way ANOVA:  $p(\text{Treatment}) = 0.0020$ ,  $p(\text{FMT Control}) = 0.0516$ ,  $p(\text{Treatment} \times \text{FMT Control}) = 0.0002$ ; Šidák's post-hoc tests for treatment effect: \*\*\*\* $p < 0.0001$  for pre-FMT Control groups,  $p > 0.05$  for post-FMT Control groups

(H, I) 3-chamber test ( $n=15/\text{group pre-FMT}$ ,  $n=14/\text{group post-FMT}$ ):

(H) Sociability index; 2-way ANOVA:  $p(\text{Treatment}) = 0.0004$ ,  $p(\text{FMT Control}) < 0.0001$ ,  $p(\text{Treatment} \times \text{FMT Control}) = 0.0032$ ; Šidák's post-hoc tests for treatment effect: \*\*\*\* $p < 0.0001$  for pre-FMT Control groups,  $p > 0.05$  for post-FMT Control groups

(I) Mean duration of each nose contact with the mouse interactor or toy mouse; 2-way ANOVA:  $p(\text{FMT Control}) = 0.9067$ ,  $p(\text{Mouse-Toy}) < 0.0001$ ,  $p(\text{FMT Control} \times \text{Mouse-Toy}) = 0.8713$ ; Šidák's post-hoc tests for Mouse vs. Toy preference: \*\*\*\* $p < 0.0001$ .

(J, K) Motor stereotypies ( $n=15/\text{group pre-FMT}$ ,  $n=15/\text{group post-FMT}$ ).

(J) Number of head shakes; 2-way ANOVA:  $p(\text{Treatment}) = 0.0021$ ,  $p(\text{FMT Control}) = 0.0715$ ,  $p(\text{Treatment} \times \text{FMT Control}) = 0.2334$ ; Šidák's post-hoc tests for treatment effect: \*\* $p < 0.01$  for pre-FMT Control groups,  $p > 0.05$  for post-FMT Control groups.

(K) Number of circling events; 2-way ANOVA:  $p(\text{Treatment}) < 0.0001$ ,  $p(\text{FMT Control}) = 0.1133$ ,  $p(\text{Treatment} \times \text{FMT Control}) = 0.5555$ ; Šidák's post-hoc tests: \* $p < 0.05$  for pre-FMT Control groups, \*\*\* $p < 0.001$  for post-FMT Control groups.

(L) PCA plots of behavioral scores recorded in the dyadic social interaction and direct monitoring of motor stereotypies (Figure 4B-G, J, K, Supplementary Figure 6I-L); ellipses of the 95% confidence intervals are indicated for each group ( $n=15/\text{group pre-FMT}$ ,  $n=14/\text{group post-FMT}$ ).

(M, N) Electrophysiological recordings of dopamine neurons activity in the VTA post-FMT Control:

(M) Representative traces of dopamine neurons activity in patch-clamp experiments performed post-FMT Control after a 200pA current injection

(N) Number of action potentials evoked by different current injection steps (n=3 animals/group, 10 cells recorded/group); 2-way ANOVA:  $p(\text{Treatment})=0.5474$ ,  $p(\text{Current})<0.0001$ ,  $p(\text{Treatment} \times \text{Current})=0.3640$ ; Šidák's post hoc tests for treatment effect:  $p>0.05$ .

(B-K) Data are presented as dot-plots featuring means  $\pm$  SD. (N) Data are presented as means  $\pm$  SD.

**Table 1. The abundance of bacterial OTU discriminating p-Cresol-treated mice from control mice correlate with social behavior/stereotypies scores.** Spearman's rank  $\rho$  correlation coefficients are annotated and color-coded: positive correlations (red), negative (blue). LEfSE score and associated p-value are also reported for each OTU. Only significant correlations are displayed (FDR-adjusted p-value < 0.05). \*, p<0.05; \*\*, p<0.01; \*\*\*, p<0.001; \*\*\*\*, p<0.0001 (n=30 animals: n=15 Control, n=15 p-Cresol). See also Supplementary Table 1 for complete LefSE analysis and Supplementary Table 2 for complete correlation analysis.

Taxonomy								LEfSE metrics		$\rho$ coefficients: OTU abundance-behavioral score											
										Social interaction					Stereotypies						
Phylum	Class	Order	Family	Genus	Species	OTU	Log <sub>10</sub> LDA score	p-val.	Social contact time (s)	# Paw contacts	Paw contact duration (s)	# Nose Contacts	Nose contact duration (s)	# Followings	# Head shakes	# Circlings					
p-Cresol	Bacteroidetes	Bacteroidia	Bacteroidales	Muribaculaceae	Unknown	Unknown	13	3.69	****	-0.57	-0.53	-0.55	-0.55								
					Unknown	Unknown	33	3.26	*	-0.62	-0.56	-0.52	-0.55	-0.57							
					Unknown	Unknown	809	2.80	*	-0.53		-0.508									
	Firmicutes	Clostridia	Clostridiales	Peptococcaceae	Unknown	Unknown	710	2.42	*		-0.49	-0.38		-0.41							
Control	Bacteroidetes	Bacteroidia	Bacteroidales	Muribaculaceae	Unknown	Unknown	838	-2.60	**				0.58								
	Firmicutes	Clostridia	Clostridiales	Clostridiales vadinBB60	Lachnospiraceae	Unknown	Unknown	45	-2.68	*	0.53										
						Blautia	Unknown	827	-2.41	**			0.61				-0.57				
						Unknown	Unknown	123	-3.15	**			0.58		0.55						
						Lachnospiraceae NK4A136	Unknown	497	-2.22	*				0.53							
						Unknown	Unknown	28	-3.84	**	0.53				0.52						
						Lachnospiraceae UCG006	Unknown	635	-2.18	**					0.54						
						Marvinbryantia	Unknown	1039	-2.48	*	0.57				0.55						
						Unknown	Unknown	409	-2.41	***	0.63	0.65	0.64	0.64	0.55	0.62					
						Unknown	Unknown	1909	-2.44	**	0.58	0.52	0.59		0.60						
						Unknown	Unknown	311	-2.50	*		0.53		0.59							
						Unknown	Unknown	375	-2.51	**	0.51				0.51	0.51					
						Unknown	Unknown	364	-2.68	***	0.57		0.60		0.65						
						Unknown	Unknown	39	-3.66	*	0.53				0.53						
									Ruminococcaceae	Ruminiclostridium	Unknown	570	-2.11	*	0.57		0.507		0.56		
										Unknown	Unknown	1354	-2.42	**	0.58	0.55	0.57		0.61		
				Ruminococcaceae UCG014	Unknown	332	-2.40	**	0.56												
				Unknown	341	-2.58	****	0.54	0.58	0.59		0.58									
				UBA1819	Multiaffiliation	268	-2.80	****	0.69	0.54	0.54	0.60	0.68								
				Unknown	Unknown	452	-2.40	*	0.51			0.55		0.55							
				Unknown	Unknown	317	-2.49	****	0.64	0.63	0.74		0.72		-0.62						
	Proteobacteria	Gammaproteobacteria	Betaproteobacteriales	Burkholderiaceae	Parasutterella	Unknown	321	-2.43	**	0.53				0.51							

## **SUPPLEMENTARY INFORMATION**

### **The microbial metabolite *p*-Cresol induces autistic-like behaviors in mice by remodeling the gut microbiota**

Microbial *p*-Cresol induces autistic-like behaviors in mice

Bermudez-Martin, P., Becker, J. A., Fernandez, S. P., Costa-Campos, R., Barbosa, S., Martinez-Gili, L., Myridakis, A., Dumas, M.-E., Bruneau, A., Cherbuy, C., Langella, P., Chabry, J., Barik, J., Le Merrer, J., Glaichenhaus, N., Davidovic, L.

#### **Supplementary information provided:**

Supplementary Materials and Methods

Supplementary figures and supplementary figures legends (6)

Supplementary tables legends (3)

## Supplementary Materials and Methods

**Ethical considerations.** Animal housing and experimentation were conducted in facilities certified by regional authorities (Direction Départementale de Protection des Populations des Alpes-Maritimes, accreditation #EC-06-152-5). The procedures involved in this study were approved by the local ethics committee for animal experimentation (Ciepal-Azur) and the Ministère de l'Enseignement Supérieur et de la Recherche, in agreement with the European Communities Council Directive (2010/63EU) for animal experiments.

**Animals treatment.** Weaned C57BL/6J mice (21 to 28 day-old) were ordered to Charles Rivers (France). This developmental stage was chosen to avoid confounding effects of maternal exposure to *p*-Cresol, while still being in the time window for late neurodevelopment during which the microbiota-gut-brain axis can intervene<sup>1</sup>. Since the sex ratio for ASD is biased towards 3 males diagnosed for 1 female suggesting a higher susceptibility of males<sup>2 3</sup>, only males were considered in this study. Animals were randomly assigned to experimental groups and housed in medium-size (up to 5 animals) open cages filled with wooden bedding, one plastic house and nesting material for enrichment, in a temperature-(22-24°C) and hygrometry- (70-80%) controlled room, under 12 hours light–dark cycle (8:00 a.m.- 8:00 p.m.). Mice had *ad libitum* access to water and standard chow (reference 4RF25, Mucedola). Mice were habituated for 6 days to our animal facility before starting treatment with *p*-Cresol (reference W233706-SAMPLE-K, Sigma-Aldrich) dispensed in sterile drinking water at a concentration of 0.25 g/L. Bottles were renewed twice weekly. This amounts in adult mice to a dose of 50mg/Kg/24 h based on a mean body mass of 25 g and a mean drinking water consumption of 5mL/24 h. This dose per day corresponded to 7 times less the reported LD50 dose of 350mg/Kg for acute oral administration of *p*-Cresol by

gavage in mice, based on available toxicity data<sup>4</sup>. Body weight, consumption of water and chow were monitored weekly.

**Quantification of *p*-Cresol in urine and serum by gas chromatography coupled to mass spectrometry (GC-MS).** Mice were individually placed in a clean empty plastic cage and urine was collected over 10 min and centrifuged (12 000 g, 5 min). The supernatant was snapped-frozen in liquid nitrogen and stored at -80°C. Blood was collected by cardiac puncture, transferred in Eppendorf tubes and allowed to clot on bench RT for 30 min. After centrifugation (12000g, 10 min, RT), serum was collected, snapped-frozen in liquid nitrogen and stored at -80°C. Prior to gas chromatography-mass spectrometry (GC-MS), urine (20 µL) and serum (100 µL) samples were prepared as follows: i) samples were spiked with 10 µL internal standard solution (myristic acid-d<sub>27</sub> in isopropanol, 750 mg/mL), ii) 850 µL of ice cold methanol were added, followed by centrifugation for 20 min (4°C, 16000 g), iii) 750 µL of supernatants were transferred to silanized dark 2mL autosampler vials and evaporated to dryness in a rotational vacuum concentrator (45°C, 20 mbar, 2 h), iv) 50 µL of methoxyamine solution (2% in pyridine) were added and the samples were incubated overnight at R, and v) 100 µL of N-methyl-trimethylsilyl-trifluoroacetamide (MSTFA)+1%,trimethylchlorosilane (TMCS) solution were added, the samples were incubated at 60°C for 1 h and transferred to dark autosampler vials with 250 µL silanized inserts. The detailed instrumental conditions for GC-MS analysis were based on a previous study<sup>5</sup>, with minor modifications to quantify *p*-Cresol. Briefly, the samples were analyzed in an Agilent 7890B-5977B Inert Plus GC-MS system. Two µL of each sample were injected in a split inlet (1:10 ratio). The chromatographic column was an Agilent ZORBAX DB5- MS (30 m X 250 µm X 0.25 µm + 10m, Duraguard). The temperature gradient was 37.5 min long and the mass analyzer was operated in full scan mode between 50-600 m/z. Blank and pooled quality control (QC) samples in

several dilutions were included in the analysis to ensure that the measurements were reproducible. There was no external contaminations and the monitored analytes were responding linearly to the detector.

## **Behavioral testing**

Behavioral phenotyping started after a 4-week treatment with *p*-Cresol and lasted for 1-2 weeks during which treatment was continued. All behavioral experiments were performed during the day. The animals followed multiple behavioral tests respecting their resting hours, with a minimum of 2 days between tests. Standard behavioral tests that have extensively been used to characterize genetic and environmental models of ASD<sup>6-10</sup> were implemented to assess the behavioral dimensions impacted in ASD.

### ***Social abilities***

*Three-chamber sociability test.* The stimulus mouse was habituated to the cylindrical cages (20 min sessions, repeated 3 days before the testing day). The apparatus consisted in a rectangular non-transparent plexiglass box (60x30cm), divided in three compartments (object chamber, empty chamber and unfamiliar mouse chamber) connected by open doors (4 cm width) to allow the mouse to move freely between the different compartments. The unfamiliar mouse or the toy mouse were placed in wired cylindrical cages. The test consisted in a habituation phase to the empty apparatus only in the presence of empty cylindrical cages during 5 min and a sociability phase where the unfamiliar mouse or the toy mouse is introduced in the cylindrical cages. Time spent in the 2 chambers were video-tracked over 10 min and analyzed *a posteriori* during the habituation and sociability phase using the ANY-maze software. The number and the time spent in close contact with each of the empty cylindrical cage (during the habituation phase) as well as with the stimulus mouse or with the toy mouse contained in wired cylindrical cage (during the sociability phase) were manually scored by an experienced experimenter blind to the experimental group. The mean duration of close contacts was calculated from these data<sup>7, 11-13</sup>. The relative position of stimulus unknown mouse (versus mouse toy) was counterbalanced between groups.

There was no bias in chamber preference, empty cylindrical cages preference or interaction ratio during the habituation phase (Supplementary Figure 2A-E, Supplementary Figure 6A-E).

*Dyadic social interactions.* Direct social interactions were recorded in open-field arena with a low light intensity (15 Lux). After a 3 min. habituation period, the subject mouse was put in presence with an unfamiliar sex- and age-matched interactor and their interaction was recorded for 10 min. Manual scoring by an experienced experimenter blind to the experimental group was performed *a posteriori* by recording time spent in social contact events, number of nose and paw contacts, time spent in nose and paw contact, number and time spent in self-grooming, number of self-grooming events after social contact, number of rearing and grooming events, number of circling episodes and head shakes. The mean duration of nose and paw contacts was calculated from these data<sup>7, 11-13</sup>.

### ***Stereotypic/perseverative behaviors***

*Motor stereotypies.* The subject mouse was placed in a clean standard home cage (21x11x17 cm) covered with a thick layer of fresh sawdust (4 cm) and recorded for 10 min with light intensity set at 40 Lux. Manual scoring by an experienced experimenter blind to the experimental group was performed *a posteriori* by computing the number of events of head shake, rearing, digging, grooming, circling episodes and total time spent digging and grooming<sup>6</sup>.

*Marble burying test.* Marble burying was used as a measure of perseverative behavior<sup>14</sup>. The subject mouse was placed in a clean standard home cage (21x11x17 cm) filled with 4 cm of fresh sawdust on which 20 glass marbles (diameter 1,5 cm) were disposed with light intensity set at 40 Lux. The number of marbles buried (more

than half of its surface outside of sawdust) during a 30 min session was monitored by an experienced experimenter blind to the experimental group<sup>6</sup>.

*Y maze spontaneous alternation task.* Spontaneous alternation behavior was used to assess behavioral flexibility and perseveration<sup>15-17</sup>. The apparatus consisted in three arms made of plexiglass (40x9x16cm) containing different symbols to be differentiated. We placed the mice in the centre and allowed it to explore the arms for 5 min with a low light intensity of 15 Lux. We measured the willingness of mice to explore new environments and we scored different patterns as spontaneous alternation (SPA), alternate arm returns (AAR) and same arm return (SAR). We then calculated the percentage of SPA, AAR and SAR<sup>6, 18</sup>.

### ***Locomotor activity***

*Actimetry.* The measurement of individual spontaneous activity was performed in actimetry chambers (Imetronic) consisting of cages equipped with infrared beams able to detect in real time horizontal and vertical movements (rearing events). Animals were individually placed in actimetry chambers under a 12-hr light/dark cycle, with free access to food and drinking water. To avoid biases in measurements due to stress possibly inducing hyperlocomotion in a novel environment, a habituation period (Day 0: 11:00 p.m. - Day 1: 8:00 a.m.) preceded the 24 h-recording of horizontal activity (Day 1: 8:00 a.m. – Day 2: 8:00 a.m.)<sup>8</sup>.

### ***Anxiety***

*Open field test.* Mice were individually placed in the corner of a white and opaque quadratic arena (40x40cm) and allowed to explore for 10 min under low illumination (40 Lux). Total distance travelled, time spent in center and number center entries were analyzed by videotracking using the ANY-Maze software<sup>8,9</sup>.

*Novelty suppressed feeding test.* Mice were food-deprived for 16 h, with unlimited access to drinking water. A pellet of food was positioned in the centre of an open-field covered with 1 cm of sawdust with light intensity set at 60 Lux. The subject mouse was then introduced in a corner of the arena and the latency (s) for the first bite in the pellet recorded. Immediately after the test, the animal was placed in a clean cage with *ad libitum* access to food and water<sup>6, 18</sup>.

### **Cognition**

*Novel object recognition test.* The novel object recognition test was performed in a rectangular arena (20cmx40cm). The test consisted of three sessions under constant light intensity (15 Lux). During the habituation session, the mice explored freely the empty arena for 5 min. For the training session, two identical objects were placed on each side of the arena and the mouse allowed to explore for 10 min. For the test session, one of the objects was replaced by a novel object and the mouse allowed to explore the objects for 10 min. The time spent exploring the familiar and novel objects by the subject animal were manually scored *a posteriori* on videorecordings of the sessions. A recognition index was calculated as the percentage of the time spent exploring the novel object over the total time spent exploring both objects<sup>19</sup>.

### **Ex vivo patch-clamp electrophysiological recordings**

Electrophysiological recordings were performed on sub-groups of control or *p*-Cresol-treated which had not been subjected to behavioral tests but nevertheless belonged to larger cohorts in which behavioral impairments in the *p*-Cresol group were observed. Mice were anesthetized (Ketamine (150 mg/kg)/ Xylazine (10 mg/kg), transcardially perfused with artificial cerebrospinal fluid (aCSF solution: NaCl 119 mM, KCl 2.5 mM, NaH<sub>2</sub>PO<sub>4</sub> 1.25 mM, MgSO<sub>4</sub> 1.3 mM, CaCl<sub>2</sub> 2.5 mM, NaHCO<sub>3</sub> 26 mM, glucose 11 mM). Brains were removed from skull and sliced sagittally in 250 µm sections using a

HM650V vibratome (Microm, France). Sections encompassing VTA were placed in ice-cold cutting solution (KCl 2.5 mM, NaH<sub>2</sub>PO<sub>4</sub> 1.25 mM, MgSO<sub>4</sub> 10 mM, CaCl<sub>2</sub> 0.5 mM, glucose 11 mM, sucrose 234 mM, NaHCO<sub>3</sub> 26 mM) bubbled with 95% O<sub>2</sub>/5% CO<sub>2</sub>. Slices were then incubated in aCSF at 37°C for 1 h, and then kept at room temperature. For recordings, sections were transferred in a thermo-controlled (32-34°C) recording chamber superfused with aCSF (2.5 ml/min). Spontaneous excitatory post-synaptic currents (sEPSCs) or excitability were measured using visualized whole-cell voltage-clamp and current-clamp recordings, respectively, using an upright microscope (Olympus France). Putative dopamine neurons were identified as previously described<sup>20</sup>. Current-clamp recordings were performed using a Multiclamp 700B device (Molecular Devices, Sunnyvale, CA). Signals were collected and stored using a Digidata 1440A converter and pCLAMP 10.2 software (Molecular Devices, CA). In all cases, access resistance was monitored by a step at -10 mV (0.1 Hz) and experiments were discarded if the access resistance increased more than 20%. Internal solution (K-D-gluconate 135 mM, NaCl 5 mM, MgCl<sub>2</sub> 2 mM, HEPES 10 mM, EGTA 0.5 mM, MgATP 2 mM, NaGTP 0.4 mM). Depolarizing (0-300 pA) or hyperpolarizing (0- 450 pA) 800 ms current steps were used to assess excitability and membrane properties of VTA dopamine neurons. sEPSCs were assessed in voltage-clamp mode at a voltage of -65mV in the presence of picrotoxin (50 µM) using the same internal solution. Off-line analyzes were performed using Clampfit 10.2 (Axon Instruments, USA).

### **Fecal microbiota analysis by 16S rRNA gene sequencing**

*Fecal DNA sample preparation.* Mice were individually placed for 10 min. in a sterile empty plastic cage, and feces were collected in Eppendorf tubes in the morning (10-11 a.m.), snapped-frozen in liquid nitrogen and stored at -80°C until further use. Genomic DNA was obtained from fecal samples using the QIAamp power fecal DNA kit

(Qiagen), and DNA quantity was determined using a TECAN Fluorometer (Qubit® dsDNA HS Assay Kit, Molecular Probes).

*16S sequencing.* The V3-V4 hypervariable region of the 16S rRNA gene was amplified by PCR using the following primers: a forward primer 5'-**CTT TCC CTA CAC GAC GCT CTT CCG ATC TAC** GGR AGG CAG CAG-3 (28-nt illumina adapter (in bold) followed the 14 nt broad range bacterial primer 343F) and a reverse primer 5'-**GGA GTT CAG ACG TGT GCT CTT CCG ATC** TTA CCA GGG TAT CTA ATC CT-3' (28-nt illumina adapter (in bold) followed by the 19 nt broad range bacterial primer 784R). The PCR reaction used 10 ng of fecal DNA as template, 0.5 µM primers, 0.2 mM dNTP, and 0.5 U of the DNA-free Taq-polymerase (MolTaq 16S, Molzym, Bremen, Germany). The amplifications were carried out using the following profile: 1 cycle at 94°C for 60 s, followed by 30 cycles at 94°C for 60 s, 65°C for 60 s, 72°C for 60 s, and finishing with a step at 72°C for 10 min. The PCR reactions were sent to the @Bridge platform (INRAe, Jouy-en-Josas, france) for sequencing (Illumina Miseq technology). Single multiplexing was performed using home-made 6 bp index, which were added to R784 during a second PCR with 12 cycles using forward primer (AAT GAT ACG GCG ACC ACC GAG ATC TAC ACT CTT TCC CTA CAC GAC) and reverse primer (CAA GCA GAA GAC GGC ATA CGA GAT-index-GTG ACT GGA GTT CAG ACG TGT). The resulting PCR products were purified and loaded onto the Illumina MiSeq cartridge according to the manufacturer instructions. Run quality was checked internally using PhiX, and sequences assigned to the corresponding based on the 6 pb index.

*Sequence analysis.* High-quality filtered reads were assembled and processed using FROGS pipeline (Find Rapidly OTU with Galaxy Solution) to obtain OTUs and their respective taxonomic assignment thanks to Galaxy instance (<https://migale.inra.fr/galaxy>)<sup>21</sup>. Paired-end sequences were merged using Flash software using at least a 10 bp overlap between the forward and reverse sequences. Then, merged sequence were pre-filtered on the following criteria (amplicons size,

presence of the 2 primers sequences, ambiguous base), yielding < 4,106 reads. The following successive steps involved de-noising and clustering of the sequences into OTUs using SWARM, chimera removal using VSEARCH yielding 21,616 clusters (< 3,106 reads). Then, cluster abundances were filtered at 0.005%, yielding 591 final clusters. Clusters were then affiliated to OTU by using a Silva123 16S reference database and the RDP (Ribosomal Database Project) classifier taxonomic assignment procedure. Taxa abundance table obtained for the dataset shows the sum of OTU abundances in each sample.

*Statistical analysis.* Richness and diversity indexes of bacterial community, as well as clustering and ordinations, were computed using the Phyloseq package (v 1.19.1) in RStudio software<sup>22</sup>. Within sample community composition ( $\alpha$ -diversity) was assessed by observed diversity (i.e. sum of unique OTUs per sample), Chao1 and Shannon index, as well as evenness-based Simpson's richness index. Divergence in community composition between samples was quantitatively assessed by calculating  $\beta$ -diversity index using Jaccard's distances matrix. Statistical difference in the microbial communities between groups were evaluated using constrained analysis of principal coordinates (PCoA) and permutational multivariate ANOVA (PERMANOVA). To identify discriminating taxa and OTU associated with the Control or *p*-Cresol class and estimate their effect size, we used the linear discriminant analysis (LDA) effect size (LEfSe) method implemented in Galaxy<sup>23</sup>.

### **Fecal matter transplantation (FMT)**

Since antibiotic treatment impacts the behavior of rodents<sup>24</sup>, we opted for an FMT procedure which did not include an antibiotic treatment step to deplete endogenous microbiota. Instead, we used a laxative treatment that was previously shown to efficiently deplete endogenous microbiota and favor the engraftment of the transplanted microbiota<sup>25</sup>.

For induction experiments (Figure 4), recipient C57BL/6J mice were received at 3 weeks of age and habituated for 5 days to our facility. From Day 1 to 3, mice were gavaged with omeprazole (Esomeprazole, Biogaran, 50mg/Kg/24 h) each morning to lower gastric acidity and favor survival of the inoculum. In the evening of Day 3, food was removed, but mice had *ad libitum* access to water. On Day 4, mice received 5 consecutive gavages of 200 $\mu$ L of Moviprep reconstituted as recommended by the manufacturer (Norgine SAS, Rueil-Malmaison, France) at 1 hr 30 min intervals. On Day 5, mice were gavaged with omeprazole. The FMT inoculum was prepared by pooling individual fecal pellets from n=15 control or n=15 *p*-Cresol treated and behaviorally phenotyped donor mice. Fecal pools were then weighted and homogenized in ice-cold ddH<sub>2</sub>O (weight:volume=1:50). Fecal slurry was filtered over a 70  $\mu$ m mesh to remove fibers and clogs. Recipient mice received 3 consecutive gavages of 200  $\mu$ L of the filtered fecal slurry at 2 h intervals. After the last gavage, mice were returned to clean cages with *ad libitum* access to food and water. Body weight was monitored on Day 4, 5 and 7 to verify that the mice recovered from the FMT procedure. Three weeks post FMT, mice were subjected to behavioral tests two days apart in the following order: dyadic social interactions and motor stereotypies.

For rescue experiments (Figure 5), mice were treated with *p*-Cresol for 4 wks as described in the animal treatment section, subjected to behavioral tests two days apart in the following order: direct social interactions, motor stereotypies and three-chamber test. Control and *p*-Cresol-treated mice were then subjected to the FMT procedure

described above. The FMT inoculum was prepared by pooling individual fecal pellets from n=15 control donor untreated mice of the same age and sex. Three weeks post FMT, mice were subjected to behavioral tests two days apart in the following order: direct social interactions, motor stereotypies and three-chamber test. The *ex vivo* electrophysiological recordings were also performed three weeks post FMT on parallel sub-groups of mice which were not subjected to behavioral testing.

## **Statistics**

Comparisons between two groups were performed using 2-tailed unpaired Mann-Whitney's non-parametric U-test. Multiple group comparisons were performed using two-way ANOVA with factors stated in legends and text. Prior to ANOVA, normality of data was assessed using Kolmogorov-Smirnov's test. *Post hoc* comparisons were performed using Šidák's correction for multiple comparison. Detailed ANOVA statistics for each panel are provided in Supplementary Table 3. For comparison analysis of frequency distributions, Kolmogorov-Smirnov's test was used. Principal Component Analysis (PCA) of behavioral data was performed for each dataset consisting of scores from the dyadic social interaction test and scores from the direct monitoring of motor stereotypies using the webtool Clustvis<sup>26</sup>. Correlations between microbial OTU abundances and behavioral scores were performed using Spearman's  $\rho$  correlation coefficient rank test with Benjamini-Hochberg's multiple testing correction. Statistical significance was set according to a two-tailed p-value or adjusted (if relevant) p-value(p)<0.05. Only significant differences are displayed on the graphs.

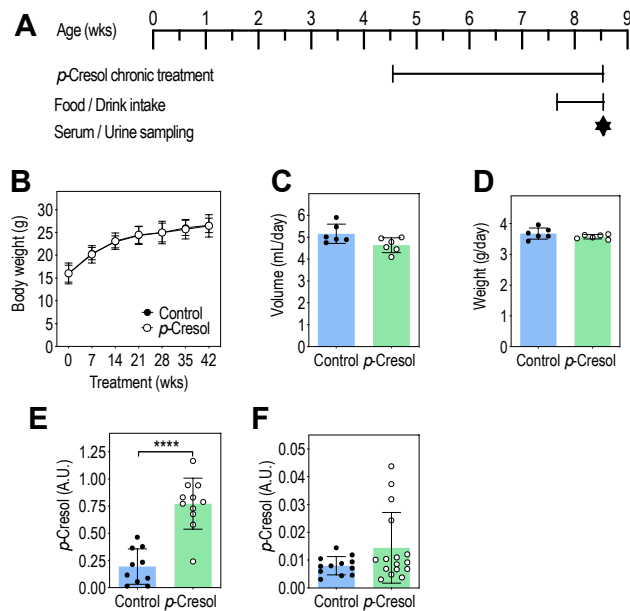
## SUPPLEMENTARY REFERENCES

1. Borre YE, O'Keeffe GW, Clarke G, Stanton C, Dinan TG, Cryan JF. Microbiota and neurodevelopmental windows: implications for brain disorders. *Trends Mol Med* 2014; **20**(9): 509-518.
2. Loomes R, Hull L, Mandy WPL. What Is the Male-to-Female Ratio in Autism Spectrum Disorder? A Systematic Review and Meta-Analysis. *J Am Acad Child Adolesc Psychiatry* 2017; **56**(6): 466-474.
3. Wayne MMY, Cheng HY. Genetics and epigenetics of autism: A Review. *Psychiatry Clin Neurosci* 2017.
4. Lewis RJ, Sax NI. Sax's Dangerous Properties of Industrial Materials. 11th Edition edn. Hoboken, N.J.; J. Wiley & Sons: Hoboken, NJ, USA, 2004, p 1004.
5. Fiehn O. Metabolomics by Gas Chromatography-Mass Spectrometry: Combined Targeted and Untargeted Profiling. *Curr Protoc Mol Biol* 2016; **114**: 30 34 31-30 34 32.
6. Becker JA, Clesse D, Spiegelhalter C, Schwab Y, Le Merrer J, Kieffer BL. Autistic-like syndrome in mu opioid receptor null mice is relieved by facilitated mGluR4 activity. *Neuropsychopharmacology* 2014; **39**(9): 2049-2060.
7. Pujol CN, Pellissier LP, Clement C, Becker JAJ, Le Merrer J. Back-translating behavioral intervention for autism spectrum disorders to mice with blunted reward restores social abilities. *Transl Psychiatry* 2018; **8**(1): 197.
8. Leboucher A, Bermudez-Martin P, Mouska X, Amri EZ, Pisani DF, Davidovic L. Fmr1-Deficiency Impacts Body Composition, Skeleton, and Bone Microstructure in a Mouse Model of Fragile X Syndrome. *Front Endocrinol (Lausanne)* 2019; **10**: 678.
9. Silverman JL, Yang M, Lord C, Crawley JN. Behavioural phenotyping assays for mouse models of autism. *Nature reviews Neuroscience* 2010; **11**(7): 490-502.

10. Becker JAJ, Kieffer BL, Le Merrer J. Differential behavioral and molecular alterations upon protracted abstinence from cocaine versus morphine, nicotine, THC and alcohol. *Addict Biol* 2017; **22**(5): 1205-1217.
11. Matsuo N, Tanda K, Nakanishi K, Yamasaki N, Toyama K, Takao K *et al.* Comprehensive behavioral phenotyping of ryanodine receptor type 3 (RyR3) knockout mice: decreased social contact duration in two social interaction tests. *Front Behav Neurosci* 2009; **3**: 3.
12. Katayama Y, Nishiyama M, Shoji H, Ohkawa Y, Kawamura A, Sato T *et al.* CHD8 haploinsufficiency results in autistic-like phenotypes in mice. *Nature* 2016; **537**(7622): 675-679.
13. Spencer CM, Alekseyenko O, Serysheva E, Yuva-Paylor LA, Paylor R. Altered anxiety-related and social behaviors in the Fmr1 knockout mouse model of fragile X syndrome. *Genes Brain Behav* 2005; **4**(7): 420-430.
14. Thomas A, Burant A, Bui N, Graham D, Yuva-Paylor LA, Paylor R. Marble burying reflects a repetitive and perseverative behavior more than novelty-induced anxiety. *Psychopharmacology (Berl)* 2009; **204**(2): 361-373.
15. Moustgaard A, Hau J, Lind NM. Effects of dopamine D4 receptor antagonist on spontaneous alternation in rats. *Behav Brain Funct* 2008; **4**: 49.
16. Le Marec N, Ethier K, Rompre PP, Godbout R. Involvement of the medial prefrontal cortex in two alternation tasks using different environments. *Brain Cogn* 2002; **48**(2-3): 432-436.
17. Delotterie D, Ruiz G, Brocard J, Schweitzer A, Roucard C, Roche Y *et al.* Chronic administration of atypical antipsychotics improves behavioral and synaptic defects of STOP null mice. *Psychopharmacology (Berl)* 2010; **208**(1): 131-141.
18. Meirsman AC, Le Merrer J, Pellissier LP, Diaz J, Clesse D, Kieffer BL *et al.* Mice Lacking GPR88 Show Motor Deficit, Improved Spatial Learning, and Low Anxiety Reversed by Delta Opioid Antagonist. *Biol Psychiatry* 2016; **79**(11): 917-927.

19. Fernandez SP, Muzerelle A, Scotto-Lomassese S, Barik J, Gruart A, Delgado-Garcia JM *et al.* Constitutive and Acquired Serotonin Deficiency Alters Memory and Hippocampal Synaptic Plasticity. *Neuropsychopharmacology* 2017; **42**(2): 512-523.
20. Fernandez SP, Broussot L, Marti F, Contesse T, Mouska X, Soiza-Reilly M *et al.* Mesopontine cholinergic inputs to midbrain dopamine neurons drive stress-induced depressive-like behaviors. *Nat Commun* 2018; **9**(1): 4449.
21. Escudie F, Auer L, Bernard M, Mariadassou M, Cauquil L, Vidal K *et al.* FROGS: Find, Rapidly, OTUs with Galaxy Solution. *Bioinformatics* 2018; **34**(8): 1287-1294.
22. McMurdie PJ, Holmes S. Phyloseq: a bioconductor package for handling and analysis of high-throughput phylogenetic sequence data. *Pac Symp Biocomput* 2012: 235-246.
23. Segata N, Izard J, Waldron L, Gevers D, Miropolsky L, Garrett WS *et al.* Metagenomic biomarker discovery and explanation. *Genome Biol* 2011; **12**(6): R60.
24. Desbonnet L, Clarke G, Traplin A, O'Sullivan O, Crispie F, Moloney RD *et al.* Gut microbiota depletion from early adolescence in mice: Implications for brain and behaviour. *Brain Behav Immun* 2015; **48**: 165-173.
25. Le Roy T, Debedat J, Marquet F, Da-Cunha C, Ichou F, Guerre-Millo M *et al.* Comparative Evaluation of Microbiota Engraftment Following Fecal Microbiota Transfer in Mice Models: Age, Kinetic and Microbial Status Matter. *Front Microbiol* 2018; **9**: 3289.
26. Metsalu T, Vilo J. ClustVis: a web tool for visualizing clustering of multivariate data using Principal Component Analysis and heatmap. *Nucleic acids research* 2015; **43**(W1): W566-570.

## Supplementary figures and supplemental figures legends (6)



### Supplementary Figure 1. *p*-Cresol treatment does not impact general physiological parameters, increases urinary *p*-Cresol excretion but not its circulating levels

(A) Timeline of the experiment

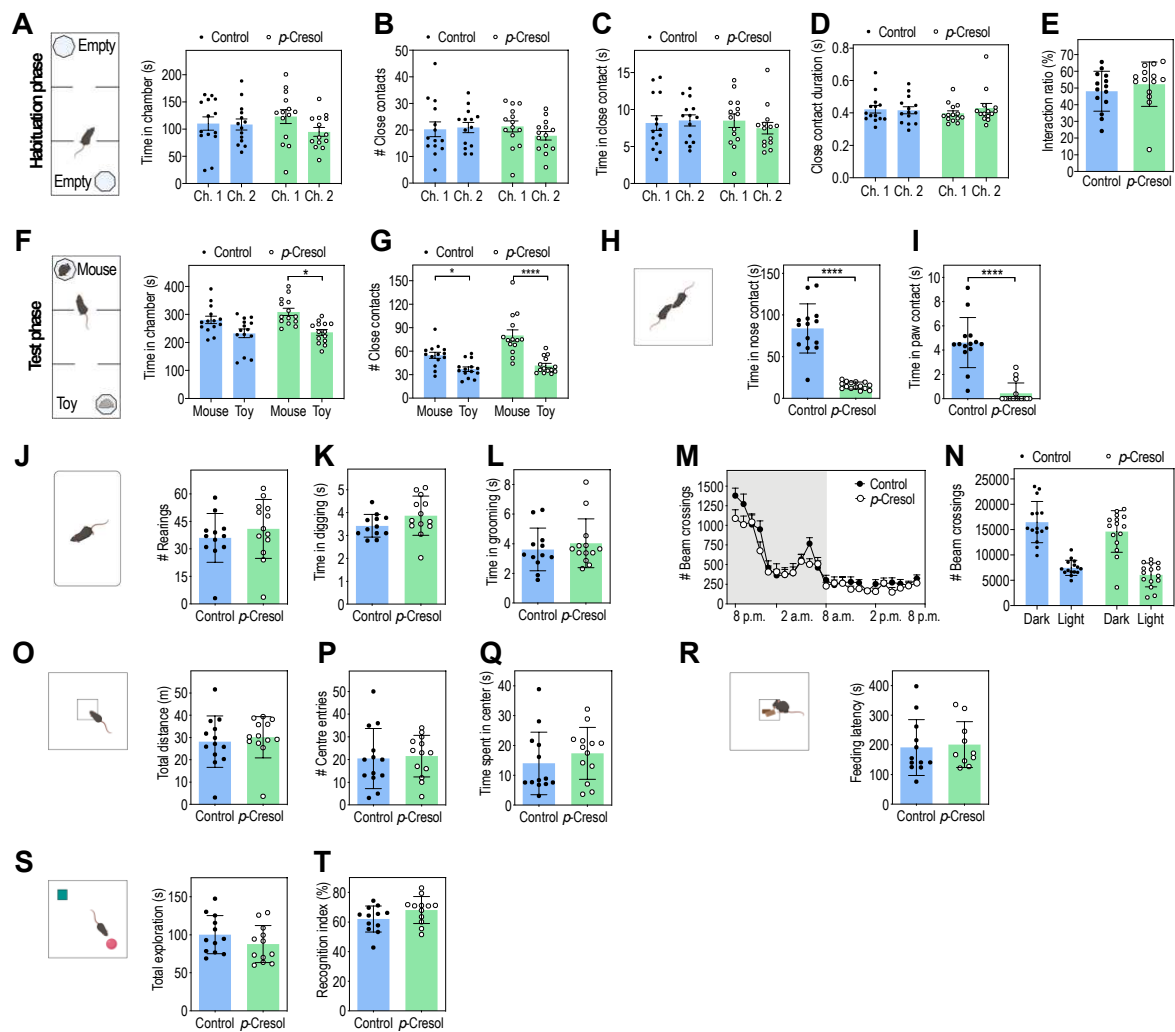
(B) Body weight follow-up (n=24/group); 2-way ANOVA:  $p(\text{Treatment})=0.8884$ ,  $p(\text{Time})<0.0001$ ,  $p(\text{Treatment} \times \text{Time})=0.9971$ ; Šidák's post hoc tests for treatment effect:  $p>0.99$ .

(C) Drink intake (n=6/group, each point representing the mean consumption per animal in one cage of 5 animals); Mann-Whitney U-test:  $p=0.0931$ .

(D) Food intake (n=6/group, each point representing the mean consumption per animal in one cage of 5 animals); Mann-Whitney U-test:  $p=0.3939$ .

(E) Urinary levels of *p*-Cresol after 4 weeks treatment (n=10 Control, n=11 *p*-Cresol); Mann-Whitney U-test: \*\*\*\*,  $p<0.0001$ .

(F) Serum levels of *p*-Cresol after 4 weeks treatment (n=12 Control, n=16 *p*-Cresol); Mann-Whitney U-test:  $p=0.3238$ .



**Supplementary Figure 2.  $\mu$ -Cresol treatment-induced behavioral alterations: additional parameters in the 3-chamber, dyadic social interactions and stereotypes tests and results from tests assessing locomotor activity, anxiety or cognition (relative to Figure 1)**

(A-E) Additional parameters during the habituation phase in the 3-chamber test (n=14/group):

(A) Time spent in each chamber; 2-way ANOVA:  $p(\text{Treatment})=0.9498$ ,  $p(\text{Chamber})=0.3018$ ,  $p(\text{Treatment} \times \text{Chamber})=0.3599$ ; Šidák's post hoc tests for chamber effect:  $p>0.05$ .

(B) Number of close contacts to the empty box in each chamber; 2-way ANOVA:  $p(\text{Treatment})=0.6839$ ,  $p(\text{Chamber})=0.4390$ ,  $p(\text{Treatment} \times \text{Chamber})=0.2648$ ; Šidák's post hoc tests for chamber effect:  $p>0.05$ .

(C) Time close contacts to the empty box in each chamber; 2-way ANOVA:  $p(\text{Treatment})=0.7265$ ,  $p(\text{Chamber})=0.6260$ ,  $p(\text{Treatment} \times \text{Chamber})=0.3188$ ; Šidák's post hoc tests for chamber effect:  $p>0.05$ .

(D) Mean duration of each close contacts to the empty box in each chamber; 2-way ANOVA:  $p(\text{Treatment})=0.8330$ ,  $p(\text{Chamber})=0.4995$ ,  $p(\text{Treatment} \times \text{Chamber})=0.3378$ ; Šidák's post hoc tests for chamber effect:  $p>0.05$ .

(E) Interaction ratio; Mann-Whitney U-test:  $p=0.265$ .

(F, G) Additional parameters during the test phase in the 3-chamber test:

(F) Time spent in each chamber containing the mouse interactor or the toy mouse; 2-way ANOVA:  $p(\text{Treatment})=0.0061$ ,  $p(\text{Mouse-Toy})=0.0019$ ,  $p(\text{Treatment} \times \text{Mouse-Toy})=0.4797$ ; Šidák's post hoc tests for Mouse vs. Toy preference effect:  $p>0.05$  for Control group, \*  $p<0.05$  for  $p$ -Cresol group.

(G) Number of close contacts with the mouse interactor or the toy mouse; 2-way ANOVA:  $p(\text{Treatment})=0.0035$ ,  $p(\text{Mouse-Toy})<0.0001$ ,  $p(\text{Treatment} \times \text{Mouse-Toy})=0.0257$ ; Šidák's post hoc tests for Mouse vs. Toy preference effect: \* $p<0.05$ , \*\*\*\* $p<0.0001$ .

(H, I) Additional parameters in the dyadic social interaction test ( $n = 14$  Control,  $n=15$   $p$ -Cresol):

(H) Total time spent in nose and (I) paw contact; Mann-Whitney U-test: \*\*\*\* $p<0.0001$ .

(J-L) Additional parameters in the motor stereotypies test ( $n=11$  Control,  $n=12$   $p$ -Cresol):

(J) Number of rearings; Mann-Whitney U-test:  $p=0.3400$ .

(K) Time spent in grooming; Mann-Whitney U-test:  $p=0.4613$ .

(L) Time spent in digging; Mann-Whitney U-test:  $p=0.1366$ .

(M, N) Locomotor activity in actimetry chambers ( $n=15/\text{group}$ ):

(M) Horizontal activity follow-up over 24 h; 2-way ANOVA:  $p(\text{Treatment})=0.1057$ ,  $p(\text{Time})<0.0001$ ,  $p(\text{Treatment} \times \text{Phase})=0.3610$ ; Šidák's post hoc tests for treatment effect:  $p>0.05$ .

(N) Cumulative activity in the dark or light phase; 2-way ANOVA:  $p(\text{Treatment})=0.0909$ ,  $p(\text{Phase})<0.0001$ ,  $p(\text{Treatment} \times \text{Phase})=0.7513$ ; Šidák's post hoc tests for treatment effect:  $p>0.05$ .

(O-Q) Open-field test ( $n=13/\text{group}$ ):

(O) Total distance travelled; Mann-Whitney U-test:  $p=0.3107$ .

(P) Number of centre entries; Mann-Whitney U-test:  $p=0.6047$ .

(Q) Time spent in the center of the area; Mann-Whitney U-test:  $p=0.3292$ .

(R) Novelty suppressed feeding (NSF) test ( $n=12$  Control,  $n=10$   $p$ -Cresol): latency to first bite; Mann-Whitney U-test:  $p=0.5707$

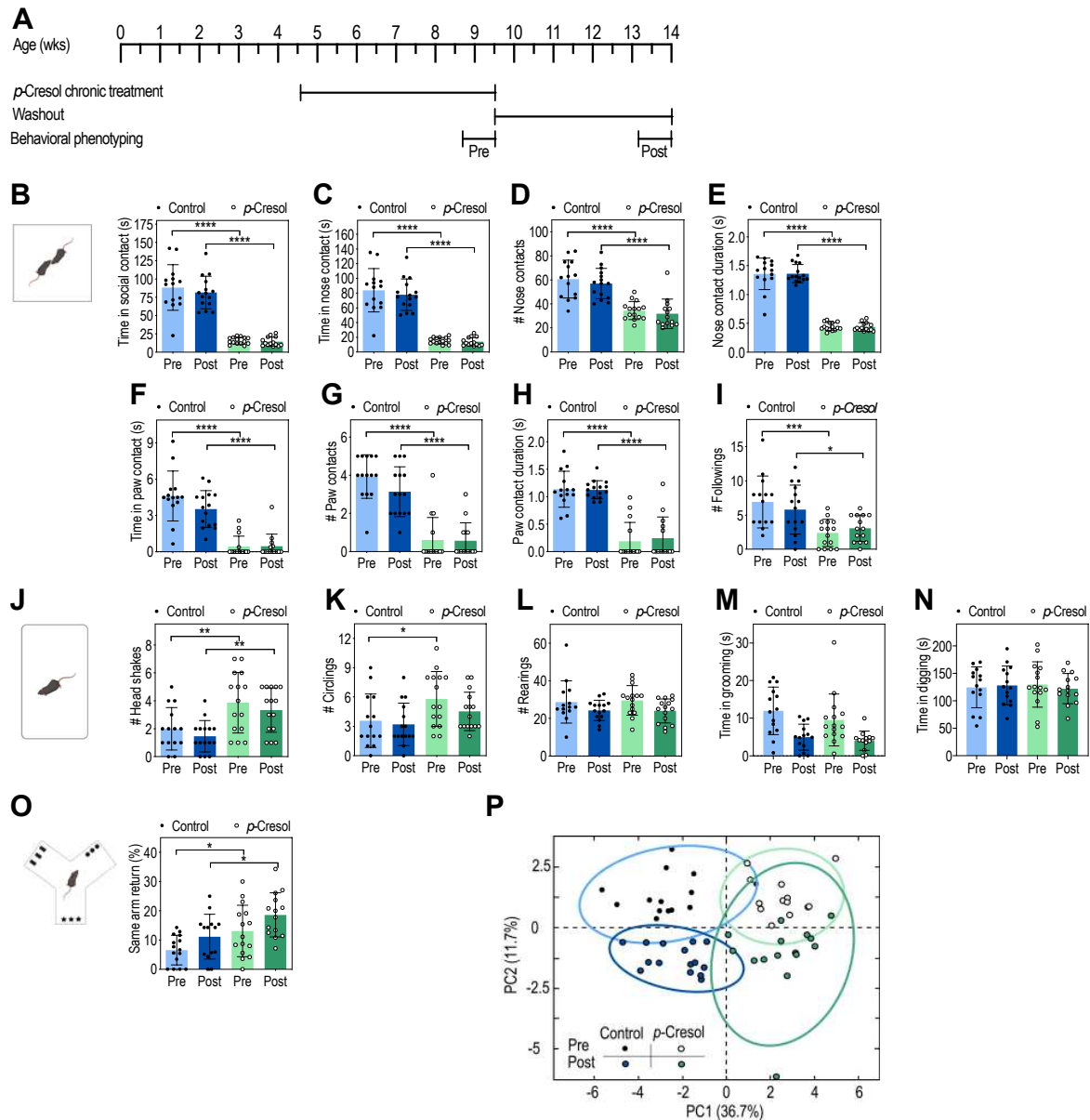
(S, T) Novel object recognition (NOR) ( $n=12/\text{group}$ ):

(S) Total time spent exploring the objects during the test phase; Mann-Whitney U-test:  $p=0.1978$ .

(T) % of time spent exploring the old vs. the new object; Mann-Whitney U-test:  $p=0.1135$ .

(A-L, N-T) Data are presented as dot-plots featuring means  $\pm$  SD.

(M) Data are shown as means  $\pm$  SD.



**Supplementary Figure 3. Autistic-like behaviors induced by *p*-Cresol persist after a 4-week washout period**

(A) Timeline of the experiment

(B-G) Dyadic social interaction test (n=14 Control, n=15 *p*-Cresol):

(B) Total time spent in social contact; 2-way ANOVA:  $p(\text{Treatment}) < 0.0001$ ,  $p(\text{Washout}) = 0.4194$ ,  $p(\text{Treatment} \times \text{Washout}) = 0.5883$ ; Šidák's post hoc tests for treatment effect: \*\*\*\* $p < 0.0001$ .

(C) Time spent in nose contact; 2-way ANOVA:  $p(\text{Treatment}) < 0.0001$ ,  $p(\text{Washout}) = 0.4525$ ,  $p(\text{Treatment} \times \text{Washout}) = 0.6450$ ; Šidák's post hoc tests for treatment effect: \*\*\*\* $p < 0.0001$ .

(D) Number of nose contacts; 2-way ANOVA:  $p(\text{Treatment}) < 0.0001$ ,  $p(\text{Washout}) = 0.3237$ ,  $p(\text{Treatment} \times \text{Washout}) = 0.8660$ ; Šidák's post hoc tests for treatment effect: \*\*\*\* $p < 0.0001$ .

(E) Mean duration of each nose contact; 2-way ANOVA:  $p(\text{Treatment}) < 0.0001$ ,  $p(\text{Washout}) = 0.9807$ ,  $p(\text{Treatment} \times \text{Washout}) = 0.8922$ ; Šidák's post hoc tests for treatment effect: \*\*\*\* $p < 0.0001$ .

(F) Time spent in paw contact; 2-way ANOVA:  $p(\text{Treatment}) < 0.0001$ ,  $p(\text{Washout}) = 0.1638$ ,  $p(\text{Treatment} \times \text{Washout}) = 0.1465$ ; Šidák's post hoc tests for treatment effect: \*\*\*\* $p < 0.0001$ .

(G) Number of paw contacts; 2-way ANOVA:  $p(\text{Treatment}) < 0.0001$ ,  $p(\text{Washout}) = 0.1793$ ,  $p(\text{Treatment} \times \text{Washout}) = 0.2109$ ; Šidák's post hoc tests for treatment effect: \*\*\*\* $p < 0.0001$ .

(H) Mean duration of each paw contact; 2-way ANOVA:  $p(\text{Treatment}) < 0.0001$ ,  $p(\text{Washout}) = 0.7906$ ,  $p(\text{Treatment} \times \text{Washout}) = 0.6926$ ; Šidák's post hoc tests for treatment effect: \*\*\*\* $p < 0.0001$ .

(I) Number of followings, 2-way ANOVA:  $p(\text{Treatment}) < 0.0001$ ,  $p(\text{Washout}) = 0.7697$ ,  $p(\text{Treatment} \times \text{Washout}) = 0.2517$ ; Šidák's post hoc tests for treatment effect: \*\*\* $p < 0.001$ , \* $p < 0.05$ .

(J-M) Motor stereotypies (n=14 Control; n=15 *p*-Cresol):

(J) Number of head shakes; 2-way ANOVA:  $p(\text{Treatment}) < 0.0001$ ,  $p(\text{Washout}) = 0.2185$ ,  $p(\text{Treatment} \times \text{Washout}) > 0.9999$ ; Šidák's post hoc tests for treatment effect: \*\* $p < 0.01$ .

(K) Number of circling events; 2-way ANOVA:  $p(\text{Treatment}) = 0.0051$ ,  $p(\text{Washout}) = 0.2605$ ,  $p(\text{Treatment} \times \text{Washout}) = 0.5796$ ; Šidák's post hoc tests for treatment effect: \* $p < 0.05$  for Control,  $p > 0.05$  for *p*-Cresol.

(L) Number of rearings; 2-way ANOVA:  $p(\text{Treatment}) = 0.8820$ ,  $p(\text{Washout}) = 0.0188$ ,  $p(\text{Treatment} \times \text{Washout}) = 0.7823$ ; Šidák's post hoc tests for treatment effect:  $p > 0.05$ .

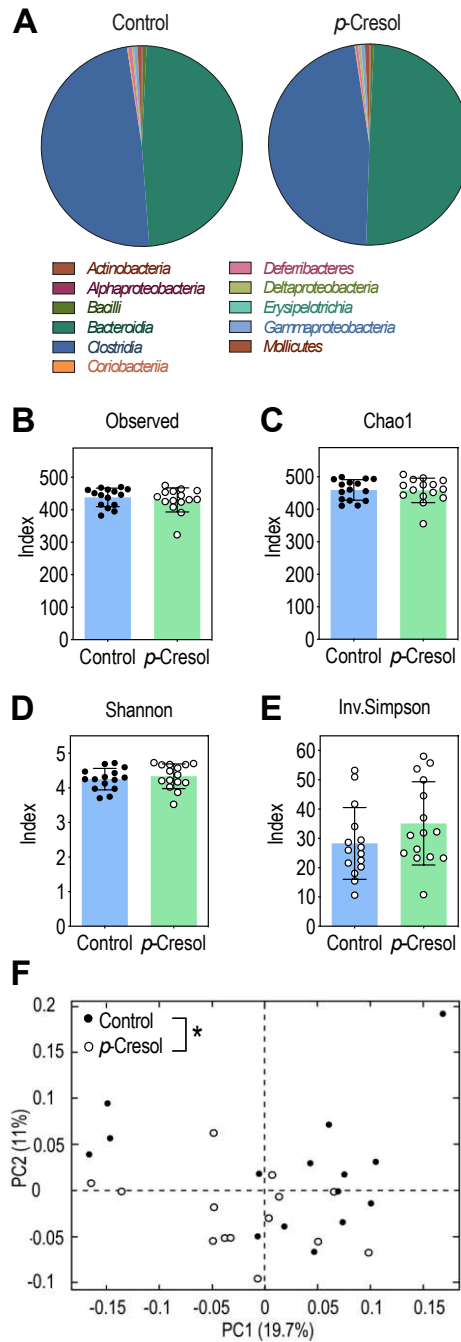
(M) Time spent in grooming; 2-way ANOVA:  $p(\text{Treatment}) = 0.2308$ ,  $p(\text{Washout}) < 0.0001$ ,  $p(\text{Treatment} \times \text{Washout}) = 0.5929$ ; Šidák's post hoc tests for treatment effect:  $p > 0.05$ .

(N) Time spent in digging; 2-way ANOVA:  $p(\text{Treatment}) = 0.9763$ ,  $p(\text{Washout}) = 0.8304$ ,  $p(\text{Treatment} \times \text{Washout}) = 0.5579$ ; Šidák's post hoc tests for treatment effect:  $p > 0.05$ .

(N) Y-maze spontaneous alternations: percentage of same arm returns (n=15 Control, n=14 *p*-Cresol): 2-way ANOVA:  $p(\text{Treatment}) = 0.0007$ ,  $p(\text{Washout}) = 0.0120$ ,  $p(\text{Interaction}) = 0.8179$ ; Šidák's post hoc tests for treatment effect: \* $p < 0.05$ .

(P) PCA plots of behavioral scores recorded in the dyadic social interaction and direct monitoring of motor stereotypies (Supplementary Figure 3B-N); ellipses of the 95% confidence intervals are indicated for each group (n=14 Control; n=15 *p*-Cresol).

(B-O) Data are presented as dot-plots featuring means  $\pm$  SD.



**Supplementary Figure 4. Microbiota analysis in  $p$ -Cresol-treated and control mice using 16S rRNA sequencing:  $\alpha$ - and  $\beta$ -diversity indexes**

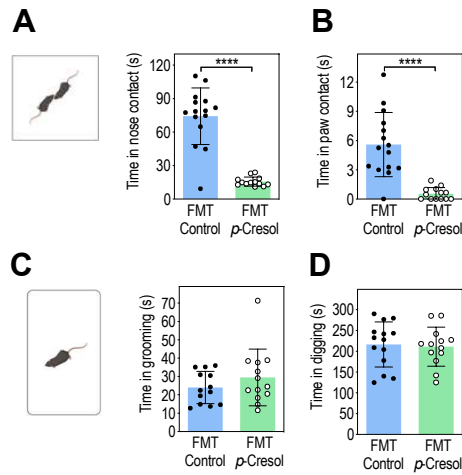
(A) Distribution of bacterial classes abundance (n=15 Control, n=15  $p$ -Cresol).

(B-E)  $\alpha$ -diversity indexes (n=15 Control, n=15  $p$ -Cresol): Observed (B), Chao1 (C), Shannon (D) Inverse Simpson (E) diversity indexes; Mann-Whitney U-test:  $p > 0.05$ .

(F)  $\beta$ -diversity index (n=15 Control, n=15  $p$ -Cresol), PCoA of Jaccard's distances; PERMANOVA:  $*p < 0.05$ .

(A) Data are presented as mean abundances for each group.

(B-E) Data are presented as dot-plots featuring means  $\pm$  SD.



**Supplementary Figure 5. FMT experiments from control or *p*-Cresol-treated mice to recipient wild-type mice: additional behavioral parameters for dyadic social interactions and stereotypes tests (relative to Figure 3)**

(A, B) Dyadic social interaction test (n=15 animals/group):

(A) Total time spent in nose contact; Mann-Whitney U-test: \*\*\*\*p<0.0001

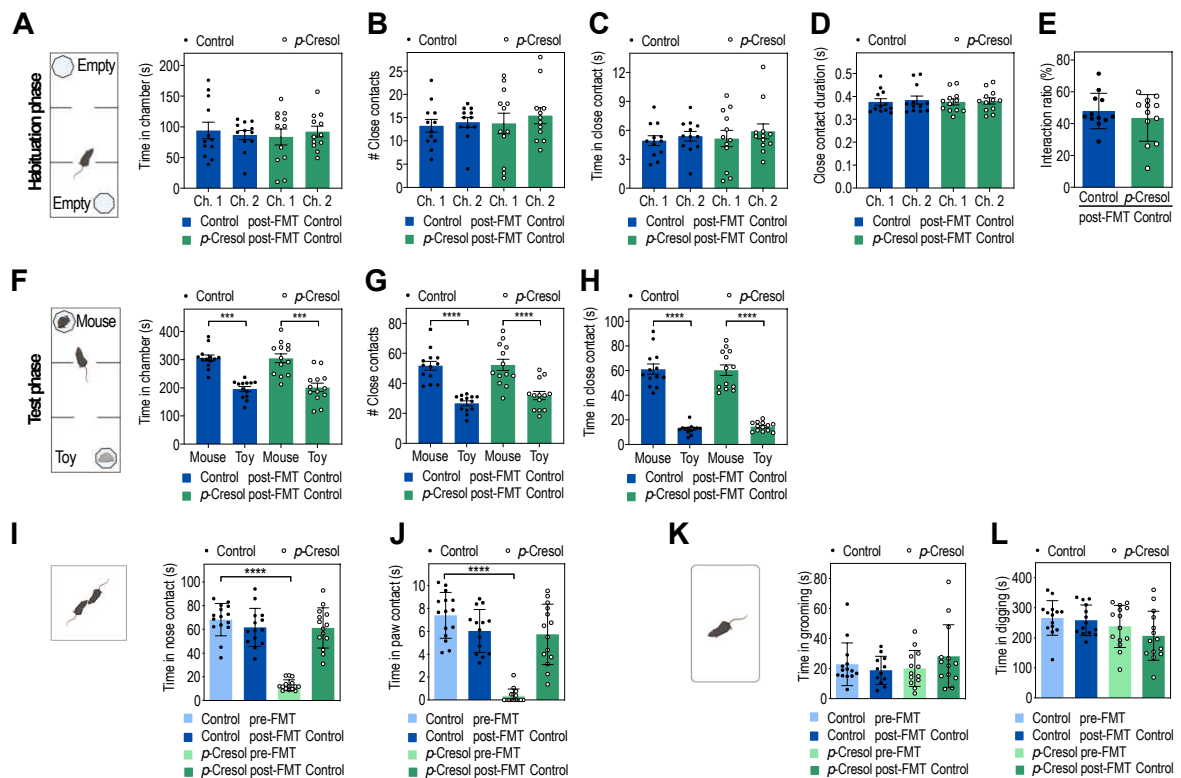
(B) Total time spent in paw contact; Mann-Whitney U-test: \*\*\*\*p<0.0001

(C, D) Motor stereotypes (n= 14 Control, n=13 *p*-Cresol):

(C) Time spent in grooming; Mann-Whitney U-test: p=0.3358.

(D) Time spent in digging; Mann-Whitney U-test: p=0.5502.

Data are presented as dot-plots featuring means  $\pm$  SD.



**Supplementary Figure 6. FMT experiments from control donors to control or *p*-Cresol treated recipient mice: additional behavioral parameters in the three-chamber, dyadic social interactions and stereotypies tests (relative to Figure 4)**

(A-E) Additional parameters during the habituation phase in the 3-chamber test post-FMT control (n=13/group):

(A) Time spent in each chamber; 2-way ANOVA:  $p(\text{Treatment})=0.8296$ ,  $p(\text{Chamber})=0.9514$ ,  $p(\text{Treatment} \times \text{Chamber})=0.4749$ ; Šidák's post hoc tests for chamber effect:  $p>0.05$ .

(B) Number of close contacts with the empty box in each chamber; 2-way ANOVA:  $p(\text{Treatment})=0.6456$ ,  $p(\text{Chamber})=0.2947$ ,  $p(\text{Treatment} \times \text{Chamber})=0.6878$ ; Šidák's post hoc tests for chamber effect:  $p>0.05$ .

(C) Time in close contact with the empty box in each chamber; 2-way ANOVA:  $p(\text{Treatment})=0.6728$ ,  $p(\text{Chamber})=0.1662$ ,  $p(\text{Treatment} \times \text{Chamber})=0.7417$ ; Šidák's post hoc tests for chamber effect:  $p>0.05$ .

(D) Mean duration of each close contact to the empty box in each chamber; 2-way ANOVA:  $p(\text{Treatment})=0.9252$ ,  $p(\text{Chamber})=0.2163$ ,  $p(\text{Treatment} \times \text{Chamber})=0.7061$ ; Šidák's post hoc tests for chamber effect:  $p>0.05$ .

(E) Interaction ratio for Chamber 1 over Chamber 2; Mann-Whitney U-test:  $p=0.755$ .

(F-H) Additional parameters during the test phase in the 3-chamber test post-FMT (n=13/group)

(F) Time spent in each chamber containing the mouse interactor or the toy mouse; 2-way ANOVA:  $p(\text{Treatment})=0.7588$ ,  $p(\text{Mouse-Toy}) < 0.0001$ ,  $p(\text{Treatment} \times \text{Mouse-Toy})=0.8356$ ; Šidák's post hoc tests for Mouse vs. Toy preference:  $***p < 0.001$ .

(G) Number of close contacts with the mouse interactor or the toy mouse; 2-way ANOVA:  $p(\text{Treatment})=0.3399$ ,  $p(\text{Mouse-Toy}) < 0.0001$ ,  $p(\text{Treatment} \times \text{Mouse-Toy})=0.4225$ ; Šidák's post hoc tests for Mouse vs. Toy preference:  $****p < 0.0001$ .

(H) Time in close contact with the mouse interactor or the toy mouse; 2-way ANOVA:  $p(\text{Treatment})=0.8480$ ,  $p(\text{Mouse-Toy}) < 0.0001$ ,  $p(\text{Treatment} \times \text{Mouse-Toy})=0.6498$ ; Šidák's post hoc tests for Mouse vs. Toy preference:  $****p < 0.0001$ .

(I, J) Additional parameters in the dyadic social interaction test pre- and post-FMT (n=15/group pre-FMT, n=14/group post-FMT):

(I) Time spent in nose contact; 2-way ANOVA:  $p(\text{Treatment}) < 0.0001$ ,  $p(\text{FMT Control}) < 0.0001$ ,  $p(\text{Treatment} \times \text{FMT Control}) < 0.0001$ ; Šidák's post hoc tests for treatment effect:  $****p < 0.0001$  for pre-FMT Control groups,  $p > 0.05$  post-FMT Control groups.

(J) Time spent in paw contact; 2-way ANOVA:  $p(\text{Treatment}) < 0.0001$ ,  $p(\text{FMT Control})=0.0002$ ,  $p(\text{Treatment} \times \text{FMT Control}) < 0.0001$ ; Šidák's post hoc tests for treatment effect:  $****p < 0.0001$  pre-FMT Control, groups  $p > 0.05$  post-FMT Control groups.

(K, L) Additional parameters in the motor stereotypies test pre- and post-FMT (n=14/group pre-FMT, n=14/group post-FMT):

(K) Time spent in grooming; 2-way ANOVA:  $p(\text{Treatment})=0.7605$ ,  $p(\text{FMT Control})=0.2801$ ,  $p(\text{Treatment} \times \text{FMT Control})=0.9682$ ; Šidák's post hoc tests for treatment effect:  $p > 0.05$ .

(L) Time spent in digging; 2-way ANOVA:  $p(\text{Treatment})=0.0295$ ,  $p(\text{FMT Control})=0.274$ ,  $p(\text{Treatment} \times \text{FMT Control})=0.5058$ ; Šidák's post hoc tests for treatment effect:  $p > 0.05$ .

### **Supplementary tables legends (3)**

#### **Supplementary Table 1. Association of bacterial taxa and OTU with Control or *p*-Cresol group (relative to Table 1)**

Taxonomic information regarding the identified bacterial taxa, linear discriminant analysis score and corresponding *p*-values as determined by LefSE analysis of bacterial taxa abundances based on 16S rRNA sequencing are indicated. OTU, operational taxonomic unit (n=15 Control, n=15 *p*-Cresol).

*Available as Excel file*

#### **Supplementary Table 2. Correlations between the abundance of discriminant microbial OTU identified by LEfSE analysis and social behavior/stereotypies scores impacted by *p*-Cresol treatment (relative to Table 1)**

Table displays taxonomic information regarding the identified OTU, Spearman's rank  $\rho$  correlation coefficients between OTU abundances and behavioral scores significantly impacted by *p*-Cresol treatment in the dyadic social interactions and motor stereotypies tests (n=30 animals: n=15 Control, n=15 *p*-Cresol). The corresponding *p*-values and adjusted *p*-values are indicated, significant  $p < 0.05$  are shaded in grey.

*Available as Excel file*

#### **Supplementary Table 3. Compilation of ANOVA statistics for behavioral data analyses and PERMANOVA statistics for Jaccard's distances analyses**

*Available as Excel file*

	Taxonomic information						LEfSE metrics							
	Phylum	Class	Order	Family	Genus	Species	OTU	Log <sub>10</sub> (LDA score)	p-val.					
Taxa associated with p-Cresol class	Actinobacteria	Coriobacteria	Coriobacteriales	Eggerthellaceae	Enterorhabdus	Unknown	675	2.664	0.0237					
	Bacteroidetes	Bacteroidia	Bacteroidales	Bacteroidaceae	Bacteroides	Unknown	19	3.490	0.0265					
				Muribaculaceae	Unknown	Unknown	18	3.864	0.0121					
					Unknown	Unknown	13	3.693	0.0002					
					Unknown	Unknown	33	3.256	0.0121					
					Unknown	Unknown	52	3.131	0.0238					
					Unknown	Unknown	40	2.884	0.0265					
					Unknown	Unknown	809	2.798	0.0261					
					Unknown	Unknown	96	2.553	0.0488					
					Unknown	Unknown	443	2.431	0.0011					
					Firmicutes	Clostridia	Clostridiales	Lachnospiraceae	Blautia	Unknown	306	2.390	0.0345	
									Lachnospiraceae NK4A136	Unknown	38	3.378	0.0020	
										Unknown	1051	2.475	0.0166	
										Unknown	290	2.367	0.0139	
										Unknown	417	2.212	0.0423	
	Lachnospiraceae UCG006	Unknown	147	2.557					0.0171					
	Roseburia	Unknown	766	2.371					0.0081					
	Unknown	Unknown	57	3.578					0.0377					
	Unknown	Unknown	31	3.368					0.0294					
	Unknown	Unknown	865	2.756					0.0052					
	Unknown	Unknown	221	2.704					0.0401					
	Unknown	Unknown	667	2.497					0.0199					
	Unknown	Unknown	997	2.410					0.0084					
	Unknown	Unknown	310	2.249					0.0152					
	Peptococcaceae	Unknown	Unknown	2,425					0.0443					
		Unknown	Unknown	2,425					0.0443					
		Unknown	Unknown	710					2.425	0.0443				
		Ruminococcaceae	Unknown	Unknown					726	2.568	0.0127			
			Ruminiclostridium	Unknown					157	2.394	0.0294			
	Proteobacteria	Gammaproteobacteria	Betaproteobacteriales	Burkholderiaceae	Parasutterella	Burkholderiales bacterium YL45	227	2.214	0.0488					
					Burkholderiales bacterium YL45	104	2.825	0.0075						
	Taxa associated with Control class	Bacteroidetes	Bacteroidia	Bacteroidales	Bacteroidaceae	Bacteroides	Multi-affiliation	130	-2.182	0.0130				
					Muribaculaceae	Unknown	Unknown	395	-2.254	0.0265				
						Unknown	Unknown	769	-2.353	0.0486				
						Unknown	Unknown	1095	-2.441	0.0259				
Unknown						Unknown	1360	-2.450	0.0196					
Unknown						Unknown	404	-2.547	0.0039					
Unknown						Unknown	1326	-2.596	0.0345					
Unknown						Unknown	838	-2.601	0.0069					
Rikenellaceae						Alistipes	Unknown	1002	-2.327	0.0074				
						Alistipes	Unknown	4	-3.744	0.0443				
Firmicutes						Clostridia	Clostridiales	Clostridiales vadinBB60	Unknown	Unknown	493	-2.462	0.0149	
									Unknown	Unknown	45	-2.679	0.0297	
								Lachnospiraceae	Blautia	Unknown	Unknown	Unknown	-3.405	0.0213
									Blautia	Unknown	Unknown	Unknown	-3.214	0.0136
		Blautia	Unknown	827	-2.412				0.0061					
		Blautia	Unknown	123	-3.146				0.0035					
		GCA_900066577	Unknown	Unknown	Unknown				-2.814	0.0401				
		GCA_900066576	Unknown	Unknown	Unknown				-2.814	0.0401				
		GCA_900066575	Unknown	484	-2.563				0.0238					
		Lachnospiraceae NK4A136	Unknown	Unknown	706				-2.189	0.0117				
			Unknown	Unknown	497				-2.215	0.0474				
			Unknown	Unknown	840				-2.370	0.0196				
			Unknown	Unknown	193				-3.102	0.0171				
			Unknown	Unknown	28				-3.840	0.0017				
			Unknown	Unknown	635				-2.181	0.0017				
		Lachnospiraceae UCG006	Unknown	Unknown	1070				-2.262	0.0100				
			Unknown	Unknown	Unknown				Unknown	-2.521	0.0443			
		Marvinbryantia	Unknown	Unknown	Unknown				Unknown	-2.525	0.0456			
		Marvinbryantia	Unknown	1039	-2.483				0.0192					
		Unknown	Unknown	409	-2.406				0.0005					
		Unknown	Unknown	1909	-2.440				0.0011					
Unknown		Unknown	311	-2.504	0.0213									
Unknown		Unknown	375	-2.514	0.0066									
Unknown		Unknown	146	-2.585	0.0213									
Unknown		Unknown	364	-2.677	0.0006									
Unknown	Unknown	97	-3.415	0.0034										
Unknown	Unknown	39	-3.658	0.0327										
Ruminococcaceae	Ruminiclostridium	Unknown	570	-2.106	0.0130									
	Unknown	Unknown	1354	-2.419	0.0034									
	Ruminococcaceae UCG014	Unknown	Unknown	685	-2.281	0.0330								
		Unknown	Unknown	332	-2.404	0.0052								
		Unknown	Unknown	262	-2.564	0.0152								
		Unknown	Unknown	341	-2.580	0.0001								
	UBA1819	Unknown	Unknown	Unknown	Unknown	-2.743	0.0095							
	UBA1819	Multi-affiliation	Unknown	Unknown	Unknown	-2.798	0.0001							
	UBA1819	Multi-affiliation	268	-2.798	0.0001									
	Unknown	Unknown	452	-2.397	0.0294									
Unknown	Unknown	317	-2.492	0.0001										
Proteobacteria	Gammaproteobacteria	Betaproteobacteriales	Burkholderiaceae	Parasutterella	Unknown	321	-2.434	0.0098						

Taxonomy		Correlation with social behavior										Correlation with stereotypes										Adjusted p-value (FDR)															
		Correlation with social behavior					Correlation with stereotypes					Correlation with social behavior					Correlation with stereotypes					Correlation with social behavior					Correlation with stereotypes										
Phylum	Class	Order	Family	Genus	Species	Total social contact time (s)	# of contacts	# of contact durations (s)	# of near contacts	# of near contact durations (s)	# of followings	# of near followings	# of near followings	# of near followings	# of near followings	# of near followings	Total social contact time (s)	# of contacts	# of contact durations (s)	# of near contacts	# of near contact durations (s)	# of followings	# of near followings	# of near followings	# of near followings	# of near followings	Total social contact time (s)	# of contacts	# of contact durations (s)	# of near contacts	# of near contact durations (s)	# of followings	# of near followings	# of near followings	# of near followings		
Actinobacteria	Corneliobactera	Corneliobacterales	Eggonellaceae	Emmornellibidus	unknown species	017	-0.285	-0.248	-0.292	-0.349	-0.220	-0.226	0.080	-0.121	0.121	0.063	0.190	0.097	0.261	0.228	0.086	0.502	0.280	0.248	0.157	0.365	0.310	0.741	0.611								
Bacteroidetes	Bacteroidia	Bacteroidales	Muribaculaceae	Muribaculum	unknown species	139	-0.132	-0.141	-0.132	-0.132	-0.132	-0.132	-0.132	-0.132	-0.132	-0.132	-0.132	-0.132	-0.132	-0.132	-0.132	-0.132	-0.132	-0.132	-0.132	-0.132	-0.132	-0.132	-0.132	-0.132	-0.132	-0.132	-0.132	-0.132	-0.132	-0.132	-0.132
Bacteroidetes	Bacteroidia	Bacteroidales	Bacteroidaceae	Bacteroides	unknown species	19	-0.363	-0.371	-0.302	-0.296	-0.423	-0.275	0.228	-0.118	0.073	0.0519	0.0065	0.1255	0.0251	0.1560	0.2426	0.5515	0.1385	0.1372	0.0505	0.2190	0.1012	0.2509	0.3266	0.6214							
Bacteroidetes	Bacteroidia	Bacteroidales	Muribaculaceae	unknown genus	unknown species	1955	0.317	0.212	0.242	0.252	0.385	0.213	-0.025	-0.248	0.1006	0.2799	0.149	0.1988	0.0562	0.2797	0.8984	0.2024	0.1903	0.3628	0.2843	0.1372	0.3390	0.9220	0.9220								
Bacteroidetes	Bacteroidia	Bacteroidales	Muribaculaceae	unknown genus	unknown species	13	-0.589	-0.531	-0.654	-0.494	-0.548	-0.380	0.186	0.067	0.0916	0.0022	0.0775	0.0025	0.0598	0.3437	0.7357	0.0273	0.0894	0.0308	0.0553	0.0308	0.1419	0.4205	0.7871								
Bacteroidetes	Bacteroidia	Bacteroidales	Muribaculaceae	unknown genus	unknown species	1236	0.262	0.125	0.131	0.107	0.321	0.003	-0.136	-0.266	0.1777	0.0266	0.3315	0.0574	0.0261	0.0699	0.4903	0.1736	0.2682	0.0994	0.1077	0.6539	0.1372	0.9001	0.3651	0.2665							
Bacteroidetes	Bacteroidia	Bacteroidales	Muribaculaceae	unknown genus	unknown species	1360	0.223	-0.020	0.148	0.125	0.274	0.126	-0.244	-0.187	0.2536	0.0937	0.4536	0.0577	0.1577	0.5206	0.2103	0.3411	0.3390	0.5315	0.5995	0.1212	0.5960	0.2990	0.4199								
Bacteroidetes	Bacteroidia	Bacteroidales	Muribaculaceae	unknown genus	unknown species	18	-0.308	-0.389	-0.323	-0.275	-0.389	-0.175	0.240	0.238	0.1113	0.0489	0.0939	0.1874	0.0407	0.3725	0.2193	0.2225	0.2024	0.1211	0.1849	0.2512	0.1211	0.4496	0.3063	0.3084							
Bacteroidetes	Bacteroidia	Bacteroidales	Muribaculaceae	unknown genus	unknown species	57	-0.618	-0.563	-0.626	-0.566	-0.657	-0.458	0.258	0.054	0.0065	0.0149	0.0041	0.0027	0.0177	0.0442	0.1946	0.7486	0.0196	0.0275	0.0378	0.0319	0.0273	0.0797	0.2764	0.8222							
Bacteroidetes	Bacteroidia	Bacteroidales	Muribaculaceae	unknown genus	unknown species	365	0.368	0.293	0.416	0.220	0.451	0.116	-0.114	-0.209	0.0422	0.1152	0.0269	0.2595	0.0160	0.5407	0.2745	0.2982	0.1231	0.2992	0.1023	0.3465	0.0554	0.6200	0.3590	0.9699							
Bacteroidetes	Bacteroidia	Bacteroidales	Muribaculaceae	unknown genus	unknown species	40	-0.300	-0.348	-0.342	-0.242	-0.413	-0.136	0.097	0.209	0.1210	0.0697	0.0752	0.2179	0.0289	0.4905	0.6241	0.2856	0.2130	0.1536	0.1619	0.3023	0.1045	0.5651	0.8893	0.3689							
Bacteroidetes	Bacteroidia	Bacteroidales	Muribaculaceae	unknown genus	unknown species	404	0.402	0.278	0.316	0.339	0.397	0.211	-0.236	-0.145	0.0338	0.1152	0.0276	0.0737	0.0383	0.2813	0.2020	0.4613	0.1114	0.2485	0.1031	0.1650	0.1310	0.3638	0.3102	0.5370							
Bacteroidetes	Bacteroidia	Bacteroidales	Muribaculaceae	unknown genus	unknown species	443	-0.380	-0.445	-0.447	-0.396	-0.343	-0.382	0.145	0.303	0.0462	0.0176	0.0171	0.0370	0.0743	0.0386	0.4615	0.1175	0.1299	0.0871	0.0871	0.1158	0.1297	0.1562	0.5370	0.2089							
Bacteroidetes	Bacteroidia	Bacteroidales	Muribaculaceae	unknown genus	unknown species	123	-0.321	-0.327	-0.314	-0.290	-0.369	-0.268	0.398	0.095	0.095	0.164	0.1342	0.0294	0.1611	0.0429	0.6290	0.1687	0.1900	0.2076	0.2294	0.1372	0.2993	0.1238	0.6993								
Bacteroidetes	Bacteroidia	Bacteroidales	Muribaculaceae	unknown genus	unknown species	769	0.229	0.031	0.194	0.129	0.328	0.079	-0.077	-0.211	0.2403	0.0771	0.3220	0.0545	0.0883	0.6050	0.6951	0.2820	0.3252	0.9047	0.4043	0.5984	0.1786	0.4744	0.7506	0.3638							
Bacteroidetes	Bacteroidia	Bacteroidales	Muribaculaceae	unknown genus	unknown species	899	-0.535	-0.447	-0.508	-0.443	-0.489	-0.491	0.269	-0.050	0.0034	0.0170	0.0058	0.0181	0.0083	0.0080	0.1659	0.7616	0.0384	0.0871	0.0472	0.0873	0.0574	0.0568	0.2581	0.8108							
Bacteroidetes	Bacteroidia	Bacteroidales	Muribaculaceae	unknown genus	unknown species	638	0.592	0.510	0.408	0.372	0.583	0.259	-0.279	-0.260	0.0064	0.109	0.0311	0.0513	0.0011	0.1833	0.1501	0.1818	0.0505	0.1988	0.1082	0.1372	0.0483	0.2152	0.2459	0.2737							
Bacteroidetes	Bacteroidia	Bacteroidales	Muribaculaceae	unknown genus	unknown species	96	-0.229	-0.229	-0.201	-0.241	-0.188	-0.280	0.017	0.158	0.2404	0.2507	0.1156	0.2170	0.3387	0.1388	0.3919	0.4451	0.3252	0.3462	0.3120	0.3037	0.4178	0.2026	0.9437	0.9206							
Bacteroidetes	Bacteroidia	Bacteroidales	Rikenellaceae	Alloprevia	unknown species	1002	0.259	0.219	0.314	0.263	0.235	0.265	-0.186	-0.147	0.1901	0.2820	0.1039	0.1170	0.2389	0.1725	0.3439	0.8123	0.2808	0.3469	0.3488	0.3665	0.4205	0.8551									
Bacteroidetes	Bacteroidia	Bacteroidales	Muribaculaceae	unknown genus	unknown species	4	0.269	0.329	0.316	0.279	0.234	0.315	-0.077	0.132	0.1658	0.0873	0.1011	0.1502	0.2313	0.1029	0.6955	0.5036	0.2581	0.1777	0.1907	0.2459	0.3152	0.1926	0.7506	0.5791							
Firmicutes	Clostridia	Clostridiales	Clostridiales within B80 group	unknown genus	unknown species	41	0.528	0.262	0.394	0.446	0.482	0.274	-0.268	-0.274	0.0041	0.1467	0.0081	0.0165	0.0382	0.1588	0.1979	0.2445	0.0378	0.2413	0.1753	0.0663	0.119	0.2519	0.1291	0.3284							
Firmicutes	Clostridia	Clostridiales	Clostridiales within B80 group	unknown genus	unknown species	123	0.368	0.398	0.312	0.304	0.460	0.071	0.036	-0.074	0.0541	0.0358	0.1063	0.0265	0.0158	0.7024	0.8481	0.7382	0.1372	0.1140	0.1970	0.1830	0.0787	0.7278	0.8878	0.7627							
Firmicutes	Clostridia	Clostridiales	Lachnospiraceae	Blautia	unknown species	463	0.487	0.427	0.583	0.275	0.560	0.254	-0.418	-0.077	0.0086	0.0233	0.0011	0.1564	0.0024	0.1915	0.0207	0.6957	0.0583	0.0988	0.0243	0.2509	0.0388	0.2008	0.1023	0.7506							
Firmicutes	Clostridia	Clostridiales	Lachnospiraceae	Blautia	unknown species	306	-0.313	-0.084	-0.015	-0.300	-0.216	-0.144	0.350	0.031	0.1051	0.0720	0.1026	0.1203	0.2691	0.4649	0.0679	0.8772	0.1996	0.7350	0.1926	0.2126	0.338	0.5402	0.1521	0.9041							
Firmicutes	Clostridia	Clostridiales	Lachnospiraceae	Blautia	unknown species	837	0.443	0.406	0.606	0.332	0.480	0.340	-0.596	0.310	0.0161	0.0323	0.0066	0.0164	0.0164	0.2104	0.0916	0.8591	0.0813	0.1108	0.0664	0.0664	0.0664	0.0664	0.0664	0.0664							
Firmicutes	Clostridia	Clostridiales	Lachnospiraceae	GC91066575	unknown species	484	0.307	0.307	0.156	0.279	0.276	0.337	0.140	-0.056	0.0067	0.3911	0.1468	0.1845	0.2459	0.4459	0.7943	0.1801	0.0911	0.0416	0.2459	0.2500	0.8626	0.8626									
Firmicutes	Clostridia	Clostridiales	Lachnospiraceae	Lachnospiraceae NK44136 group	unknown species	1051	-0.325	-0.304	-0.341	-0.343	-0.333	-0.101	0.318	-0.010	0.0911	0.1157	0.168	0.0743	0.0652	0.6087	0.0995	0.9884	0.1815	0.2074	0.3037	0.1607	0.1446	0.6736	0.1901	0.9670							
Firmicutes	Clostridia	Clostridiales	Lachnospiraceae	Lachnospiraceae NK44136 group	unknown species	193	0.454	0.265	0.350	0.470	0.401	0.236	-0.368	0.245	0.0130	0.1738	0.0675	0.0716	0.0368	0.2259	0.3838	0.2084	0.0766	0.2665	0.1521	0.0704	0.1120	0.3102	0.1372	0.2970							
Firmicutes	Clostridia	Clostridiales	Lachnospiraceae	Lachnospiraceae NK44136 group	unknown species	29	0.507	0.290	0.418	0.523	0.436	0.246	-0.496	-0.353	0.0040	0.1339	0.0270	0.0055	0.0043	0.0086	0.0174	0.0650	0.0378	0.2254	0.1023	0.1135	0.0883	0.0388	0.0549	0.9499							
Firmicutes	Clostridia	Clostridiales	Lachnospiraceae	Lachnospiraceae NK44136 group	unknown species	290	-0.338	-0.359	-0.304	-0.319	-0.379	-0.501	0.053	0.157	0.0783	0.0606	0.1159	0.0384	0.0444	0.7963	0.3637	0.4263	0.1650	0.1428	0.2074	0.1999	0.1299	0.8414	0.7005	0.5047							
Firmicutes	Clostridia	Clostridiales	Lachnospiraceae	Lachnospiraceae NK44136 group	unknown species	38	-0.365	-0.338	-0.389	-0.287	-0.425	-0.192	0.391	0.031	0.0561	0.0784	0.0407	0.0121	0.0238	0.0394	0.8771	0.1372	0.1650	0.1211	0.1372	0.1650	0.1211	0.0466	0.1194	0.9047							
Firmicutes	Clostridia	Clostridiales	Lachnospiraceae	Lachnospiraceae NK44136 group	unknown species	417	-0.213	-0.193	-0.253	-0.160	-0.253	-0.122	0.208	0.019	0.2754	0.3239	0.1946	0.4156	0.1946	0.5366	0.2889	0.9239	0.3590	0.4046	0.2838	0.4031	0.2838	0.6033	0.3694	0.9407							
Firmicutes	Clostridia	Clostridiales	Lachnospiraceae	Lachnospiraceae NK44136 group	unknown species	497	0.426	0.459	0.449	0.532	0.386	0.386	-0.305	0.069	0.0296	0.0388	0.0088	0.0088	0.0088	0.0088	0.0088	0.0088	0.0088	0.0088	0.0088	0.0088	0.0088	0.0088	0.0088	0.0088							
Firmicutes	Clostridia	Clostridiales	Lachnospiraceae	Lachnospiraceae NK44136 group	unknown species	706	0.397	0.192	0.417	0.167	0.445	0.176	-0.340	-0.272	0.0477	0.3267	0.0773	0.39																			

# Conclusions and Perspectives

## A. Conclusions

Our study has demonstrated the impact of the bacterial metabolite *p*-Cresol on social and repetitive behaviour, the core symptoms of ASD by remodelling of microbiota community. This reveals the possible role of bacterial metabolites on the alteration of behaviour, impacting the reward circuit. Our study has allowed the development of environmental mouse model (mice treated with *p*-Cresol) that allows studying how the intestinal microbiota communicates with the brain and impacts the behaviour. Furthermore, we have been able to recover behavioural alterations thanks to the transfer of faecal material that allows the normalization of the microbial community and which could be a safe therapeutic strategy for ASD patients.

## B. Perspectives in the *p*-Cresol Mouse Model

### 1. Understanding the Cellular and Molecular Pathways Impacted by *p*-Cresol

Our study has demonstrated a causal relationship between dysbiosis, *p*-Cresol and ASD-like behaviours. However, the mechanisms underlying the action of *p*-Cresol on social behaviour remain to be elucidated; in particular the cellular and molecular changes induced by *p*-Cresol, both centrally and peripherally, as well as the route of communication involved remain to be identified.

In the short term, we will therefore:

- ◆ *Determine if mice exposed to p-Cresol display abnormalities in the ENS, intestinal epithelial and immune cells*

Given that the microbiota influences the ENS and intestinal epithelium physiology, we wish to explore possible dysfunctions in these systems. To do this, we will perform a structural exploration of the ENS on whole-mount colonic tissue where we will label different population of enteric neurons (cholinergic with anti-ChAT and nitrinergic with anti-nNOS) and analyse the organization of the ENS network (Aubert et al., 2019).

We will also carry out histological staining to study the distribution and morphology of different epithelial cell types. Cell nuclei will be labelled with haematoxylin, cytoplasm with eosin and mucin-secreting goblet cells with alcian blue. Finally, enterochromaffin cells will be labelled with anti-Chromogranin A antibodies and their density will be determined.

Finally, we will perform immunofluorescence analysis of fixed intestinal tissue to monitor signs of inflammation. We will study the density of macrophages (labelled with anti-F4/80 antibodies) and T cells (labelled with anti-CD3 antibodies) in the submucosa/mucosa and the muscle/myenteric plexus layers.

- ◆ *Determine the molecular changes induced by p-Cresol treatment in brain areas related to the social reward circuit*

To this aim, we will perform real-time quantitative PCR (RT-QPCR) analyses to identify variations in the levels of transcripts related to ASD genes. Notably mRNA relative to neurotransmitter transport and biosynthesis, the GABAergic, glutamatergic, oxytocinergic and dopaminergic systems known to be associated with ASD (Becker et al., 2014) will be quantified in punches of brain regions related to the social reward circuit such as VTA, PFC, NAc and amygdala.

In the longer term, we will:

- ◆ *Determine whether the alterations identified above can be induced or alleviated by microbiota manipulation.*

We will focus on the cellular and molecular abnormalities identified in the previous experiments. First, we will assess whether these abnormalities are transmitted along with social behaviour deficits in recipient wild-type mice transplanted with faeces from *p*-Cresol-treated mice. Second, we will investigate whether the restoration of a healthy microbiota in *p*-Cresol-treated mice, which we know normalises social behaviour is accompanied by a normalisation of these abnormalities.

These experiments should allow to understand better the molecular and cellular changes induced by *p*-Cresol both peripherally and centrally and contributing to social behaviour deficits.

◆ *Explore the role of vagus nerve in p-Cresol-induced behavioural effects*

To further explore the route of communication involved in *p*-Cresol effects on behaviour, we will primarily investigate the contribution of the vagus nerve. We have shown that *p*-Cresol treatment produces a decrease in dopamine neurons excitability in the VTA, an important region in the reward circuit. This structure is connected to several brain regions that form the mesolimbic circuit. Our goal is to find out how signals from the gut microbiota reach the brain. An important candidate for this signal transmission is the vagus nerve. Wild-type mice will be vagotomised mice and subjected to chronic treatment with *p*-Cresol. After 4 weeks, social behaviour and stereotypic/perseverative behaviours will be evaluated. If vagotomy abolishes *p*-Cresol effects on behaviour, it would demonstrate that the vagus mediates the effects of *p*-Cresol on behaviour. In the same way, we will assess if vagotomy blocks the development of abnormal behaviours in recipient wild-type mice transplanted with feces from *p*-Cresol-treated mice. While these experiments should allow to validate the possible contribution of vagus nerve signalling, it remains possible that the *p*-Cresol-induced dysbiotic microbiota signals through other pathways (neuroendocrine, immune) to communicate with the brain. For example, a study showed that microbiota depletion induced by the administration of antibiotics increased anxious behaviours, and these effects were also induced in vagotomised mice (Bercik et al., 2011b). Therefore, microbiota effects on behaviour can use pathways not involving the vagus nerve. If this is the case, we will explore neuroendocrine and immune pathways if anomalies in these pathways were determined in the short-term experiments.

## 2. Possible Therapeutic Strategies to Explore in the *p*-Cresol Model

◆ *Pharmacological interventions*

First, we will test pharmacological interventions to restore social behaviour deficits in *p*-Cresol-treated mice. Candidate pharmacological targets will derive from the analysis of brain transcripts in brain areas related to the social reward circuit. We will manipulate the most relevant neuronal population and brain region using pharmacological interventions targeting the identified cell populations to restore social behaviour deficits in *p*-Cresol treated mice.

#### ◆ *Interventions targeting the microbiota*

Two strategies will be tested involving probiotic or prebiotic treatment of *p*-Cresol mice. One interesting candidate probiotic is *L. reuteri* which restores both social interaction deficits and VTA dopamine neurons excitability in genetic and environmental ASD models (Buffington et al., 2016, Sgritta et al., 2019). This probiotic unlikely acts by normalising the gut microbiota; rather *L. reuteri* enhances the synaptic plasticity of dopaminergic neurons in the VTA region (Sgritta et al., 2019), which is altered in *p*-Cresol mice. Other probiotics derived from human studies could be used. *p*-Cresol is produced exclusively by bacterial metabolism, therefore, *p*-Cresol urinary levels reflect the production of this metabolite by the bacteria. Therefore, the administration of probiotics could help to modify the populations of *p*-Cresol-producer bacteria, restore the bacterial balance and recover some of the behavioural abnormalities observed in *p*-Cresol mice. Two probiotics, *Lactobacillus casei* and *Bifidobacterium breve*, were shown to decrease *p*-Cresol urinary levels in healthy volunteers, and could be tested in *p*-Cresol-treated mice (De Preter et al., 2004, 2007).

Another interesting candidate is the prebiotic oligofructose-enriched inulin (Synergy 1 mix, Orafiti®) that reduces the urinary excretion of *p*-Cresol in healthy volunteers (De Preter et al., 2007). We will test the behavioural effect in *p*-Cresol-treated mice to see if we improve or restore the behavioural abnormalities. In this case, we will treat the mice with *p*-Cresol and then we will administer the prebiotic in the drinking water. Then, we will analyse the social behaviours and stereotypies.

### 3. Possible Therapeutic Intervention Strategies Targeting the Microbiota in ASD

In this section, we will detail the therapeutic avenues derived from our preclinical data that could be explored to treat core ASD symptoms by targeting the microbiota and *p*-Cresol production in ASD patients.

#### a. FMT

In our study, we have shown that FMT from normal mice normalises social behaviour deficits in *p*-Cresol-treated mice. This was also shown in the DIO model of ASD (Buffington et al., 2016). Also, recolonization of GF mice with a conventional

microbiota normalised their social behaviour deficits (Desbonnet et al., 2014). These findings demonstrate that restoring a normal microbiota via FMT can alleviate ASD-like behavioural symptoms in rodents. Evaluating the potential of FMT is currently the subject of active clinical research in the ASD field. FMT appears as the most effective microbial therapy and its effects are sustained over time. FMT involves collecting stools from neurotypical patients and preparing these stools for transplantation to ASD patients. Until now, FMT has mainly been used in patients with recurrent infections with *Clostridioides difficile* and antibiotic resistance (e.g. vancomycin) (Davidovics et al., 2019; Van Nood et al., 2013). Since microbiota dysbiosis is prevalent in a large proportion of ASD patients, a pilot study has evaluated its safety and efficacy to treat ASD GI and core behavioural symptoms. Kang and colleagues conducted a clinical trial on 18 ASD patients and have shown that this microbial therapy is safe and well tolerated by young ASD patients. They observed significant improvements of both GI symptoms and behavioural problems, notably clear improvements in social skills and reduction of stereotypies/repetitive behaviours) after FMT (Kang et al., 2017). In addition, they showed that these beneficial effects were maintained over time, up to two years after FMT (Kang et al., 2019). One limitation of this study is its small sample size. Nevertheless, microbial therapy *via* FMT appears to be safe and have long-lasting beneficial effects on GI and behavioural ASD symptoms.

In future studies, the cohorts should be of larger sample size, with an established age range and with similar severity in terms of gastrointestinal and behavioural symptoms. Several clinical trials are being conducted around the world to test on larger sample of patients the safety and efficacy of FMT for ASD patients (<https://clinicaltrials.gov/ct2/results?cond=Autism+Spectrum+Disorder&term=fecal+matter&cntry=&state=&city=&dist=>).

#### b. Probiotic and Prebiotic Treatment

Another strategy targeting the microbiota could be through the use of specific probiotics and prebiotics to help reduce endogenous production of *p*-Cresol by the dysbiotic microbiota of ASD patients. Some clinical trials have already investigated the effects of probiotics in ASD patients with mixed results. The administration of probiotics such as *Lactobacillus casei* and *Bifidobacterium longum* improves gastrointestinal symptoms in

ASD children, reducing inflammation and normalising intestinal microbiota (Tomova et al., 2015), however, their effect on behavioural impairments appear limited.

The administration of the probiotic *L. casei* decreases *p*-Cresol urinary levels in healthy volunteers (De Preter et al., 2004). Another probiotic that could be used is *Bifidobacterium breve* Yakult, which decreases the urinary levels of *p*-Cresol in healthy volunteers (De Preter et al., 2007). Further, another study conducted on healthy volunteers have shown that the administration of the *Lactobacillus casei* Shirota strain produces positive effects on mood and cognition (Benton et al., 2007). Therefore *L. casei* would be an interesting candidate probiotic to test in ASD patients presenting high levels of *p*-Cresol.

The effect of prebiotics on *p*-Cresol excretion has also been studied. One study has shown that the  $\beta$ -galactosido-fructose administration reduces the urinary excretion of *p*-Cresol in healthy volunteers (De Preter et al., 2004). Similarly, short- and long-term administration of oligofructose-enriched inulin reduces the urinary excretion of *p*-Cresol in healthy volunteers (De Preter et al., 2007)

These findings suggest that the use of pre- and probiotics in ASD patients may help reduce *p*-Cresol levels, improve gastrointestinal and maybe even behavioural symptoms. For this, more clinical trials are required to test the efficacy of pre- and probiotic treatment in ASD.

# Chapter 3: Peripheral Phenotypes in Fragile X Syndrome

## I. Context

This section is dedicated to my PhD work related to Fragile X Syndrome. The absence of the RNA-binding protein FMRP induces deregulations in the CNS which are thought to be at the basis of the behavioural impairment in FXS patients. However, FMRP is widely expressed, including in peripheral organs, FXS patients display somatic symptoms and a few studies in animal models have shown that the absence of FMRP could also have consequences outside the CNS and in particular on metabolic homeostasis, whole body composition and on the immune system. Based on this, we hypothesised that loss of FMRP could impact each of these peripheral systems. During my PhD, I contributed to three publications related to the identification of peripheral phenotypes in Fragile X Syndrome.

## Metabolic Anomalies in FXS: Publication #1

### A. Research Hypothesis and Objectives of the Study

Several studies suggested that *FMRI*-deficiency in human impacted the levels of circulating lipids (Berry-Kravis et al., 2015; Lisik et al., 2016), suggesting possible metabolic anomalies. In this study, our hypothesis was that *FMRI*-deficiency, could impact metabolic homeostasis both in FXS patients and in the FXS mouse model. Our objectives were:

1. To uncover global changes in metabolic homeostasis in the *Fmr1*-KO mouse model and in FXS patients
2. To characterise the dysregulations of metabolic homeostasis in the *Fmr1*-KO mouse model

3. To understand the role of translation dysregulation in the metabolic changes induced by the loss of the translational repressor FMRP

To meet these objectives, we investigated the metabolic consequences of *Fmr1*-deficiency notably on glucose and lipid metabolism in FXS mouse model *in vivo*, *ex vivo* in adipose tissue explants and in *in vitro* models. To assess the translationality of the findings, we also measured metabolic markers in the serum of FXS patients.

My contribution to this article was to assist Laetitia Davidovic and Antoine Leboucher, the postdoctoral researcher in charge of the project, for *in vivo* experiments, and notably insulin and glucose tolerance tests. I also performed semi-quantitative western-blotting analysis of proteins and phospho-proteins involved in the insulin receptor pathway and quantitative RT-PCR to measure transcripts related to adipose tissue markers.

## B. Results

The results are presented in the following publication.

*Publication #1:*

Leboucher A, Pisani DF, Martinez-Gili L, Chilloux J, **Bermudez-Martin P**, Van Dijck A, Ganief T, Macek B, Becker JA, Le Merrer J, Kooy RF, Amri EZ, Khandjian EW, Dumas ME, Davidovic L (2019). The translational regulator FMRP controls lipid and glucose metabolism in mice and humans. *Molecular Metabolism*. 21:22-35.

To summarise, in this study, we have shown that *Fmr1*-KO mice display an increase in glucose tolerance and insulin sensitivity, as well as a reduction in adiposity due to an increase in lipid utilization as energetic substrate. Further, FXS patients have similar metabolic deregulation with reduced circulating glucose and insulin and increased levels of free fatty acids. This study contributed to a better understanding of the consequences of *FMRI* gene inactivation in the periphery and its importance in metabolic homeostasis.

## C. Manuscript

# The translational regulator FMRP controls lipid and glucose metabolism in mice and humans

Antoine Leboucher<sup>1,9</sup>, Didier F. Pisani<sup>2</sup>, Laura Martinez-Gili<sup>3</sup>, Julien Chilloux<sup>3</sup>, Patricia Bermudez-Martin<sup>1</sup>, Anke Van Dijck<sup>4</sup>, Tariq Ganief<sup>5</sup>, Boris Macek<sup>5</sup>, Jérôme A.J. Becker<sup>6</sup>, Julie Le Merrer<sup>6</sup>, R. Frank Kooy<sup>4</sup>, Ez-Zoubir Amri<sup>2</sup>, Edouard W. Khandjian<sup>7,8</sup>, Marc-Emmanuel Dumas<sup>3</sup>, Laetitia Davidovic<sup>1,\*</sup>

## ABSTRACT

**Objectives:** The Fragile X Mental Retardation Protein (FMRP) is a widely expressed RNA-binding protein involved in translation regulation. Since the absence of FMRP leads to Fragile X Syndrome (FXS) and autism, FMRP has been extensively studied in brain. The functions of FMRP in peripheral organs and on metabolic homeostasis remain elusive; therefore, we sought to investigate the systemic consequences of its absence.

**Methods:** Using metabolomics, *in vivo* metabolic phenotyping of the *Fmr1*-KO FXS mouse model and *in vitro* approaches, we show that the absence of FMRP induced a metabolic shift towards enhanced glucose tolerance and insulin sensitivity, reduced adiposity, and increased  $\beta$ -adrenergic-driven lipolysis and lipid utilization.

**Results:** Combining proteomics and cellular assays, we highlight that FMRP loss increased hepatic protein synthesis and impacted pathways notably linked to lipid metabolism. Mapping metabolomic and proteomic phenotypes onto a signaling and metabolic network, we predicted that the coordinated metabolic response to FMRP loss was mediated by dysregulation in the abundances of specific hepatic proteins. We experimentally validated these predictions, demonstrating that the translational regulator FMRP associates with a subset of mRNAs involved in lipid metabolism. Finally, we highlight that FXS patients mirror metabolic variations observed in *Fmr1*-KO mice with reduced circulating glucose and insulin and increased free fatty acids.

**Conclusions:** Loss of FMRP results in a widespread coordinated systemic response that notably involves upregulation of protein translation in the liver, increased utilization of lipids, and significant changes in metabolic homeostasis. Our study unravels metabolic phenotypes in FXS and further supports the importance of translational regulation in the homeostatic control of systemic metabolism.

Crown Copyright © 2019 Published by Elsevier GmbH. This is an open access article under the CC BY-NC-ND license (<http://creativecommons.org/licenses/by-nc-nd/4.0/>).

**Keywords** Fragile X mental retardation protein; RNA-binding protein; Translation; Metabolism; Glucose; Lipids

## 1. INTRODUCTION

The Fragile X Mental Retardation Protein (FMRP) is an RNA-binding protein, which associates with polyribosomes to regulate mRNA translation together with its homologues FXR1P and FXR2P [1–4]. A current model states that FMRP exerts repressive activity on translation by reversibly stalling ribosomes on its target mRNA [5,6]. So far, FMRP functions and the mRNAs it targets have been mostly explored in the context of the central nervous system (CNS). Indeed, inactivation of the X-linked *FMR1* gene, which encodes FMRP, is associated with neurodevelopmental defects, intellectual disability, and autism spectrum disorders in Fragile X Syndrome (FXS), a syndrome affecting 1:6,000 new-borns [7,8]. Numerous studies have used the *Fmr1*-KO mouse

models [9,10] to show that loss of FMRP expression affects the translation of a wide range of mRNA, compromising brain translation homeostasis with deleterious consequences on synaptic plasticity and thus on behavior [4,11].

Despite the wide expression of FMRP in peripheral tissues [12,13], thus far, the consequences of its absence outside the CNS are only starting to be elucidated. In *dfmr1*-KO *Drosophila*, the loss of FMRP was shown to elevate insulin signaling in the brain and intestine, inducing developmental defects in those organs [14–16]. Another study in the *Drosophila* model of FXS, highlighted reduced whole-body carbohydrate and lipid stores, hypersensitivity to starvation, and altered mitochondrial functions [17]. Although no overt metabolic alterations was reported in the first generation FXS mouse

<sup>1</sup>Université Côte d'Azur, CNRS, Institut de Pharmacologie Moléculaire et Cellulaire, Valbonne, France <sup>2</sup>Université Côte d'Azur, CNRS, Inserm, Institut de Biologie Valrose, Nice, France <sup>3</sup>Division of Integrative Systems Medicine and Digestive Diseases, Department of Surgery and Cancer, Imperial College London, Exhibition Road, South Kensington, London SW7 2AZ, United Kingdom <sup>4</sup>Department of Medical Genetics, University and University Hospital of Antwerp, Prins Boudewijnlaan 43/6, 2650 Edegem, Belgium <sup>5</sup>Proteome Center Tübingen, Germany <sup>6</sup>Physiologie de la Reproduction et des Comportements, INRA UMR-0085, CNRS UMR-7247, Inserm, Université François Rabelais, IFCE, 37380, Nouzilly, France <sup>7</sup>Centre de Recherche CERVO, Institut en Santé Mentale de Québec, PQ, Canada <sup>8</sup>Département de Psychiatrie et des Neurosciences, Faculté de Médecine, Université Laval, Québec, PQ, Canada

<sup>9</sup> Present address: German Institute of Human Nutrition Potsdam-Rehbruecke (DIfE), Nuthetal, Germany.

\*Corresponding author. IPMC CNRS UMR7275, 660 Route des Lucioles, 06560 Valbonne, France. E-mail: [davidovic@ipmc.cnrs.fr](mailto:davidovic@ipmc.cnrs.fr) (L. Davidovic).

Received December 2, 2018 • Revision received January 2, 2019 • Accepted January 8, 2019 • Available online xxx

<https://doi.org/10.1016/j.molmet.2019.01.002>

## Original Article

model (*Fmr1*-KO1) [9], the *Fmr1/Fxr2* double KO mouse displayed increased glucose tolerance and insulin sensitivity, reduced adiposity, and reduced circulating glucose [18]. Finally, independent clinical studies reported reduced levels of lipids, including cholesterol, in FXS patients compared to healthy controls [19–21]. These data supported possible functions for FMRP in the control of glucose and lipid metabolism, but mechanisms by which FMRP could impact metabolism and its mRNA targets in peripheral organs remain mostly unknown.

Here, we demonstrated that loss of FMRP in mice markedly impacted glucose and lipid metabolism. We further showed that loss of FMRP elevates hepatic protein synthesis and that FMRP likely controls the translation of key hepatic proteins involved in lipid metabolism. Finally, we provided clinical evidence that circulating metabolic markers were altered in FXS patients as compared to healthy controls.

## 2. MATERIALS AND METHODS

Detailed experimental procedures are available in the [Supplemental Information Appendix](#).

### 2.1. Animal procedures

*Fmr1*-KO2 mice described in [10] were housed in a temperature (22–24 °C) and hygrometry (70–80%)-controlled room with a 12-h light–dark cycle (lights on at 07:00) and fed on standard chow (reference 4RF25, Mucedola). All the described experiments were performed on male littermates at 4-months of age, with the exception of initial blood sampling of fed animals for metabolic profiling (presented in [Figure 1](#)) that was performed on 4 to 6 months-old animals.

### 2.2. Clinical samples

25 fragile X patients and 29 sex- and age-matched healthy subjects were enrolled at the University of Antwerp (Antwerp, Belgium). Written informed consent was obtained from each participant or his legal guardian before research participation. The absence/presence of the Fragile X full mutation in the 5' UTR of *FMR1* gene was confirmed in FXS patients by an accredited laboratory, using a CGG-repeat PCR and Southern Blotting on DNA isolated from blood. All patients had a number of CGG repeats above 200, yielding *FMR1* gene inactivation (Pieretti et al., 1991). To avoid stress induced by fasting to Fragile X patients, individuals involved in the study were not advised to fast prior to venous blood sampling.

### 2.3. Metabolic profiling

For metabolome studies in mice, blood was sampled between 9 and 11 a.m., either in nonfasted animals, i.e. fed *ad libitum*, or after an overnight fast. For FXS controls and patients, sera were obtained from nonfasted individuals. NMR experiments were carried out using a Bruker Avance spectrometer (Bruker GmbH, Rheinstetten, Germany) operating at 600 MHz as described previously [22]. Structural assignment was performed using data from literature, HMDB (<http://www.hmdb.ca/>), S-Base (Bruker GmbH, Rheinstetten, Germany) and in-house databases [23]. <sup>1</sup>H NMR spectra were pre-processed and exported into Matlab for multivariate statistical analyses using orthogonal partial least square discriminant analysis (O-PLS-DA) as previously reported [24].

### 2.4. Blood chemistry and hormones measurements

Glucose was measured using a glucometer (AccuCheck Mobile, Roche). The determination of circulating TG, FFA, and total cholesterol

was subcontracted to the Genotoul Anexplo Platform (Toulouse, France). Leptin and insulin were measured using dedicated ELISA kits (MesoScaleDiscovery). TG determination in liver was performed using a dedicated kit (Sigma Aldrich).

### 2.5. Insulin (ITT) and glucose tolerance tests (GTT)

These experiments were conducted according to the IMPReSS guidelines (International Mouse Phenotyping Resource of Standardized Screens). Mice were respectively fasted overnight (GTT) or 6 h (ITT) prior to i.p. injection of glucose (2 g/Kg, Sigma–Aldrich) or insulin (0.75 U/Kg, Humalog, Lilly) as per recommended procedures [25]. Glucose was measured in freely moving unrestrained animals using a glucometer (AccuCheck Mobile, Roche) in a drop of blood obtained after incision of the tip of the tail.

### 2.6. In vivo tissue insulin response measurement

Mice were fasted overnight then injected with insulin (0.75 U/Kg, Humalog, Lilly) or saline. Five minutes after injection, mice were sacrificed by cervical dislocation, and tissues were rapidly dissected and stored at –80 °C until further analyses. The western-blotting procedure and a list of antibodies and dilutions used are provided in [Appendix](#).

### 2.7. Quantitative RT-PCR

Real-time PCR reactions procedures are detailed in [Appendix](#). Primers used are available in [Table S6](#).

### 2.8. Microcomputed tomography analysis and adipose tissue histology

Anesthetized animals were introduced in a SkyScan-1178 X-ray tomograph and analyzed as previously described [26]. Epididymal adipose tissue was fixed in 4% paraformaldehyde, paraffin-embedded, and stained with hematoxylin and eosin.

### 2.9. Lipolysis assays

For *in vivo* lipolysis experiments, 6 hrs-fasted *Fmr1*-KO and WT were injected intraperitoneally either with saline or isoproterenol at 1 mg/kg and blood sampled 15 min post injection. For *ex vivo* lipolysis experiments, 6 hrs-fasted *Fmr1*-KO and WT mice were sacrificed, and intra-abdominal white epididymal fat depots were cut in explants then treated with 1 μM isoproterenol or vehicle. Preparation of stromal vascular fraction (SVF) of epididymal adipose tissue was performed as described in [27]. Adipocytes derived from hMADS cells were obtained as described in [28,29] and transfected with anti-*FMR1* or control *siRNA* (Invitrogen) detailed in [Appendix](#). Lipolysis experiments of SVF-derived adipocytes and hMADS adipocytes were performed as described in [27].

### 2.10. Indirect calorimetry

Indirect calorimetry experiments were performed using indirect calorimetry chambers (Phenomaster System, TSE) at the Anexplo Genotoul metabolic phenotyping platform (Toulouse, France).

### 2.11. Liver proteome analysis

Livers from 4 months-old overnight fasted animals were quickly collected after cervical dislocation, snapped frozen in liquid nitrogen and kept at –80 °C until further analysis. Proteins were digested by in-solution digestion and measured on an EASY-nLC 1200 coupled to an Orbitrap Elite mass spectrometer (Thermo Fisher Scientific). All acquired MS data were processed with the MaxQuant software suite [30,31] version 1.5.2.8 against the complete mouse UniProt database

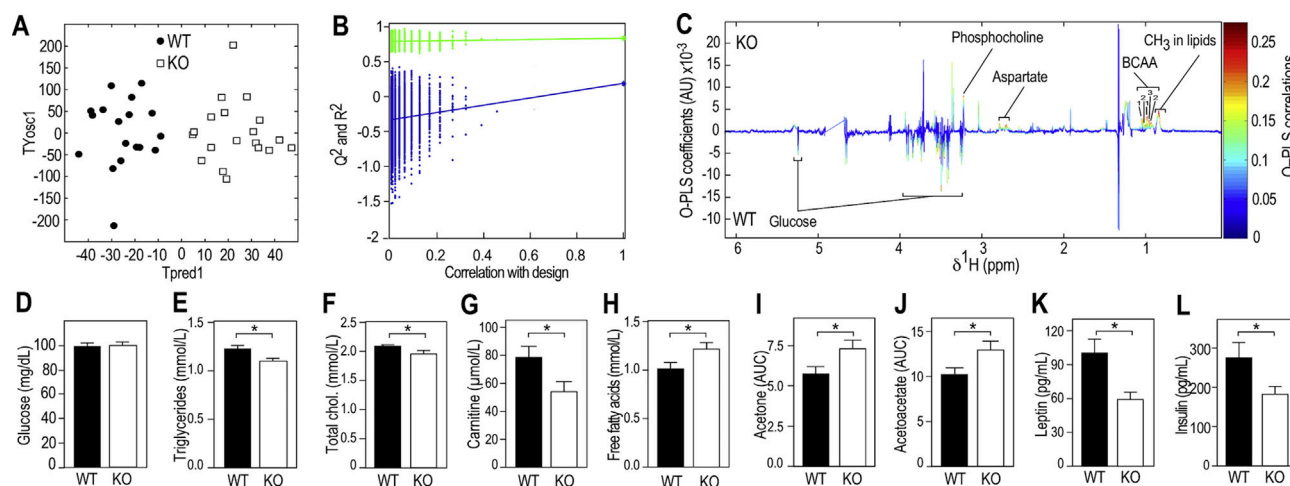


**Figure 1: *Fmr1*-deficiency modifies metabolic profiles in the fed and fasting state.** (A) Orthogonal Partial Least Square Discriminant Analysis (OPLS-DA) of plasma  $^1\text{H}$  NMR spectra from fed *Fmr1*-KO and WT mice. PLS components (TPred1 & TYosc1) corresponding to a combination of the initial NMR spectral variables were computed for each individual.  $n = 18$  WT,  $n = 19$  KO. (B) Permutation testing to assess significance of the OPLS-DA model ( $n = 10,000$  random iterations,  $p = 0.01$ ). (C) Pseudo-spectrum representation of OPLS-DA model to highlight spectral regions discriminating *Fmr1*-KO from -WT samples. s. Positive and negative model coefficients respectively correspond to significantly higher or lower metabolite concentrations in *Fmr1*-KO animals as compared to WT.  $^1\text{H}$  NMR signals corresponding to glucose, aspartate, phosphocholine, the branched amino acids (BCAA) valine (1), isoleucine (2) and leucine (3), and broad resonances from  $\text{CH}_3$  methyl groups present in lipids are highlighted. (D) Fasting plasmatic levels of glucose in *Fmr1*-KO and WT animals. Data are means  $\pm$  SEM;  $n = 11$  WT,  $n = 12$  KO; 2-tailed Student's T-test: ns. (E) Fasting plasmatic levels of triglycerides (TG) in *Fmr1*-KO and WT animals. Data are means  $\pm$  SEM;  $n = 28$  WT,  $n = 28$  KO; 2-tailed Student's T-test: \*,  $p < 0.05$ . (F) Fasting plasmatic levels of total cholesterol in *Fmr1*-KO and WT animals. Data are means  $\pm$  SEM;  $n = 27$  WT,  $n = 28$  KO; 2-tailed Student's T-test: \*,  $p < 0.05$ . (G) Fasting plasmatic levels of carnitine in *Fmr1*-KO and WT animals. Data are means  $\pm$  SEM;  $n = 13$  WT,  $n = 9$  KO; 2-tailed Student's T-test: \*,  $p < 0.05$ . (H) Fasting plasmatic levels of free fatty acids (FFA) in *Fmr1*-KO and WT animals. Data are means  $\pm$  SEM;  $n = 26$  WT,  $n = 25$  KO; 2-tailed Student's T-test: \*,  $p < 0.05$ . (I) Relative quantification of  $^1\text{H}$  NMR signal from acetone (2.22 ppm) in fasting *Fmr1*-KO and WT animals. Data are means  $\pm$  SEM;  $n = 12$  WT,  $n = 13$  KO; 2-tailed Student's T-test: \*,  $p < 0.05$ . (J) Relative quantification of  $^1\text{H}$  NMR signal from acetoacetate (2.27 ppm) in fasting *Fmr1*-KO and WT animals. Data are means  $\pm$  SEM;  $n = 12$  WT,  $n = 13$  KO; 2-tailed Student's T-test: \*,  $p < 0.05$ . (K) Fasting leptin in *Fmr1*-KO and WT animals. Data are means  $\pm$  SEM;  $n = 21$  WT,  $n = 18$  KO; 2-tailed Student's T-test: \*,  $p < 0.05$ . (L) Fasting insulin in *Fmr1*-KO and WT animals. Data are means  $\pm$  SEM;  $n = 11$  WT,  $n = 12$  KO; 2-tailed Student's T-test: \*,  $p < 0.05$ .

(taxonomy ID10090). Comparison analysis for individual protein levels between genotype was run on normal rank-based inverse log-transformed label-free quantification (LFQ) values and individual FDR were calculated. GO analysis was performed using String (v10.5) [32] and Panther (v12.0) expression analysis tools [33,34].

### 2.12. Puromycin-labeling of neosynthesized peptides

The hepatic cell line FL83B was transduced with a lentivirus expressing *shFmr1* or *shControl* and FACS-sorted based on eGFP expression, as described in [35]. FMRP was tested using the m1C3 monoclonal antibody against FMRP in western-blotting [36] or the avian IgY#C10 polyclonal antibodies by immunofluorescence staining [6,37,38]. The puromycin-labeling assay was performed according to [39]. Puromycin (10  $\mu\text{g}/\text{mL}$ ) incorporation was performed in the presence or absence of cycloheximide (50  $\mu\text{g}/\text{mL}$ ) for 15 or 30 min. Proteins were visualized after protein transfer to nitrocellulose membranes by Ponceau staining and puromycin-labeled neosynthesized peptides were visualized by immunoblotting with anti-puromycin 12D10 antibody (Millipore) followed by HRP-coupled secondary antibodies and electrochemiluminescence detection using a Fusion VX-Imager (Vilber). Puromycin signals were quantified in each lane by densitometric analysis using the ImageJ software, normalized to Ponceau signal in the corresponding lane and then adjusted to average signal in control cells at 15 min.

### 2.13. Metabolic network analysis

MetaboSignal R package [40,41] was used to build the shortest paths network from FMRP to the metabolites of interest (Table S5), integrating the proteins dysregulated in the liver as extra nodes to the network (Table S6). Pivotal betweenness was then computed (Table S7).

### 2.14. Immunoaffinity (IA) capture of FMRP complexes in FL83B cells or liver extracts

FL83B cells or *Fmr1*-WT and -KO liver were homogenized in IA buffer (10 mM Tris pH 7.4, 150 mM NaCl, 1.25 mM  $\text{MgCl}_2$ , 0.5% NP40, 1 mM DTT, 5 U/mL RNasin (Invitrogen)). The lysates were centrifuged at 10,000 g for 15 min at 4  $^{\circ}\text{C}$ . The collected supernatant was then raised to 400 mM NaCl and 30 mM EDTA [37]. For each IA assay, 500  $\mu\text{g}$  of proteins from FL83B cells or liver extract was incubated in the presence of 60  $\mu\text{g}$  of anti-FMRP IgY#C10 antibodies or non-immune IgY immobilized on 15  $\mu\text{L}$  of anti-chicken IgY agarose beads (Gallus Immunotech Inc.). Samples were incubated overnight under rotation at 4  $^{\circ}\text{C}$  and washed 4 times with buffer containing 10 mM Tris pH 7.4, 400 mM NaCl, 10 mM EDTA, 0.5% NP40. 1/5th of each assay was used for immunoblot analyses using anti-FMRP mAb1C3 antibody [36] IA-captured mRNA were then phenol-extracted, precipitated with sodium acetate, and resuspended in water and subjected to reverse transcription (RT) using the SuperScript III system (Invitrogen). RT products were subjected to polymerase chain reaction (PCR), using a PCR Master Kit (Promega) and primers detailed in Table S8. PCR products were visualized on a 2.5% TAE agarose gel and amplicon size was verified using the BenchTop DNA ladder (Promega).

### 2.15. Statistics

Normality of data was assessed using Kolmogorov–Smirnov's test. To compare 2 groups, 2-tailed unpaired Student's T-test was used. For non-normal data, raw data were log-transformed to meet normality criteria prior to Student's T-test. If sample size  $n < 8$  or if normality was not reached after log-transformation, data were analyzed using Mann & Whitney's non-parametrical U-test. Multiple group

## Original Article

comparisons were performed ANOVAs and detailed statistics appear in Table S9. *Post hoc* comparisons were performed either using Šidák's correction for multiple comparison or Fisher's Least Significance Difference test (if less than 6 comparisons were performed), as stated in the legends. Statistical significance was set according to a two-tailed p-value ( $p < 0.05$ ). Statistical analysis was performed using GraphPad Prism version 6.00 for iOS (GraphPad Software, USA).

### 2.16. Study approvals

All animal studies were conducted in facilities accredited by legal authorities (Direction Départementale de Protection des Populations des Alpes-Maritimes, accreditation #C-06-152-5) using procedures approved by the Ministère de l'Enseignement Supérieur et de la Recherche (agreement #00788.01 and #05224.01). Samples and data collection from Fragile X patients and controls were approved by the medical ethics committee of the University of Antwerp in Belgium (agreement #B300201523589). The study was conducted in accordance with statutes and regulations regarding the protection of the right and welfare of human subjects' participation in biomedical research (World Declaration of Helsinki).

## 3. RESULTS

### 3.1. *Fmr1*-deficiency alters plasmatic metabolites in FXS mouse model

To study the potential impact of *Fmr1*-deficiency on general metabolic homeostasis, we used proton nuclear magnetic resonance ( $^1\text{H}$  NMR) spectroscopy to profile the plasma metabolome of 4-months old *Fmr1*-WT and -KO male littermates fed *ad libitum*. Supervised multivariate statistical modelling of  $^1\text{H}$  NMR data indicated that *Fmr1*-KO animals displayed a characteristic plasmatic metabolic signature, significantly distinct from controls (Figure 1A,B). In *Fmr1*-KO plasma, we identified a significant decrease in signals from glucose, paralleled by an increase in signals from branched chain amino acids, aspartate, and phosphocholine (Figure 1C).  $-\text{CH}_3$  resonances from fatty acid (FA) methyl groups at  $\sim 0.9$  ppm [42] were also significantly increased in *Fmr1*-KO animals compared to WT (Figure 1C). These results suggest that *Fmr1*-deficiency induces possible dysregulations of glucose and lipid metabolism observable in the fed state.

We then examined the levels of a number of metabolic markers after an overnight fast. Fasting glycemia appeared unaffected by *Fmr1*-deficiency as glycemia from *Fmr1*-WT and KO animals were both reached standard fasting glucose levels of 100 mg/dL (Figure 1D). In contrast, we observed reduced circulating levels of triglycerides (TG) and total cholesterol in fasted *Fmr1*-KO animals, accompanied by a reduction in plasma carnitine, a quaternary amine involved in lipid metabolism (Figure 1E–G). Conversely, we observed significant increases in free FA (FFA) and  $^1\text{H}$  NMR signals from the ketone bodies (KB) acetone and acetoacetate (Figure 1H–J). Finally, we highlighted that *Fmr1*-deficiency reduced the fasting circulating levels of the metabolic hormones leptin and insulin (Figure 1K,L). Collectively, these variations in metabolic markers both in the fasted and fed state pointed towards dysregulations in glucose and lipid homeostasis in *Fmr1*-KO mice.

### 3.2. *Fmr1*-deficiency enhances glucose tolerance and insulin response

To further explore these dysregulations, we challenged energy homeostasis in *Fmr1*-WT and -KO littermates by performing glucose and insulin tolerance tests (GTT and ITT, respectively). After an overnight or a 6 h fast, fasting glycemia was comparable for both genotypes (TO,

Figure 2A,B). During the course of the GTT, there was a significant effect of genotype on glycemia over time (Figure 2A). Post injection of glucose, glycemia was significantly lower in *Fmr1*-KO animals at 30, 45 and 60 min, when compared to WT animals (Figure 2A). During ITT, there was also a significant effect of genotype on glycemia over time after insulin injection. At 90 and 120 min, glycemia of *Fmr1*-KO animals were significantly lower than in *Fmr1*-WT controls (Figure 2B). Cumulative glycemia calculated over the course of the GTT and ITT were also significantly decreased in *Fmr1*-KO animals (Figure 2C,D). We further investigated the insulin response at the molecular level in *Fmr1*-KO and WT liver. Injection of a bolus of insulin triggered activation and autophosphorylation of the insulin receptor (InsR) in the liver, leading to an increased phosphorylation at Tyr<sup>1146</sup> and Tyr<sup>1151/1151</sup> in both groups. In *Fmr1*-KO animals, the phosphorylation of InsR was increased both in basal conditions and upon insulin injection when compared to *Fmr1*-WT liver (Figure 2E). We then monitored the phosphorylation status of Akt at Ser<sup>473</sup>. Following insulin injection, the increase in Akt phosphorylation was significantly steeper in the *Fmr1*-KO liver (Figure 2E). These data suggested that loss of FMRP in the liver was accompanied by an increased response to insulin stimulation.

### 3.3. *Fmr1*-deficiency reduces adiposity and shifts metabolism towards a higher use of lipid as energy substrates

As several classes of circulating lipids were impacted in *Fmr1*-KO mice (Figure 1C,E–K) and leptin was reduced, we then sought to investigate the impact of *Fmr1*-deficiency on adipose tissue, the main tissue for lipid storage, as well as a site of expression for FMRP (Figure S1). We used  $\mu\text{CT}$  X-ray tomography and showed that *Fmr1*-deficiency differentially affected intra-abdominal adipose tissue (IAAT) and subcutaneous adipose tissue (SCAT). The volume of IAAT was significantly reduced by 53.4% in *Fmr1*-KO animals, whilst SCAT was not affected (Figure 3A). Further, fat pads of *Fmr1*-KO mice displayed smaller adipocytes, with a reduced average surface as compared to control animals (Figure 3B,C). Considering that adipocytes had a spherical shape, we extrapolated their volume from the adipocyte area measures and estimated that the mean adipocyte volume was decreased by 40.1% in *Fmr1*-KO animals (mean WT adipocyte volume =  $1.76 \pm 0.05 \times 10^4 \mu\text{m}^3$  vs. mean KO adipocyte volume =  $1.052 \pm 0.17 \times 10^4 \mu\text{m}^3$ ). This was within the range of the total WAT volume ratio (53.4%, Figure 3A) and suggests that the total number of adipocytes is likely preserved in the absence of FMRP.

In parallel, we showed that *Fmr1*-KO and WT WAT express similar mRNA levels for the adipocyte precursor marker *Pdgfra* [43], suggesting that the adipocyte precursor pool is not impacted in WAT (Figure S2A). Also, FMRP expression increased upon differentiation of adipocytes derived from the stromal vascular fraction (SVF) of WAT (Figure S2B). However, analysis of SVF-derived *Fmr1*-KO adipocytes did not reveal clear adipogenesis defects when compared to *Fmr1*-WT adipocytes (Figure S2C). In addition, human multipotent adipose-derived stem (hMADS) cells repressing *FMR1* did not display alterations in the course of differentiation or expression of the mature adipocyte markers *PLIN1* and *FABP4* (Figure S3A,B). Thus, the reduction in fat mass observed in *Fmr1*-KO animals appeared unlikely to be due to impaired adipogenesis but rather to reduced fat storage in adipocytes *in vivo*. We also observed a reduction in hepatic triglycerides storage in *Fmr1*-KO animals as compared to controls (Figure S4).

Reduced fat storage both in liver and WAT could reflect a higher consumption of lipids as energetic substrate in *Fmr1*-deficient animals. We therefore used indirect calorimetry chambers to

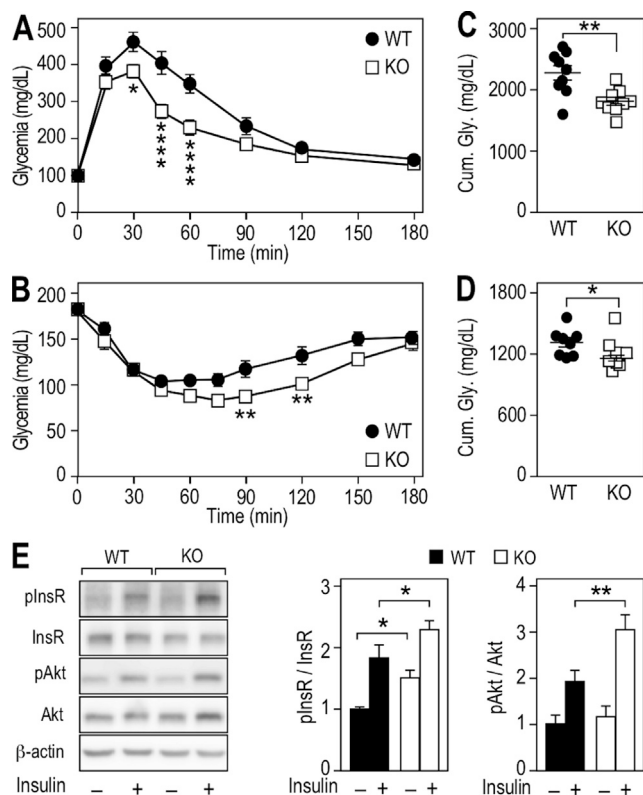


**Figure 2: *Fmr1*-deficiency improves glucose tolerance and insulin sensitivity in liver.** (A) Glucose tolerance test (GTT) in *Fmr1*-KO and WT animals. Data are means  $\pm$  SEM; n = 9 WT, n = 9 KO; 2-way ANOVA: p(Genotype) = 0.0034, p(Time) < 0.0001, p(Interaction) < 0.0001; Sidák's post hoc tests for genotype-wise comparisons: \*, p < 0.05, \*\*\*\*, p < 0.0001. (B) Insulin tolerance test (ITT) in *Fmr1*-KO and WT animals. Data are means  $\pm$  SEM; n = 8 WT, n = 8 KO; 2-way ANOVA: p(Genotype) = 0.0117, p(Time) < 0.0001, p(Interaction) = 0.0134; Sidák's post hoc tests for genotype-wise comparisons: \*\*, p < 0.01. (C) Cumulative glycemia over the 3 h course of GTT. Data are means  $\pm$  SEM; n = 9 WT, n = 9 KO; 2-tailed Student's T-test: \*\*, p < 0.01. (D) Cumulative glycemia over the 3 h course of ITT. Data are means  $\pm$  SEM; n = 8 WT, n = 8 KO; 2-tailed Student's T-test: \*, p < 0.05. (E) Western-blot and densitometric analysis of insulin receptor (InsR) and Akt phosphorylation status in liver from *Fmr1*-KO and WT animals injected with saline or insulin. Densitometric analysis is presented as means  $\pm$  SEM of phosphoproteins signals ratios relative to total protein, all signals being normalized to  $\beta$ -actin. InsR-Saline: n = 6 animals/group, InsR-Insulin: n = 5 animals/group; 2-way ANOVA: p(Genotype) = 0.0027, p(Treatment) < 0.0001, p(Interaction) = 0.7424; Fisher's LSD post hoc tests for genotype-wise comparisons: \*, p < 0.05. Akt: n = 5 animals/group; 2-way ANOVA: p(Genotype) = 0.0215, p(Treatment) < 0.0001, p(Interaction) = 0.0924; Fisher's LSD post hoc tests for genotype-wise comparisons: \*\*, p < 0.01.

measure circadian ingestive behavior, activity, O<sub>2</sub> consumption, and CO<sub>2</sub> production. No significant variations in drinking water intake, food consumption, or total cumulative activity were detected in *Fmr1*-KO animals over the course of indirect calorimetry recordings (Figure S5A–D). Furthermore, *Fmr1*-deficiency did not affect the energetic expenditure (EE) and its average over 24 h (Figure S5E,F). The respiratory exchange rate (RER), which provides information about metabolic substrate utilization (lipid or carbohydrate), was calculated by dividing the volume of CO<sub>2</sub> produced (VCO<sub>2</sub>) over the volume of oxygen consumed (VO<sub>2</sub>) [44]. The RER profile of *Fmr1*-KO animals over 24 h appeared shifted towards lower RER values (Figure 3D). Furthermore, its average

was significantly decreased in *Fmr1*-KO animals as compared to controls (Figure 3E), indicating that *Fmr1*-deficiency contributes to shift metabolism towards an enhanced utilization of lipid substrates as energetic substrate.

#### 3.4. *Fmr1*-deficiency increases lipolysis in adipocytes

In white adipose tissue (WAT), fat accumulation is regulated by activation of  $\beta$ -adrenergic receptors, which elicits intracellular TG hydrolysis and release of glycerol and FFA to the general circulation. We monitored lipolysis *in vivo* in *Fmr1*-KO and WT littermates in basal conditions and upon systemic injection of isoproterenol, a pan  $\beta$ -adrenergic receptor agonist. Isoproterenol treatment induced an increase in peripheral plasma glycerol release in both *Fmr1*-WT and -KO mice. Independently of isoproterenol treatment, glycerol release was significantly increased in *Fmr1*-deficient animals (Figure 4A). We mirrored those results in WAT explants from *Fmr1*-KO and WT animals (Figure 4B). This suggests a constitutive overactivation of lipolysis in the absence of FMRP. Also, in *Fmr1*-KO SVF-derived adipocytes, there was a significant increase in glycerol release when isoproterenol was applied, suggestive of a higher sensitivity to  $\beta$ -adrenergic receptor agonists (Figure 4C). Finally, we performed time-course experiments of isoproterenol-induced lipolysis in hMADs transiently transfected with a *siRNA* that efficiently repressed *FMR1* mRNA (Figure S3B). As a readout of lipolysis, in addition to glycerol release, we monitored intracellular TG and FFA release in the medium (Figure 4D). In both *siFMR1* and *siCt1*-transfected cells, isoproterenol treatment impacted intracellular TG levels (Figure 4D). After an initial phase of intracellular TG depletion, *de novo* TG synthesis took over and likely accounted for the progressive recovery in TG levels, hindering the identification of a significant effect of *FMR1*-knockdown over the course of the experiment (Figure 4D). In contrast, when considering FFA and glycerol release induced by isoproterenol treatment, there was a significant impact of *FMR1*-knockdown (Figure 4D). By 120 min, *siFMR1*-transfected adipocytes had released significantly more glycerol and FFA than *siCt1*-transfected adipocytes. These data collectively suggest that loss of FMRP overactivates the  $\beta$ -adrenergic response and increases lipolysis, both in mouse and human adipocytes.

#### 3.5. The absence of FMRP leads to profound changes in the hepatic proteome and increases hepatic protein synthesis

Since FMRP is expressed in the liver (Figure S1), a key organ for the regulation of both glucose and lipid homeostasis, we reasoned that molecular changes in the hepatic proteome could help refine the molecular events underlying the broad metabolic effects driven by FMRP loss. We used quantitative Mass Spectrometry (MS) to characterize the liver proteome of *Fmr1*-KO and WT littermates (Table S1). The Volcano plot representing statistical significance against fold-of-change (FC KO vs WT) for the 2,087 detected proteins appeared dissymmetric (Figure 5A). Among the 307 proteins with a false discovery rate (FDR)  $\leq$  0.01 whose abundance was increased or decreased by at least 1.5-fold (absFC  $\geq$  1.5; Figure 5A), there was a shift towards higher FC with strongest changes in terms of abundance observed for upregulated proteins in the absence of FMRP. Further clustering analysis on these 307 proteins revealed that protein abundance patterns were consistent genotype-wise (Figure 5B). GO analysis of the 307 dysregulated proteins clearly pointed to selective enrichment in pathways linked to lipid metabolism, with the *Fmr1*-KO liver notably displaying increased levels of enzymes or transporters involved in the main routes of FA catabolism (Figure 5C, Table S2–S4). Consistent with this, there was a reduced abundance in

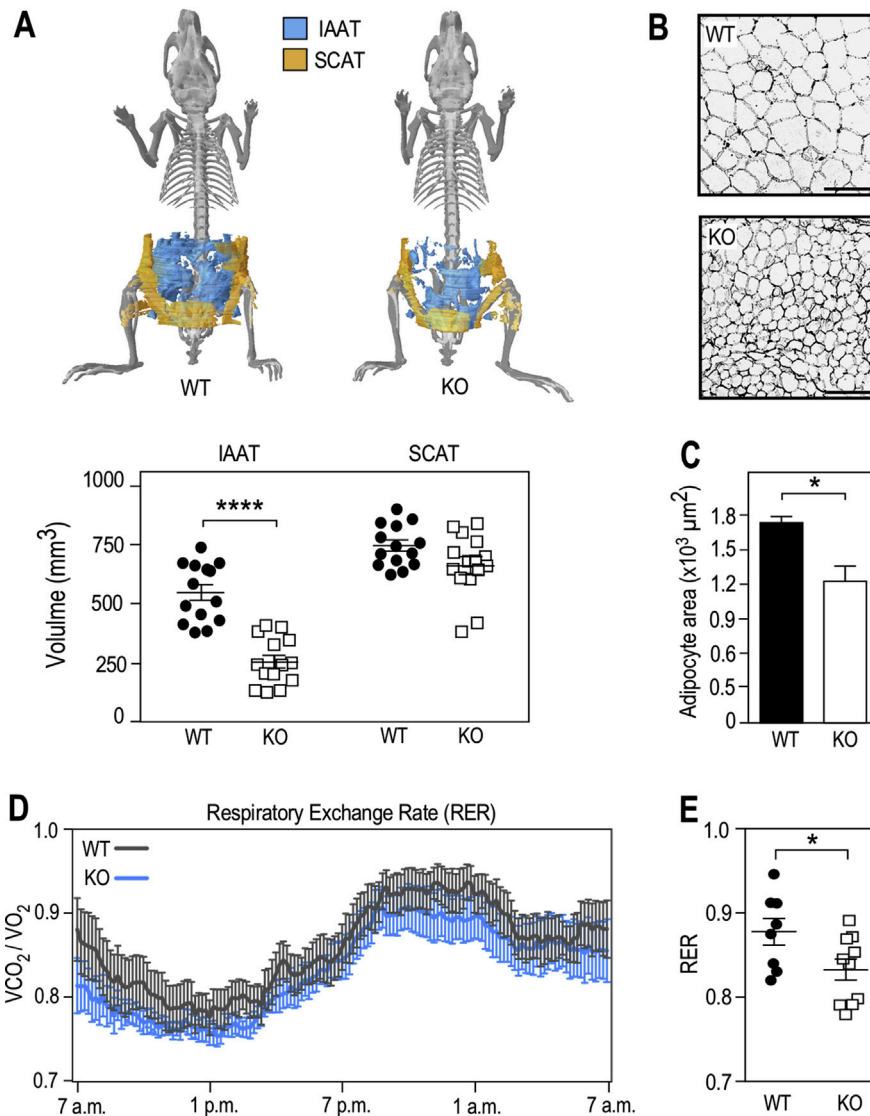


**Figure 3: *Fmr1*-deficiency reduces adiposity, enhances lipolysis, and shifts metabolism towards a better utilization of lipids.** (A) X-ray computerized tomography 3D reconstruction of intra-abdominal (IAAT) and subcutaneous (SCAT) adipose tissues and calculated volumes of IAAT and SCAT in *Fmr1*-WT and KO animals. Data are presented as means  $\pm$  SEM; n = 14 KO, n = 14 WT; 2-way ANOVA: p(Genotype) < 0.0001; p(AT type) < 0.0001; p(Interaction) = 0.0004; LSD post hoc tests for genotype-wise comparisons: \*\*\*\*, p < 0.0001. (B) Representative sections of *Fmr1*-WT and KO IAAT stained with hematoxylin and eosin, black bars represent 100  $\mu$ m. (C) Average adipocyte area in *Fmr1*-WT and KO IAAT. Data are presented as means  $\pm$  SEM; n = 6 WT, n = 6 KO; 2-tailed Mann & Whitney U-test: \*, p < 0.05. (D) Respiratory exchange rate (RER) follow-up over 24 h in 4 months-old *Fmr1*-KO and WT mice. Data are means  $\pm$  SEM every 10 min; n = 8 WT, n = 10 KO. (E) Average RER over 24 h in *Fmr1*-KO and WT mice. Data are means  $\pm$  SEM; n = 8 WT, n = 10 KO; 2-tailed Student's T-test: \*, p < 0.05.

proteins involved in lipid storage and formation of lipoprotein particles in the absence of FMRP (Figure 5C, Table S2–S4), in agreement with the significant reduction in hepatic TG content in *Fmr1*-KO liver (Figure S4). This supported that molecular changes in the liver in the absence of FMRP could participate to metabolic phenotypes linked to lipids in *Fmr1*-KO animals. In contrast to the numerous pathways linked to lipid metabolism highlighted with the GO analysis, only one pathway related to glucose was significantly enriched “starch and glucose metabolism” (Figure 5C, Table S3).

Besides clear overrepresentation of pathways involved in lipid metabolism, the primary enriched pathways involved ribosome, RNA translation, RNA-binding proteins, and amino-acyl-tRNA biosynthesis (Figure 5C, Table S2–S4). Notably, core ribosomal proteins and translation elongation factors were markedly upregulated in the

absence of FMRP (Table S2–S4). We reasoned these changes could reflect a possible increase in hepatic translation in the absence of FMRP. We therefore monitored protein synthesis in the FL83B murine hepatocyte cell line by labeling neosynthesized polypeptides with puromycin [39]. We inactivated FMRP expression by lentiviral transduction of an *shFmr1* or control *shCtl*. Transduced cells expressing the *shFmr1* or control *shCtl* were selected based on their co-expression of eGFP. Immunofluorescence staining using the avian IgY#C10 antibodies revealed a strong reduction of FMRP expression in *shFmr1* cells as compared to *shCtl* cells, while the signal from the ribosomal protein S6 remained unaffected (Figure 5D). Western blot analysis of FMRP expression confirmed that this repression is stable over passages in *shFmr1*-transduced cells (Figure S6A). Puromycin labeling of neosynthesized peptides was strongly decreased when the

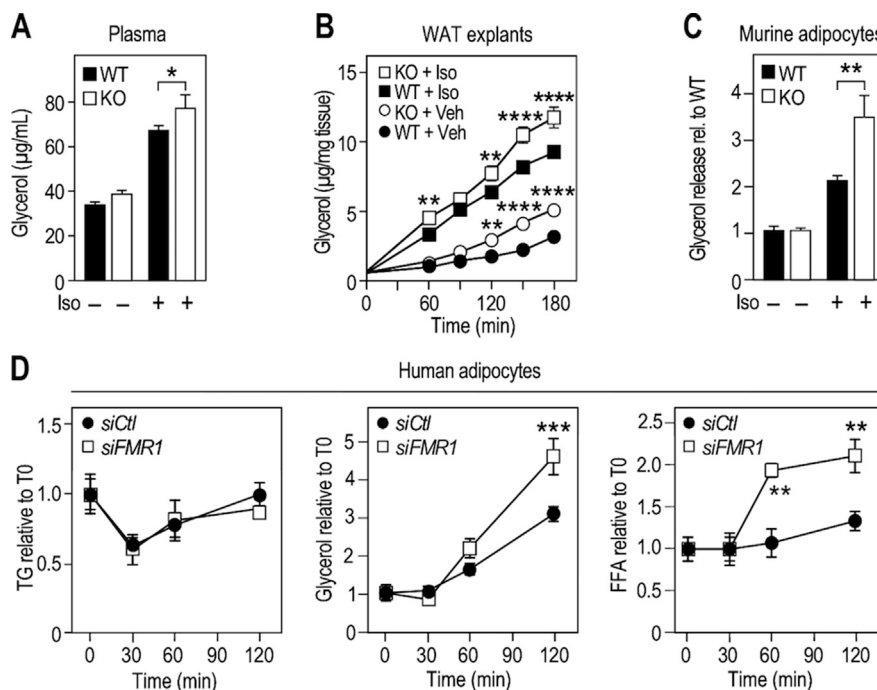


**Figure 4: *Fmr1*-deficiency increases lipolysis in murine and human adipocytes.** (A) Glycerol release in serum as readout of lipolysis in *Fmr1*-KO and WT animals before and 15 min after injection of isoproterenol (Iso). Data are presented as means  $\pm$  SEM;  $n = 13$  WT,  $n = 12$  KO; 2-way ANOVA:  $p(\text{Genotype}) = 0.0327$ ;  $p(\text{Treatment}) < 0.0001$ ;  $p(\text{Interaction}) = 0.4161$ ; LSD post hoc tests for genotype-wise comparisons: \*,  $p < 0.05$ . (B) Glycerol release as readout of lipolysis following treatment with Iso in *ex-vivo* culture supernatant of epididymal white adipose tissue (WAT) explants. Data were normalized to individual WAT explant weight and presented as means  $\pm$  SEM;  $n = 8/\text{condition}$ ; 3-way ANOVA:  $p(\text{Genotype}) < 0.0001$ ,  $p(\text{Treatment}) < 0.0001$ ,  $p(\text{Time}) < 0.0001$ ,  $p(\text{Genotype} \times \text{Treatment}) = 0.4884$ ,  $p(\text{Genotype} \times \text{Time}) < 0.0001$ ,  $p(\text{Treatment} \times \text{Time}) < 0.0001$ ,  $p(\text{Genotype} \times \text{Treatment} \times \text{Time}) = 0.5818$ ; Sidák's post hoc tests for genotype-wise comparisons: \*\*,  $p < 0.01$ ; \*\*\*\*,  $p < 0.0001$ . (C) Glycerol release as readout of lipolysis following treatment with Iso *in vitro* in SVF-derived adipocytes from *Fmr1*-WT and KO animals. Data were normalized to protein content and presented as means ratios relative to control WT - Iso  $\pm$  SEM;  $n = 6$  WT,  $n = 6$  KO; 2-way ANOVA:  $p(\text{Genotype}) < 0.0205$ ;  $p(\text{Treatment}) < 0.0001$ ;  $p(\text{Interaction}) = 0.0102$ ; LSD post hoc tests for genotype-wise comparisons: \*\*,  $p < 0.01$ . (D) Intracellular TG and release of glycerol and FFA following isoproterenol-induced lipolysis in human hMADS cells differentiated into adipocytes, transiently transfected with anti-*FMR1* (*siFMR1*) or control siRNA (*siCtl*). Data were normalized to protein content and presented as means ratios relative to *siCtl* - Iso  $\pm$  SEM;  $n = 4/\text{condition}$ ; 2-way ANOVA:  $p(\text{siRNA}_{\text{TG}}) = 0.7478$ ,  $p(\text{Time}_{\text{TG}}) = 0.0049$ ,  $p(\text{Interaction}_{\text{TG}}) = 0.9339$ ;  $p(\text{siRNA}_{\text{Glycerol}}) = 0.0102$ ,  $p(\text{Time}_{\text{Glycerol}}) < 0.0001$ ,  $p(\text{Interaction}_{\text{Glycerol}}) = 0.0048$ ;  $p(\text{siRNA}_{\text{FFA}}) = 0.0008$ ,  $p(\text{Time}_{\text{FFA}}) < 0.0001$ ,  $p(\text{Interaction}_{\text{FFA}}) = 0.0081$ ; LSD post hoc tests for siRNA-wise comparisons: \*\*,  $p < 0.01$ ; \*\*\*\*,  $p < 0.0001$ .

translation inhibitor cycloheximide was applied, showing the specificity of the labeling (Figure S6B). After both 15 min and 30 min of treatment, we observed a significant increase in puromycin incorporation in the FL83B-*shFmr1* cell line as compared to the FL83B-*shCtl* cell line (Figure 5E,F). These data supported that FMRP loss exaggerated protein synthesis in hepatocytes, in line with the shift towards higher protein abundances in the *Fmr1*-KO liver and the significant enrichment in GO terms related to "Translation" or "Ribosome" highlighted in the study of the *Fmr1*-KO liver proteome (Figure 5A,C, Table S3, S4).

### 3.6. FMRP targets hepatic mRNAs linked to lipid homeostasis

To functionally connect FMRP to the observed metabolic phenotypes and identify the molecular pathways involved, we used a network-based approach integrating directed metabolic and signaling networks [40,41]. We first compiled an extended list of metabolites deriving from the metabolic biomarkers identified in our initial metabolomics and biochemical measurements (Figure 1, Table S5) and imputed a number of interactions (Table S6). Notably, the network displays in the inner circle close around FMRP the putative interactions with the 307 proteins significantly dysregulated by at least 1.5-fold in the liver in its absence (Table S2). Then, to identify metabolic nodes forming functional paths between FMRP and its associated metabolites, we analyzed the topology of the resulting network (Figure 6A) and derived the relative importance of each node within the network using

a measure of centrality (pivotal betweenness (PB) described in [45], Table S7). Among the 307 dysregulated proteins in the *Fmr1*-KO liver, 175 displayed PB distinct from 0 (Table S7), indicating that they are likely to contribute to the observed metabolic signature. The resulting network (Figure 6A) highlights a number of protein nodes dysregulated in the *Fmr1*-KO liver and connecting FMRP to the metabolites with single-step paths (Figure 6A,B).

To further validate *in vivo* the network predictions and ascertain that FMRP could directly regulate the translation of some pivotal proteins, we tested whether FMRP interacted in hepatocyte with a series of mRNAs encoding proteins appearing in the network with PB distinct from zero and with functions directly involved in lipid and glucose metabolism (Figure 6A,B). FMRP-associated messenger ribonucleoproteins (mRNPs) from FL83B hepatocytes were efficiently trapped by immune-affinity (IA) capture, as shown by the enrichment in FMRP in the IA preparations and the concomitant strong depletion in FMRP signal in the post-IA supernatant (Figure 6C). *Cpt1a*, *Slc16a1*, *Aldh3a2*, *Abcd3*, and *Tecr* mRNA, as well as *Fmr1* mRNA, itself an extensively validated mRNA target of FMRP [46], were detected by RT-PCR in IA-captured FMRP complexes and not recovered in the control fraction (Figure 6D). In contrast, the unrelated mRNA *Actb*, *Ckdn1a*, *Hprt*, and *Gapdh* or mRNAs encoding proteins with a null PB such as *Plin3* were not detected (Figure 6D, Figure S6C). Also, the mRNAs encoding the pivotal proteins Agl, Gys2, or Apoa2 were not recovered in FMRP mRNA

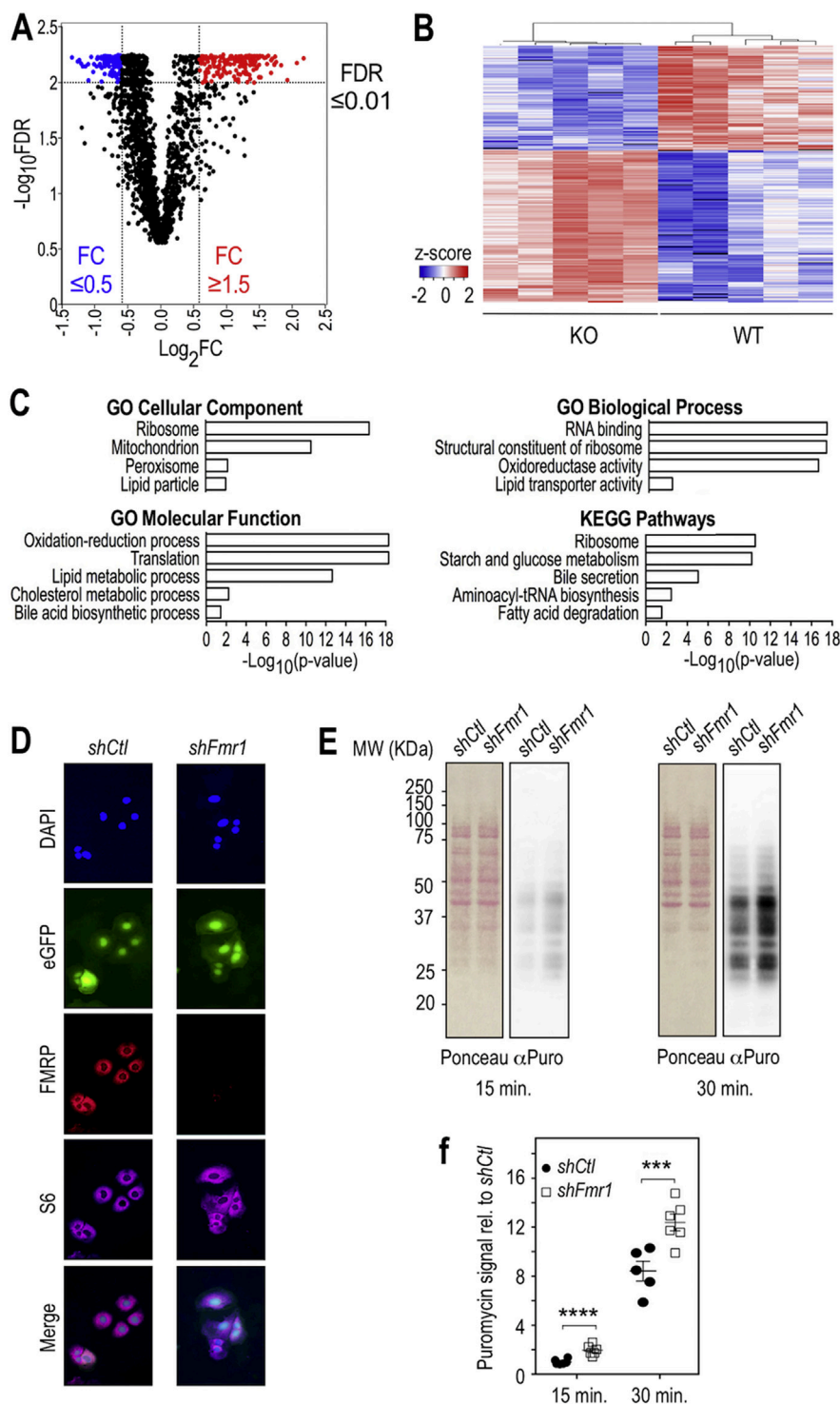


**Figure 5: Loss of FMRP provokes profound changes in the hepatic proteome and enhances translation.** (A) Volcano plot of statistical significance presented as  $-\log_{10}$  transformed false-discovery rate (FDR) against fold-of-change for each quantified protein in *Fmr1*-KO and WT liver.  $n = 5$  WT,  $n = 5$  KO. Significantly upregulated proteins and downregulated proteins ( $\text{FDR} < 0.01$ ) appear respectively in red and blue. (B) Heatmap visualization and clustering analysis of significantly affected proteins whose abundance was increased or decreased by at least 1.5-fold (see list in [SI Appendix, Table S2](#)).  $n = 5$  WT,  $n = 5$  KO. Color code refers to the calculated z-score, missing values appear in black. (C) Selection of GO terms significantly enriched in the list of proteins presented in [b](#) and [Table S2](#) (see [SI Appendix](#)) and associated adjusted p-value ([Table S3, S4](#)). (D) Immunofluorescence analysis of FMRP expression in the FL83B hepatic cell line transduced with a virus driving the expression of a control shRNA (*shCtl*) or an shRNA targeting *Fmr1* (*shFmr1*) coupled to eGFP (green). FMRP was detected with IgY#C10 anti-FMRP antibodies (red) and the ribosomal protein S6 with anti-S6 antibodies (purple). Nuclei were counterstained with DAPI (blue) and merge images are shown in the last panel. The same exposure time was used for image captures of *shFmr1*- and *shCtl* transduced cells. (E) Translation monitoring assay using puromycin-labeled proteins in the *shFmr1*- or *shControl* (*shCtl*)- inactivated cells. Cells were labeled with puromycin for 15 and 30 min. Cell homogenates were analyzed by SDS-PAGE and proteins transferred to nitrocellulose membranes. Separated proteins were stained with Red Ponceau followed by immunoblotting with an anti-puromycin antibody ( $\alpha$ -Puro) that labels neosynthesized peptides. (F) Densitometric analysis of puromycin signal in (E). Data were normalized to total protein Ponceau

complexes, suggesting selectivity in FMRP mRNA recognition (Figure S6C). To further validate that the identified associations also occurred *in vivo*, we performed IA-capture experiments in liver homogenates obtained from *Fmr1*-WT and -KO mice and confirmed the presence of *Cpt1a*, *Slc16a1*, *Aldh3a2*, *Abcd3* and *Tecr* mRNA in FMRP-containing mRNPs (Figure S7). These experiments suggest that FMRP associates with mRNA encoding pivotal enzymes and transporters in the network and likely controls their translation in the liver. This could contribute to the lipid-related metabolotypes observed in *Fmr1*-KO animals.

### 3.7. FXS patients display reduced glycemia, insulinemia and increased circulating FFA

To further assess the clinical relevance of the identified metabolic effects induced by loss of FMRP in FXS mouse model, we collected sera samples in a cohort of 25 FXS patients, bearing *FMR1* full-mutation (above 200 CGG repeats in the 5'UTR of the gene) which leads to *FMR1* gene inactivation and loss of FMRP [47], and 29 sex and age-matched controls (Figure S8A,B). Distributions of body mass indexes were not different between patients and controls (Figure S8C). Sera of patients and controls were collected randomly during the day, but the distribution of sample collection time was not differing between control and patient groups (Figure S8D). We then used <sup>1</sup>H-NMR to profile the serum metabolome of controls and FXS patients. O-PLS-DA modelling of <sup>1</sup>H-NMR data showed that FXS patients display a characteristic serum metabolic signature that is significantly different from controls (Figure 7A,B). Serum from FXS patients displayed a significant decrease in signals from glucose (Figure 7C,D), similarly to *Fmr1*-KO animals in the nonfasted state (Figure 1C). In FXS patients, there was also a significant decrease in signals from glutamine and alanine, paralleled by an increase in creatine signals (Figure 7C). Finally, FXS patients displayed a significant reduction in insulin levels and a significant increase in circulating FFA as compared to controls (Figure 7E,F).

## 4. DISCUSSION

Here, we provide an in-depth metabolic phenotyping of the FXS mouse model and highlight the consequences of the loss of the translational regulator FMRP on metabolic homeostasis in mice and humans. We further highlighted the contributing molecular mechanisms, as we show that loss of FMRP increased hepatic synthesis of proteins notably involved in lipid metabolism.

### 4.1. The absence of the translational regulator FMRP dysregulates hepatic protein synthesis with consequences on systemic metabolism

In this study, we demonstrate that the absence of FMRP leads to an increase in protein synthesis, as supported by our proteomics data in the *Fmr1*-KO liver in combination with quantification of protein synthesis in *Fmr1*-deficient hepatocytes. This depicts FMRP as a regulator of hepatic translation, in agreement with its presence on polyribosomes from mouse liver [2]. Biological network integration of metabolomics and proteomics data enabled us to identify key mRNA targets of FMRP linked to the metabolic phenotypes observed in *Fmr1*-KO animals: *Cpt1a*, *Slc16a1*, *Aldh3a2*, *Abcd3*, and *Tecr*. Importantly, these mRNA were previously identified as putative FMRP targets in

large-scale screenings [5,48] and we have experimentally validated their association with FMRP and the overabundance of the corresponding proteins in the *Fmr1*-KO liver. These data support the fact that FMRP functions as a translational repressor in the liver for this subset of mRNAs and directly controls translation of the cognate protein. Our work indicates that loss of FMRP determines increased abundances of key enzymes or transporters cooperating in FA hepatic metabolism either through direct translational regulation, or indirectly possibly through compensatory or adaptive mechanisms. Although we cannot exclude the fact that the activity of these enzymes and transporters could be downregulated to compensate for their overabundance, dysregulated hepatic expression of these proteins could explain the variations in the circulating levels of a number of metabolites and contribute to the global metabolic changes observed in *Fmr1*-KO animals. Notably, in the absence of FMRP, overabundance of *Cpt1a*, the rate limiting enzyme of FA mitochondrial  $\beta$ -oxidation which transfers the acyl group of LCFA-CoA conjugates onto carnitine [49], could directly improve the mitochondrial uptake of long-chain fatty acids and their subsequent mitochondrial  $\beta$ -oxidation. This is in agreement with previous work showing that increase in CPT1A activity enhanced  $\beta$ -oxidation rates both *in vitro* and *in vivo*, reduced hepatocyte TG accumulation and secretion and increased KB formation [50,51], in agreement with our findings in *Fmr1*-KO mice. In the absence of FMRP, the increased synthesis of the monocarboxylate transporter *Slc16a1* [52] could also favour hepatic export of KB, the terminal breakdown products of mitochondrial  $\beta$ -oxidation, contributing to elevate the circulating levels of the KB acetone and acetoacetate in *Fmr1*-KO mice. Furthermore, overabundance of the FA transporter *Abcd3* and of the aldehyde dehydrogenase *Aldh3a2* could also be indicative of increased peroxisomal  $\beta$ -oxidation of lipids [53]. All these data suggest a direct link between loss of the translational regulator FMRP in liver and lipid homeostasis. FMRP is expressed in all peripheral tissues, except in adult muscle [13,54]. Further studies are now required to understand the impact on translation of FMRP loss in extra-hepatic peripheral tissues with metabolic roles, and how it could disrupt their metabolic interplay.

### 4.2. The absence of FMRP perturbs key metabolic pathways

In the absence of FMRP, we also show that key metabolic signaling pathways are over-activated: the insulin-mediated control of glucose homeostasis and the  $\beta$ -adrenergic control of lipolysis. Excessive insulin signaling in the brain [14,15] and in the intestine [16] was previously described in the *dfmr1* FXS drosophila model and also associated with excessive *Akt* phosphorylation. Our work further extends these findings to the liver in the *Fmr1*-KO mouse model and suggests that FMRP is generally required for the fine-tuning of the response to insulin. Increased sensitivity to insulin in the liver could explain the improved glucose tolerance in *Fmr1*-KO animals, while the reduced circulating levels of insulin might result from a physiological adaptation to counteract excessive insulin signaling. Defective insulin signaling in other peripheral organs might participate to the glucose-related phenotypes we describe in the present study. In mice, intestinal gluconeogenesis is essential to maintain glycemia in the absence of hepatic glucose production [55]. Furthermore, bone is also a tissue exerting some control on metabolism, and notably on the insulin system [56]. Given the fact that FMRP is not expressed in adult muscle [13,54], we anticipate that the consequences of FMRP loss in muscle

signal, adjusted to average signal in *shCtrl* cells at 15 min and presented as means  $\pm$  cSEM; n = 6 independent measures/group, except for WT 30 min, n = 5; 2-way ANOVA: p(shRNA) < 0.0001, p(Time) < 0.0001, p(Interaction) = 0.4288; LSD post hoc tests for shRNA-wise comparisons: \*\*\*, p < 0.001; \*\*\*\*, p < 0.0001.

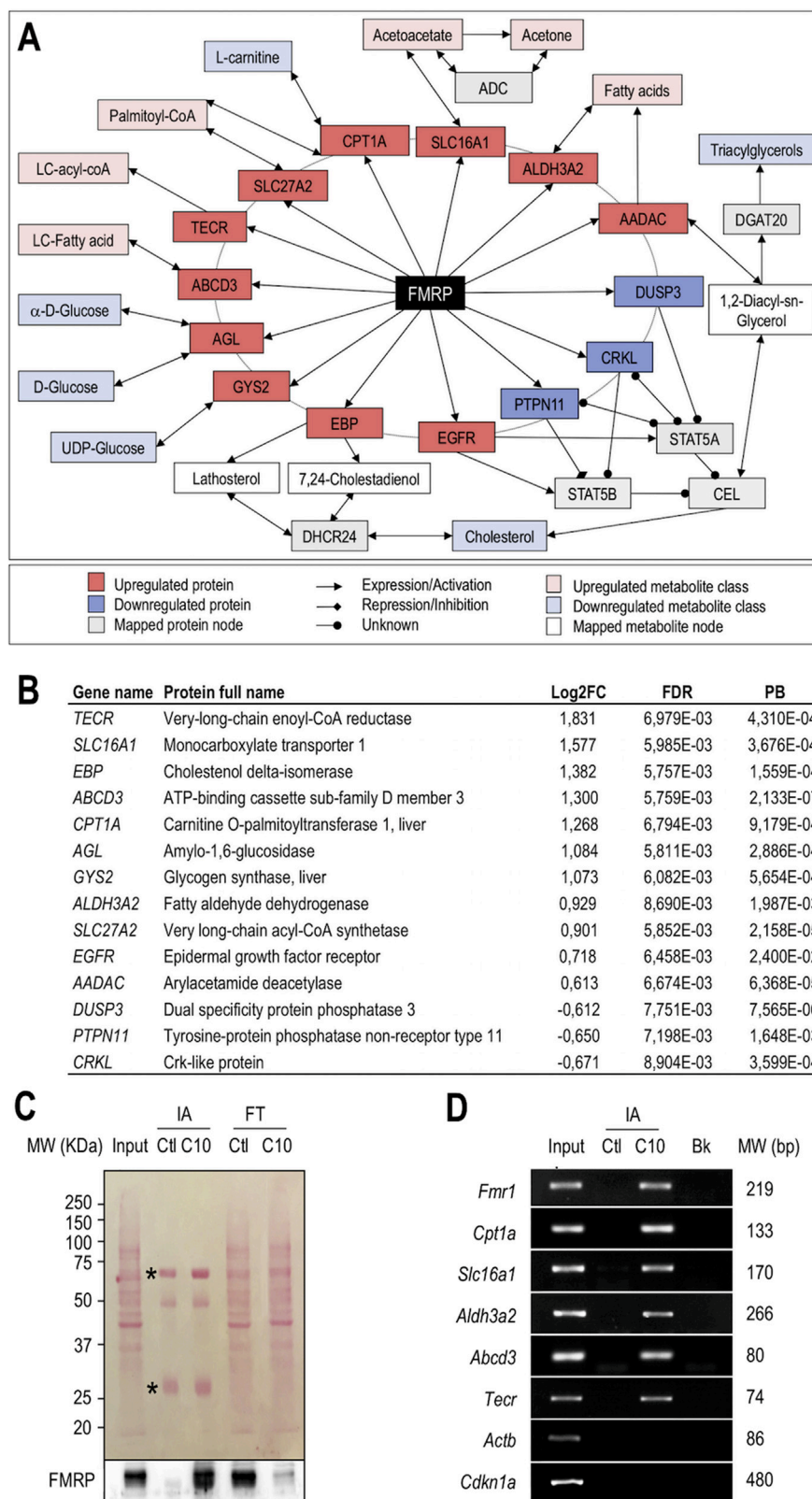


**Figure 6: Metabolic network mapping links FMRP to metabolic dysregulations via specific mRNA targets involved in lipid catabolism.** (A) Classes of circulating metabolites and hepatic proteins significantly dysregulated in *Fmr1*-KO animals were mapped onto the interactome. The resulting network allows connecting the causal protein FMRP to the downstream metabolic consequences of its absence. (B) Pivotal proteins of the network, Log<sub>2</sub> fold-of-change (FC) in the *Fmr1*-KO vs WT liver, associated adjusted p-value (FDR) and normalized pivotal betweenness scores (PB). (C) Cell homogenates from FL83B hepatocytes (Input), immuno-affinity (IA) purified complexes, captured with control IgY (IA Ctl) or anti-FMRP IgY#C10 (IA C10) antibodies and corresponding post-IA flowthrough (FT) supernatants were separated by SDS-PAGE, transferred onto a nitrocellulose membrane

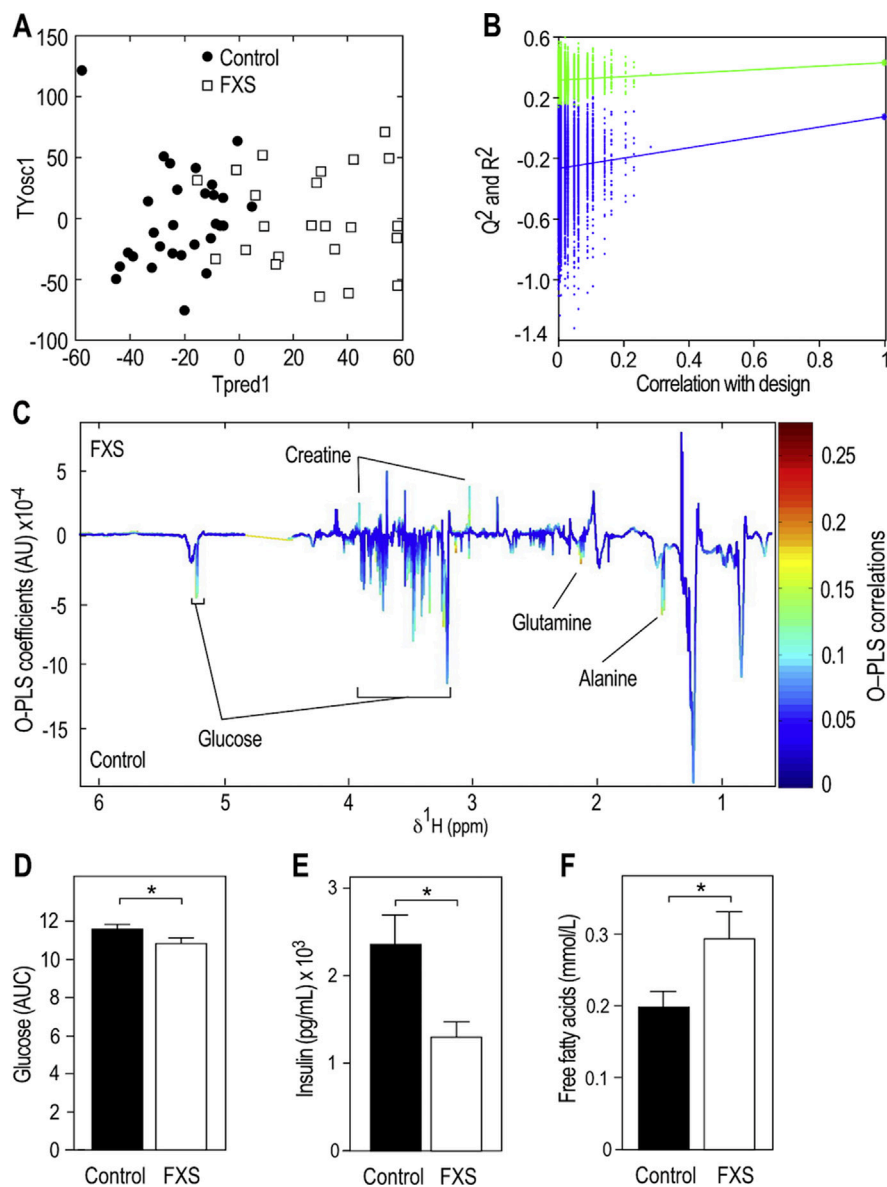


**Figure 7: *FMR1*-deficiency in Fragile X Syndrome patients reduces glucose and insulin and increases circulating FFA.** (A) OPLS-DA of <sup>1</sup>H NMR spectra from sera of FXS patients and sex-, aged-, BMI-matched controls and computation of PLS scores maximizing the segregation of the groups (TPred1 & TYosc1). Sera were collected in the fed state. (B) Permutation testing to assess significance of the O-PLS-DA model presented in (A) (n = 10,000 random iterations, p = 0.026). (C) Pseudo-spectrum representation of OPLS-DA model coefficients to highlight spectral regions responsible for discrimination between FXS and control samples. Positive and negative model coefficients respectively correspond to significantly higher or lower metabolite concentrations in FXS patients as compared to controls. <sup>1</sup>H NMR signals corresponding to glucose, glutamine, alanine and creatine are highlighted. (D) Relative quantification of the <sup>1</sup>H NMR signal corresponding to glucose peak at 5.25 ppm in sera from controls and FXS patients. Data are means ± SEM; n = 28 controls, n = 24 FXS patients; 2-tailed Student's T-test on log-transformed data: \*, p < 0.05. (E) Circulating levels of insulin in controls and FXS patients. Data are means ± SEM; n = 29 controls, n = 25 FXS patients; 2-tailed Student's T-test on log-transformed data: \*, p < 0.05. (F) Circulating levels of FFA in controls and FXS patients. Data are means ± SEM; n = 28 controls, n = 25 FXS patients; 2-tailed Student's T-test on log-transformed data: \*, p < 0.05.

tissue would only be indirect or secondary to the alterations we describe in the liver.

We also highlight that *Fmr1*-deficient experimental models display an enhancement of the β-adrenergic agonist-driven lipolytic response in WAT, which could underpin the reduced adiposity in

*Fmr1*-KO animals. Further, the increased release of FFA from WAT could enhance the bioavailability of lipid substrates for hepatic β- and ω-oxidation and contribute to the shift towards a higher utilization of lipids substrates observed in *Fmr1*-KO mice using indirect calorimetry.

and stained with Ponceau (upper panel). IgY heavy chains and light chains are indicated by an asterisk. Immunoblotting with anti-FMRP mAb1C3 antibody (lower panel). Note the depletion in FMRP load in the post-IA C10 flowthrough with IgY#C10 (FT C10), as compared to input and control IgY IA (FT CtI). (D) RT-PCR analysis of mRNA associated with FMRP. Total RNA was extracted from the input cell lysate and IA preparations described in (C), and used as a template for RT-PCR. PCR products obtained from input, control IgY IA (IA CtI) or IgY#C10 (IA C10) IA complexes as well as control blank PCR (Bk) performed in the absence of matrix were separated and visualized by agarose gel electrophoresis. The molecular weights (MW) of PCR amplicons are specified on the right side.

## Original Article

### 4.3. The Fragile X family of proteins and RNA-binding proteins have possible conserved roles in the control of metabolic homeostasis

We show that the absence of FMRP provokes profound changes in glucose and lipid metabolism in the *Fmr1*-KO2 mouse model, while no overt metabolic alterations were previously reported in the *Fmr1*-KO1 mouse model of FXS [18]. Besides differences in the breeding, housing or diet used for the *Fmr1*-KO1 and KO2 models, possible explanation for this could be the age of the animals studied and different experimental design for *in vivo* metabolic phenotyping. However, Lumaban & Nelson showed that the *Fmr1/Fxr2* double knock out mouse exhibits metabolic abnormalities overlapping with our observations: enhanced glucose tolerance and insulin response, hypoglycemia, and reduced adiposity [18]. This suggests a conserved role for the Fragile X Related family of genes in the regulation of metabolic homeostasis. In keeping with this notion, a recent study indicates that the *Drosophila* FXS model displays anomalies in energy metabolism, with decreased whole-body glucose and lipid stores and impaired mitochondrial functions [17]. In addition, we show both in mouse and human that *FMR1*-deficiency impacts the circulating metabolome and notably reduces glucose and insulin levels. This suggests that FXS may also be accompanied by yet under reported modifications in insulin sensitivity and glucose homeostasis in humans, similar to that seen in our FXS mouse model and in FXS fly model [17]. We highlighted reduced levels of FFA in FXS patients; lower blood cholesterol was previously reported in FXS patients [19–21], and we now report it in the *Fmr1*-KO2 mouse model, suggesting that lipid homeostasis is generally impacted by *FMR1*-deficiency. Other translational regulators such as the translation initiation factors EIF6 [57] and EIF4BP1 [58] or the ribosomal protein S6 kinase p70S6K [59] have previously been described as modulators of metabolic phenotypes and notably of lipid homeostasis. In particular, similarly to *Fmr1*-KO mice, *S6k1*-KO and *Eif4bp1*-KO mice have reduced body fat mass, increased lipolysis, and decreased adipocyte size. Our study therefore strengthens the importance of RNA-binding proteins and translation regulators in the general control of metabolic homeostasis.

### 4.4. Clinical relevance of findings

Regarding the clinical relevance of our findings of reduced adiposity in FXS mouse model, there is a lack of large-scale epidemiological studies on adiposity in the general FXS population. Although severe obesity is reported in less than 10% of FXS patients, known as Prader Willi-like (PWL) [60,61], obesity is not described in typical FXS patients [7,62], such as the patients enrolled in our study. On one hand, obese FXS patients are likely to benefit at the behavioral and metabolic level from treatment with the anti-diabetic drug metformin, as recently shown in seven FXS cases [63]. On the other hand, we show that typical FXS patients are likely to present metabolic phenotypes distinct from type 2 diabetes (T2D) with reduced glycemia and insulinemia. One study even mentioned a lower incidence of T2D in FXS population [63]. In the same line, earlier studies have reported that FXS patients are not prone to hyperlipidemia since they display reduced cholesterol and TG [19–21], in agreement with our findings in FXS mouse model. Treatment with the cholesterol-lowering agent lovastatin improved behavioral outcome in FXS patients [64], but the authors also observed an unexpectedly strong diminution in TG and cholesterol levels after 3 months of treatment [20,64]. This raises the issue that the possible untoward effects of metabolic drugs should be considered in clinical trials involving FXS patients not harbouring T2D features or hyperlipidemia.

### 4.5. Conclusions

Our study identifies metabolic phenotypes in FXS and supports a role for FMRP-mediated translation in the homeostatic control of systemic metabolism. Furthermore, this work underlines the importance to further investigate the metabolic roles of translational regulators, both in fundamental biology and from a clinical standpoint.

### AUTHOR CONTRIBUTIONS

LD designed the project. AL, DP, JC, LMG, PBM, TG, BM, EZA, EWK, MED, and LD designed and carried out the experiments. AL, DP, JC, LMG, TG, BM, EZA, EWK, MED, and LD treated and interpreted data. FK and AVD provided human samples, contributed and interpreted clinical data. LD and MED wrote the manuscript.

### ACKNOWLEDGEMENTS

We thank N. Durand and the IPMC animal facility for expert animal care. We acknowledge H. Van Esch for help with patient recruitment and are very grateful to the families and patients who have participated in this study. We thank the Anexplor phenotyping platform (Genotoul, Rangueil, Toulouse). LD thanks the generous support of FRAXA Research Foundation, Agence Nationale de la Recherche (ANR JCJC SVE6 MetaboXFra), Conseil Général 06, Fondation Jérôme Lejeune and the CNRS PICS program. LD and MED acknowledge the support of the Royal Society-CNRS International Exchange Program (IE120728). LD, BM and MED are grateful to the European Community 7th Framework Program under Coordinated Action NEURON-ERANET (grant agreement 291840). The MED lab is funded by METACARDIS (HEALTH-F4-2012-305312) and the UK Medical Research Council (MRC grant MR/M501797/1). RFK and AVD have received grants from FRAXA Research Foundation and Jérôme Lejeune Foundation. EWK was supported by grants from the CIHR and NSERC. JAJB and JLM thank Region Centre-Val de Loire (ARD2020 Biomedicaments—GPCRab) and the Labex MablImprove for financial support and the Experimental Unit PAO #1297 (EU0028) of INRA Centre Val de Loire for animal housing.

### CONFLICTS OF INTEREST

None declared.

### APPENDIX A. SUPPLEMENTARY DATA

Supplementary data to this article can be found online at <https://doi.org/10.1016/j.molmet.2019.01.002>.

### REFERENCES

- [1] Khandjian, E.W., Corbin, F., Woerly, S., Rousseau, F., 1996. The fragile X mental retardation protein is associated with ribosomes. *Nature Genetics* 12(1):91–93.
- [2] Khandjian, E.W., Huot, M.E., Tremblay, S., Davidovic, L., Mazroui, R., Bardoni, B., 2004. Biochemical evidence for the association of fragile X mental retardation protein with brain polyribosomal ribonucleoproteins. *Proceedings of the National Academy of Sciences of the United States of America* 101(36):13357–13362.
- [3] Stefani, G., Fraser, C.E., Darnell, J.C., Darnell, R.B., 2004. Fragile X mental retardation protein is associated with translating polyribosomes in neuronal cells. *Journal of Neuroscience* 24(33):7272–7276.
- [4] Darnell, J.C., Klann, E., 2013. The translation of translational control by FMRP: therapeutic targets for FXS. *Nature Neuroscience* 16(11):1530–1536.
- [5] Darnell, J.C., Van Driesche, S.J., Zhang, C., Hung, K.Y., Mele, A., Fraser, C.E., et al., 2011. FMRP stalls ribosomal translocation on mRNAs linked to synaptic function and autism. *Cell* 146(2):247–261.

- [6] El Fatimy, R., Davidovic, L., Tremblay, S., Jaglin, X., Dury, A., Robert, C., et al., 2016. Tracking the fragile X mental retardation protein in a highly ordered neuronal ribonucleoparticles population: a link between stalled polyribosomes and RNA granules. *PLoS Genetics* 12(7):e1006192.
- [7] Kidd, S.A., Lachiewicz, A., Barbooth, D., Blitz, R.K., Delahunty, C., McBrien, D., et al., 2014. Fragile X syndrome: a review of associated medical problems. *Pediatrics* 134(5):995–1005.
- [8] Penagarikano, O., Mulle, J.G., Warren, S.T., 2007. The pathophysiology of fragile X syndrome. *Annual Review of Genomics and Human Genetics* 8:109–129.
- [9] Consortium, T.D.-B.F.X., 1994. Fmr1 knockout mice: a model to study fragile X mental retardation. *Cell* 78(1):23–33.
- [10] Mientjes, E.J., Nieuwenhuizen, I., Kirkpatrick, L., Zu, T., Hoogveen-Westerveld, M., Severijnen, L., et al., 2006. The generation of a conditional Fmr1 knock out mouse model to study Fmrp function in vivo. *Neurobiology of Disease* 21(3):549–555.
- [11] Richter, J.D., Bassell, G.J., Klann, E., 2015. Dysregulation and restoration of translational homeostasis in fragile X syndrome. *Nature Reviews Neuroscience* 16(10):595–605.
- [12] Davidovic, L., Tremblay, S., Gravel, M., De Koninck, P., Khandjian, E.W., 2006. The fragile X syndrome: one protein missing and 1001 disoriented mRNA. *Medical Science (Paris)* 22(1):41–46.
- [13] Khandjian, E.W., Bardoni, B., Corbin, F., Sittler, A., Giroux, S., Heitz, D., et al., 1998. Novel isoforms of the fragile X related protein FXR1P are expressed during myogenesis. *Human Molecular Genetics* 7(13):2121–2128.
- [14] Callan, M.A., Clements, N., Ahrendt, N., Zarnescu, D.C., 2012. Fragile X protein is required for inhibition of insulin signaling and regulates glial-dependent neuroblast reactivation in the developing brain. *Brain Research* 1462:151–161.
- [15] Monyak, R.E., Emerson, D., Schoenfeld, B.P., Zheng, X., Chambers, D.B., Rosenfelt, C., et al., 2017. Insulin signaling misregulation underlies circadian and cognitive deficits in a drosophila fragile X model. *Molecular Psychiatry* 22(8):1140–1148.
- [16] Luhur, A., Buddika, K., Ariyapala, I.S., Chen, S., Sokol, N.S., 2017. Opposing post-transcriptional control of InR by FMRP and LIN-28 adjusts stem cell-based tissue growth. *Cell Reports* 21(10):2671–2677.
- [17] Weisz, E.D., Towheed, A., Monyak, R.E., Toth, M.S., Wallace, D.C., Jongens, T.A., 2018. Loss of drosophila FMRP leads to alterations in energy metabolism and mitochondrial function. *Human Molecular Genetics* 27(1):95–106.
- [18] Lumaban, J.G., Nelson, D.L., 2015. The fragile X proteins Fmrp and Fxr2p cooperate to regulate glucose metabolism in mice. *Human Molecular Genetics* 24(8):2175–2184.
- [19] Berry-Kravis, E., Levin, R., Shah, H., Mathur, S., Darnell, J.C., Ouyang, B., 2015. Cholesterol levels in fragile X syndrome. *American Journal of Medical Genetics* 167A(2):379–384.
- [20] Caku, A., Seidah, N.G., Lortie, A., Gagne, N., Perron, P., Dube, J., et al., 2017. New insights of altered lipid profile in fragile X Syndrome. *PLoS One* 12(3):e0174301.
- [21] Lisik, M.Z., Gutmajster, E., Sieron, A.L., 2016. Low levels of HDL in fragile X syndrome patients. *Lipids* 51(2):189–192.
- [22] Dona, A.C., Jimenez, B., Schafer, H., Humpfer, E., Spraul, M., Lewis, M.R., et al., 2014. Precision high-throughput proton NMR spectroscopy of human urine, serum, and plasma for large-scale metabolic phenotyping. *Analytical Chemistry* 86(19):9887–9894.
- [23] Dona, A.C., Kyriakides, M., Scott, F., Shephard, E.A., Varshavi, D., Veselkov, K., et al., 2016. A guide to the identification of metabolites in NMR-based metabolomics/metabolomics experiments. *Computational and Structural Biotechnology Journal* 14:135–153.
- [24] Dumas, M.E., Barton, R.H., Toye, A., Cloarec, O., Blancher, C., Rothwell, A., et al., 2006. Metabolic profiling reveals a contribution of gut microbiota to fatty liver phenotype in insulin-resistant mice. *Proceedings of the National Academy of Sciences of the United States of America* 103(33):12511–12516.
- [25] Ayala, J.E., Samuel, V.T., Morton, G.J., Obici, S., Croniger, C.M., Shulman, G.I., et al., 2010. Standard operating procedures for describing and performing metabolic tests of glucose homeostasis in mice. *Disease Models and Mechanisms* 3(9–10):525–534.
- [26] Beranger, G.E., Pisani, D.F., Castel, J., Djedaini, M., Battaglia, S., Amiaud, J., et al., 2014. Oxytocin reverses ovariectomy-induced osteopenia and body fat gain. *Endocrinology* 155(4):1340–1352.
- [27] Pisani, D.F., Beranger, G.E., Corinus, A., Giroud, M., Ghandour, R.A., Altirriba, J., et al., 2016. The K<sup>+</sup> channel TASK1 modulates beta-adrenergic response in brown adipose tissue through the mineralocorticoid receptor pathway. *The FASEB Journal* 30(2):909–922.
- [28] Rodriguez, A.M., Elabd, C., Delteil, F., Astier, J., Vernochet, C., Saint-Marc, P., et al., 2004. Adipocyte differentiation of multipotent cells established from human adipose tissue. *Biochemical and Biophysical Research Communications* 315(2):255–263.
- [29] Pisani, D.F., Djedaini, M., Beranger, G.E., Elabd, C., Scheideler, M., Ailhaud, G., et al., 2011. Differentiation of human adipose-derived stem cells into "Brite" (brown-in-white) adipocytes. *Frontiers in Endocrinology (Lausanne)* 2:87.
- [30] Cox, J., Hubner, N.C., Mann, M., 2008. How much peptide sequence information is contained in ion trap tandem mass spectra? *Journal of the American Society for Mass Spectrometry* 19(12):1813–1820.
- [31] Cox, J., Mann, M., 2008. MaxQuant enables high peptide identification rates, individualized p.p.b.-range mass accuracies and proteome-wide protein quantification. *Nature Biotechnology* 26(12):1367–1372.
- [32] Jensen, L.J., Kuhn, M., Stark, M., Chaffron, S., Creevey, C., Muller, J., et al., 2009. STRING 8—a global view on proteins and their functional interactions in 630 organisms. *Nucleic Acids Research* 37(Database issue):D412–D416.
- [33] Thomas, P.D., Campbell, M.J., Kejariwal, A., Mi, H., Karlak, B., Daverman, R., et al., 2003. PANTHER: a library of protein families and subfamilies indexed by function. *Genome Research* 13(9):2129–2141.
- [34] Thomas, P.D., Kejariwal, A., Guo, N., Mi, H., Campbell, M.J., Muruganujan, A., et al., 2006. Applications for protein sequence-function evolution data: mRNA/protein expression analysis and coding SNP scoring tools. *Nucleic Acids Research* 34(Web Server issue):W645–W650.
- [35] Khalfallah, O., Jarjat, M., Davidovic, L., Nottet, N., Cestele, S., Mantegazza, M., et al., 2017. Depletion of the fragile X mental retardation protein in embryonic stem cells alters the kinetics of neurogenesis. *Stem Cells* 35(2):374–385.
- [36] Devys, D., Lutz, Y., Rouyer, N., Bellocq, J.P., Mandel, J.L., 1993. The FMR-1 protein is cytoplasmic, most abundant in neurons and appears normal in carriers of a fragile X premutation. *Nature Genetics* 4(4):335–340.
- [37] El Fatimy, R., Tremblay, S., Dury, A.Y., Solomon, S., De Koninck, P., Schrader, J.W., et al., 2012. Fragile X mental retardation protein interacts with the RNA-binding protein Caprin1 in neuronal RiboNucleoProtein complexes. *PLoS One* 7(6):e39338.
- [38] Dury, A.Y., El Fatimy, R., Tremblay, S., Rose, T.M., Cote, J., De Koninck, P., et al., 2013. Nuclear fragile X mental retardation protein is localized to cajal bodies. *PLoS Genetics* 9(10):e1003890.
- [39] Schmidt, E.K., Clavarino, G., Ceppi, M., Pierre, P., 2009. SUNSET, a non-radioactive method to monitor protein synthesis. *Nature Methods* 6(4):275–277.
- [40] Rodriguez-Martinez, A., Ayala, R., Posma, J.M., Dumas, M.E., 2018. Exploring the genetic landscape of metabolic phenotypes with MetaboSignal. *Current Protocols in Bioinformatics* 61(1), 14 14 11–14 14 13.
- [41] Rodriguez-Martinez, A., Ayala, R., Posma, J.M., Neves, A.L., Gauguier, D., Nicholson, J.K., et al., 2017. MetaboSignal: a network-based approach for topological analysis of metabolite regulation via metabolic and signaling pathways. *Bioinformatics* 33(5):773–775.
- [42] Ouldamer, L., Nadal-Desbarats, L., Chevalier, S., Body, G., Goupille, C., Bougnoux, P., 2016. NMR-based lipidomic approach to evaluate controlled

## Original Article

- dietary intake of lipids in adipose tissue of a rat mammary tumor model. *Journal of Proteome Research* 15(3):868–878.
- [43] Berry, R., Rodeheffer, M.S., 2013. Characterization of the adipocyte cellular lineage in vivo. *Nature Cell Biology* 15(3):302–308.
- [44] Even, P.C., Nadkarni, N.A., 2012. Indirect calorimetry in laboratory mice and rats: principles, practical considerations, interpretation and perspectives. *American Journal of Physiology - Regulatory, Integrative and Comparative Physiology* 303(5):R459–R476.
- [45] Davidovic, L., Navratil, V., Bonaccorso, C.M., Catania, M.V., Bardoni, B., Dumas, M.E., 2011. A metabolomic and systems biology perspective on the brain of the Fragile X syndrome mouse model. *Genome Research* 12:2190–2202.
- [46] Schaeffer, C., Bardoni, B., Mandel, J.L., Ehresmann, B., Ehresmann, C., Moine, H., 2001. The fragile X mental retardation protein binds specifically to its mRNA via a purine quartet motif. *The EMBO Journal* 20(17):4803–4813.
- [47] Pieretti, M., Zhang, F.P., Fu, Y.H., Warren, S.T., Oostra, B.A., Caskey, C.T., et al., 1991. Absence of expression of the FMR-1 gene in fragile X syndrome. *Cell* 66(4):817–822.
- [48] Ascano Jr., M., Mukherjee, N., Bandaru, P., Miller, J.B., Nusbaum, J.D., Corcoran, D.L., et al., 2012. FMRP targets distinct mRNA sequence elements to regulate protein expression. *Nature* 492(7429):382–386.
- [49] Miyazawa, S., Ozasa, H., Osumi, T., Hashimoto, T., 1983. Purification and properties of carnitine octanoyltransferase and carnitine palmitoyltransferase from rat liver. *Journal of Biochemistry* 94(2):529–542.
- [50] Lin, X., Yue, P., Chen, Z., Schonfeld, G., 2005. Hepatic triglyceride contents are genetically determined in mice: results of a strain survey. *American Journal of Physiology - Gastrointestinal and Liver Physiology* 288(6):G1179–G1189.
- [51] Stefanovic-Racic, M., Perdomo, G., Mantell, B.S., Sipula, I.J., Brown, N.F., O'Doherty, R.M., 2008. A moderate increase in carnitine palmitoyltransferase 1a activity is sufficient to substantially reduce hepatic triglyceride levels. *American Journal of Physiology. Endocrinology and Metabolism* 294(5):E969–E977.
- [52] Jackson, V.N., Halestrap, A.P., 1996. The kinetics, substrate, and inhibitor specificity of the monocarboxylate (lactate) transporter of rat liver cells determined using the fluorescent intracellular pH indicator, 2',7'-bis(carboxyethyl)-5(6)-carboxyfluorescein. *Journal of Biological Chemistry* 271(2):861–868.
- [53] Wanders, R.J., Waterham, H.R., Ferdinandusse, S., 2015. Metabolic interplay between peroxisomes and other subcellular organelles including mitochondria and the endoplasmic reticulum. *Frontiers in Cell and Developmental Biology* 3:83.
- [54] Davidovic, L., Sacconi, S., Bechara, E.G., Delplace, S., Allegra, M., Desnuelle, C., et al., 2008. Alteration of expression of muscle specific isoforms of the fragile X related protein 1 (FXR1P) in facioscapulohumeral muscular dystrophy patients. *Journal of Medical Genetics* 45(10):679–685.
- [55] Penhoat, A., Fayard, L., Stefanutti, A., Mithieux, G., Rajas, F., 2014. Intestinal gluconeogenesis is crucial to maintain a physiological fasting glycemia in the absence of hepatic glucose production in mice. *Metabolism* 63(1):104–111.
- [56] Ferron, M., Wei, J., Yoshizawa, T., Del Fattore, A., DePinho, R.A., Teti, A., et al., 2010. Insulin signaling in osteoblasts integrates bone remodeling and energy metabolism. *Cell* 142(2):296–308.
- [57] Brina, D., Miluzio, A., Ricciardi, S., Clarke, K., Davidsen, P.K., Viero, G., et al., 2015. eIF6 coordinates insulin sensitivity and lipid metabolism by coupling translation to transcription. *Nature Communications* 6:8261.
- [58] Tsukiyama-Kohara, K., Poulin, F., Kohara, M., DeMaria, C.T., Cheng, A., Wu, Z., et al., 2001. Adipose tissue reduction in mice lacking the translational inhibitor 4E-BP1. *Nature Medicine* 7(10):1128–1132.
- [59] Carnevalli, L.S., Masuda, K., Frigerio, F., Le Bacquer, O., Um, S.H., Gandin, V., et al., 2010. S6K1 plays a critical role in early adipocyte differentiation. *Developmental Cell* 18(5):763–774.
- [60] Nowicki, S.T., Tassone, F., Ono, M.Y., Ferranti, J., Croquette, M.F., Goodlin-Jones, B., et al., 2007. The Prader-Willi phenotype of fragile X syndrome. *Journal of Developmental and Behavioral Pediatrics* 28(2):133–138.
- [61] McLennan, Y., Polussa, J., Tassone, F., Hagerman, R., 2011. Fragile X syndrome. *Current Genomics* 12(3):216–224.
- [62] Hagerman, R.J., Berry-Kravis, E., Hazlett, H.C., Bailey Jr., D.B., Moine, H., Kooy, R.F., et al., 2017. Fragile X syndrome. *Nature Reviews Disease Primers* 3:17065.
- [63] Dy, A.B.C., Tassone, F., Eldeeb, M., Salcedo-Arellano, M.J., Tartaglia, N., Hagerman, R., 2017. Metformin as targeted treatment in fragile X syndrome. *Clinical Genetics* 93(2):216–222.
- [64] Caku, A., Pellerin, D., Bouvier, P., Riou, E., Corbin, F., 2014. Effect of lovastatin on behavior in children and adults with fragile X syndrome: an open-label study. *American Journal of Medical Genetics, Part A* 164A(11):2834–2842.

# Appendix

## Supplemental information

### **The translational regulator FMRP controls lipid and glucose metabolism in mice and humans**

Antoine Leboucher, Didier F. Pisani, Laura Martinez-Gili, Julien Chilloux, Patricia Bermudez-Martin, Anke Van Dijck, Tariq Ganief, Boris Macek, Jérôme A. J. Becker, Julie Le Merrer, Frank R. Kooy, Ez-Zoubir Amri, Edouard W. Khandjian, Marc-Emmanuel Dumas, Laetitia Davidovic

#### **This PDF file includes:**

Supplemental materials and methods

Figures S1 to S8

Tables S1 to S9 legends

#### **Other supplemental materials for this manuscript include the following:**

Tables S1 to S9, available as Excel files

## Supplemental material and methods

*Animal procedures.* C57Bl6/J *Fmr1*-KO2 mice used in this study are described in [1]. Animals were housed in an SPF facility in medium-size (up to 5 animals/cage) or large cages (up to 10 animals/cage) filled with wooden bedding, one plastic house and nesting material for enrichment. All *Fmr1*-WT and *Fmr1*-KO male used in this study were littermates born to heterozygous females. Pups were weaned at 28 days of age, identified by ear tags, and genotyped by PCR as described [1]. Pups from various litters were then randomly grouped according to their genotype in cages and had *ad libitum* access to water and standard chow (reference 4RF25, Mucedola) composed of cereals (53.7%), animal proteins (4.7%), vegetal proteins (30.5%), lipids (soy oil, 1.4%), vitamins and minerals (4.1%), amino acids (0.1%). Animals were housed in a temperature (22-24°C) and hygrometry (70-80%)- controlled room with a 12 hrs light-dark cycle (lights on at 07:00). All the described experiments were performed on male animals at exactly 4-months (16 weeks) of age, to the exception of initial blood sampling of fed animals for metabolic profiling presented in Figure 1 that was performed on fed *Fmr1*-KO and WT animals between 4 and 6 months of age. Blood was withdrawn in the morning between 9 and 10 a.m. in heparinated tubes (Terumo) from *Fmr1*-KO and WT animals in nonfasting or fasting conditions as stated. In nonfasting conditions, animals were fed *ad libitum* and in fasting conditions animals were fasted overnight for 16 hr. Plasma was collected from tubes after

centrifugation at 1200g for 10 min. For experiments involving treatment, animals from the same genotype were randomly assigned to experimental groups.

*Metabolic profiling.* NMR experiments were carried out using a Bruker Avance spectrometer (Bruker GmbH, Rheinstetten, Germany) operating at 600 MHz. Briefly, 15  $\mu$ L of plasma or serum was mixed with 335  $\mu$ L of water and 350  $\mu$ L of buffer (0.075M  $\text{NaH}_2\text{PO}_4$ , 0.8% TSP, 0.04%  $\text{NaN}_3$ , 20%  $\text{D}_2\text{O}$ , pH 7.4), centrifuged (12000g, 4  $^\circ\text{C}$ , 5 min). Six hundred  $\mu$ L of the resulting supernatant was transferred into a SampleJet NMR tube for  $^1\text{H}$  NMR analysis using a spectrometer (Bruker) operating at 600.22 MHz as described previously [2]. Structural assignment was performed using data from literature, HMDB (<http://www.hmdb.ca/>), S-Base (Bruker GmbH, Rheinstetten, Germany) and in-house databases [3].  $^1\text{H}$  NMR spectra were pre-processed and exported in to Matlab for multivariate statistical analyses using orthogonal partial least square discriminant analysis (O-PLS-DA) as previously reported [4].

*Blood chemistry and hormones measurements.* The determination of circulating TG, FFA and total cholesterol was subcontracted to the Genotoul Anexplo Platform (Toulouse, France) and performed on 16 hr fasted *Fmr1*-WT and KO plasma samples. The determination of triglyceride content in liver was made using an enzymatic test (ETGA-200, Bioassay Systems) on tissue homogenates from 16 hr fasted animals. Briefly, tissues of *Fmr1* WT and KO mice were homogenized in proportion to their mass using a water-based buffer containing

isopropanol and Triton X100. The resulting homogenate was then centrifuged and the supernatant submitted to enzymatic hydrolysis of TG, followed by a chemical determination of glycerol, proportional to the amount of TG in the original sample, using a biochemical colorimetric kit (Sigma Aldrich). Leptin and insulin were measured on murine plasma sampled after a 16 hr fast using an Electro-Chemo-Luminescence (ECL)-based assay (v-plex®, MesoScaleDiscovery). The same platform was used to measure insulin in sera from FXS patients and controls.

*Insulin (ITT), glucose tolerance tests (GTT).* These experiments were conducted according to the IMPReSS guidelines (International Mouse Phenotyping Resource of Standardized Screens) and in agreement with [5] and [6]. Mice were respectively fasted 16 hr (GTT) or 6 hr (ITT) prior to i.p. injection of glucose (2 g/Kg, Sigma-Aldrich) or insulin (0.75 U/Kg, Humalog, Lilly) as per recommended procedures [6]. Glycemia was then measured by tail blood sampling at 0, 15, 30, 60, 90, 120 and 180 min post injection using a glucometer (AccuCheck Mobile, Roche) and a drop of blood collected after an incision at the tip of the tail. During the course of the experiment, mice were freely moving and unrestrained (including during blood sampling for glycemia measure) and had continuous access to water.

*In vivo tissue insulin sensitivity measurement.* Mice were fasted 16 hours, then injected with insulin (0.75 U/Kg, Humalog, Lilly) or saline. Five minutes after

injection, mice were sacrificed by cervical dislocation and tissues were rapidly dissected, snapped frozen in liquid nitrogen and stored at -80°C until further analyses.

*Western-blotting.* Samples were homogenized by sonication in a buffer containing 50 mM Tris pH 7.4, NaCl 150 mM, MgCl<sub>2</sub> 1.25 mM, Triton 0.5 % and containing protease and phosphatase inhibitors (Pierce, Thermo-Scientific). 17,000 g supernatants were dosed using the Bradford method (Biorad). 30 µg of proteins were diluted in Laemmli buffer, separated on 11% acrylamide gels and transferred to nitrocellulose membranes (Amersham). Membranes were probed with Anti-Akt (#9272; 1:2000), anti-pSer<sup>473</sup>-Akt (#9271; 1:500), anti-Insulin receptor (#3025; 1:1000), anti-pTyr<sup>1150/1151</sup>-Insulin receptor/pTyr<sup>1135-1136</sup>Igf receptor (#3024; 1:250) polyclonal antibodies from Cell Signalling Technologies, monoclonal anti-β-Actin (#A2228) or anti-GAPDH (#G8795) antibodies (1:30,000; Sigma-Aldrich) and HRP-coupled secondary antibodies (1:1000; Jackson Laboratories). Signal was visualized using ECL kits (Perkin) and a Fusion VX-Imager (Vilber). Protein and phospho-proteins signals were quantified by densitometric analysis using the ImageJ software. For each tissue, two gels were run in parallel. One membrane was used for total proteins quantification and the other for phosphoproteins. β-actin signals were used to control for variability in loading/transfer. Total protein and phospho-protein signal intensities were normalized to the respective β-actin signals. The ratio between normalized phospho-epitopes signals and the corresponding normalized total protein signal

was then calculated. Scans of the fully uncut Ponceau-stained membranes as well as western-blots are available upon request.

*Quantitative RT-PCR.* Total RNA was extracted from tissues using the RNeasy kit (Qiagen, Hilden, Germany) and digested with DNAase I (Turbo DNAse, Ambion). Reverse transcription (RT) reaction was performed using the Superscript II RT-PCR system (Invitrogen, Carlsbad, California, USA) according to the manufacturers' protocol. Real-time PCR reactions were carried out using the Syber Green I qPCR core Kit (Eurogentec, Liège, Belgium) in a LightCycler system (Roche, USA). The comparative threshold cycle ( $C_t$ ) for the amplicons of each sample was determined by the LightCycler software and normalised to the corresponding  $C_t$  of *TATA Box Binding Protein (Tbp)* mRNA for murine samples and *Glyceraldehyde phosphate dehydrogenase (GAPDH)* for human samples. Finally, the  $2^{-\Delta\Delta C_t}$  method [7] was used to analyse the relative changes in the various studied mRNAs. The following primers were used: *Tbp* (AGGCCAGACCCCACAACCTC; GGGTGGTGCCTGGCAA), *Pdgfra* (ACTACATCTCCAAAGGCAGCACCT, TGTAGAACTGGTCGTTTCATGGGC A), human *GAPDH* (CCACATCGCTCAGACACCAT; GACCAGGCGCCCAAT), human *FMR1* (CATGCACTTTCGGAGTCTG; GAAATCTCGAGGCAAGCTG). Primers for human *PERILIPIN1* and *FABP4* are described in [8].

*Microcomputed tomography analysis.* Anesthetised animals were introduced in a SkyScan-1178 X-ray tomograph and analysed as previously described [9]. In

brief, mice were scanned using the following parameters: 104  $\mu\text{m}$  voxel size, 49 kV, 0.5 mm thick aluminum filter and a rotation step of  $0.9^\circ$ . Subcutaneous and intra-abdominal adipose tissue volumes were determined in 250 slides of a 20.5 mm segment in the abdominal cavity between the lumbar vertebra 3 (L3) and the caudal vertebra 1 (C1) using NRecon and CTAn softwares (Bruker, Kontich, Belgium).

*Adipose tissue histology.* Epididymal adipose tissue was collected, fixed for 24 hours in 4% paraformaldehyde, paraffin-embedded and serially cut in 4  $\mu\text{m}$  sections using a microtome HM340E (Leica). Slices were then deparaffinated and stained with hematoxylin and eosin. Micrographs were obtained with a DMD108 digital microscope and automated analysis of adipocytes surface was performed using an in-house ImageJ software macro.

*Cell culture.* Preparation of stromal vascular fraction (SVF) of epididymal adipose tissue was performed as described in [10]. Briefly, intra-abdominal white epididymal fat depots were collected, washed in PBS, minced then digested for 30 min at  $37^\circ\text{C}$  in DMEM supplemented with 2 mg/ml collagenase A (Roche) and 20 mg/ml bovine serum albumin (Sigma-Aldrich). The lysate was successively filtered through 250, 100, and 27  $\mu\text{m}$  nylon meshes and centrifuged for 5 min at 500 g. The pellet containing SVF cells were plated and maintained in DMEM containing 10% FBS until confluence. Differentiation was induced in the same medium supplemented with 1  $\mu\text{M}$  dexamethasone, 0.5 mM

isobutylmethylxanthine, and 340 nM insulin for 2 days. Cells were then maintained for 10 days in the presence of 340 nM insulin for the induction of adipogenesis. hMADS cells were described in [8, 11], transfected with anti-*FMR1* *siRNA* (Invitrogen): CCCACCUCCUGUAGGUUAAUAAA/UUUUAUUUAACCU ACAGGAGGUGG) or control *siRNA* (Stealth, Invitrogen), using HiPerFect Transfection Reagent (Qiagen) and differentiated into adipocytes as described in [8, 11].

*Lipolysis assays.* For *in vivo* lipolysis experiments, 6 hours-fasted *Fmr1*-KO and WT were injected intraperitoneally with either saline or isoproterenol at 1 mg/Kg. Fifteen minutes after injection, blood was sampled for glycerol determination in serum. For *ex vivo* lipolysis experiments, 6 hours-fasted *Fmr1*-KO and WT mice were sacrificed, and intra-abdominal white epididymal fat depots were sampled, washed in PBS, then cut in explants of 15-20 mg each, and weighed. Explants were then incubated for 1 hr in DMEM low glucose (1 g/L) supplemented with 15 mM HEPES, 0.5 % bovine serum albumin (Sigma-Aldrich) and then treated with 1  $\mu$ M isoproterenol or vehicle. A sample of medium was taken for determination of glycerol content at 0, 60, 90, 120, 150 and 180 min after treatment. Glycerol release was then normalized to initial explant mass. Glycerol concentration in serum or medium was determined using Glycerol Free reagent kit (Sigma-Aldrich), according to the manufacturer's instructions. Lipolysis experiments of SVF-derived adipocytes were performed as described in [10], using 1  $\mu$ M of isoproterenol for 1 hr 30 min. Lipolysis of human hMAD-derived adipocytes was

performed after 10 days of differentiation. Cells were over-night insulin deprived and then submitted to 1 $\mu$ M isoproterenol treatment in fresh media. At indicated times, sampled media were used to measure glycerol and free fatty acid release using Free Glycerol Reagent and Free Fatty Acid Quantification Assay Kit (Abcam) according to the manufacturer's instructions. Concomitantly, cells were lysed with NaOH 0.2N and neutralized with HCl 0.2N. Lysates were used to evaluate triglyceride content using Triglyceride and Free Glycerol reagents (Sigma-Aldrich) and protein content using BCA kit (Sigma-Aldrich) according to the manufacturer's instructions. TG, glycerol and FFA levels were then normalized to protein content in the corresponding well.

*Indirect calorimetry.* Indirect calorimetry experiments were performed at the Anexplo Genotoul metabolic phenotyping platform (Toulouse, France). 4-mths old male *Fmr1*-KO and WT animals were habituated for 24 hr in indirect calorimetry chambers (Phenomaster System, TSE). Over the following 24 hr, the automated device recorded drink and food consumption, activity monitored by the number of infrared beam breaks, O<sub>2</sub> consumption (VO<sub>2</sub> in mL/h/kg<sup>0.75</sup>) and CO<sub>2</sub> production (VCO<sub>2</sub> in mL/h/kg<sup>0.75</sup>). Energetic expenditure (H<sub>2</sub> in kcal/h/kg<sup>0.75</sup>) and Respiratory Exchange Ratio (RER) were then calculated as described [12].

*Proteome analysis.* Livers from 4 months-old overnight fasted animals were quickly collected after cervical dislocation, snapped frozen in liquid nitrogen and kept at -80°C until further analysis. Livers were lysed in lysis buffer (25 mM Tris-

HCl pH 7.6, 150 mM NaCl, 1% NP-40, 1% sodium deoxycholate, 0.1% SDS), disrupted with ceramic beads using the FastPrep apparatus (MP Biomedicals) set at Power 6 for 40 s. Lysates were centrifuged at 12,000g, 20 min at 4°C. 100 µL of supernatant were precipitated overnight at -20°C with 900 µL of an acetone:methanol solution (8:1), centrifuged at 2,200g, 20 min at 4°C. Pellet was further rinsed with 80% acetone, then air-dried. The dried protein pellets were resuspended in denaturation buffer (6 M urea, 2 M thiourea in 10 mM Tris, pH 8.5) and quantified using the Bradford assay (Bio-Rad, Munich, Germany). Proteins were digested by in-solution digestion. Briefly, proteins were reduced with 3 mM dithiothreitol, alkylated with 9 mM iodoacetamide, predigested for three hours with 1:100 (w/w) Lys-C (Wako, Germany) and digested with 1:100 (w/w) trypsin (Promega, USA) for 14 hours shaking at room temperature. Before trypsin digestion, samples were diluted with 6 volumes of 50 mM ammonium bicarbonate. Following digestion, samples were acidified with formic acid (FA) to a final concentration of 0.5 % (v/v). Samples were measured on an EASY-nLC 1200 (Thermo Fisher Scientific) coupled to an Orbitrap Elite mass spectrometer (Thermo Fisher Scientific). Peptides were chromatographically separated using 75 µm (ID), 15 cm columns packed in-house with reversed-phase ReproSil-Pur 120 C18-AQ 1.9 µm resin (Dr. Maisch GmbH). Peptides were then eluted using a 169 min non-linear gradient of solvent B (80% ACN, 0.1% formic acid) in the increments; 8 % - 27 % over 142 min, 27 % – 35 % over 24 min and 35 % – 50 % over 3 min. Full-scans were recorded between 300-2000 Thomson at a resolution of 120,000 with a target value of 1E6. The top 15 most intense ions

from each full scan were selected for fragmentation (MS/MS) by higher-energy collisional dissociation (HCD) using a collision energy of 35% at a target value of 5000 charges. Both MS and MS/MS scans were recorded in the orbitrap. All acquired MS data were processed with the MaxQuant software suite [13] version 1.5.2.8 against the complete mouse UniProt database (taxonomy ID 10090) containing 54,506 sequences and a database of 248 frequently observed contaminants. Precursor mass tolerance was set to 6 ppm and 0.5 Da for MS/MS fragment ions. A maximum of two missed cleavages resulting in a minimal length of seven amino acids and full tryptic enzyme specificity were required. Oxidation of methionine and protein N-terminal acetylation were defined as variable modifications and carbamidomethylation of cysteines was used as fixed modification. False discovery rate was set to 1% for peptide and protein identifications. For label-free quantification (LFQ), runs with a 0.7 min matching window were selected. MS proteomics data have been deposited to the ProteomeXchange Consortium via the PRIDE partner repository[14] with the dataset identifier PXD007241 (Username: [reviewer52669@ebi.ac.uk](mailto:reviewer52669@ebi.ac.uk); Password: dc4JzXam). Comparison analysis for individual protein levels between genotype was run on normal rank-based inverse log-transformed label-free quantification (LFQ) values and individual FDR were calculated. GO analysis on significantly affected proteins was performed on the subset of proteins with  $FDR \leq 0.01$  and absolute  $FC \geq 1.5$  using String (v10.5) [15] and Panther (v12.0) expression analysis tools [16, 17].

*Generation of the FL83B cell lines.* The FL83B embryonic hepatocytic cell line was ordered to ATCC (CRL-2390) and cultured according to the guidelines in F12K complete medium containing 10% fetal bovine serum. FL83B cells were transduced as described in [18], using a lentivirus expressing either an anti-*Fmr1* shRNA targeting *Fmr1* constitutive exon 1 (*shFmr1*) or a control shRNA (*shControl*). Co-expression of the shRNA is coupled to eGFP expression to enable sorting of transduced cells using a FACS Aria III (BD) based on eGFP fluorescence as described in [18].

*Immunofluorescence.* FL83B cells were grown subconfluent, fixed in 4% paraformaldehyde and subjected to immunofluorescence labeling using anti-S6 polyclonal rabbit antibodies (Cell signalling) and anti-FMRP Y#C10 polyclonal avian antibodies [19] and secondary antibodies coupled either to Alexa594 or Alexa647, as described in [20]. After counterstaining with DAPI, coverslips were mounted on slides with anti-fading reagent and observed using a Zeiss Axioplan2 epifluorescence microscope equipped with a CoolSNAP HQ CCD cooled camera (Roper Scientific). Micrographs were then analysed with ImageJ software.

*Puromycin labeling of neosynthesized peptides.* The assay was performed as described in [21]. In brief, FL83B cells were seeded at a density of 100,000 cells/well in 12 well plates. 48 hr post seeding, complete medium was changed for fresh F12K medium. After 5 hr, puromycin was added to the wells at a final concentration of 10  $\mu\text{g}/\text{mL}$ . After 15 and 30 min, incorporation of puromycin was

stopped by washing the cells 3 times in ice-cold PBS. Control experiments were performed by preincubating cells for 30 min with the translation blocker cycloheximide (50  $\mu\text{g}/\text{mL}$ ). Cells were scraped in lysis buffer (10 mM Tris pH 7.4, 150 mM NaCl, 1.25 mM  $\text{MgCl}_2$ , 0.5% NP40) containing a complete antiprotease cocktail (Pierce). 20  $\mu\text{g}$  of proteins were loaded on a 11% SDS-PAGE and transferred on a nitrocellulose membrane. Ponceau staining was performed to quantify the total protein load in each lane, as described [21, 22]. Puromycin-labeled neosynthesized peptides were visualized by western-blotting using the anti-puromycin 12D10 antibody (Millipore). Signal was visualized using ECL kits (Perkin) and a Fusion VX-Imager (Vilber). Puromycin signal was normalized to total protein Ponceau signal, with both signals quantified in each lane by densitometric analysis using the ImageJ software. Scans of the fully uncut Ponceau-stained membranes as well as anti-puromycin western-blot images are available upon request.

*Metabolic network reconstruction.* The MetaboSignal R package (<https://bioconductor.org/packages/release/bioc/html/MetaboSignal.html>) was used to build the shortest paths network of relevant proteins and metabolites [23, 24]. An extended list of metabolites (Table S5) was built to recapitulate the classes of metabolites of interest identified using metabolomics or biochemical measurements of circulating markers presented in Figure 1. A network of human pathways was then built merging KEGG, OmniPath and TRRUST databases. A number of interactions were manually implemented (Table S6): interactions for

acetone, L-carnitine, GYS2, AGL, ABCD3, and SLC16A1 were manually curated from the literature [25-30] and proteins significantly dysregulated in the *Fmr1*-KO liver were mapped in the first network of interaction with FMRP. Since human pathways are more complete in those databases, we used human Entrez ID, at the expense of 22 significant mouse proteins with no human homolog that were not considered in the network analysis: *Cyp2a12*, *Cyp3a25*, *Cyp2c37*, *Cyp2c50*, *Cyp2c67*, *Cyp2c54*, *Cyp2j5*, *Hsd3b5*, *Slco1a1*, *Rdh7*, *Ugt2b7*, *Chil3*, *Ugt1a9*, *Ngp*, *Cyp2d22*, *Cyp2a5*, *Cyp2d26*, *Gulo*, *Cyp2c23*, *Cyp2d10*, *Cyp2d9*, *Ighv1-31*. Shortest paths network from FMRP to the metabolites of interest were then computed and visualised in Cytoscape [31]. Finally, the network metric of pivotal betweenness (PB, [32]) was computed for each protein mapped onto the network (Table S7).

*Immunoaffinity (IA) capture of FMRP complexes in FL83B cells or liver extracts.* Either FL83B cells or *Fmr1*-WT and -KO liver were homogenized in IA buffer (10 mM Tris pH 7.4, 150mM NaCl, 1.25 mM MgCl<sub>2</sub>, 0.5% NP40, 1mM DTT, 5U/mL RNasin (Invitrogen)). Homogenates were centrifuged at 10,000g for 15 min at 4°C. The supernatant was then raised to 400mM NaCl and 30 mM EDTA and pre-cleared for 1 hr with 60 µL of agarose beads recognizing avian IgY (Gallus) (pre-blocked with 0.1 mg/ml yeast tRNA, and glycogen (Invitrogen)) and with 120 µL of untreated agarose beads (Gallus). Per IA assay, 500 µg of supernatant was incubated in the presence of 60 µg of anti-FMRP Y#C10 antibodies or unrelated IgY (Gallus) immobilized on 15 µL of agarose beads. Samples were

incubated overnight rotating at 4°C and washed 4 times with IA wash buffer (10 mM Tris pH 7.4, 400mM NaCl, 10 mM EDTA, 0.5% NP40). 1/5th of each assay was used for protein analysis using anti-FMRP mAb1C3 antibody [33] and the remaining was subjected to DNAase I treatment (Ambion) for 15 min on ice followed by proteinase K treatment (Roche) for 15 min at RT. IA-captured mRNAs were then phenol-extracted, precipitated with sodium acetate and resuspended in water. The integrity of RNAs extracted from the input and the flowthrough post-IA supernatant was verified on a 1.5% agarose gel. RNA from input lysates and IA assays were subjected to reverse transcription (RT) using the SuperScript III system (Invitrogen), according to the manufacturer's instructions. RT products were subjected to polymerase chain reaction (PCR), using a PCR Master Kit (Promega). Primers used and amplicons lengths are listed in Table S9. The PCR program consisted in 10 min of initial denaturation at 95°C followed by 28 to 35 cycles consisting of 30 s at 95°C, 15 s at 58°C, 15 s at 72°C, and a final elongation step of 10 min at 72°C. PCR products were visualised on a 2.5% TAE agarose gel and amplicon size was verified using the BenchTop DNA ladder (Promega). Primers used are detailed in Table S8.

*Clinical samples.* Twenty-nine healthy subjects (24 males, 5 females) and 25 fragile X patients (20 males, 5 females) of matching ages and ethnicity were enrolled at the University of Antwerp (Antwerp, Belgium). The absence/presence of the Fragile X full mutation in the 5' UTR of *FMR1* gene was confirmed in all participants by an accredited laboratory, using a CGG-repeat PCR and Southern

Blotting on DNA isolated from blood. All patients were between 6-18 years of age and had a number of CGG repeats above 200 yielding *FMR1* gene inactivation (Pieretti et al., 1991). Informed consent was obtained from each participant or his legal guardian before research participation. For this study, we privileged unmedicated patients or under stable treatment for the past 8 wks. Patients under anti-psychotic treatment were systematically excluded. Out of the 25 patients involved, 3 were under Ritaline treatment and were advised not to take the drug on the day of sampling. Exclusion criteria were: recent history of seizure, epilepsy, or blackouts, clinically unstable medical disease, progressive CNS disease/disorder, history of psychiatric disorders, behavioural dysfunction to the point that subject cannot cooperate for testing and history of pathologies which could modify blood biochemistry (e.g. diabetes). To avoid stress induced by fasting to Fragile X patients, individuals involved in the study were not advised to fast prior sampling. Blood was withdrawn in serum collection tubes (BD Vacutainer Serum Separator Tubes), incubated for at least 30 min at room temperature then centrifuged at 2000 rpm, 10 min, at room temperature. Serum was collected, aliquoted and immediately snapped-frozen in liquid nitrogen prior storage at -80°C until use.

*Measures in human samples.* <sup>1</sup>H-NMR metabolic profiling of nonfasting sera samples from FXS patients and controls was performed as described for murine samples. The determination of circulating FFA was subcontracted to the Genotoul Anexplo Platform (Toulouse, France). Insulin was measured using an

Electro-Chemo-Luminescence (ECL)-based assay (v-plex®, MesoScaleDiscovery).

*Statistics.* Normality of data was assessed using Kolmogorov-Smirnov's test. To compare 2 groups, 2-tailed unpaired Student's T-test was used. For non-normal data, log-transformation was applied to meet normality criteria prior to Student's T-test. If sample size  $n < 8$  or if normality was not reached after log-transformation, data were analyzed using Mann & Whitney's non-parametrical U-test. Multiple group comparisons were performed using two-way ANOVA with Genotype (or *siRNA* or *shRNA*) and Treatment or Time as factors or using three-way ANOVA with Genotype, Treatment and Time as factors as stated in legends and text. *Post hoc* comparisons were performed either using Šidák's correction for multiple comparison or Fisher's Least Significance Difference test (if less than 6 comparisons were performed), as stated in the legends. The details of ANOVA statistics are presented in Table S9. Statistical significance was set according to a two-tailed  $p$  value ( $p < 0.05$ ). Only significant differences are displayed on the graphs. Statistical analysis was performed using GraphPad Prism version 6.00 for iOS (GraphPad Software, USA).

*Study approvals.* All animal studies were conducted in facilities accredited by legal authorities (Direction Départementale de Protection des Populations des Alpes-Maritimes, accreditation #C-06-152-5). Procedures involving animal experimentation were approved by the local animal experimentation ethics

committee (Comité Institutionnel d'Éthique Pour l'Animal de Laboratoire) and registered at the Ministère de l'Enseignement Supérieur et de la Recherche (agreement #00788.01 and #05224.01). Samples and data collection from Fragile X patients and controls was approved by the medical ethics committee of the University of Antwerp in Belgium (agreement #B300201523589). The study was conducted in accordance with statutes and regulations regarding the protection of the right and welfare of human subjects' participation in biomedical research (World Declaration of Helsinki).

## Supplemental figures

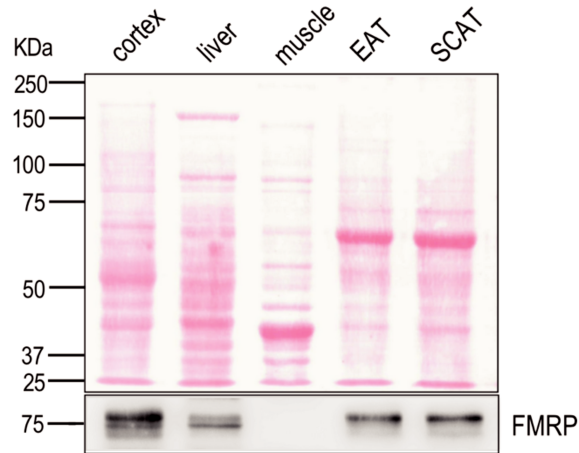


**Figure S1. Expression of FMRP in various tissues.**

Ponceau staining of membrane and Western-blot using anti-FMRP mAb1C3 monoclonal antibody in cortex, liver, muscle (quadriceps), epididymal (EAT) and sub-cutaneous (SCAT) adipose tissues of a 4-months old WT mouse. Note the expression of FMRP in the cortex, liver and both adipose tissues (EAT and SCAT) and the lack of expression in muscle in agreement with [34], supporting the specificity of the staining.

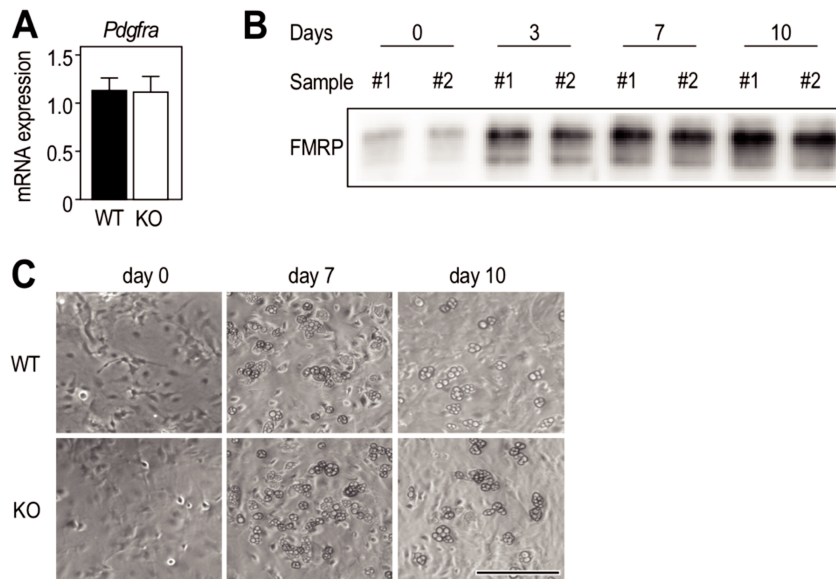


**Figure S2. *Fmr1*-deficiency does not affect adipocytes differentiation**

(A) mRNA levels of adipocyte progenitor marker *Pdgfra* in *Fmr1*-WT and -KO WAT. Data are means  $\pm$  SEM of mRNA level relative to WT; n=8 WT, n=9 KO. 2-tailed Student's T-test: ns.

(B) Western-blot analysis of FMRP expression in cells derived from two independent preparations (#1 and #2) of epididymal adipose tissue-derived stromal vascular fraction (SVF) cells at 0, 3, 7 and 10 days of differentiation into adipocytes. 15 $\mu$ g of proteins were loaded in each lane.

(C) Microphotographs showing the course of differentiation of SVF derived adipocytes from *Fmr1*-KO and WT WAT. Black bar represents 200  $\mu$ m.

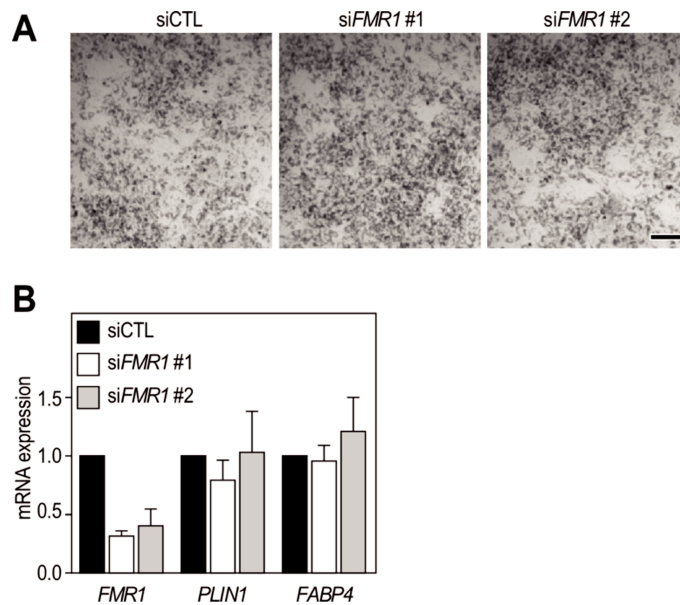


**Figure S3. *Fmr1*-deficiency does not affect hMADs differentiation into adipocytes.**

(A) Microphotographs of hMADs-derived adipocytes transfected with a silencing RNA targeting *FMR1* transcript constitutive exon (*siFMR1*) or a control (*siCtl*) siRNA. Black bar represents 200  $\mu$ m.

(B) Quantitative RT-PCR determination of *FMR1*, *PLIN1* and *FABP4* mRNA expression in hMADs-derived adipocytes transfected with *siFMR1* or *siCtl*. Data are means  $\pm$  SEM relative to *siCtl*; n=4/condition; 2-way ANOVA: p(siRNA)=0.001, p(Transcript)=0.0144, p(Interaction)=0.0144; Šidák's post hoc tests: \*\*\*, p<0.001.

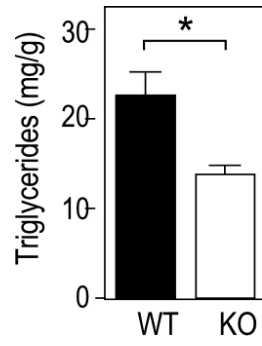


**Figure S4. *Fmr1*-deficiency reduces hepatic TG content.** Data are means TG levels per gram of tissue  $\pm$  SEM; n=9 WT, n=9 KO; 2-tailed Student's T-test: \*,  $p < 0.05$ .

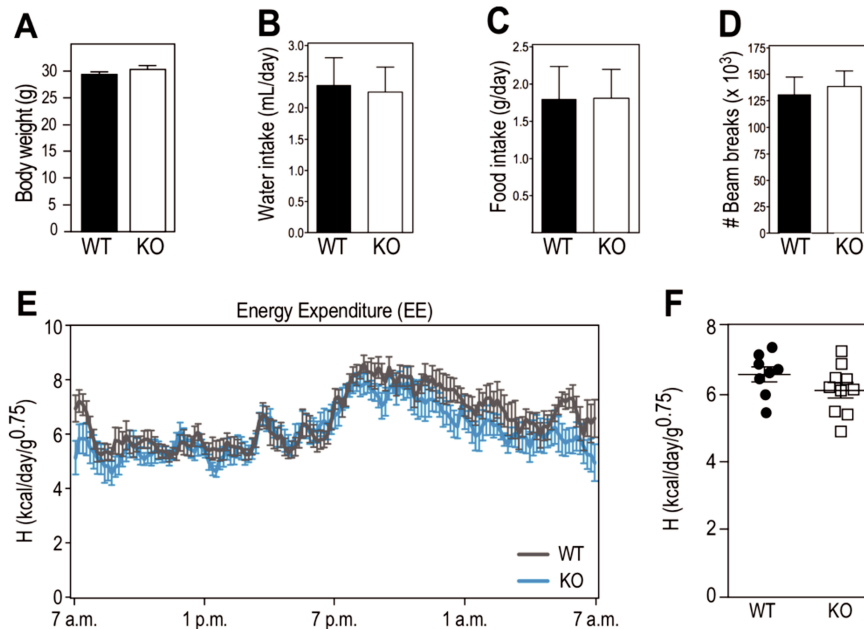


**Figure S5. *Fmr1*-deficiency does not modify body weight, water intake, food intake, locomotor activity or energetic expenditure.**

(A) Body weight in 4-mths old *Fmr1*-KO and WT littermates. Data are means  $\pm$  SEM; n=8 WT, n=10 KO; 2-tailed Student's T-test: ns.

(B) Drinking water intake over 24 hrs. Data are means  $\pm$  SEM; n=8 WT, n=10 KO; 2-tailed Student's T-test: ns.

(C) Food intake over 24 hrs. Data are means  $\pm$  SEM; n=8 WT, n=10 KO; 2-tailed Student's T-test: ns.

(D) Total activity measured by the number of infrared beam breaks over 24 hrs. Data are means  $\pm$  SEM; n=8 WT, n=10 KO; 2-tailed Student's T-test: ns.

(E) Energy expenditure follow-up by over 24 hrs (10 min bin). n=8 WT, n=10 KO.

(F) Average EE over 24 hrs. Data are means  $\pm$  SEM; n=8 WT, n=10 KO; 2-tailed Student's T-test: ns.

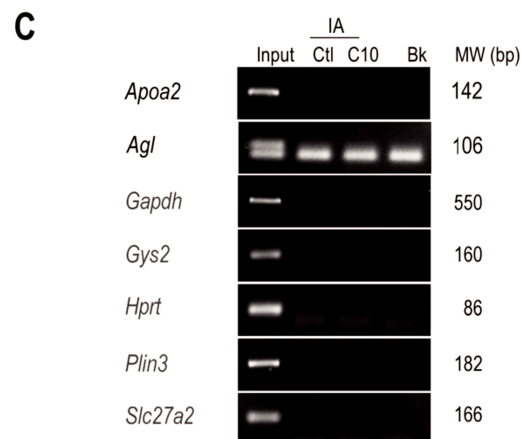
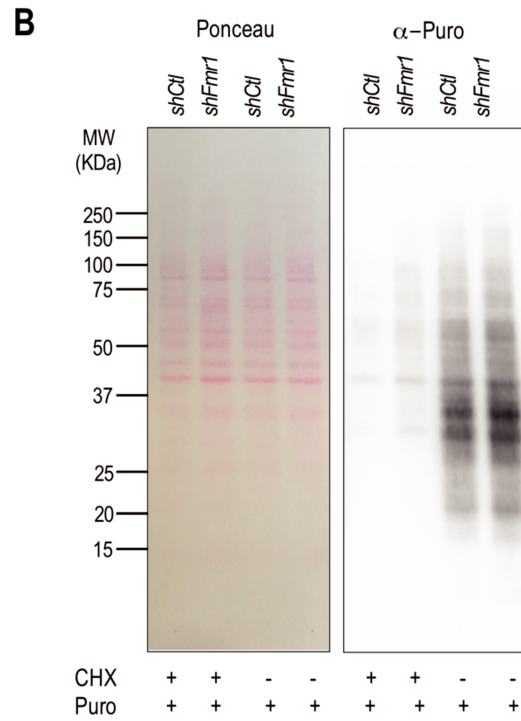
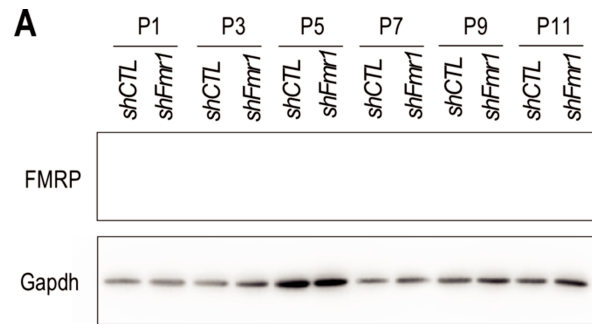


**Figure S6. Controls for *Fmr1* repression, Sunset and IA experiments in the FL83B hepatocytic cell line.**

(A) FL83B cells transduced with *shFmr1* show stable depletion of FMRP over passages as compared to *shCtl*-transduced cells. Western-blot using anti-FMRP mAb1C3 antibody in *shControl* (*shCtl*) and *shFmr1* cell lines at different passages (P). Gapdh was used as a loading control. 15  $\mu$ g of proteins were loaded per lane.

(B) Anti-puromycin antibody selectively label neosynthesized peptides in *shFmr1* and *shCtl* FL83B cell lines. Cells were pretreated with the translation inhibitor cycloheximide (CHX) for 30 min or with vehicle as indicated and then labelled with puromycin (puro) for 30 min. Cell homogenates were analyzed by Ponceau or western blot with anti-puromycin antibody ( $\alpha$ -Puro). Note the strong reduction in puromycin signal in the presence of CHX. 15  $\mu$ g of proteins were loaded per lane.

(C) RT-PCR analysis of mRNAs associated with FMRP in FL83B hepatocytes. Total RNA was extracted from the input cell lysate and IA preparations described in (Figure 6B), and used as a template for RT-PCR. PCR products obtained from input, control IgY (IA Ctl) or IgY#C10 (IA C10) IA complexes as well as control blank PCR (Ctl) performed in the absence of matrix were separated and visualized by agarose gel electrophoresis. PCR amplicons lengths (bp) are specified on the right side. (\*) Amplicon likely to correspond to aspecific primer dimers amplification. The *Agf* specific band is the upper one only detected in the Input.

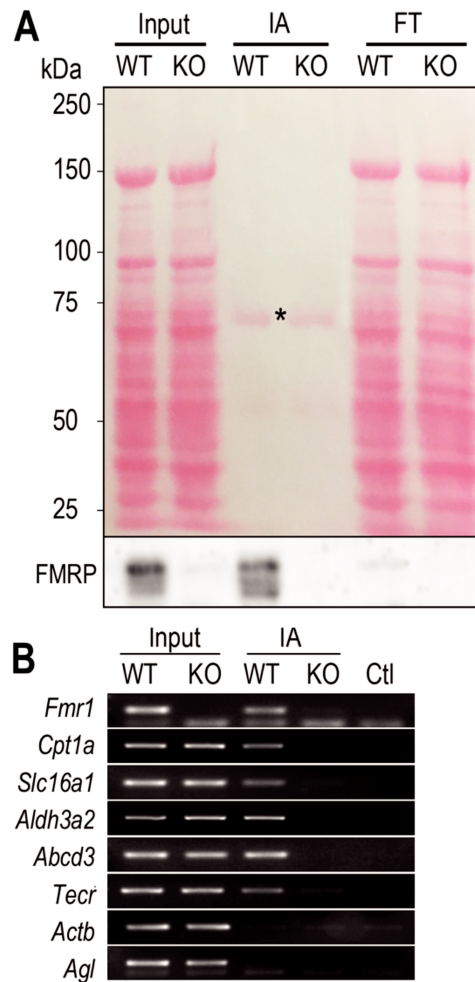


**Figure S7. FMRP associates with selective mRNAs in the liver**

(A) Liver homogenates from *Fmr1*-WT and KO fasted mice were subjected to immuno-affinity (IA) capture with anti-FMRP IgY#C10 avian antibodies and the eluted proteins as well as the post-IA flowthrough supernatant (FT) were analyzed by immunoblotting using anti-FMRP mAb1C3. IgY heavy chains are labeled with an asterisk on the Ponceau (upper panel). Note that depletion in FMRP load in the post-immunoprecipitation supernatant in the presence of IgY#C10 as compared to *Fmr1*-WT input.

(B) RT-PCR analysis of mRNAs associated with FMRP in the liver. Total RNA was extracted from the input *Fmr1*-WT and KO liver lysates and FMRP IA-captured complexes and used as a template for RT-PCR. RT-PCR products obtained from input *Fmr1*-WT or KO liver (lanes 1, 2) and IgY#C10 IA preparations from *Fmr1*-WT or KO liver (lanes 3, 4), as well as control PCR (lane 5) performed in the absence of matrix were separated and visualized by agarose gel electrophoresis. This reveals that the known FMRP mRNA target *Fmr1* is selectively recovered in the IgY#C10 IA-captured complexes from *Fmr1*-WT liver. The mRNAs *Cpt1a*, *Slc16a1*, *Aldh3a2*, *Abcd3*, *Tecr* are also selectively recovered in the IgY#C10 immunoprecipitate, while the mRNA *Actb* and *Agl* were not recovered. The molecular weights of PCR amplicons are specified on the right side.

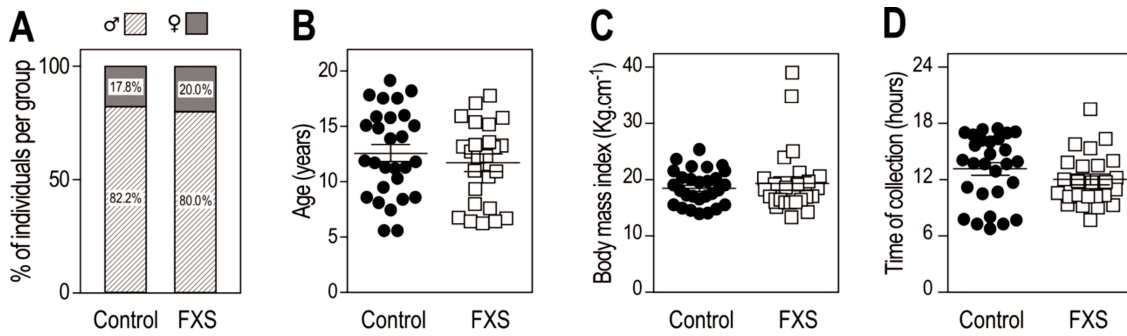


**Figure S8. Characteristics of the FXS and control individuals involved in the clinical study.**

(A) Sex distribution; n=29 controls and n=25 FXS patients; Chi-square test: ns.

(B) Age distribution. Data are means  $\pm$  SEM; n=29 controls and n=25 FXS patients; 2-tailed Student's T-test: ns.

(C) Body mass index distribution. Data are means  $\pm$  SEM; n=29 controls and n=25 FXS patients; 2-tailed Mann & Whitney U-test: ns.

(D) Distribution of sample collection's time. Data are means  $\pm$  SEM; n=29 controls and n=25 FXS patients; 2-tailed Mann & Whitney U-test: ns.

## Supplementary tables legends

**Table S1. Individual LFQ scores for the samples used in proteome analysis.**

*Available as Excel file*

**Table S2. List of 307 proteins showing a significant change in abundance of at least 1.5-fold ( $FDR \leq 0.01$ ) in *Fmr1*-deficient fasted liver as compared to control.**

*Available as Excel file*

**Table S3. String-based Gene Ontology analysis of pathways significantly overrepresented in list of 307 of proteins showing a significant change ( $FDR \leq 0.01$ ) and absolute fold-of-change in abundance of at least 1.5 in *Fmr1*-deficient fasted liver as compared to control.**

*Available as Excel file*

**Table S4. Panther-based Gene Ontology analysis of pathways significantly overrepresented in list of 307 of proteins showing a significant change ( $FDR \leq 0.01$ ) and absolute fold-of-change in abundance of at least 1.5 in *Fmr1*-deficient fasted liver as compared to control.**

*Available as Excel file*

**Table S5. Metabolic network extended metabolite list.**

*Available as Excel file*

**Table S6. Metabolic network extended node list.** Gene (EntrezGene ID) or metabolite (KEGG ID), reference for interaction

*Available as Excel file*

**Table S7. Metabolic network metrics.** Human Entrez Gene IDs, Gene name, Protein name and normalized pivotal betweenness (PB) score for proteins mapped on the network.

*Available as Excel file*

**Table S8. List of primers.**

*Available as Excel file*

**Table S9. ANOVA statistics.**

*Available as Excel file*

## References

- [1] Mientjes, E.J., Nieuwenhuizen, I., Kirkpatrick, L., Zu, T., Hoogeveen-Westerveld, M., Severijnen, L., et al., 2006. The generation of a conditional Fmr1 knock out mouse model to study Fmrp function in vivo. *Neurobiol Dis* 21(3):549-555.
- [2] Dona, A.C., Jimenez, B., Schafer, H., Humpfer, E., Spraul, M., Lewis, M.R., et al., 2014. Precision high-throughput proton NMR spectroscopy of human urine, serum, and plasma for large-scale metabolic phenotyping. *Anal Chem* 86(19):9887-9894.
- [3] Dona, A.C., Kyriakides, M., Scott, F., Shephard, E.A., Varshavi, D., Veselkov, K., et al., 2016. A guide to the identification of metabolites in NMR-based metabonomics/metabolomics experiments. *Comput Struct Biotechnol J* 14:135-153.
- [4] Dumas, M.E., Barton, R.H., Toye, A., Cloarec, O., Blancher, C., Rothwell, A., et al., 2006. Metabolic profiling reveals a contribution of gut microbiota to fatty liver phenotype in insulin-resistant mice. *Proc Natl Acad Sci U S A* 103(33):12511-12516.
- [5] Heikkinen, S., Argmann, C.A., Champy, M.F., Auwerx, J., 2007. Evaluation of glucose homeostasis. *Curr Protoc Mol Biol* Chapter 29:Unit 29B 23.
- [6] Ayala, J.E., Samuel, V.T., Morton, G.J., Obici, S., Croniger, C.M., Shulman, G.I., et al., 2010. Standard operating procedures for describing and performing metabolic tests of glucose homeostasis in mice. *Dis Model Mech* 3(9-10):525-534.
- [7] Livak, K.J., Schmittgen, T.D., 2001. Analysis of relative gene expression data using real-time quantitative PCR and the 2<sup>-</sup>(Delta Delta C(T)) Method. *Methods* 25(4):402-408.
- [8] Rodriguez, A.M., Elabd, C., Delteil, F., Astier, J., Vernochet, C., Saint-Marc, P., et al., 2004. Adipocyte differentiation of multipotent cells established from human adipose tissue. *Biochemical and biophysical research communications* 315(2):255-263.

- [9] Beranger, G.E., Pisani, D.F., Castel, J., Djedaini, M., Battaglia, S., Amiaud, J., et al., 2014. Oxytocin reverses ovariectomy-induced osteopenia and body fat gain. *Endocrinology* 155(4):1340-1352.
- [10] Pisani, D.F., Beranger, G.E., Corinus, A., Giroud, M., Ghandour, R.A., Altirriba, J., et al., 2016. The K<sup>+</sup> channel TASK1 modulates beta-adrenergic response in brown adipose tissue through the mineralocorticoid receptor pathway. *FASEB J* 30(2):909-922.
- [11] Pisani, D.F., Djedaini, M., Beranger, G.E., Elabd, C., Scheideler, M., Ailhaud, G., et al., 2011. Differentiation of Human Adipose-Derived Stem Cells into "Brite" (Brown-in-White) Adipocytes. *Front Endocrinol (Lausanne)* 2:87.
- [12] Even, P.C., Nadkarni, N.A., 2012. Indirect calorimetry in laboratory mice and rats: principles, practical considerations, interpretation and perspectives. *Am J Physiol Regul Integr Comp Physiol* 303(5):R459-476.
- [13] Cox, J., Mann, M., 2008. MaxQuant enables high peptide identification rates, individualized p.p.b.-range mass accuracies and proteome-wide protein quantification. *Nat Biotechnol* 26(12):1367-1372.
- [14] Vizcaino, J.A., Csordas, A., Del-Toro, N., Dianas, J.A., Griss, J., Lavidas, I., et al., 2016. 2016 update of the PRIDE database and its related tools. *Nucleic Acids Res* 44(22):11033.
- [15] Jensen, L.J., Kuhn, M., Stark, M., Chaffron, S., Creevey, C., Muller, J., et al., 2009. STRING 8--a global view on proteins and their functional interactions in 630 organisms. *Nucleic Acids Res* 37(Database issue):D412-416.
- [16] Thomas, P.D., Campbell, M.J., Kejariwal, A., Mi, H., Karlak, B., Daverman, R., et al., 2003. PANTHER: a library of protein families and subfamilies indexed by function. *Genome Res* 13(9):2129-2141.
- [17] Thomas, P.D., Kejariwal, A., Guo, N., Mi, H., Campbell, M.J., Muruganujan, A., et al., 2006. Applications for protein sequence-function evolution data: mRNA/protein

expression analysis and coding SNP scoring tools. *Nucleic Acids Res* 34(Web Server issue):W645-650.

[18] Khalfallah, O., Jarjat, M., Davidovic, L., Nottet, N., Cestele, S., Mantegazza, M., et al., 2017. Depletion of the Fragile X Mental Retardation Protein in Embryonic Stem Cells Alters the Kinetics of Neurogenesis. *Stem Cells* 35(2):374-385.

[19] El Fatimy, R., Tremblay, S., Dury, A.Y., Solomon, S., De Koninck, P., Schrader, J.W., et al., 2012. Fragile X mental retardation protein interacts with the RNA-binding protein Caprin1 in neuronal RiboNucleoProtein complexes [corrected]. *PLoS ONE* 7(6):e39338.

[20] Dury, A.Y., El Fatimy, R., Tremblay, S., Rose, T.M., Cote, J., De Koninck, P., et al., 2013. Nuclear Fragile X Mental Retardation Protein is localized to Cajal bodies. *PLoS genetics* 9(10):e1003890.

[21] Schmidt, E.K., Clavarino, G., Ceppi, M., Pierre, P., 2009. SUnSET, a nonradioactive method to monitor protein synthesis. *Nat Methods* 6(4):275-277.

[22] Gantois, I., Khoutorsky, A., Popic, J., Aguilar-Valles, A., Freemantle, E., Cao, R., et al., 2017. Metformin ameliorates core deficits in a mouse model of fragile X syndrome. *Nat Med* 23(6):674-677.

[23] Rodriguez-Martinez, A., Ayala, R., Posma, J.M., Dumas, M.E., 2018. Exploring the Genetic Landscape of Metabolic Phenotypes with MetaboSignal. *Curr Protoc Bioinformatics* 61(1):14 14 11-14 14 13.

[24] Rodriguez-Martinez, A., Ayala, R., Posma, J.M., Neves, A.L., Gauguier, D., Nicholson, J.K., et al., 2017. MetaboSignal: a network-based approach for topological analysis of metabotype regulation via metabolic and signaling pathways. *Bioinformatics* 33(5):773-775.

- [25] Koorevaar, G., Van Stekelenburg, G.J., 1976. Mammalian acetoacetate decarboxylase activity. Its distribution in subfractions of human albumin and occurrence in various tissues of the rat. *Clin Chim Acta* 71(2):173-183.
- [26] Miyazawa, S., Ozasa, H., Osumi, T., Hashimoto, T., 1983. Purification and properties of carnitine octanoyltransferase and carnitine palmitoyltransferase from rat liver. *J Biochem* 94(2):529-542.
- [27] Algranati, I.D., Cabib, E., 1960. The synthesis of glycogen in yeast. *Biochim Biophys Acta* 43:141-142.
- [28] Whelan, W.J., 1971. Enzymic explorations of the structures of starch and glycogen. *Biochem J* 122(5):609-622.
- [29] Imanaka, T., Aihara, K., Takano, T., Yamashita, A., Sato, R., Suzuki, Y., et al., 1999. Characterization of the 70-kDa peroxisomal membrane protein, an ATP binding cassette transporter. *J Biol Chem* 274(17):11968-11976.
- [30] Halestrap, A.P., 2013. The SLC16 gene family - structure, role and regulation in health and disease. *Mol Aspects Med* 34(2-3):337-349.
- [31] Shannon, P., Markiel, A., Ozier, O., Baliga, N.S., Wang, J.T., Ramage, D., et al., 2003. Cytoscape: a software environment for integrated models of biomolecular interaction networks. *Genome Res* 13(11):2498-2504.
- [32] Davidovic, L., Navratil, V., Bonaccorso, C.M., Catania, M.V., Bardoni, B., Dumas, M.E., 2011. A metabolomic and systems biology perspective on the brain of the Fragile X syndrome mouse model. *Genome Res* 12:2190-2202.
- [33] Devys, D., Lutz, Y., Rouyer, N., Bellocq, J.P., Mandel, J.L., 1993. The FMR-1 protein is cytoplasmic, most abundant in neurons and appears normal in carriers of a fragile X premutation. *Nat Genet* 4(4):335-340.

[34] Khandjian, E.W., Bardoni, B., Corbin, F., Sittler, A., Giroux, S., Heitz, D., et al., 1998. Novel isoforms of the fragile X related protein FXR1P are expressed during myogenesis. *Hum Mol Genet* 7(13):2121-2128.

# Skeletal Anomalies in FXS: Publication #2

## A. Research Hypothesis and Objectives of the Study

Bone abnormalities such as dental, mandibular, craniofacial and skeletal abnormalities had been previously observed in FXS patients (Davids et al., 1990; Heulens et al., 2013; Sabbagh-Haddad et al., 2016). Therefore, our hypothesis was that *Fmr1*-deficiency could impact whole body composition and bone structure in FXS mouse model.

To test this hypothesis, we used exclusively the *Fmr1*-KO FXS mouse model and our objectives were:

1. To investigate whole-body composition and skeletal defects in *Fmr1*-KO mouse model
2. To investigate the behavioural changes which could contribute to bone structural changes

To achieve the first goal, we used 4-month old *Fmr1*-KO and WT male mice littermates. We used microcomputerised X-ray tomography to analyse skeletal morphology and femora bone microstructure. We also performed behavioural tests to measure locomotor activity and actimetry chambers to analyse diurnal and nocturnal activity.

My contribution to this article was the realization, analysis and interpretation of behavioural tests in *Fmr1*-KO and WT animals.

## B. Results

The results of this study are presented in the following publication:

*Publication #2:*

Leboucher A, **Bermudez-Martin P**, Mouska X, Amri EZ, Pisani DF, Davidovic L (2019) *Fmr1*-deficiency impacts body composition, skeleton and bone microstructure in a mouse model of Fragile X Syndrome. *Frontiers in Endocrinology*. 10:678. doi: 10.3389/fendo.2019.00678. eCollection 2019.

To summarise, in this study we have shown that *Fmr1*-KO mice display overweight and overgrowth accompanied by an increase in muscular mass and a reduction of intra-abdominal adiposity. We have shown that this is accompanied by structural changes in bone morphology. Moreover, *Fmr1*-KO displayed increased physical activity in the open-field and in actimetry chambers. This study opens the way for future research to study the relationship between hyperactivity and skeletal changes found in Fragile X patients.

## C. Manuscript



# *Fmr1*-Deficiency Impacts Body Composition, Skeleton, and Bone Microstructure in a Mouse Model of Fragile X Syndrome

Antoine Leboucher<sup>1†</sup>, Patricia Bermudez-Martin<sup>1</sup>, Xavier Mouska<sup>1</sup>, Ez-Zoubir Amri<sup>2</sup>, Didier F. Pisani<sup>3</sup> and Laetitia Davidovic<sup>1\*</sup>

<sup>1</sup> Université Côte d'Azur, CNRS, IPMC, Valbonne, France, <sup>2</sup> Université Côte d'Azur, CNRS, Inserm, IBV, Nice, France,

<sup>3</sup> Université Côte d'Azur, CNRS, LP2M, Nice, France

## OPEN ACCESS

### Edited by:

Chandi C. Mandal,  
Central University of Rajasthan, India

### Reviewed by:

Michaël R. Laurent,  
University Hospitals Leuven, Belgium  
Stéphane Blouin,  
Ludwig Boltzmann Institute of  
Osteology (LBIO), Austria

### \*Correspondence:

Laetitia Davidovic  
davidovic@ipmc.cnrs.fr

### † Present address:

Antoine Leboucher,  
German Institute of Human Nutrition  
Potsdam-Rehbrücke (DIfE),  
Nuthetal, Germany

### Specialty section:

This article was submitted to  
Bone Research,  
a section of the journal  
Frontiers in Endocrinology

Received: 27 May 2019

Accepted: 18 September 2019

Published: 02 October 2019

### Citation:

Leboucher A, Bermudez-Martin P,  
Mouska X, Amri E-Z, Pisani DF and  
Davidovic L (2019) *Fmr1*-Deficiency  
Impacts Body Composition, Skeleton,  
and Bone Microstructure in a Mouse  
Model of Fragile X Syndrome.  
*Front. Endocrinol.* 10:678.  
doi: 10.3389/fendo.2019.00678

Fragile X syndrome (FXS) is a neurodevelopmental disorder associated with intellectual disability, hyperactivity, and autism. FXS is due to the silencing of the X-linked *FMR1* gene. Murine models of FXS, knock-out (KO) for the murine homolog *Fmr1*, have been generated, exhibiting CNS-related behavioral, and neuronal anomalies reminiscent of the human phenotypes. As a reflection of the almost ubiquitous expression of the *FMR1* gene, FXS is also accompanied by physical abnormalities. This suggests that the *FMR1*-deficiency could impact skeletal ontogenesis. In the present study, we highlight that *Fmr1*-KO mice display changes in body composition with an increase in body weight, likely due to both increase of skeleton length and muscular mass along with reduced visceral adiposity. We also show that, while *Fmr1*-deficiency has no overt impact on cortical bone mineral density (BMD), cortical thickness was increased, and cortical eccentricity was decreased in the femurs from *Fmr1*-KO mice as compared to controls. Also, trabecular pore volume was reduced and trabecular thickness distribution was shifted toward higher ranges in *Fmr1*-KO femurs. Finally, we show that *Fmr1*-KO mice display increased physical activity. Although the precise molecular signaling mechanism that produces these skeletal and bone microstructure changes remains to be determined, our study warrants further investigation on the impact of *FMR1*-deficiency on whole-body composition, as well as skeletal and bone architecture.

**Keywords:** fragile X syndrome, bone microstructure, skeleton, tomography, trabecula, muscle, physical activity

## INTRODUCTION

Fragile X syndrome (FXS) is a neurodevelopmental disorder associated with intellectual disability, attention deficits, and hyperactivity disorders, and autism spectrum disorders (1, 2). FXS affects 1/4,000 males and 1/7,000 females worldwide and is caused by the silencing of the X-linked Fragile X Mental Retardation 1 (*FMR1*) gene located in a fragile chromosomal site in 27q3 (3, 4). In FXS patients, abnormal expansions of CGG trinucleotide repeats in the 5' untranslated region of the *FMR1* gene lead to an hypermethylation of the upstream CpG island in the gene promotor and to *FMR1* silencing (3–5). Murine *Fmr1*-knock-out (KO) models of FXS have been generated, exhibiting CNS-related behavioral, and neuronal anomalies reminiscent of the human phenotypes (6, 7). The *FMR1* gene is not only expressed in the central nervous system (CNS) but also

in a variety of peripheral tissues, including adipose tissue, and liver (8–11). Adult skeletal and cardiac muscle are the only peripheral tissues tested so far not expressing FMRP, while both white adipose tissue (WAT) and brown adipose tissue (BAT) express FMRP (8–12). This suggests that long-term pathological consequences of *FMRI*-deficiency are not solely confined to the central nervous system disorders and more likely extend to physiological dysfunctions in peripheral systems. We have previously demonstrated in FXS mouse model how *Fmr1*-deficiency increased systemic utilization of lipids, reduced adiposity and provoked significant changes in metabolic homeostasis, some of which were also translatable to FXS patients (11). Besides presenting metabolic phenotypes, FXS is also accompanied by physical abnormalities (13). In subsets of FXS patients, morphometric studies have highlighted increased stature and height (14) and a general overgrowth in prepubertal boys affected by FXS (13, 15). FXS patients present connective tissue dysplasia (16), dental and mandibular anomalies (17), orthopedic anomalies such as scoliosis (18), and abnormal metacarpophalangeal pattern profile (19). In addition, FXS patients display specific craniofacial abnormalities with reduced facial depth, hypoplasticity of the nasal bone–cartilage interface and narrow mid-facial width exaggerating ear prominence (20). This suggests that *Fmr1*-deficiency could have widespread peripheral effects, including on skeletal ontogenesis. Besides subtle craniofacial anomalies with morphometric changes in the mandible and skull (20), skeletal particularities, and bone microstructure have not yet been studied in FXS mouse model. In this study, we examined in details body composition and bone microstructure of adult *Fmr1*-KO male mice.

## MATERIALS AND METHODS

### Animals Procedures

*Fmr1*-KO2 mice on the C57Bl/6J background used in this study were originally described in Mientjes et al. (7) and were named *Fmr1*-KO all throughout the manuscript. *Fmr1*-heterozygous females and *Fmr1*-KO male founders were obtained from Rob Willemsen (Erasmus University, Rotterdam, Netherlands) and backcrossed for at least 10 generations on a C57Bl6/J WT background (Janvier Labs, France). All *Fmr1*-WT and *Fmr1*-KO male used in this study were littermates born to *Fmr1* heterozygous females mated with *Fmr1*-KO males. Pups were weaned at 28 days of age, identified by ear tags, and genotyped by PCR as described (7). Pups from various litters were then randomly grouped according to their genotype in cages and had *ad libitum* access to water and standard chow (reference 4RF25, Mucedola) composed of cereals (53.7%), animal proteins (4.7%), vegetal proteins (30.5%), lipids (soy oil, 1.4%), vitamins and minerals (4.1%), amino acids (0.1%). Animals were housed in a temperature (22–24°C) and hygrometry (70–80%)- controlled room with a 12 h light-dark cycle (lights on at 08:00). Animals were housed in medium-size (up to 5 animals/cage) or large cages (up to 10 animals/cage) filled with wooden bedding, one plastic house and nesting material for enrichment. All the described experiments were performed on male animals at exactly 4-months (16 weeks) of age. After cervical dislocation, muscle

*Tibialis anterior*, visceral, and subcutaneous WAT, as well as interscapular BAT were dissected by trained personnel and weighed with a precision balance.

### Osteocalcin Measure

Animals were anesthetized and blood was withdrawn by cardiac puncture, incubated for at least 30 min at room temperature (RT) then centrifuged at 400 g, 10 min, RT. Serum was collected and immediately snapped-frozen in liquid nitrogen prior storage at  $-80^{\circ}\text{C}$  until use. Osteocalcin was measured in serum using a dedicated ELISA kit (Takara), according strictly to the manufacturer's instructions.

### Microcomputerised Tomography Analysis: Skeleton Morphology

For the analysis of whole-body bone morphology (Figure 1), anesthetised animals were introduced in a SkyScan  $\mu\text{CT}$  –1178 X-ray tomograph (Bruker) and analyzed as previously described (11, 21). Mice were scanned using the following parameters:  $104\ \mu\text{m}$  pixel size, 49 kV, 0.5 mm thick aluminum filter and a rotation step of  $0.9^{\circ}$ . 3D reconstructions and analysis of skeleton, vertebra and femur lengths as well as skeleton volume were performed using NRecon and CTAn software (Skyscan). Skeleton volume was calculated using CTAn software by extracting from  $\mu\text{CT}$  scans all voxels exceeding a single global CT threshold value, ensuring that differences between study groups are due to experimental effects rather than image-processing effects. The representative skeleton reconstruction from one *Fmr1*-WT animal (Figure 1D) was obtained by further processing of the 3D reconstructed sections using the ImageJ plugin 3D viewer and the BoneJ plugin (22). Bone and skeleton lengths were calculated using the 3D coordinates of the structure extremities specified in Figure 1D. For skeleton length we used the anterior coordinate of the nasal bone and the posterior coordinate of the first caudal vertebra. For femur length, we used the extreme coordinate of the femoral epiphysis and the extreme coordinate of the proximal epiphysis (measured on both femurs and averaged). For L3-L6 vertebra length we used the anterior extreme coordinate of L3 vertebra and the posterior extreme coordinate of L6 vertebra.

### Microcomputerised Tomography Analysis: Bone Microstructure

For measurements of bone mineral density (BMD) and microstructure, we proceeded according to the guidelines for Assessment of Bone Microstructure in Rodents Using Micro-Computed Tomography (23). After necropsy, femora were individually scanned with a SkyScan  $\mu\text{CT}$ -1173 X-ray tomograph (Bruker) set with the following parameters:  $7.76\ \mu\text{m}$  pixel size, 45 kV, 1 mm thick aluminum filter,  $0.5^{\circ}$  of rotation step, as previously described (21). 3D reconstructions and bone microstructure analysis were performed using NRecon and CTAn software (Skyscan). Bone microstructure was reconstructed using CTAn software by extracting from  $\mu\text{CT}$  scans all voxels exceeding a single global CT value.

The region of interest (ROI) for calculations of femur cortical bone microstructure parameters was defined as a mid-shaft segment of  $400\ \mu\text{m}$  starting at 55% of the total femur length from

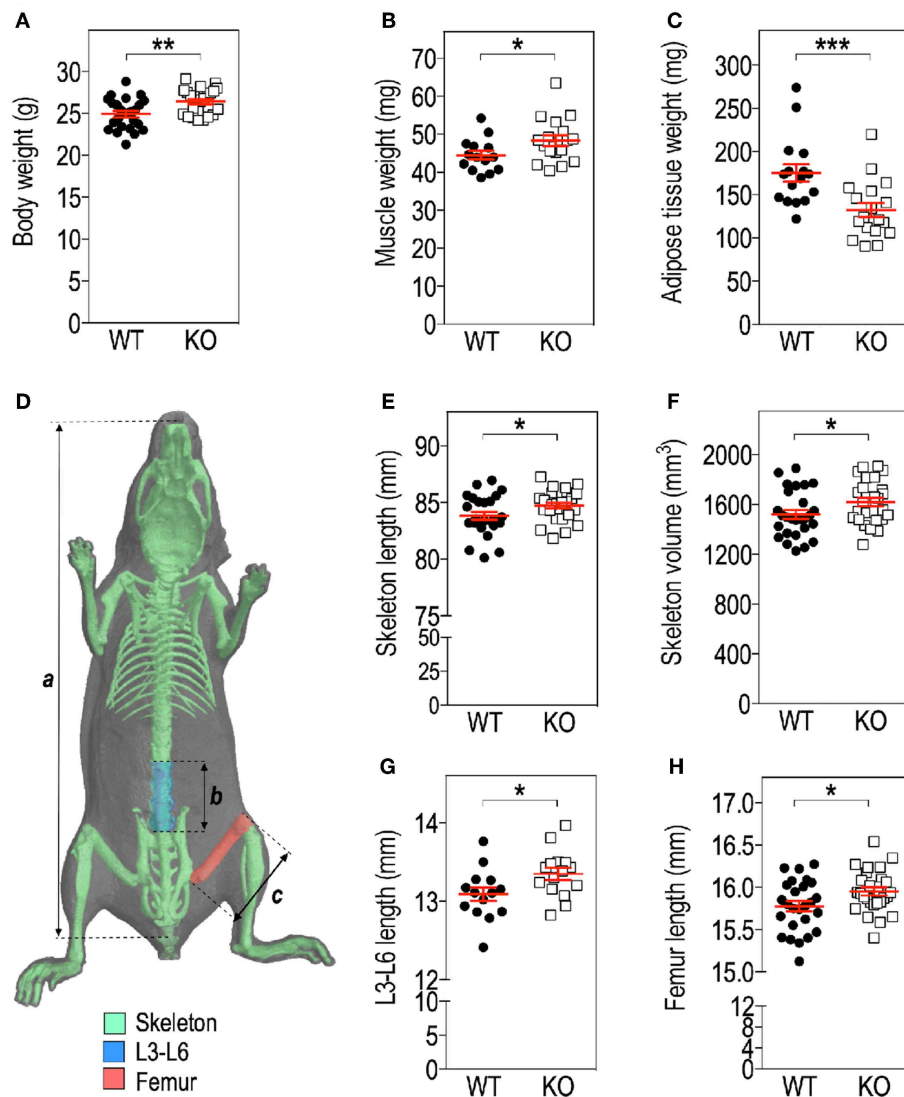


**FIGURE 1 |** *Fmr1*-deficiency modifies body mass distribution. Body weight (A), *Tibialis anterior* muscle (B), as well as visceral white adipose tissue (WAT) (C) weights in *Fmr1*-KO and WT 4-months old male mice. (D) Anatomical coordinates used for analysis of: a, skeleton length; b, vertebral L3-L6 length; c, maximal femur length. Skeleton length (E), skeleton volume (F), vertebral L3-L6 length (G), and femoral length (H) were measured in 3D reconstructions of skeleton following X-ray tomography. Data are presented as dot-plots featuring means  $\pm$  SEM in red. Statistical significance of differences was measured using 2-tailed Student's *T*-test. \**p* < 0.05; \*\**p* < 0.01; \*\*\**p* < 0.001. For (A,E,F,H), *n* = 24–27 animals/group; for (B,C,G), *n* = 15–18 animals/group.

the proximal epiphysis extremity (corresponding on average to a distance of 8.68 mm for WT animals and 8.77 mm for KO animals) and extending up to 400  $\mu$ m distally. The ROI for calculations of femur trabecular bone microstructure parameters was defined as a 900  $\mu$ m-segment of the distal metaphysis, located on average 450  $\mu$ m away from the epiphyseal line and excluding cortical bone. The segment started at a distance equivalent to 13.5% of the total femur length measured from the distal extremity of the femur, corresponding on average to a distance of 2.13 mm in the WT and 2.15 mm in the KO.

For volumetric cortical BMD calculation, a BMD phantom rod pair supplied by the manufacturer and suitable for mouse

bone analysis (2 mm of diameter) with different known densities (0.25 and 0.75 g.cm<sup>-3</sup> calcium hydroxyapatite) was scanned along with the samples, using scan settings identical to those for acquisitions on femurs. Individual cortical (total cross-sectional object area, object area per slice, cortical area fraction, cortical thickness, mean polar moment of inertia (MMI), eccentricity) and trabecular (bone volume fraction, trabecular number, trabecular thickness, trabecular separation, total volume of trabecular pores) bone microstructure parameters were extracted on each section of the corresponding 3D ROI, using the CTAN software and then averaged as recommended in Bouxsein et al. (23). Their means and standard deviations (SD) for each group

**TABLE 1** | Comparison analysis of variables for cortical bone morphology in *Fmr1*-KO and WT femurs.

Abbreviation	Variable description	Unit	Mean WT	SD WT	Mean KO	SD KO	p-value
vBMD	Volumetric bone mineral density	mg/cm <sup>3</sup>	1.2310	0.0593	1.2190	0.0334	0.5403 <sup>a</sup>
Tt.Ar	Mean total cross-sectional object area	mm <sup>2</sup>	0.9402	0.1002	1.0010	0.1179	0.1548 <sup>a</sup>
Ct.Ar	Average object area per slice	mm <sup>2</sup>	0.4788	0.0729	0.3885	0.1812	0.1214 <sup>a</sup>
Ct.Ar/Tt.Ar	Cortical area fraction	%	53.62	12.28	40.31	20.61	0.0574 <sup>a</sup>
Ct.Th	Average cortical thickness	mm	0.1748	0.0106	0.1856	0.0098	<b>0.0128<sup>a</sup></b>
MMI	Mean polar moment of inertia	mm <sup>4</sup>	0.526	0.102	0.544	0.113	0.6613 <sup>a</sup>
Ecc	Eccentricity	A. U.	0.7056	0.0717	0.6338	0.0680	<b>0.0148<sup>b</sup></b>

Mean and standard deviations (SD) to the mean are reported for *Fmr1*-WT and KO animals, as well as p-value for the Student's *T*-test (<sup>a</sup>) or the Mann & Whitney *U*-test (<sup>b</sup>). Significant p-values ( $p < 0.05$ ) are bolded.  $n = 13$ – $15$  animals/group.

**TABLE 2** | Comparison analysis of variables for trabecular bone microarchitecture in *Fmr1*-KO and WT femurs.

Abbreviation	Variable description	Unit	Mean WT	SD WT	Mean KO	SD KO	p-value
BV/TV	Bone volume fraction	%	18.6300	5.1660	22.3700	5.5000	<b>0.0469<sup>b</sup></b>
Tb.N	Trabecular number	nb/mm	1.1110	0.5512	1.1160	0.9092	0.5164 <sup>b</sup>
Tb.Th	Trabecular thickness	mm	0.06106	0.007229	0.06624	0.00632	0.0619 <sup>a</sup>
Tb.Sp	Trabecular separation	mm	0.2140	0.0257	0.2005	0.0292	0.2295 <sup>a</sup>
Tb.Po	Total volume of trabecular pores	mm <sup>3</sup>	1.7320	0.1008	1.5510	0.1443	<b>0.0007<sup>a</sup></b>

Mean and standard deviations (SD) are reported for *Fmr1*-WT and KO animals, as well as p-value for the Student's *T*-test (<sup>a</sup>) or the Mann & Whitney *U*-test (<sup>b</sup>). Significant p-values ( $p < 0.05$ ) are bolded.  $n = 12$ – $15$  animals/group.

are reported in **Tables 1, 2**. Representative cortical and trabecular ROI from one *Fmr1*-WT and one *Fmr1*-KO animal were obtained by further processing of the 3D reconstructed segments using the ImageJ plugin 3D viewer and the BoneJ plugin (22).

## Locomotor Activity Recordings

Gross locomotor activity was determined in an open field arena. Animals were placed in a brightly illuminated arena (200 Lux) and their movements were recorded for 10 min. An automated tracking system (Anymaze) was used to determine total distance moved, rotations number and number of center entries. The measurement of individual spontaneous activity was made using actimetry chambers (Imetronic) consisting of cages equipped with infrared beams able to detect in real time horizontal and vertical movements (rearings). Animals were individually placed in actimetry chambers under a 12-h light/dark cycle, with free access to food and drinking water. To avoid biases in measurements due to stress possibly inducing hyperlocomotion in a novel environment, an habituation period (Day 0: 11:00 p.m. to Day 1: 8:00 a.m.) preceded the 24 h-recording of horizontal and vertical activity (Day 1: 8:00 a.m. to Day 2: 8:00 a.m.).

## Statistics

Normality of data was assessed using Kolmogorov-Smirnov's test and outliers removed using the robust regression and outlier removal (ROUT) method (24). To compare 2 groups, 2-tailed unpaired Student's *T*-test was used. For non-normal data, raw data were log-transformed to meet normality criteria prior

to Student's *T*-test. If normality was not reached after log-transformation, data were analyzed using Mann & Whitney's non-parametrical *U*-test. Multiple group comparisons were performed using 2-way ANOVA, followed by *post-hoc* tests as indicated in figures legends. Statistical significance was set according to a two-tailed *p*-value ( $p < 0.05$ ). Statistical analysis was performed using GraphPad Prism version 6.00 for iOS (GraphPad Software, USA).

## RESULTS

### *Fmr1*-Deficiency Impacts Skeleton and Body Mass Distribution

We assessed several basic parameters in 4-months old *Fmr1*-KO and WT male littermates (**Figure 1**). *Fmr1*-KO mice display a significant increase in total body weight as compared to WT (**Figure 1A**). Furthermore, we weighed *Tibialis anterior* muscle and epididymal fat depots and showed that muscle weight was significantly increased in *Fmr1*-KO mice, to the expense of visceral adipose tissue that was reduced (**Figures 1B,C**). In contrast, subcutaneous or BAT weights were similar in *Fmr1*-WT and KO animals (**Supplementary Figure 1**). This agreed with the reduction of visceral adipose tissue volume and lack of variation in subcutaneous adipose tissue volume observed in a previous study in *Fmr1*-KO animals (11).

To precisely study the skeleton, we measured a number of skeletal parameters on 3D reconstructions of skeleton from micro-computerized X-ray tomography data (**Figure 1D**). We

found that *Fmr1*-deficiency is accompanied by a significant increase in total mouse length, as well as in skeletal volume (Figures 1E,F). Femur maximal length and L3-L6 vertebral length, which are reliable indicators of general skeleton length, were also both significantly increased in *Fmr1*-deficient animals (Figures 1G,H).

Finally, the ratios: muscle weight/body weight, femur length/body length, L4-L6 length/body length were not significantly different between *Fmr1*-KO and WT animals (Supplementary Table 1), indicating that *Fmr1*-KO animals exhibited similar proportions to WT animals.

## *Fmr1*-Deficiency Determines Changes in Bone Microstructure

To further resolve the microstructure of bone in *Fmr1*-WT and KO mice, we analyzed BMD and structure of femurs at the level of the mid-shaft cortical bone, using high resolution micro-computerized X-ray tomography (Figure 2A, Table 1). Volumetric BMD measured in the mid-shaft was not significantly affected by *Fmr1*-deficiency (Table 1, Figure 2B). We did not observe changes in the mean total cross-sectional object area, the mean object area per slice or the mean cortical area fraction (Table 1).

Qualitative analysis of transversal sections of mid-shaft cortical bone showed that *Fmr1*-deficiency impact the cortical pattern and skews toward higher ranges the cortical thickness distribution (Figure 2C). Quantitative analysis over a 400  $\mu$ m mid-shaft block revealed that *Fmr1*-KO mice exhibit a significant increase in average cortical thickness as compared to WT (Table 1, Figure 2D). Furthermore, the mean polar MMI, an estimator of bone strength was not significantly impacted in *Fmr1*-KO mice (Table 1).

We also assessed cortical eccentricity, a measure of bone cross-sectional geometry, which is known to influence biomechanical response of the bone during habitual loading. Cortical eccentricity appeared significantly shifted toward lower values in *Fmr1*-KO femurs (Table 1, Figure 2E). This is indicative of a rounder shape of the bone at the mid-shaft level in *Fmr1*-KO animals as compared to WT.

We then studied bone trabecular microstructure by analyzing transversal sections of a 900  $\mu$ m segment located in the distal femoral metaphysis (Figure 3A). *Fmr1*-KO mice displayed a significant increase in the bone volume fraction as compared to WT littermates (Table 2, Figure 3B). The average trabecular numbers, average trabecular separation, and average trabecular thickness were not significantly impacted by *Fmr1*-deficiency (Table 2). However, when looking in closer details at the trabecular thickness distributions over the 900  $\mu$ m segment, we observed that *Fmr1*-deficiency significantly shifted to higher ranges the trabecular thickness (Figure 3C), and this shift was significant (Figure 3D). Furthermore, the total volume of trabecular pores was significantly decreased in *Fmr1*-KO animals (Table 2), in line with the increase in bone volume fraction.

Finally, we measured circulating osteocalcin, a bone-hormone exclusively secreted by osteoblasts with roles in bone formation, metabolism, and adaptation to exercise (25). In *Fmr1*-KO

animals, serum osteocalcin levels were similar to *Fmr1*-WT levels (Supplementary Figure 2).

## *Fmr1*-Deficiency Leads to Increased Physical Activity in Mouse

Physical activity is a strong contributor to adaptations in bone architecture (26) and the changes we observed in *Fmr1*-KO mouse in terms of body composition and bone microstructure recapitulate the ones observed in mice subjected to exercise (27). We therefore monitored the impact of *Fmr1*-deficiency on spontaneous locomotor activity. In the open field test, *Fmr1*-KO mice were significantly more active than WT littermates in total distance traveled (Figure 4A), number of rotations (Figure 4B) and showed a higher number of center entries (Figure 4C). As open-field recordings are performed over a short period of time (10 min.), we then monitored continuous locomotor activity in *Fmr1*-KO and WT littermates in actimetry chambers over 24 h in a standard dark-light cycle. Independently of genotypes, horizontal (Figures 4D,E) and vertical activities (rearings, Figures 4F,G) display a characteristic nycthemeral rhythm, with two nocturnal peaks and reduced movements during the light phase. There was a significant effect of genotype over time on horizontal activity (Figure 4D). Cumulative horizontal activity was significantly increased in the nocturnal phase for *Fmr1*-KO animals as compared to their WT littermates (Figure 4E). Similarly, there was a significant effect of genotype over time on vertical activity (Figure 4F). Cumulative vertical activity was significantly increased in the nocturnal phase for *Fmr1*-KO animals as compared to their WT littermates (Figure 4G). These results indicate that *Fmr1*-deficient mice display a sustained hyperactivity as compared to wildtype mice.

## DISCUSSION

In the present study, we show that *Fmr1*-deficiency in mice, as a model of FXS pathology, translates into increased body weight, skeleton length, and volume. Some studies report a general overgrowth in boys affected by FXS (13, 15) and increased stature and height (14), which is in line with our observations in *Fmr1*-KO mice. In *Fmr1*-KO mice, overweight and overgrowth are accompanied by an increase in muscular mass and a reduction of intra-abdominal adiposity. The later result corroborates our previous observations of reduced WAT, decreased circulating leptin and increased lipid catabolism in *Fmr1*-KO mice (11) and previous findings of reduced lipid storage in FXS *Drosophila* model (28). This suggests that *Fmr1*-deficiency provokes fat mass redistribution impacting visceral WAT and sparing subcutaneous WAT and BAT. Whole-body energy expenditure, that is critically regulated by BAT, was also not impacted by *Fmr1*-deficiency, as we have previously shown using indirect calorimetry (11). Also, body temperature of *Fmr1*-KO mice was similar to WT (Leboucher & Davidovic, unpublished observations). All these data confirm the lack of overt phenotype related to BAT in *Fmr1*-KO animals and suggest that this tissue is unlikely involved in the described phenotypes. No epidemiological study on the FXS population is available to-date regarding the adiposity in typical

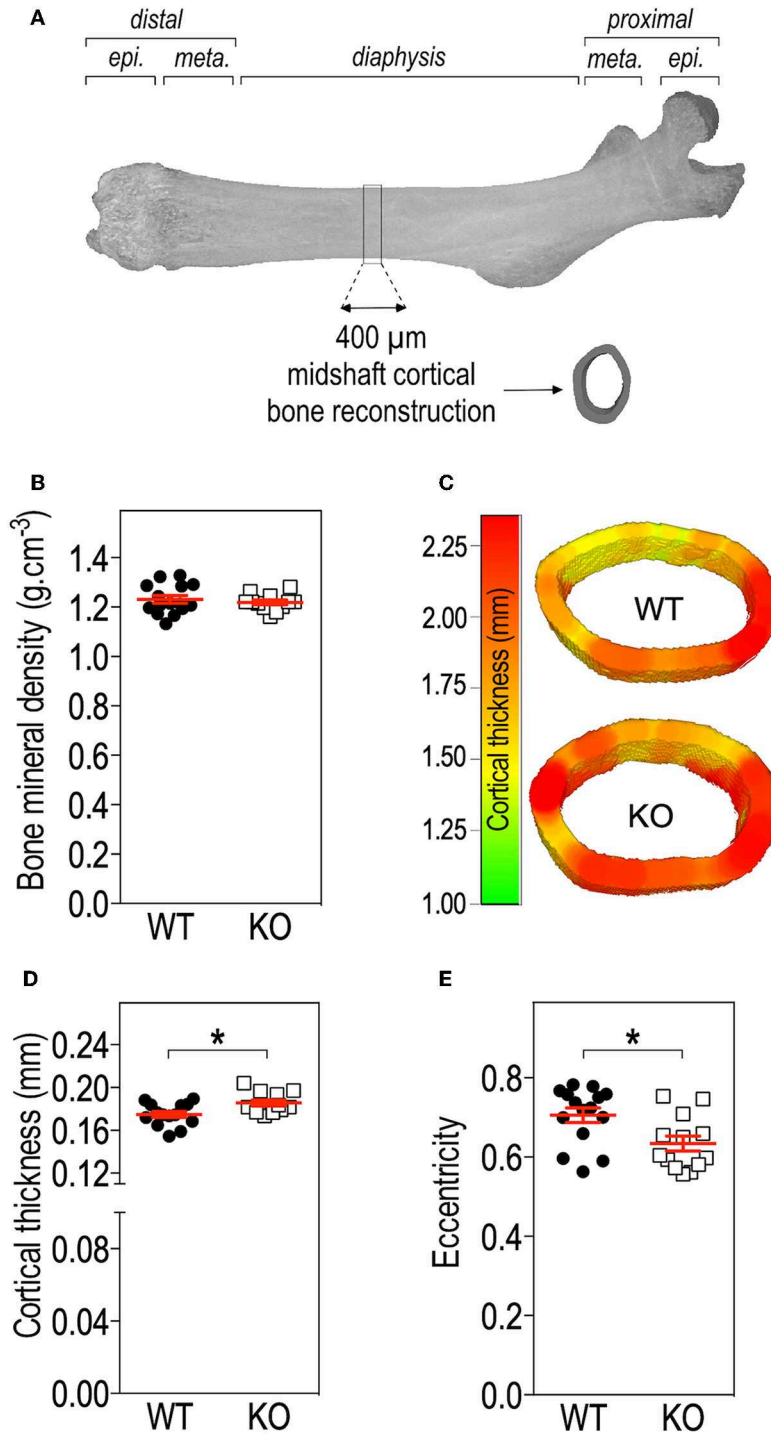
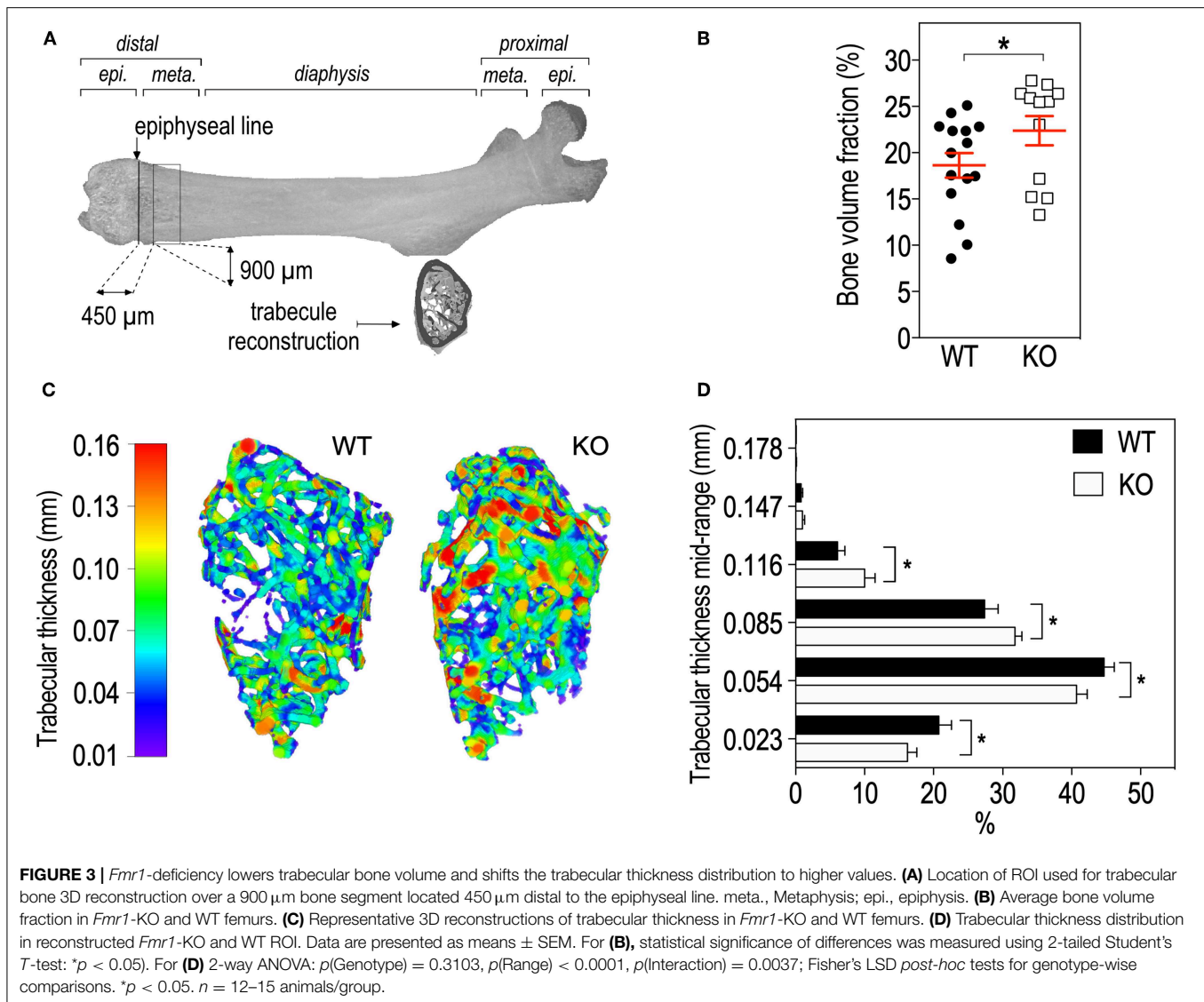


**FIGURE 2** | *Fmr1*-deficiency does not impact bone mineral density (BMD) but modifies cortical bone architecture. **(A)** Location of ROI used for mid-shaft cortical bone 3D reconstruction of a 400  $\mu\text{m}$  diaphysis section. meta., metaphysis; epi., epiphysis. **(B)** Bone mineral density. **(C)** Representative 3D reconstructions of cortical thickness in *Fmr1*-KO and WT femurs. Average cortical thickness **(D)** and cortical bone eccentricity **(E)** in *Fmr1*-KO and WT 4 months-old male animals. For **(B,D,E)**, data are presented as dot-plots featuring means  $\pm$  SEM in red. Statistical significance of differences was measured using 2-tailed Student's *T*-test **(D)** or Mann & Whitney *U*-test **(E)**. \* $p < 0.05$ .  $n = 12$ –15 animals/group.



FXS patients. The reduced adiposity we observed in *Fmr1*-KO mice could at first sight be contradictory with the reports of hyperphagia and obesity in a rare subset of Fragile X patients displaying Prader Willi-like (PWL) phenotypes (29). However, these traits are not observed in typical FXS patients (11, 13, 30). Our results warrant further clinical studies to characterize body composition in FXS patients.

When looking closer at bone microstructure parameters, we observed that BMD was not significantly affected by *Fmr1*-deficiency, indicating that the bone mineralization process is unlikely affected in *Fmr1*-KO animals. However, bone architecture of *Fmr1*-KO mice is impacted, with decreased volume of trabecular pore, increased trabecular bone volume fraction and a shift toward higher trabecular thickness ranges, accompanied by increased cortical thickness, and eccentricity. The changes in bone microstructure which we highlight in *Fmr1*-KO animals resemble the ones observed in humans (31) or animals (27) subjected to long-term physical exercise. Indeed,

physical activity is not only a strong contributor to adaptations in bone architecture but it also provokes body mass redistribution, notably a decrease in fat mass and an increase in the lean mass (26), which is what we observe in *Fmr1*-KO mice as compared to control mice. Also, the changes in shape of the proximal femur with an increased eccentricity could reflect the changing loading pattern during growth due to increased physical activity. Indeed, changes in bone morphology and strength can be enhanced through functional loading as shown in human studies (32, 33). As bone architecture reflects the history load originating both from muscle contractions as well as from the effect of gravity, the increased cortical thickness and the shift toward higher trabecular thickness in *Fmr1*-KO animals could correspond to a functional adaptation to the mechanical stress induced by increased physical activity and body weight. We therefore hypothesize that the increased physical activity observed in *Fmr1*-KO mice could indirectly participate to changes in body composition. Importantly, physical activity

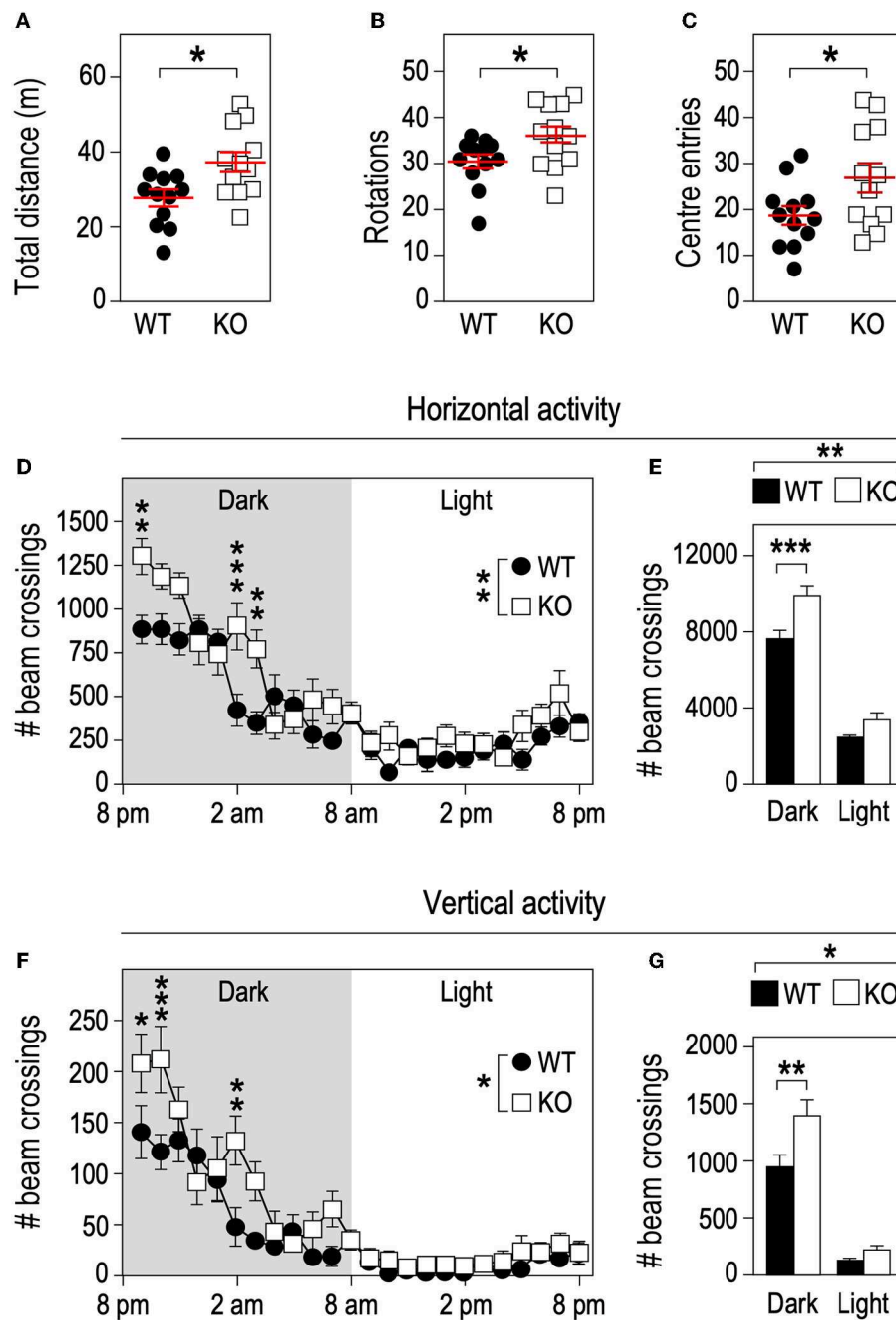


**FIGURE 4 |** *Fmr1*-deficiency increases locomotor activity. *Fmr1*-KO and WT adult male littermates were monitored for 10 min in an open-field arena and total distance traveled (**A**), number of rotations (**B**), and center entries (**C**) were calculated. Horizontal activity measured in actimetry chambers over 24 h (**D**) and corresponding histograms of cumulative activity in dark/light phases (**E**). Vertical activity measured in actimetry chambers over 24 h (**F**) and corresponding histograms of cumulative activity in dark/light phases (**G**).  $n = 12$  animals/group. For (**A–C**), data are presented as dot-plots featuring means  $\pm$  SEM. Statistical significance of differences was measured using 2-tailed Student's *T*-tests. \* $p < 0.05$ . For (**D–G**), data are presented as means  $\pm$  SEM. For (**D**) 2-way ANOVA:  $p(\text{Genotype}) = 0.0053$ ,  $p(\text{Time}) < 0.0001$ ,  $p(\text{Interaction}) = 0.0002$ ; Holm-Šidák's *post-hoc* tests for genotype-wise comparisons. \*\* $p < 0.01$ ; \*\*\* $p < 0.001$ . For (**E**) 2-way ANOVA:  $p(\text{Genotype}) = 0.0024$ ,  $p(\text{Phase}) < 0.0001$ ,  $p(\text{Interaction}) = 0.0599$ ; Holm-Šidák's *post-hoc* tests for genotype-wise comparisons. \*\* $p < 0.01$ ; \*\*\* $p < 0.0001$ . For (**F**) 2-way ANOVA:  $p(\text{Genotype}) = 0.0394$ ,  $p(\text{Phase}) < 0.0001$ ,  $p(\text{Interaction}) = 0.0006$ ; Holm-Šidák's *post-hoc* tests for genotype-wise comparisons. \* $p < 0.05$ , \*\* $p < 0.01$ ; \*\*\* $p < 0.001$ . For (**G**) 2-way ANOVA:  $p(\text{Genotype}) = 0.0348$ ,  $p(\text{Phase}) < 0.0001$ ,  $p(\text{Interaction}) = 0.042$ ; Holm-Šidák's *post-hoc* tests for genotype-wise comparisons. \* $p < 0.05$ , \*\* $p < 0.01$ .

behavior is mostly centrally regulated and thus could be a possible consequence of *Fmr1*-deficiency in the CNS. Increased daily locomotor activity alterations had been previously well-documented in *Drosophila* FXS model (34) and in younger 8 weeks-old male *Fmr1*-KO animals (35). Our results indicate that 4-months old *Fmr1*-deficient mice display a sustained increase in physical activity as compared to wildtype mice, suggesting that hyperactivity-related phenotypes are not transient and persist in adulthood. This agrees with attention deficits and hyperactivity disorder (ADHD) being a frequent comorbidity diagnosed in FXS patients (13). Furthermore, physical activity is known to trigger beneficial metabolic changes, notably reduction in circulating triglycerides and cholesterol and better response to insulin, which are phenotypes we have recently described in the *Fmr1*-KO mice (11). All these data point toward important roles for *FMR1* gene at multiple levels in the organism: both central and peripheral.

FMRP, the protein encoded by the *FMR1* gene is a RNA-binding protein which controls mRNA translation. FMRP is widely expressed in the organism, including in adipose tissue, however, FMRP is absent from the adult muscle (8–12). It is therefore unlikely that FMRP will directly participate to muscle remodeling. In addition to increased physical activity, dysregulated translation regulation in bone tissue in the absence of FMRP could also participate to the skeletal and bone microstructure changes we observed here. Also, craniofacial abnormalities have been previously identified in both FXS patients and FXS mouse model (20), and this occurs independently of physical activity, suggesting that FMRP could have a direct role on bone formation/resorption processes. Further molecular studies would be required to identify FMRP mRNA targets in bone and its contribution to the shaping of bone microstructure.

Our study has some limitations. First, we have assessed bone phenotypes at a single age (4-month-old) and only in male animals. The stability of these phenotypes over time (during growth and aging) and the impact of sex should be further investigated. Circulating bone hormones, including osteocalcin levels, could also be assessed during growth. Second, detailed histo-morphometric studies of bone coupled to *in vitro* studies in osteoblasts and osteoclasts derived from *Fmr1*-KO and WT mice could contribute to identify the mechanism by which *Fmr1*-deficiency regulates bone morphology. Third, to estimate whether the changes in body composition are accompanied with improved physical capacities, *Fmr1*-KO mice could be subjected to forced exercise training in a treadmill combined with indirect calorimetry. Finally, further studies in FXS patients are warranted to assess the translationality of our findings in FXS mouse model. In this context, the use of Dual Energy X-Ray Absorptiometry (DEXA) technology, easily amenable both to mice, and humans to study visceral fat mass and lean body mass would enable an in-depth characterization of body mass distribution in FXS.

To our knowledge, this study is the first to document changes in body mass composition, skeleton, and bone architecture induced by *Fmr1*-deficiency in mice. These changes may result in part from adaptations to the hyperactivity and increased body weight that we highlight in *Fmr1*-KO mice or from the

loss of the translational regulator FMRP in bone or adipose tissue. We have previously shown that *Fmr1*-KO mice present a variety of metabolic changes, notably increased glucose, and insulin tolerance as well as a metabolic shift toward increased lipid catabolism, this being likely mediated by the loss of FMRP-mediated hepatic translation repression (11). To which extend these metabolic abnormalities could also be linked to increased physical activity remains to be investigated. Given that recent studies have shown that a dynamic crosstalk between peripheral organs is required for the optimal control of metabolic homeostasis (36, 37), our study further paves the way for further investigation of skeletal and metabolic changes in FXS patients.

## DATA AVAILABILITY STATEMENT

The datasets generated for this study are available on request to the corresponding author.

## ETHICS STATEMENT

All animal studies were conducted in facilities accredited by French legal authorities (Direction Départementale de Protection des Populations des Alpes-Maritimes, accreditation #C-06-152-5). Procedures involving animal experimentation were approved by the local animal experimentation ethics committee and the French Ministère de l'Enseignement Supérieur et de la Recherche (agreement #00788.01 and #05224.01).

## AUTHOR CONTRIBUTIONS

LD designed the project and wrote the manuscript. AL, PB-M, DP, and LD carried out the experiments. AL, DP, and LD analyzed the data. XM provided advices for tomography acquisition and 3D reconstruction. AL performed 2D analyses and 3D modelisation. E-ZA interpreted the tomography data. AL, PB-M, E-ZA, XM, and DP revised the manuscript.

## FUNDING

LD thanks the generous support of FRAXA Research Foundation and Agence Nationale de la Recherche (ANR JCJC SVE6 MetaboXFra). E-ZA acknowledges the support of the CNRS for this study.

## ACKNOWLEDGMENTS

We thank the IPMC animal facility for expert animal care, in particular N. Guy, V. Thieffin, and B. Donay. We are greatly indebted to MD Dr. Sattonet (Polyclinique Saint-Jean, Cagnes-sur-Mer) for providing access to the high energy  $\mu$ CT Skyscan and for helpful advices for its use.

## SUPPLEMENTARY MATERIAL

The Supplementary Material for this article can be found online at: <https://www.frontiersin.org/articles/10.3389/fendo.2019.00678/full#supplementary-material>

## REFERENCES

- Chelly J, Khelifaoui M, Francis F, Cherif B, Bienvenu T. Genetics and pathophysiology of mental retardation. *Eur J Hum Genet.* (2006) 14:701–13. doi: 10.1038/sj.ejhg.5201595
- Gez J, Shoubridge C, Corbett M. The genetic landscape of intellectual disability arising from chromosome X. *Trends Genet.* (2009) 25:308–16. doi: 10.1016/j.tig.2009.05.002
- Hagerman PJ. The fragile X prevalence paradox. *J Med Genet.* (2008) 45:498–9. doi: 10.1136/jmg.2008.059055
- Oberle I, Rousseau F, Heitz D, Kretz C, Devys D, Hanauer A, et al. Instability of a 550-base pair DNA segment and abnormal methylation in fragile X syndrome. *Science.* (1991) 252:1097–102. doi: 10.1126/science.252.5009.1097
- Penagarikano O, Mulle JG, Warren ST. The pathophysiology of fragile X syndrome. *Annu Rev Genom Hum Genet.* (2007) 8:109–29. doi: 10.1146/annurev.genom.8.080706.092249
- Consortium FX TDB. Fmr1 knockout mice: a model to study fragile X mental retardation. *Cell.* (1994) 78:23–33. doi: 10.1016/0092-8674(94)90569-X
- Mientges EJ, Nieuwenhuizen I, Kirkpatrick L, Zu T, Hoogeveen-Westerveld M, Severijnen L, et al. The generation of a conditional Fmr1 knock out mouse model to study Fmrp function *in vivo*. *Neurobiol Dis.* (2006) 21:549–55. doi: 10.1016/j.nbd.2005.08.019
- Devys D, Lutz Y, Rouyer N, Bellocq JP, Mandel JL. The FMR-1 protein is cytoplasmic, most abundant in neurons and appears normal in carriers of a fragile X premutation. *Nat Genet.* (1993) 4:335–40. doi: 10.1038/ng0893-335
- Khandjian EW, Fortin A, Thibodeau A, Tremblay S, Cote F, Devys D, et al. A heterogeneous set of FMR1 proteins is widely distributed in mouse tissues and is modulated in cell culture. *Hum Mol Genet.* (1995) 4:783–9. doi: 10.1093/hmg/4.5.783
- Davidovic L, Tremblay S, Gravel M, De Koninck P, Khandjian EW. [The fragile X syndrome: one protein missing and 1001 disoriented mRNAs]. *Med Sci.* (2006) 22:41–6. doi: 10.1051/medsci/200622141
- Leboucher A, Pisani DF, Martinez-Gili L, Chilloux J, Bermudez-Martin P, Van Dijk A, et al. The translational regulator FMRP controls lipid and glucose metabolism in mice and humans. *Mol Metab.* (2019) 21:22–35. doi: 10.1016/j.molmet.2019.01.002
- Davidovic L, Sacconi S, Bechara EG, Delplace S, Allegra M, Desnuelle C, et al. Alteration of expression of muscle specific isoforms of the fragile X related protein 1. (FXR1P) in facioscapulohumeral muscular dystrophy patients. *J Med Genet.* (2008) 45:679–85. doi: 10.1136/jmg.2008.060541
- Kidd SA, Lachiewicz A, Barbooth D, Blitz RK, Delahunty C, McBrien D, et al. Fragile X syndrome: a review of associated medical problems. *Pediatrics.* (2014) 134:995–1005. doi: 10.1542/peds.2013-4301
- Butler MG, Pratesi R, Watson MS, Breg WR, Singh DN. Anthropometric and craniofacial patterns in mentally retarded males with emphasis on the fragile X syndrome. *Clin Genet.* (1993) 44:129–38. doi: 10.1111/j.1399-0004.1993.tb03863.x
- de Vries BB, Robinson H, Stolte-Dijkstra I, Tjon Pian Gi CV, Dijkstra PF, van Doorn J, et al. General overgrowth in the fragile X syndrome: variability in the phenotypic expression of the FMR1 gene mutation. *J Med Genet.* (1995) 32:764–9. doi: 10.1136/jmg.32.10.764
- Hagerman RJ, Van Housen K, Smith AC, McGavran L. Consideration of connective tissue dysfunction in the fragile X syndrome. *Am J Med Genet.* (1984) 17:111–21. doi: 10.1002/ajmg.1320170106
- Sabbagh-Haddad A, Haddad DS, Michel-Crosato E, Arita ES. Fragile X syndrome: panoramic radiographic evaluation of dental anomalies, dental mineralization stage, and mandibular angle. *J Appl Oral Sci.* (2016) 24:518–23. doi: 10.1590/1678-775720160170
- Davids JR, Hagerman RJ, Eilert RE. Orthopaedic aspects of fragile-X syndrome. *J Bone Joint Surg Am.* (1990) 72:889–96. doi: 10.2106/00004623-199072060-00015
- Butler MG, Fletcher M, Gale DD, Meaney FJ, McLeod DR, Fagan J, et al. Metacarpophalangeal pattern profile analysis in fragile X syndrome. *Am J Med Genet.* (1988) 31:767–73. doi: 10.1002/ajmg.1320310406
- Heulens I, Suttie M, Postnov A, De Clerck N, Perrotta CS, Mattina T, et al. Craniofacial characteristics of fragile X syndrome in mouse and man. *Eur J Hum Genet.* (2013) 21:816–23. doi: 10.1038/ejhg.2012.265
- Beranger GE, Pisani DF, Castel J, Djedaini M, Battaglia S, Amiaud J, et al. Oxytocin reverses ovariectomy-induced osteopenia and body fat gain. *Endocrinology.* (2014) 155:1340–52. doi: 10.1210/en.2013-1688
- Doube M, Klosowski MM, Arganda-Carreras I, Cordelieres FP, Dougherty RP, Jackson JS, et al. BoneJ: free and extensible bone image analysis in ImageJ. *Bone.* (2010) 47:1076–9. doi: 10.1016/j.bone.2010.08.023
- Bouxsein ML, Boyd SK, Christiansen BA, Guldberg RE, Jepsen KJ, Müller R. Guidelines for assessment of bone microstructure in rodents using micro-computed tomography. *J Bone Miner Res.* (2010) 25:1468–86. doi: 10.1002/jbmr.141
- Motulsky HJ, Brown RE. Detecting outliers when fitting data with nonlinear regression - a new method based on robust nonlinear regression and the false discovery rate. *BMC Bioinform.* (2006) 7:123. doi: 10.1186/1471-2105-7-123
- Moser SC, van der Eerden BCJ. Osteocalcin-A versatile bone-derived hormone. *Front Endocrinol.* (2018) 9:794. doi: 10.3389/fendo.2018.00794
- Thompson D, Karpe F, Lafontan M, Frayn K. Physical activity and exercise in the regulation of human adipose tissue physiology. *Physiol Rev.* (2012) 92:157–91. doi: 10.1152/physrev.00012.2011
- Dominguez JM II, Prisyb RD, Muller-Delp JM, Allen MR, Delp MD. Increased nitric oxide-mediated vasodilation of bone resistance arteries is associated with increased trabecular bone volume after endurance training in rats. *Bone.* (2010) 46:813–9. doi: 10.1016/j.bone.2009.10.029
- Weisz ED, Towheed A, Monyak RE, Toth MS, Wallace DC, Jongens TA. Loss of Drosophila FMRP leads to alterations in energy metabolism and mitochondrial function. *Hum Mol Genet.* (2018) 27:95–106. doi: 10.1093/hmg/ddx387
- Nowicki ST, Tassone F, Ono MY, Ferranti J, Croquette MF, Goodlin-Jones B, et al. The prader-Willi phenotype of fragile X syndrome. *J Dev Behav Pediatr.* (2007) 28:133–8. doi: 10.1097/01.DBP.0000267563.18952.c9
- Hagerman RJ, Berry-Kravis E, Hazlett HC, Bailey DB Jr, Moine H, Kooy RF, et al. Fragile X syndrome. *Nat Rev Dis Primers.* (2017) 3:17065. doi: 10.1038/nrdp.2017.66
- Best A, Holt B, Troy L, Hamill J. Trabecular bone in the calcaneus of runners. *PLoS ONE.* (2017) 12:e0188200. doi: 10.1371/journal.pone.0188200
- Sugiyama T, Price JS, Lanyon LE. Functional adaptation to mechanical loading in both cortical and cancellous bone is controlled locally and is confined to the loaded bones. *Bone.* (2010) 46:314–21. doi: 10.1016/j.bone.2009.08.054
- Travison TG, Araujo AB, Esche GR, Beck TJ, McKinlay JB. Lean mass and not fat mass is associated with male proximal femur strength. *J Bone Miner Res.* (2008) 23:189–98. doi: 10.1359/jbmr.071016
- McBride SM, Bell AJ, Jongens TA. Behavior in a drosophila model of fragile X. *Results Probl Cell Differ.* (2012) 54:83–117. doi: 10.1007/978-3-642-21649-7\_6
- Gaudissard J, Ginger M, Premoli M, Memo M, Frick A, Pietropaolo S. Behavioral abnormalities in the Fmr1-KO2 mouse model of fragile X syndrome: the relevance of early life phases. *Autism Res.* (2017) 10:1584–96. doi: 10.1002/aur.1814
- Wei J, Ferron M, Clarke CJ, Hannun YA, Jiang H, Blaner WS, et al. Bone-specific insulin resistance disrupts whole-body glucose homeostasis via decreased osteocalcin activation. *J Clin Invest.* (2014) 124:1–13. doi: 10.1172/JCI72323
- Karsenty G, Mera P. Molecular bases of the crosstalk between bone and muscle. *Bone.* (2018) 115:43–9. doi: 10.1016/j.bone.2017.04.006

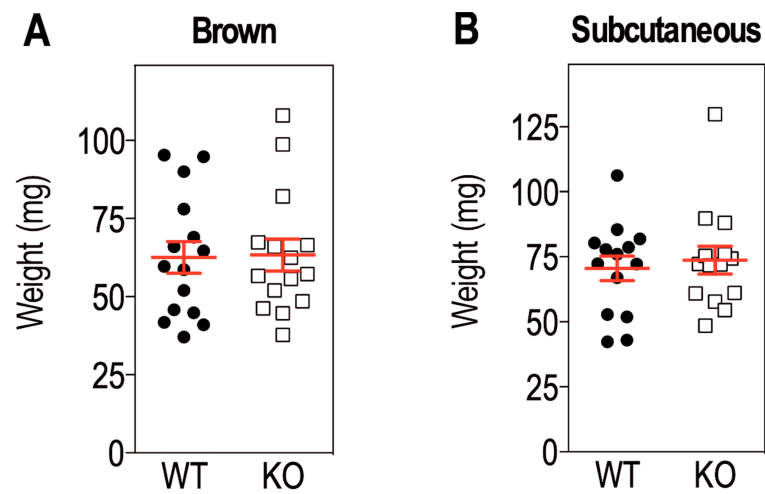
**Conflict of Interest:** The authors declare that the research was conducted in the absence of any commercial or financial relationships that could be construed as a potential conflict of interest.

Copyright © 2019 Leboucher, Bermudez-Martin, Mouska, Amri, Pisani and Davidovic. This is an open-access article distributed under the terms of the Creative Commons Attribution License (CC BY). The use, distribution or reproduction in other forums is permitted, provided the original author(s) and the copyright owner(s) are credited and that the original publication in this journal is cited, in accordance with accepted academic practice. No use, distribution or reproduction is permitted which does not comply with these terms.

## *Supplementary Material*

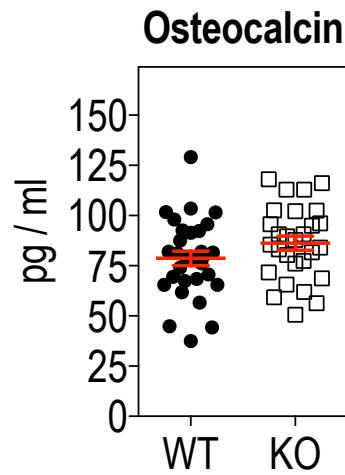
**Supplementary Table 1. Comparison analysis of ratios relative to body mass distribution and skeleton in *Fmr1*-KO and WT littermates (Relative to Figure 1).** For calculations, *Tibialis anterior* and adipose tissue weights were in mg and body weight in g. All lengths were in mm. Mean and standard deviations (SD) are reported for *Fmr1*-WT and KO animals, as well as p-value for the Student's T-test. n=15-18 animals/group.

<b>Ratio</b>	<b>Mean WT</b>	<b>SD WT</b>	<b>Mean KO</b>	<b>SD KO</b>	<b>p-value</b>
<i>Tibialis anterior</i> weight / Body weight	1.800	0.198	1.854	0.225	0.4858
Femur length / Skeleton length	0.188	0.005	0.188	0.004	0.7664
L3-L6 length / Skeleton length	0.147	0.003	0.149	0.003	0.0780



**Supplementary Figure 1. *Fmr1*-deficiency does not impact brown or subcutaneous white adipose tissue weight (relative to Figure 1).**

Weight of interscapular brown adipose tissue (*A*) and subcutaneous white adipose tissues (*B*) in 4 months-old *Fmr1*-WT and KO mice. Data are presented as dot-plots featuring means  $\pm$  SEM in red. Student T-test p-value: 0.912 (*A*), 0.637 (*B*). n=13-15 animals/group.



**Supplementary Figure 2. *Fmr1*-deficiency does not impact the levels of circulating osteocalcin.**

Serum levels of osteocalcin in 4 months-old *Fmr1*-WT and KO mice. Data are presented as dot-plots featuring means  $\pm$  SEM in red. Student T-test p-value: 0.134. n=28-30 animals/group.

# Immune Anomalies in FXS: Publication #3

## A. Research Hypothesis and Objectives of the Study

Previous studies suggested that FXS patients could present immune anomalies (Ashwood et al., 2010; Careaga et al., 2014). In this study, our working hypothesis was that immune dysfunction in FXS patients would translate into altered levels of circulating immune biomarkers measured in the serum.

To test this hypothesis, we relied on serum samples from FXS and healthy patients and our objectives were:

1. To investigate the profiles of immune biomarkers in the serum of FXS patients and controls
2. To identify an immune signature associated with FXS

To achieve these objectives, we assessed the levels of 52 circulating markers (cytokines, chemokines, growth factors) in the serum of n=25 FXS patients and n=29 age- and sex-matched healthy individuals. We then used univariate and multivariate statistics as well as clustering analysis to model the ability of immune biomarkers to separate FXS patients from controls based on their immune profile.

My contribution to this article was the measurement of several cytokines and chemokines using an electrochemiluminescence-based immunoassay in serum samples from FXS patients and controls.

## B. Results

The results of this study are presented in the following publication:

*Publication #3:*

Van Dijck A, Barbosa S, **Bermudez-Martin P**, Khalfallah O, Gilet C, Martinuzzi E, Elinck E, Kooy RF, Glaichenhaus N, Davidovic L (2020) Reduced serum levels of pro-inflammatory chemokines in Fragile X Syndrome. *BMC Neurology*. 15;20(1):138.

To summarise, in this study, we have shown that FXS patients exhibited decreased levels of nine chemokines, which are important immune mediators. These alterations could contribute to immune impairments in FXS patients, but this remains to be investigated. This study allowed the identification of biomarkers that may be biologically relevant to Fragile X Syndrome.

## C. Manuscript

RESEARCH ARTICLE

Open Access

# Reduced serum levels of pro-inflammatory chemokines in fragile X syndrome



Anke Van Dijck<sup>1†</sup>, Susana Barbosa<sup>2†</sup>, Patricia Bermudez-Martin<sup>2</sup>, Olfa Khalfallah<sup>2</sup>, Cyprien Gilet<sup>3</sup>, Emanuela Martinuzzi<sup>2</sup>, Ellen Elinck<sup>1</sup>, R. Frank Kooy<sup>1</sup>, Nicolas Glaichenhaus<sup>2</sup> and Laetitia Davidovic<sup>2\*</sup>

## Abstract

**Background:** Fragile X syndrome (FXS) is the most frequent cause of inherited intellectual disability and the most commonly identified monogenic cause of autism. Recent studies have shown that long-term pathological consequences of FXS are not solely confined to the central nervous system (CNS) but rather extend to other physiological dysfunctions in peripheral organs. To gain insights into possible immune dysfunctions in FXS, we profiled a large panel of immune-related biomarkers in the serum of FXS patients and healthy controls.

**Methods:** We have used a sensitive and robust Electro Chemi Luminescence (ECL)-based immunoassay to measure the levels of 52 cytokines in the serum of  $n = 25$  FXS patients and  $n = 29$  healthy controls. We then used univariate statistics and multivariate analysis, as well as an advanced unsupervised clustering method, to identify combinations of immune-related biomarkers that could discriminate FXS patients from healthy individuals.

**Results:** While the majority of the tested cytokines were present at similar levels in FXS patients and healthy individuals, nine chemokines, CCL2, CCL3, CCL4, CCL11, CCL13, CCL17, CCL22, CCL26 and CXCL10, were present at much lower levels in FXS patients. Using robust regression, we show that six of these biomarkers (CCL2, CCL3, CCL11, CCL22, CCL26 and CXCL10) were negatively associated with FXS diagnosis. Finally, applying the K-sparse unsupervised clustering method to the biomarker dataset allowed for the identification of two subsets of individuals, which essentially matched the FXS and healthy control categories.

**Conclusions:** Our data show that FXS patients exhibit reduced serum levels of several chemokines and may therefore exhibit impaired immune responses. The present study also highlights the power of unsupervised clustering methods to identify combinations of biomarkers for diagnosis and prognosis in medicine.

**Keywords:** Fragile X syndrome, Cytokines, Chemokines, Biomarkers, Clustering, Autism spectrum disorders, Intellectual disability

## Background

Fragile X syndrome (FXS) is the most frequent cause of inherited intellectual disability (ID) and the most commonly identified monogenic cause of autism spectrum disorders (ASD) [1, 2]. This X-linked genetic disease is caused by the silencing of the Fragile X Mental Retardation 1

(*FMR1*) gene positioned in Xq27.3 [3]. FXS is more prevalent in males (1.4:1000) than in females (0.9/10,000) and females tend to display milder impairments [4]. In FXS patients, a dynamic mutation abnormally increases the number of CGG repeats in the first exon of the *FMR1* gene, above the premutation threshold of 200 repeats, leading to their hypermethylation and the subsequent absence of its gene product FMRP, an RNA-binding protein controlling translation [5, 6]. Although a monogenic disorder, FXS is a disease of complex aetiology. FXS prominent phenotypes

\* Correspondence: davidovic@ipmc.cnrs.fr

<sup>†</sup>Anke Van Dijck and Susana Barbosa contributed equally to this work.

<sup>2</sup>Université Côte d'Azur, CNRS, Institut de Pharmacologie Moléculaire et Cellulaire, Valbonne, France

Full list of author information is available at the end of the article



© The Author(s). 2020 **Open Access** This article is licensed under a Creative Commons Attribution 4.0 International License, which permits use, sharing, adaptation, distribution and reproduction in any medium or format, as long as you give appropriate credit to the original author(s) and the source, provide a link to the Creative Commons licence, and indicate if changes were made. The images or other third party material in this article are included in the article's Creative Commons licence, unless indicated otherwise in a credit line to the material. If material is not included in the article's Creative Commons licence and your intended use is not permitted by statutory regulation or exceeds the permitted use, you will need to obtain permission directly from the copyright holder. To view a copy of this licence, visit <http://creativecommons.org/licenses/by/4.0/>. The Creative Commons Public Domain Dedication waiver (<http://creativecommons.org/publicdomain/zero/1.0/>) applies to the data made available in this article, unless otherwise stated in a credit line to the data.

notably include intellectual disability, epilepsy, anxiety linked to sensory hyperarousal, attention deficits and hyperactivity disorder [7]. Furthermore, stereotypies and social interaction deficits lead to ASD diagnosis in 60% of boys and 25% of girls with FXS [8]. FXS is also accompanied by physical and anatomical abnormalities (macroorchidism, elongated face, hyperextensible finger joints) and recurrent health problems such as gastro-intestinal dysfunctions [7, 9]. Recurrent media otitis are frequent in FXS patients (52.6% versus 12.6% in neurotypical controls), as well sinusitis, although the incidence of other types of infections is not different in FXS patients [9, 10]. This suggests that the long-term pathological consequences of this neurodevelopmental disorder are not solely confined to the central nervous system and could extend to other physiological dysfunctions in peripheral systems.

To study possible peripheral consequences of *FMRI*-deficiency, some authors have compared the levels of serum and plasma biomarkers between FXS patients and healthy controls. Prior studies have focused on metabolic markers and have highlighted reduced levels of cholesterol [11–13] and abnormal abundances of the metabolic hormones leptin and adiponectin [14]. In a translational study addressing metabolic consequences of *FMRI*-deficiency both in a FXS mouse model and in FXS patients, we have recently shown that FXS patients display reductions in circulating glucose and increases in both free fatty acids and insulin, underlining metabolic anomalies in FXS [15]. Regarding possible immune dysfunctions in FXS, only a few studies have characterized FXS patients for immune biomarkers such as cytokines. These small circulating molecules are secreted by both immune and non-immune cell types and include notably interleukins (IL), chemokines, interferons (IFN) and members of the Tumour Necrosis Factor (TNF) family. Cytokines regulate the differentiation, activation and effector function of all immune cell types [16]. While inflammatory chemokines attract immune cells to inflammatory sites, homeostatic chemokines control cell migration during development. To our knowledge, only two studies have investigated possible immune dysfunction in FXS patients. In a first study, Ashwood et al. have assessed plasma samples from FXS male patients ( $n = 40$  FXS with ASD;  $n = 64$  FXS without ASD) and typically developing controls ( $n = 19$ ) for the levels of 22 cytokines. Compared to healthy controls, the authors found that FXS patients exhibited higher plasma levels of the pro-inflammatory cytokine IL-1 $\alpha$  and IL-12p40, and lower levels of the chemokines CCL2, CCL5, CCL11 and CXCL10 [17]. In a second study, Careaga et al. compared peripheral blood mononuclear cells (PBMC) from FXS children ( $n = 27$ ) and healthy age-matched individuals ( $n = 8$ ) for their ability to secrete pro-inflammatory

cytokines in response to lipopolysaccharides (LPS) and Phytohemagglutinin (PHA) [18]. While the basal immune responsiveness of PBMC to LPS and PHA was not impacted, PBMC from FXS patients secreted higher levels of the pro-inflammatory cytokines IL-6 and IL-12p40 compared to those from healthy controls in the presence of the group I mGluR agonist DHPG. Taken together, these two studies suggested that FXS patients may exhibit immune dysfunction. To further investigate this issue, we have used a highly sensitive and robust multiplex immunoassay to assess serum samples from FXS patients ( $n = 25$ ) and age- and sex-matched controls ( $n = 29$ ) for the level of 52 immune-related biomarkers. We then analysed this dataset using both standard univariate statistical method, robust Elastic Net regression and an advanced unsupervised clustering method.

## Methods

### Study sample

This study entitled “Identification of Fragile X Syndrome soluble biomarkers” was approved by the medical ethics committee of the University of Antwerp in Belgium Protocol agreement #: B300201523589) and conducted in accordance with statutes and regulations regarding the protection of the right and welfare of human subjects’ participation in biomedical research (World Declaration of Helsinki). In a previous study which found significant alterations in circulating cytokine levels in FXS patients compared to healthy controls [17], the exact effect sizes were not indicated and we therefore could not use previous knowledge to compute power. We therefore conducted a power analysis to determine the sample size required to identify differences for a theoretical large effect size (Cohen’s  $\delta > 0.75$ ) with a power of 80% and an error rate set at 5%. Since we had no a priori knowledge regarding the normality of the to be obtained data, we computed the sample sizes under two comparison conditions and found that  $n = 26$  individuals/group would be required for Student’s T-test comparisons, while  $n = 30$ /group would be required for Mann & Whitney non-parametric comparisons between the two groups. Based on this, we aimed to recruit  $n = 30$  patients and  $n = 30$  matching controls, at the Centre for Medical Genetics of the University of Antwerp (Antwerp, Belgium), at which patients are regularly received for a yearly consultation.

As a result, 29 healthy subjects (24 males, 5 females) and 25 fragile X patients (20 males, 5 females) of matching ages and ethnicity were enrolled (Table 1). The absence/presence of the fragile X mutation was confirmed in all participants by an accredited laboratory, using a CGG-repeat PCR and Southern Blotting on DNA isolated from blood. Inclusion criteria were age 6–18 and a stable medication regimen for the previous 8 weeks. Out of the 54

**Table 1** Characteristics of FXS patients and healthy controls

ID	Sex	Age #	BMI (kg/m <sup>2</sup> )	Time of sampling
<b>Controls</b>				
C1	Male		17.4	15:10
C2	Female		16.9	13:40
C3	Male		16.9	13:44
C4	Male		17.9	16:57
C5	Male		14.4	11:10
C6	Male		20.1	07:40
C7	Male		19.4	10:28
C8	Female		18.9	14:05
C9	Female		19.9	13:55
C10	Male		18.0	10:40
C11	Male		21.4	16:20
C12	Male		23.5	14:45
C13	Male	Age range	22.1	13:40
C14	Female	of control	15.4	08:00
C15	Male	group:	21.4	07:15
C16	Male	5.7–19.3 yrs	25.2	07:15
C17	Male		22.4	07:40
C18	Male		14.6	17:00
C19	Male		16.4	17:38
C20	Male		20.2	17:20
C21	Male		22.2	17:26
C22	Male		15.4	16:45
C23	Male		16.4	17:05
C24	Male		14.8	16:00
C25	Male		13.9	16:10
C26	Female		18.9	15:40
C27	Male		13.8	12:53
C28	Male		17.1	06:45
C29	Male		19.6	07:45
<b>FXS Patients</b>				
X1	Male		16.3	15:45
X2	Male		18.1	12:10
X3	Male		16.3	16:20
X4	Male		23.7	11:00
X5	Male		16.9	15:20
X6	Male		21.2	12:00
X7	Male		16.4	09:00
X8	Male		16.7	14:00
X9	Male		15.9	11:45
X10	Male		13.0	19:30
X11	Male	Age range	14.1	11:30
X12*	Male	of FXS	15.0	11:50
X13	Female	group:	18.4	10:45

**Table 1** Characteristics of FXS patients and healthy controls (Continued)

ID	Sex	Age #	BMI (kg/m <sup>2</sup> )	Time of sampling
X14	Male	6.3–17.9 yrs	16.9	10:55
X15	Male		18.3	10:15
X16	Female		19.5	10:20
X17	Female		34.5	07:40
X18	Male		15.9	13:25
X19	Male		15.8	10:45
X20	Male		38.8	19:30
X21	Male		19.0	09:20
X22	Male		20.1	13:50
X23	Female		24.8	09:15
X24	Male		18.9	09:10
X25*	Female		20.3	10:30
Control	82.7%	12.0	18.0	13:55
FXS	80.0%	12.5	18.1	11:30
<i>p</i> -value	1	0.3769	0.8803	0.2527

For the sex variable, percentage of males in each group and *p*-value for Fisher's exact test are indicated. For the other variables, range or medians of each group and *p*-values for Mann & Whitney tests are indicated. Patients under treatment are labelled with \*. (#) To preserve anonymity, instead of individual ages, age ranges are specified for each group

subjects enrolled, 2 FXS patients were actually under Ritalin treatment (X12 and X25) and were advised not to take the drug on the day of sampling. The other subjects were not under any type of medication. Clinical examination and parental questionnaire confirmed that none of the enrolled subjects presented with a recent infection episode on the day of sampling. Exclusion criteria were: recent history of seizure, epilepsy, blackouts, clinically unstable medical disease, progressive CNS disease/disorder, history of psychiatric disorders, behavioural dysfunction to the point that subject cannot cooperate for testing and history of pathologies which could modify blood biochemistry. Written informed consent was obtained from each participant or his/her legal guardian before research participation. To avoid stress induced by fasting to Fragile X patients, individuals involved in the study were not advised to fast prior sampling. Blood was withdrawn in serum collection tubes (BD Vacutainer Serum Separator Tubes), incubated for at least 30 min at room temperature then centrifuged at 2000 rpm, 10 min, at room temperature. Serum was collected, aliquoted and immediately snapped-frozen in liquid nitrogen prior storage at  $-80^{\circ}\text{C}$  until use. Information regarding sex, age, body mass index (BMI) and time of blood sampling were also retrieved.

#### Biomarkers measurements

Serum samples were assessed for biomarker levels using the V-plex<sup>®</sup> kits for the Meso Scale Discovery (MSD)

analytical platform, according to manufacturer's instructions. We used the following kits: Human Cytokine 30-Plex, V-PLEX Plus Th17 Panel 1, Human Chemokine Panel 2 and Vascular Injury Panel 2 to measure immune-related biomarkers: CCL1, CCL2, CCL3, CCL4, CCL11, CCL13, CCL15, CCL17, CCL19, CCL20, CCL22, CCL26, CCL27, CXCL1, CXCL5, CXCL10, CXCL11, CXCL12, CX3CL1, GM-CSF, IFN- $\gamma$ , IL-1 $\alpha$ , IL-1 $\beta$ , IL-2, IL-4, IL-5, IL-6, IL-7, IL-8, IL-10, IL-12p40, IL-12p70, IL-13, IL-15, IL-16, IL-17A, IL-17B, IL-17E, IL-17A/F, IL-21, IL-22, IL-23, IL-27, IL-31, IL-33, TNF- $\alpha$ , TNF- $\beta$ , C-reactive protein (CRP), Macrophage Migration Inhibitory Factor (MIF), SAA, sICAM-1, sVCAM-1 and VEGF-A. All 54 samples (sera from  $n = 29$  controls and  $n = 25$  FXS patients) were systematically analysed on the same plate to limit measurements biases. The concentration of each marker was calculated using the MSD software. The 0 value was imputed for concentrations which appeared below the lower limit of detection as determined by the MSD software.

### Statistical analysis

The distribution of biomarkers levels appeared non-normal in both groups, even when log-transformation was applied. Therefore, comparison analyses were performed using the non-parametric Mann & Whitney U-test with Bonferroni's multiple test correction. Statistical significance was set according to a corrected  $p$ -value ( $p$ )  $< 0.05$ . Only significant differences are displayed on the graphs. We computed the  $r$  effect size statistic for the Mann–Whitney U-test, which corresponds to the  $Z$  value from the test divided by the total number of observations. Statistics of effect size for the Mann–Whitney U-test assesses the degree to which one group has data with higher ranks compared to the other group and unlike  $p$ -values, they are not affected by sample size.

Elastic Net logistic regression models were implemented with the aim of performing variable selection, leading to sparser final model, in agreement with previous recommendations [19]. To study the association between 9 dysregulated chemokines identified by univariate analysis (CCL2, CCL3, CCL4, CCL11, CCL13, CCL17, CCL22, CCL26 and CXCL10) and FXS diagnosis, adjusting for age, BMI and time of sampling, we used robust regression with 2000 subsampling steps. We used the recent R package *enetLTS*: Robust and Sparse Methods for High Dimensional Linear and Logistic Regression developed by Kurnaz et al. [20, 21]. As this method currently does not handle categorical variables such as sex, the analysis was also rerun on a reduced dataset consisting of male subjects only.

Correlations between cytokine pairs identified in the clustering analysis were computed using the Spearman's  $\rho$  correlation coefficient rank test with Benjamini & Hochberg's multiple test correction.

Statistical analyses were performed using R and graphs generated using GraphPad Prism version 6.00 for iOS (GraphPad Software, USA).

### Over-representation analysis

To generate the chemokine receptor interaction table (Additional file 1: Fig. S1), we used the InnateDB database [22], the expert-curated reference database in the IUPHAR/BPS Guide to Pharmacology [23] and a recent review of literature [16]. The webtool from the InnateDB database [22] was used to determine over-represented pathways within the set of 9 dysregulated chemokines.

### Clustering analysis

Clustering analysis was performed using K-sparse algorithm [24]. K-sparse clustering aims at identifying discriminated clusters, by transforming the space of the features' (biomarkers concentration) and removing the features which appear the less pertinent for the identification of clusters. As an input dataset, we enter the raw values of concentrations for each feature and each subject in the K-sparse algorithm. A pre-processing step is embedded in the K-sparse algorithm, which allows the automated normalization of the features to guarantee the convergence of the algorithm, as described in [24]. Then, for some initial labels  $Y$ , the first step of K-sparse computes a weighted projection matrix  $W$  which linearly combines the features such that most samples are projected close to the centroid of their associated cluster. The clustering computed by K-sparse therefore considers the possible presence of outliers or extreme values through the weighted linear combination of the selected features. A sparsity constraint on  $W$  allows removal of features which are not sufficiently relevant to discriminate these clusters according to the fixed labels  $Y$ . The second step aims to fix this optimized weighted matrix  $W$  and to minimize the Within Cluster Sum of Squares (WCSS) by running the  $k$ -means algorithm in the projected space. In other words, this second step aims to update the labels according to the previously weighted and combined features. By repeating these two alternating steps, K-sparse algorithm converges to a solution. Finally, the  $t$ -Distributed Stochastic Neighbour Embedding ( $t$ -SNE) method is used to render a graphical output of clustering. Complete code of the K-sparse algorithm will be made available upon request.

## Results

### Immune markers analysis

We have analysed serum samples of 25 FXS patients ( $n = 20$  males;  $n = 5$  females) and 29 healthy controls ( $n = 24$  males;  $n = 5$  females) (Table 1). The two groups did not differ in terms of sex proportions, age, BMI or time of sampling (Table 1). Fifty-two cytokines and

inflammation and tissue damage markers were quantified. Out of these biomarkers, 6 cytokines (IL-1 $\alpha$ , IL-1 $\beta$ , IL-2, IL-4, IL-5 and IL-13) were below the lower limit of detection in more than 20% of control samples (Additional file 2: Table S1) and were therefore not retained for downstream analysis. We then used univariate statistical methods to compare the levels of the remaining biomarkers in FXS patients and healthy controls. The majority of these biomarkers were present at similar levels in patients and controls (Additional file 3: Table S2). In contrast, 10 biomarkers were differentially expressed between FXS patients and controls ( $p$ -value < 0.05, Additional file 3: Table S2): CCL2, CCL3, CCL4, CCL11, CCL13, CCL17, CCL22,

CCL26, CXCL10 and IL-15. After multiple testing correction, only the 9 chemokines appeared significantly decreased in FXS patients, as compared to controls (adjusted  $p$ -value < 0.05, Additional file 3: Table S2, Fig. 1). Large effect sizes ( $0.5 < r$  coefficient < 0.8) were observed for all dysregulated chemokines except for CCL4 in which the effect size was medium ( $0.2 < r$  coefficient < 0.5) (Additional file 3: Table S2). The same 10 biomarkers were significantly dysregulated in the dataset reduced to male subjects ( $p$ -value < 0.05, Additional file 3: Table S2). After multiple testing correction, seven out of the 9 chemokines identified in the full dataset (CCL2, CCL11, CCL13, CCL17, CCL22, CCL26 and CXCL10) were also significantly reduced in FXS male

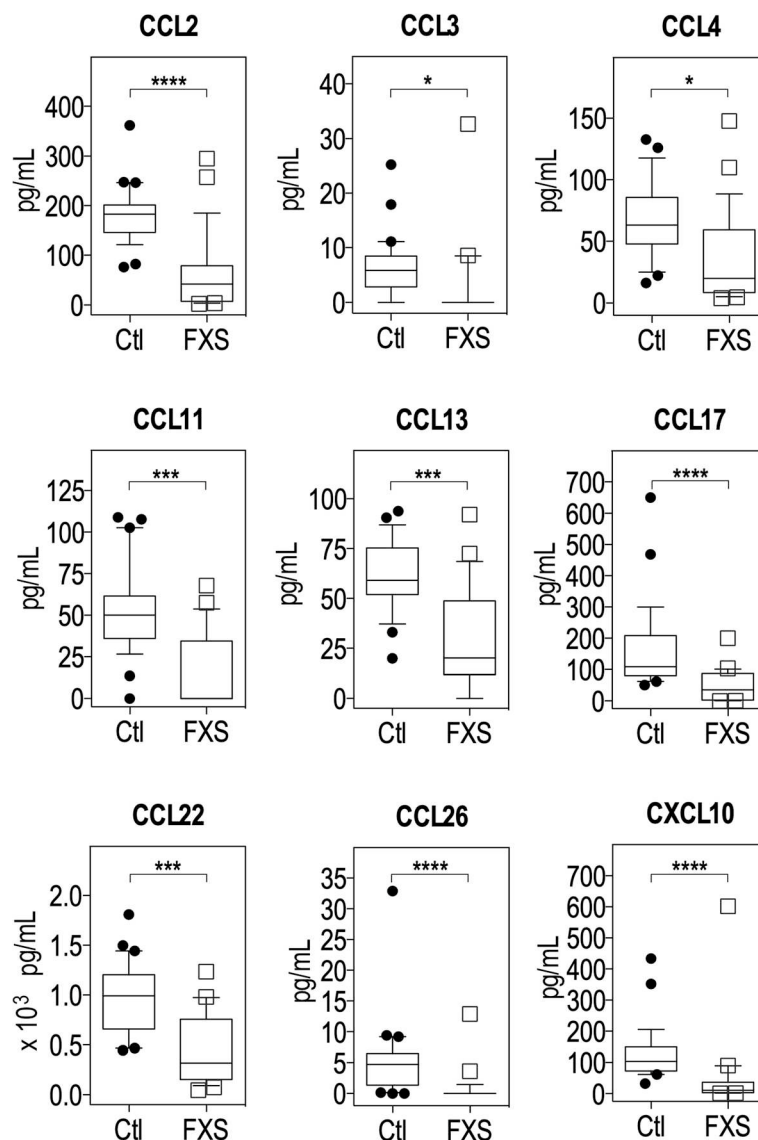


**Fig. 1** Levels of chemokines downregulated in FXS patients as compared to controls. Data are presented as a box-and-whiskers plot;  $n = 29$  controls,  $n = 25$  FXS patients. The box plots the first quartile, median and third quartile of the values. The whiskers are drawn down to the 10th percentile and up to the 90th. Points below and above the whiskers are drawn as individual dots. Statistical significance of differences was measured using the Mann-Whitney U-test based on adjusted  $p$ -values. \*:  $p < 0.01$ ; \*\*\*:  $p < 0.001$ ; \*\*\*\*:  $p < 0.0001$

patients as compared to male controls (adjusted  $p$ -value < 0.05, Additional file 3: Table S2). Although the small number of females in our dataset ( $N = 10$  out of  $N = 54$  subjects) precluded a clear analysis of the effect of sex, the later results suggest a minimal impact of sex on chemokine levels.

To ascertain the results of univariate statistics, we conducted a multivariate analysis using robust Elastic Net penalized regression to evaluate the association between chemokine levels and FXS diagnosis, adjusting for covariates possibly impacting the levels of chemokines (age, BMI, time of sampling). As compared to non-robust Elastic Net regression, robust regression presented the advantage of downweighing the effect of extreme values and potential outliers in terms of biomarkers' concentrations, which could affect the stability of the analysis (Fig. 1, Additional file 3: Table S2). This analysis revealed that the levels of CCL2, CCL3, CCL11, CCL22, CCL26 and CXCL10 were negatively associated with increased odds of FXS diagnosis, while the covariates age, BMI and time of sampling were not (Table 2). Sex being another possible confounding factor and as robust regression currently does not handle categorical variables, we rerun the robust regression analysis on a sample restricted to male individuals. We confirmed that 5 chemokines CCL2, CCL11, CCL22, CCL26 and CXCL10 remained stably associated with increased odds of FXS diagnosis in the dataset restricted to male subjects, reflecting a minimal impact of sex on these associations (Table 2). However,

CCL4, CCL13 and CCL17 appeared associated with FXS diagnosis only in the dataset restricted to males. This supports the stability of our results for CCL2, CCL11, CCL22, CCL26 and CXCL10 and possible sex differences in the expression of chemokines for CCL3, CCL4, CCL13 and CCL17.

While some chemokines bind to several receptors, some chemokine receptors bind different chemokines [16]. To gain further insight into the immune pathways that could be impacted by chemokine dysregulation, we constructed an interaction map using available databases (see Material & Methods for extensive list of sources). We identified six chemokine receptors, CCR1, CCR2, CCR3, CCR4, CCR5 and CXCR5, whose signalling could be impacted (Additional file 1: Fig. S1A). We then performed a pathway over-representation analysis on the list of the nine downregulated chemokines in FXS patients (Additional file 1: Fig. S1B, Additional file 4: Table S3). Biological processes related to chemotaxis of innate and adaptive immune cell types were over-represented: CCL2 and CCL3 for lymphocytes, monocytes, macrophages and neutrophils, CCL3, CCL11 and CCL13 for eosinophils, neutrophils, granulocytes, CCL3 and CXCL10 for T cells, CCL3 and CCL4 for NK cells. Several chemokines were also involved in response to viral infection (CCL4, CCL11, CXCL10), bacterial infection (CCL2, CCL3, CXCL10), as well as to toxic substances insults (CCL3, CCL4).

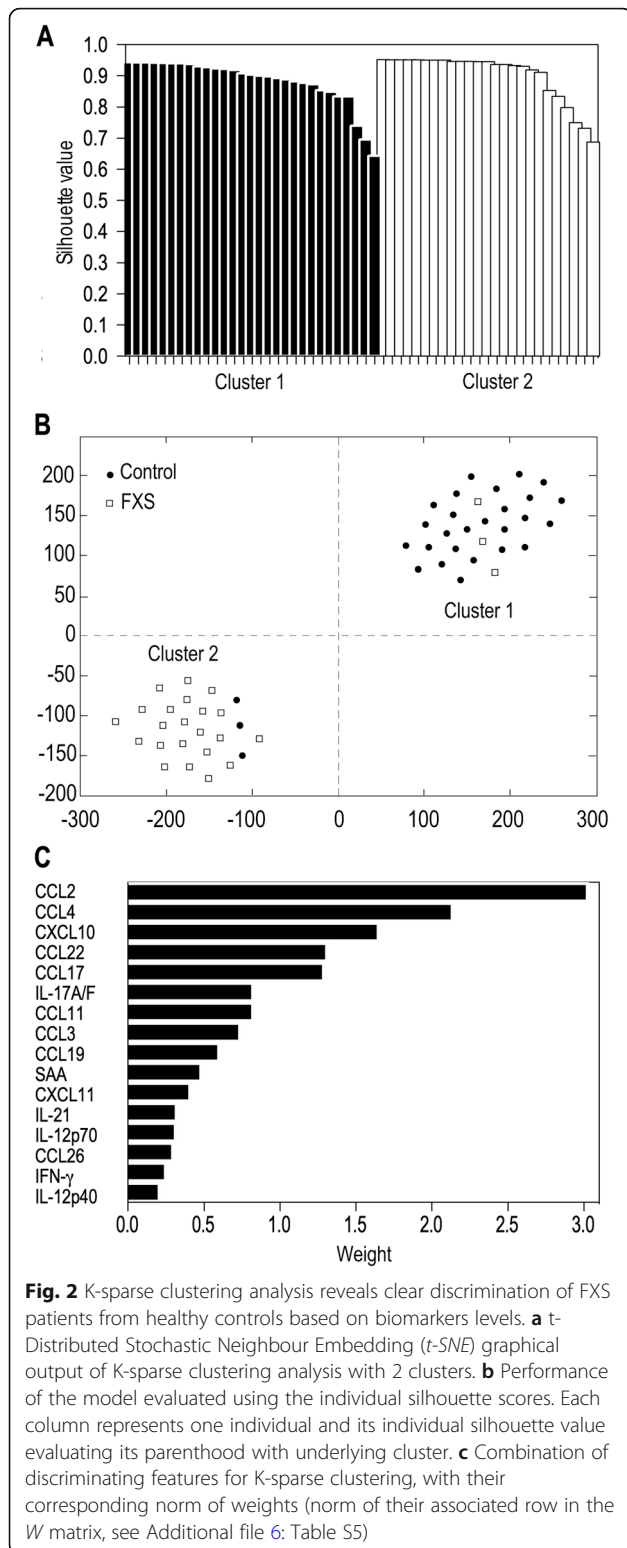
### Clustering analysis

In contrast to univariate methods that assess the differential expression of cytokines at the single feature level, unsupervised clustering methods allows for identifying combinations of variables with the best joint discriminative ability to separate the classes of samples. We therefore applied unsupervised classification to the dataset encapsulating the levels of the studied biomarkers for each of the 54 individuals included in our study. To partition the samples in two clusters, we used the K-sparse algorithm which not only identifies underlying homogeneous clusters but also selects the combination of biomarkers relevant to discriminate each cluster. We have previously proven the superior efficacy of K-sparse clustering towards more classical PCA k-means clustering [24]. In order to assess the quality of this K-sparse partitioning in two clusters, we computed the silhouette value for each patient. Silhouette value measures how similar a patient is to the patients in its own cluster (i.e. the intra-cluster cohesion), compared to patients in other clusters (i.e. the inter-cluster separation). The closest the silhouette coefficient (average of all the silhouette values) approaches 1, the better the intra-cluster consistency is. The mean silhouette coefficient associated to our clustering was equal to 0.892 and most of the individual silhouette values were close to 1 (Fig. 2a, Additional file 5: Table S4), which

**Table 2** Associations between chemokines and FXS diagnosis adjusted for age, BMI and time of sampling

	Dataset	
	Males + Females ( $N = 54$ )	Males ( $N = 44$ )
<b>Covariates</b>		
Age	0	0
Time of sampling	0	-0.04093
BMI	0	-0.15352
<b>Chemokines</b>		
<b>CCL2</b>	<b>-0.03703</b>	<b>-0.05208</b>
CCL3	-0.01263	0
CCL4	0	0.06623
<b>CCL11</b>	<b>-0.01220</b>	<b>-0.01161</b>
CCL13	0	-0.05315
CCL17	0	-0.00101
<b>CCL22</b>	<b>-0.00060</b>	<b>-0.00743</b>
<b>CCL26</b>	<b>-0.04703</b>	<b>-1.04540</b>
<b>CXCL10</b>	<b>-0.01051</b>	<b>-0.03173</b>

Coefficients were obtained using robust Elastic Net regression with 2000 subsampling steps on the whole dataset (males and females subjects:  $N = 54$ ,  $n = 25$  FXS patients,  $n = 29$  controls) and in a dataset reduced to male subjects ( $N = 44$ ,  $n = 20$  FXS patients,  $n = 24$  controls). Coefficients distinct from zero are shaded in grey and convergent associations across the two datasets are bolded



indicated the appropriateness of our clustering and which revealed that the 2 clusters are well distinct in the projected space (Fig. 2b). Since clustering analysis was unsupervised, the model was not a priori informed of the samples class

(i.e. Control or FXS). We therefore compared our clusters labels to these class' labels (Fig. 2b). Among the 29 individuals in Cluster 1, 26 were healthy controls and 3 were FXS patients. In contrast, among the 25 individuals in Cluster 2, 22 were FXS patients and 3 were healthy controls. This revealed that our partitioning matches well with the two classes Control and FXS.

The procedure of features selection proposed by K-sparse algorithm allowed for identifying relevant biomarkers that could discriminate the two clusters using the weighted projection matrix  $W$  associated to this clustering (Additional file 6: Table S5). K-sparse clustering discriminated healthy controls from FXS patients on the basis of the combination of 16 cytokines (Fig. 2c). This combination of biomarkers overlaps with the list of chemokines displaying the largest significant changes (CCL2, CCL3, CCL4, CCL11, CCL17, CCL22, CCL26, CXCL10, Fig. 1) to the exception of CCL13 which was not selected (Fig. 1, 2c). It also highlighted that CCL19, CXCL11, IL-12p40, IL-12p70, IL-17A/F, IL-21, INF- $\gamma$  and SAA have discriminative capacities, although these markers were not differentially expressed between FXS and controls in univariate analysis (Fig. 2c).

To identify potential relationships between these 16 biomarkers, we performed correlation analyses in healthy controls and FXS patients respectively (Fig. 3, Additional file 7: Table S6). IL-12p70, IL-17A/F, IL-21 and SAA did not display significant correlations with any of the markers in both controls and patients, to the exception of the IL-17A/F and IL-21 interleukin pair (Fig. 3). Similar correlation patterns were observed in control individuals and in FXS patients for combinations of the chemokines CCL2, CCL3, CCL4, CCL11, CCL17, CCL22 and CXCL10. In contrast, CCL19, CCL26, IL-12p40 and IFN- $\gamma$  displayed divergent patterns of correlation. Medium to strong positive correlations were observed in FXS patients for the combinations of 7 chemokines (CCL2, CCL3, CCL4, CCL17, CCL19, CCL22 and CXCL10) and IFN- $\gamma$  correlated with CCL3, CCL4 and CXCL10. This suggests the presence of coordinated variations in the levels of those biomarkers in FXS patients (Fig. 3).

## Discussion

### Reduced levels of pro-inflammatory chemokines in FXS patients

Compared to healthy individuals, Ashwood et al. found that FXS patients with ASD exhibited higher plasma levels of IL-1 $\alpha$  and IL-12p40 and reduced levels of CCL2, CCL5, CCL11 and CXCL10, but similar levels of IL-1 $\beta$ , IL-2, IL-3, IL-4, IL-5, IL-6, IL-7, IL-8, IL-10, IL-12p70, IL-13, IL-15, GM-CSF, IFN- $\gamma$ , TNF- $\alpha$  and CCL3 [17]. They also found that FXS patients without ASD exhibited higher plasma levels of IL-1 $\alpha$  and reduced levels of CCL5 and CXCL10, but similar levels of the other

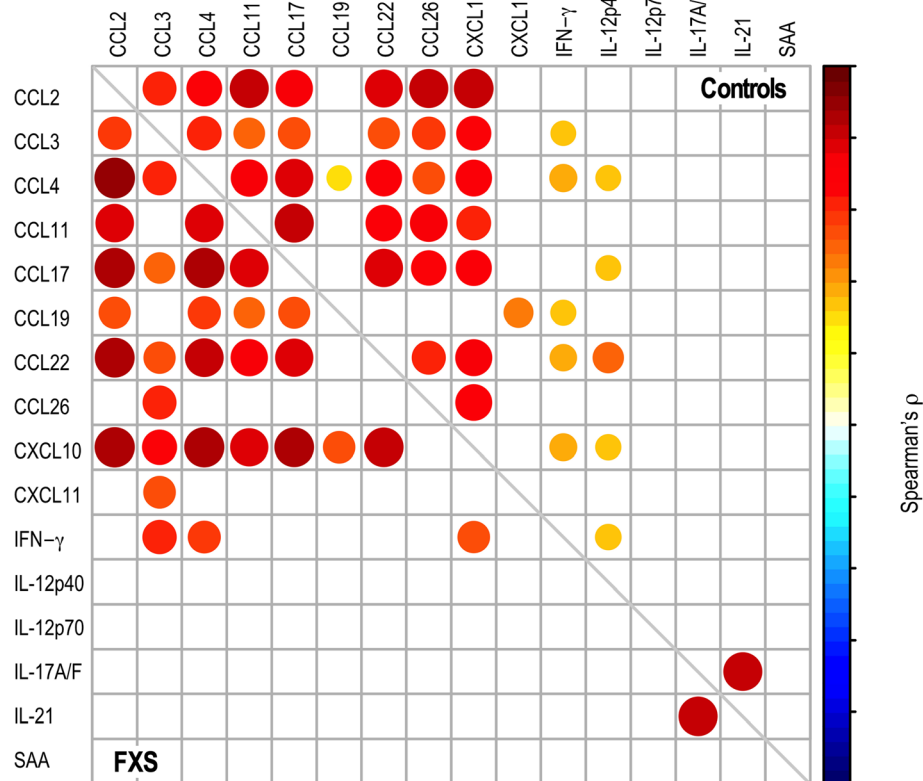


**Fig. 3** Correlation analysis of the serum levels of the 16 discriminating cytokines identified by K-sparse clustering in healthy controls and FXS patients. Mirror heatmap representation of correlations. Spearman's  $\rho$  coefficients are color-coded and proportional to dot area. Only significant correlations are displayed (adjusted  $p$ -value < 0.05)

biomarkers [17]. While seven interleukins, i.e. IL-1 $\alpha$ , IL-1 $\beta$ , IL-2, IL-4, IL-5 and IL-13 were readily detected in plasma samples by Ashwood et al. using a different immunoassay, these IL were below the lower level of detection in our serum samples. In agreement with this previous study, we found that IL-6, IL-7, IL-8, IL-10, IL-12p40, IL-12p70, IL-15, GM-CSF, IFN- $\gamma$  and TNF- $\alpha$  were present at similar levels in FXS patients and healthy controls. However, we did not highlight an increase in IL-12p40 in FXS patients and we show a decrease in CCL3. These apparent discrepancies could be explained by the type of matrix used (plasma versus serum), the analytical platform used (bead-array versus ECL assay) or differences in the statistical methods used. However, both our study and the one by Ashwood et al. suggest that FXS patients do not exhibit a clear low-grade pro-inflammatory profile that would be characterized by higher levels of multiple pro-inflammatory cytokine and acute phase proteins such as CRP. In agreement with this observation in FXS patients, serum levels of the two pro-inflammatory cytokines TNF- $\alpha$  and IFN- $\gamma$  were reported to be identical in *Fmr1*-KO mice and their non-transgenic littermates [25].

Chemokines are well known for their ability to induce directed chemotaxis in nearby responsive cells. Here, we

have found that FXS patients exhibit reduced serum levels of CCL2, CCL3, CCL4, CCL11, CCL13, CCL17, CCL22, CCL26 and CXCL10. Furthermore, CCL2, CCL3, CCL11, CCL22, CCL26 and CXCL10 were negatively associated with FXS diagnosis in a robust regression model in which we adjusted for age, BMI and time of sampling. Five of these chemokines (CCL2, CCL11, CCL22, CCL26 and CXCL10) were also retained in a dataset reduced to male subjects, strengthening our findings for these chemokines. Finally, CCL2, CCL3, CCL11, CCL22, CCL26 and CXCL10 are also selected by our K-sparse clustering as features discriminating the clusters, in combination with 10 additional biomarkers. Importantly, a previous report highlighted that the plasmatic levels of CCL2, CCL11 and CXCL10 were significantly decreased in a larger sample of male FXS patients [17]. All these data support the fact that dysregulation of at least a subset of specific pro-inflammatory chemokines could contribute to FXS.

The subset of chemokines exhibiting reduced levels in FXS patients indicated possible decreased signalling from six chemokine receptors: CCR1, CCR2, CCR3, CCR4, CCR5 and CXCR3. This could possibly impact the chemotaxis of a number of cell types and pathways

ontologically related to “inflammatory response”, including “response to viral infection”, “response to LPS” or “response to toxic insults”. CXCR3 is expressed primarily by activated NK cells and T lymphocytes, and by epithelial cells [26]. Th1 cells co-express CXCR3 and CCR5 while Th2 cells express CCR3 and CCR4. CXCR3 ligands that attract Th1 cells can concomitantly block the migration of Th2 cells in response to CCR3 ligands, thus enhancing the polarization of effector T cell recruitment [26]. Reduced serum levels of CXCL10 might dampen CXCR3 signalling, while decreased levels of CCL3 and CCL5 could reduce CCR3 and CCR4 signalling. This could ultimately cause T cell dysfunction in FXS patients. CCL2 is the most strongly dysregulated chemokine in FXS patients as compared to controls. Through signalling via CCR2 and CCR4 receptors, CCL2 mediates chemotaxis of monocytes and dendritic cells, as well as memory T cells to the sites of inflammation upon tissue injury or infection [27, 28]. Decreased levels of circulating CCL2 could therefore contribute to reduce the local immune response to infection in FXS patients.

A general health survey on FXS patients highlighted an increased occurrence of ear, throat and nose infections such as sinusitis and otitis in FXS patients [9, 10]. However, anatomical particularities and malformations of the ear conducts and sinuses are likely to explain the specificity of these infections [9], as FXS patients do not appear more sensitive to other types of infections. This would have been expected, if there was a general defective chemokine receptor signalling during infection in FXS patients. Nevertheless, it may be envisioned that reduced chemokine levels in FXS patients may be associated with a reduced capacity of the immune system of FXS patients to respond to specific pathogens. Of note, one study in the *Drosophila melanogaster* model of FXS showed that the *dfmr1* mutants exhibit increased sensitivity to bacterial infection and decreased phagocytosis of bacteria by systemic immune cells [29], suggesting that *dfmr1* gene is required for the activation of phagocytic immune cells and therefore for their immune responsiveness.

Although immune responsiveness to LPS and PHA of PBMC from FXS patients did not differ from those of healthy controls [18], a few studies have been performed in asymptomatic individuals carrying the *FMRI* premutation. Notably, an increase in IL-10 secretion by PBMC in the absence of immune challenge was described in *FMRI* premutation carriers [30]. Furthermore, a decreased cytokine secretion response was observed in LPS-stimulated PBMC from individuals carrying the *FMRI* premutation [31]. This suggests that dysregulation in the *FMRI* gene could alter immune responsiveness under yet to be defined conditions. FMRP, the *FMRI* gene product, is an RNA-binding protein and a translational regulator [6].

Although majorly described as a translational repressor, some studies suggest that FMRP can activate the translation of some of its mRNA targets [6]. Further work would be required to determine whether the mRNAs encoding the six dysregulated cytokines are bona fide mRNA targets for translational activation by FMRP or whether their decreased levels indirectly result from compensatory or adaptive mechanisms.

#### Possible neuro-immune alterations in FXS

Interactions between the nervous and the immune system are critical not only during early neurodevelopment but also in adolescence and adulthood [32]. As a consequence, immune dysfunction may cause changes in brain connectivity associated with neurodevelopmental disorders and this has been mostly studied in the context of ASD [33]. Chemokine and their cognate receptors are widely expressed in the developing and adult CNS and disruption of their patterns of expression have been involved in CNS disorders, including ASD [34]. Notably, CCL2, CCL3, CCL4, CCL5 and CCL11 are required, via signalling through CCR2, CCR3 and CCR5 receptors, for microglia chemotaxis [35–37]. In addition, CCL2 regulates migration of neural stem cells in the brain [38]. Although peripheral levels of those chemokines might not reflect their actual levels in the CNS, alterations in CCL2, CCL3, CCL4, CCL5 and CCL11 signalling could participate to the defects in CNS patterning observed in FXS patients. In addition, alterations in chemokine secretion or immune response could enhance the sensitivity of FXS patients to neurological damages induced by environmental sources, including infections and xenobiotics exposure. In line with this, and although chemokines were not assessed, one study has shown that cortical astrocytes derived from the brain of FXS mouse model secreted more IL-6 in response to LPS stimulation. Furthermore, the authors provide evidence that the abnormal elevation of IL-6 in the cortex of *Fmr1*-KO mouse could be linked to the synaptic phenotypes [39].

#### Immune-related biomarkers enable clustering of samples in FXS and control cases

The K-sparse clustering strategy we applied to the biomarkers’ dataset enabled discrimination of FXS samples from control samples relying principally on a combination of 16 immune-related markers. A number of efficient methods already exist to perform unsupervised classification of samples based on datasets encapsulating biological features. It is common practice to use PCA k-means to perform clustering analysis. k-means does not perform both clustering and feature selection, therefore providing minimal insights into the discriminating features and therefore into the underlying biology. The K-sparse method we have used alternates k-means with

projection-gradient minimization to promote sparsity and enable features selection, with significant improvements in clustering performances as compared to k-means standard algorithm in terms of clustering performances [24]. By considering the weighted linear combination of the selected features, the clustering computed by K-sparse also presented the advantage of handling extreme values and outliers which are frequently observed in biomarker datasets. The K-sparse clustering highlighted that 8 of the 9 significantly dysregulated chemokines contribute to separation between controls and FXS cases. It further identified additional immune-related molecules with discriminative abilities: CCL19, CXCL11, IL-12p40, IL-12p70, IL-17F, IL-21, INF- $\gamma$  and SAA. K-sparse highlights the contribution of biomarkers which do not differ in univariate analysis and regression analysis. This can be explained by the fact that K-sparse relies on weighted linear combination of the selected features and not on the individual distribution of values among each class. Correlations are observed between a subset of the 16 biomarkers selected by K-sparse, showing that relationships between biomarkers can be of biological relevance. Our study supports that K-sparse clustering can complement classical univariate and regression analyses to identify relevant biomarkers of disease. It paves the way for the use of K-sparse clustering analysis for the identification of combinations of disease biomarkers, but also for the stratification of patients in homogenous subtypes bearing similar biological patterns.

### Limitations of the study

Our study has some limitations. First, the sample size is relatively small ( $n = 25$  FXS patients;  $n = 29$  sex and age-matched controls), which may lead to an overestimation of the effect size owing to reduced power, but also limit the generalization of our findings. Second, the methodological choices we have made based on our dataset constraints, e.g. the use of robust Elastic Net regression instead of classical logistic regression, may limit the interpretation of the identified associations. Indeed, coefficients are shrunk and computation of confidence interval and asymptotically valid  $p$ -values are not yet available in the robust regression framework. However, among the six chemokines that we have shown here to be negatively associated with FXS, three (CCL2, CCL11, CXCL10) have already been demonstrated to be present at lower levels in an independent cohort of FXS patients ( $n = 64$ ) compared to healthy controls ( $n = 19$ ) [17], therefore strengthening the validity of our conclusions. Third, although we have adjusted the associations between specific chemokines and FXS diagnosis for a number of covariates which could impact serum cytokines (age, BMI and time of sampling), we cannot rule out the contribution of additional unmeasured covariates. Fourth, we acknowledge that the present study provides limited insight into possible underlying

mechanisms. However, it is noteworthy that almost nothing is known on possible immune-related dysfunctions in FXS patients. Exploratory studies are therefore needed to provide the rationale for new studies investigating specific underlying mechanisms.

### Conclusions

Our data suggest that immune dysfunction could participate to the physio-pathological processes involved in FXS. The dysregulated immune markers are pro-inflammatory chemokines which are reduced, suggesting that inflammation is not a hallmark of FXS. Further studies are required to decipher the possible role played by immune molecules, and in particular chemokines, in the pathophysiology of FXS and other neurodevelopmental disorders.

### Supplementary information

Supplementary information accompanies this paper at <https://doi.org/10.1186/s12883-020-01715-2>.

**Additional file 1: Figure S1.** Pathways associated with significantly dysregulated chemokines in FXS patients. (A) Interaction map for the subset of chemokines dysregulated in FXS patients and their cognate receptors CCR1, CCR2, CCR4, CCR5 and CXCR10. (B) Selection of GO terms significantly over-represented in the list of dysregulated chemokines presented in Fig. 1.

**Additional file 2: Table S1.** Percentage of detection of biomarkers in FXS patients vs. healthy controls and inclusion of analytes

**Additional file 3: Table S2.** Comparison analysis of serum biomarkers levels in FXS patients and controls in the whole dataset ( $N = 54$ ) and in a reduced dataset consisting of male individuals ( $N = 44$ ). Minimum (Min), first quartile (Q1), median, third quartile (Q3), maximum (Max), mean, standard deviation (SD) are indicated for each group. The  $r$  effect size statistic, raw  $p$ -values ( $p$ -value) and adjusted  $p$ -values for the Mann-Whitney U-test, are indicated both for the full dataset ( $N = 54$ ,  $n = 25$  FXS patients,  $n = 29$  controls) and for the dataset reduced to male individuals ( $N = 44$ ,  $n = 20$  FXS patients,  $n = 24$  controls).

**Additional file 4: Table S3.** Over-represented pathways based on the list of significantly downregulated chemokines in FXS patients

**Additional file 5: Table S4.** Silhouette values for each individual in the K-sparse clustering analysis with  $k = 2$  and clustering accuracy based on samples class

**Additional file 6: Table S5.**  $W$  matrix highlighting the respective discriminative weight of each feature in the 4 dimensions of the K-sparse model

**Additional file 7: Table S6.** Correlations and associated adjusted  $p$ -values for each biomarker pair among the 16 features identified by K-sparse clustering in healthy controls and FXS patients. For each biomarker pair, correlations  $r$  coefficients and the corresponding adjusted  $p$ -values are presented in upper triangle and lower triangle, respectively. Adjusted  $p$ -values  $< 0.05$  are highlighted in bold.

### Abbreviations

FXS: Fragile X Syndrome; CNS: central nervous system; *FMR1*: Fragile X Mental Retardation 1 gene; IL: interleukin; LPS: lipopolysaccharides; PBMC: peripheral blood mononuclear cells; ASD: autism spectrum disorder; TNF: Tumor Necrosis Factor; IFN: interferon

### Acknowledgements

We acknowledge H. Van Esch for help with patient recruitment and are very grateful to the families and patients who have participated in this study.

**Authors' contributions**

AVD, FK and EE recruited patients and controls and performed serum sampling. LD, PBM, OK and EM performed experiments. LD and SB performed statistical analysis. CG performed clustering analysis. LD, OK and NG wrote the manuscript. LD designed the study. All authors read and approved the final manuscript.

**Funding**

LD thanks the generous support of FRAXA Research Foundation, l'Agence Nationale de la Recherche (ANR JCJC SVE6 MetaboXFra). RFK and AVD have received grants from FRAXA Research Foundation and Jérôme Lejeune Foundation. Funding bodies were not involved in the design of the study and collection, analysis, and interpretation of data and in writing the manuscript.

**Availability of data and materials**

The datasets used and analysed during the current study as well as the complete code for K-sparse clustering are available from the corresponding author on reasonable request.

**Ethics approval and consent to participate**

Collection of samples and data from Fragile X patients and healthy controls was approved by the medical ethics committee of the University of Antwerp in Belgium (Agreement #B300201523589). The study was conducted in accordance with statutes and regulations regarding the protection of the right and welfare of human subjects' participation in biomedical research (World Declaration of Helsinki). Written informed consent was obtained from each participant or his/her legal guardian before research participation.

**Consent for publication**

Not applicable.

**Competing interests**

The authors declare that they have no competing interests.

**Author details**

<sup>1</sup>Department of Medical Genetics, University and University Hospital of Antwerp, Edegem, Belgium. <sup>2</sup>Université Côte d'Azur, CNRS, Institut de Pharmacologie Moléculaire et Cellulaire, Valbonne, France. <sup>3</sup>Université Côte d'Azur, CNRS, Laboratoire Informatique Signaux et Systèmes de Sophia Antipolis, Valbonne, France.

Received: 31 July 2019 Accepted: 1 April 2020

Published online: 15 April 2020

**References**

- Chelly J, Khelifaoui M, Francis F, Cherif B, Bienvenu T. Genetics and pathophysiology of mental retardation. *Eur J Hum Genet.* 2006;14(6):701–13.
- Geçez J, Shoubridge C, Corbett M. The genetic landscape of intellectual disability arising from chromosome X. *Trends Genet.* 2009;25(7):308–16.
- Verkerk AJ, Pieretti M, Sutcliffe JS, Fu YH, Kuhl DP, Pizzuti A, et al. Identification of a gene (FMR-1) containing a CGG repeat coincident with a breakpoint cluster region exhibiting length variation in fragile X syndrome. *Cell.* 1991;65(5):905–14.
- Hunter J, Rivero-Arias O, Angelov A, Kim E, Fotheringham I, Leal J. Epidemiology of fragile X syndrome: a systematic review and meta-analysis. *Am J Med Genet A.* 2014;164A(7):1648–58.
- Davidovic L, Tournier B, Khandjian EW. The fragile X syndrome. *Encyclopedia of Life Sciences: John Wiley & Sons;* 2007.
- Banerjee A, Ifrim MF, Valdez AN, Raj N, Bassell GJ. Aberrant RNA translation in fragile X syndrome: From FMRP mechanisms to emerging therapeutic strategies. *Brain Res.* 2018;1693(Pt A):24–36.
- Hagerman RJ, Berry-Kravis E, Hazlett HC, Bailey DB Jr, Moine H, Kooy RF, et al. Fragile X syndrome. *Nat Rev Dis Primers.* 2017;3:17065.
- Kaufmann WE, Kidd SA, Andrews HF, Budimirovic DB, Esler A, Haas-Givler B, et al. Autism Spectrum disorder in fragile X syndrome: Cooccurring conditions and current treatment. *Pediatrics.* 2017;139(Suppl 3):S194–206.
- Kidd SA, Lachiewicz A, Barbooth D, Blitz RK, Delahunty C, McBrien D, et al. Fragile X syndrome: a review of associated medical problems. *Pediatrics.* 2014;134(5):995–1005.
- Hagerman RJ, Altshul-Stark D, McBogg P. Recurrent otitis media in the fragile X syndrome. *Am J Dis Child.* 1987;141(2):184–7.
- Berry-Kravis E, Levin R, Shah H, Mathur S, Darnell JC, Ouyang B. Cholesterol levels in fragile X syndrome. *Am J Med Genet.* 2015;167A(2):379–84.
- Lisik MZ, Gutmajster E, Sieron AL. Low levels of HDL in fragile X syndrome patients. *Lipids.* 2016;51(2):189–92.
- Caku A, Seidah NG, Lortie A, Gagne N, Perron P, Dube J, et al. New insights of altered lipid profile in fragile X syndrome. *PLoS One.* 2017;12(3):e0174301.
- Lisik MZ, Gutmajster E, Sieron AL. Plasma levels of Leptin and Adiponectin in fragile X syndrome. *Neuroimmunomodulation.* 2016;23(4):239–43.
- Leboucher A, Pisani DF, Martinez-Gili L, Chilloux J, Bermudez-Martin P, Van Dijck A, et al. The translational regulator FMRP controls lipid and glucose metabolism in mice and humans. *Mol Metab.* 2019;21:22–35.
- Hughes CE, Nibbs RJB. A guide to chemokines and their receptors. *FEBS J.* 2018.
- Ashwood P, Nguyen DV, Hessel D, Hagerman RJ, Tassone F. Plasma cytokine profiles in fragile X subjects: is there a role for cytokines in the pathogenesis? *Brain Behav Immun.* 2010;24(6):898–902.
- Careaga M, Noyon T, Basuta K, Van de Water J, Tassone F, Hagerman RJ, et al. Group I metabotropic glutamate receptor mediated dynamic immune dysfunction in children with fragile X syndrome. *J Neuroinflammation.* 2014;11:110.
- Pavlou M, Ambler G, Seaman S, De Iorio M, Omar RZ. Review and evaluation of penalised regression methods for risk prediction in low-dimensional data with few events. *Stat Med.* 2016;35(7):1159–77.
- Kurnaz FS, Hoffmann I, Filzmoser P. Robust and sparse estimation methods for high-dimensional linear and logistic regression. *Chemometr Intell Lab Syst.* 2018;172:211–22.
- Kurnaz FS, Hoffmann I, Filzmoser P. enetLTS: robust and sparse methods for high dimensional linear and logistic regression. R package version 0.1.0 <https://CRAN.R-project.org/package=enetLTS>. 2018.
- Breuer K, Foroushani AK, Laird MR, Chen C, Sribnaia A, Lo R, et al. InnateDB: systems biology of innate immunity and beyond—recent updates and continuing curation. *Nucleic Acids Res.* 2013;41(Database issue):D1228–33.
- Sharman JL, Harding SD, Southan C, Faccenda E, Pawson AJ, Davies JA, et al. Accessing Expert-Curated Pharmacological Data in the IUPHAR/BPS Guide to PHARMACOLOGY. *Curr Protoc Bioinformatics.* 2018;61(1):1–34. 1–46.
- Gilet C, Deprez M, Caillaud JB, Barlaud M. Clustering with feature selection using alternating minimization, Application to computational biology. *arXiv.* 2017;1711.02974v3.
- Yuskaitis CJ, Beurel E, Jope RS. Evidence of reactive astrocytes but not peripheral immune system activation in a mouse model of fragile X syndrome. *Biochim Biophys Acta.* 2010;1802(11):1006–12.
- Qin S, Rottman JB, Myers P, Kassam N, Weinblatt M, Loetscher M, et al. The chemokine receptors CXCR3 and CCR5 mark subsets of T cells associated with certain inflammatory reactions. *J Clin Invest.* 1998;101(4):746–54.
- Fantuzzi L, Borghi P, Ciolli V, Pavlakis G, Belardelli F, Gessani S. Loss of CCR2 expression and functional response to monocyte chemotactic protein (MCP-1) during the differentiation of human monocytes: role of secreted MCP-1 in the regulation of the chemotactic response. *Blood.* 1999;94(3):875–83.
- Andrew DP, Ruffing N, Kim CH, Miao W, Heath H, Li Y, et al. C-C chemokine receptor 4 expression defines a major subset of circulating nonintestinal memory T cells of both Th1 and Th2 potential. *J Immunol.* 2001;166(1):103–11.
- O'Connor RM, Stone EF, Wayne CR, Marcinkiewicz EV, Ulgherait M, Delventhal R, et al. A Drosophila model of fragile X syndrome exhibits defects in phagocytosis by innate immune cells. *J Cell Biol.* 2017;216(3):595–605.
- Marek D, Papin S, Ellefsen K, Niederhauser J, Isidor N, Ransijn A, et al. Carriers of the fragile X mental retardation 1 (FMR1) premutation allele present with increased levels of cytokine IL-10. *J Neuroinflammation.* 2012;9:238.
- Careaga M, Rose D, Tassone F, Berman RF, Hagerman R, Ashwood P. Immune dysregulation as a cause of autoinflammation in fragile X premutation carriers: link between FMRI CGG repeat number and decreased cytokine responses. *PLoS One.* 2014;9(4):e94475.
- Dantzer R. Neuroimmune interactions: from the brain to the immune system and vice versa. *Physiol Rev.* 2018;98(1):477–504.
- Meltzer A, Van de Water J. The role of the immune system in autism Spectrum disorder. *Neuropsychopharmacology.* 2017;42(1):284–98.
- Stuart MJ, Singhal G, Baune BT. Systematic review of the neurobiological relevance of chemokines to psychiatric disorders. *Front Cell Neurosci.* 2015;9:357.

35. Cross AK, Woodroffe MN. Chemokines induce migration and changes in actin polymerization in adult rat brain microglia and a human fetal microglial cell line in vitro. *J Neurosci Res.* 1999;55(1):17–23.
36. Skuljec J, Sun H, Pul R, Benardais K, Ragancokova D, Moharreggh-Khiabani D, et al. CCL5 induces a pro-inflammatory profile in microglia in vitro. *Cell Immunol.* 2011;270(2):164–71.
37. Selenica ML, Alvarez JA, Nash KR, Lee DC, Cao C, Lin X, et al. Diverse activation of microglia by chemokine (C-C motif) ligand 2 overexpression in brain. *J Neuroinflammation.* 2013;10:86.
38. Wiedera D, Holtkamp W, Entschladen F, Niggemann B, Zanker K, Kaltschmidt B, et al. MCP-1 induces migration of adult neural stem cells. *Eur J Cell Biol.* 2004;83(8):381–7.
39. Krasovska V, Doering LC. Regulation of IL-6 secretion by astrocytes via TLR4 in the fragile X mouse model. *Front Mol Neurosci.* 2018;11:272.

### Publisher's Note

Springer Nature remains neutral with regard to jurisdictional claims in published maps and institutional affiliations.

**Ready to submit your research? Choose BMC and benefit from:**

- fast, convenient online submission
- thorough peer review by experienced researchers in your field
- rapid publication on acceptance
- support for research data, including large and complex data types
- gold Open Access which fosters wider collaboration and increased citations
- maximum visibility for your research: over 100M website views per year

**At BMC, research is always in progress.**

Learn more [biomedcentral.com/submissions](https://biomedcentral.com/submissions)



## Conclusions on FXS Work

Fragile X syndrome (FXS) is the leading genetic cause of ASD. Most of the studies on FXS focussed on the study of CNS alterations induced by *Fmr1*-deficiency, and more specifically on brain function and behavioural impairments. In these three studies, we explored possible metabolic, skeletal and immune anomalies in the FXS mouse model and in FXS patients.

Regarding metabolic anomalies, we reveal that the loss of FMRP induces a systemic response that leads to decreased adiposity and broad changes in metabolic homeostasis with increased circulating free fatty acids and reduced glucose and insulin. We also found that FXS mouse model displays increased insulin sensitivity and improved glucose tolerance, associated with enhanced utilization of lipids as energetic substrate. Furthermore, we demonstrated that the FMRP protein regulates the translation of key mRNA involved in hepatic lipid metabolism. These findings suggest that FXS is accompanied by metabolic phenotypes. To which extent metabolic anomalies could contribute to brain dysfunction and behavioural impairments in FXS remains to be further explored.

We also describe for the first time the changes in body mass composition, skeleton, and bone architecture induced by *Fmr1*-deficiency in mice. Similar findings at the bone level were observed in FXS patients with an unusual overgrowth including macrocephaly and increased stature (Penagarikano et al., 2007). One study had also previously shown that the *Fmr1*-KO mouse and FXS patients display changes in craniofacial bone morphology (Heulens et al., 2013). These abnormalities could reflect an adaptation of the body to enhanced physical activity or be due to direct effects of FMRP absence. Further work is required to understand whether FMRP plays a direct role on skeletal ontogenesis.

Finally, we identified a specific immune profile in FXS patients characterised by decreased levels of 9 chemokines, suggestive of possible immune dysfunction. To which extent these nine cytokines could constitute immune biomarkers of FXS remain to be further investigated in larger samples of patients.

Overall our work strongly argues that *FMRI*-deficiency not only impacts the CNS but also whole-body homeostasis.

# Take-Home Message

ASD have a significant societal impact due to their high incidence and dramatic consequences on the quality of life of patients and their families. Early research focused on identifying abnormalities in the CNS and generating drug treatments targeting the brain. Despite active research in the ASD field, there is still no specific treatment, particularly to improve social interactions. In this Thesis, we have studied the involvement of the periphery, and notably the metabolic, immune and microbiota contribution to ASD, our work suggests their possible involvement in ASD aetiology and symptoms. Importantly, we have demonstrated a causal relationship between the microbial metabolite *p*-Cresol in ASD and ASD core behavioural symptoms; strongly suggest that manipulation of the gut microbiota is a therapeutic target to be further explored for the treatment of ASD.

# Bibliography

- Adams, J.B., Johansen, L.J., Powell, L.D., Quig, D., and Rubin, R.A. (2011). Gastrointestinal flora and gastrointestinal status in children with autism - comparisons to typical children and correlation with autism severity. *BMC Gastroenterol.* *11*, 22.
- Ahluwalia, B., Magnusson, M.K., and Öhman, L. (2017). Mucosal immune system of the gastrointestinal tract: maintaining balance between the good and the bad. *Scand. J. Gastroenterol.* *52*, 1185–1193.
- Allison, C., Baron-Cohen, S., Wheelwright, S., Charman, T., Richler, J., Pasco, G., and Brayne, C. (2008). The Q-CHAT (Quantitative CHECKlist for Autism in Toddlers): A normally distributed quantitative measure of autistic traits at 18-24 months of age: Preliminary report. *J. Autism Dev. Disord.* *38*, 1414–1425.
- Altieri, L., Neri, C., Sacco, R., Curatolo, P., Benvenuto, A., Muratori, F., Santocchi, E., Bravaccio, C., Lenti, C., Saccani, M., et al. (2011). Urinary p-cresol is elevated in small children with severe autism spectrum disorder. *Biomarkers* *16*, 252–260.
- Amodeo, D.A., Jones, J.H., Sweeney, J.A., and Ragozzino, M.E. (2012). Differences in BTBR T+ tf/J and C57BL/6J mice on probabilistic reversal learning and stereotyped behaviors. *Behav. Brain Res.* *227*, 64–72.
- De Angelis, M., Piccolo, M., Vannini, L., Siragusa, S., De Giacomo, A., Serrazanetti, D.I., Cristofori, F., Guerzoni, M.E., Gobetti, M., and Francavilla, R. (2013). Fecal Microbiota and Metabolome of Children with Autism and Pervasive Developmental Disorder Not Otherwise Specified. *PLoS One*.
- Ashwood, P., and Wakefield, A.J. (2006). Immune activation of peripheral blood and mucosal CD3+ lymphocyte cytokine profiles in children with autism and gastrointestinal symptoms. *J. Neuroimmunol.* *173*, 126–134.
- Ashwood, P., Wills, S., and Van de Water, J. (2006). The immune response in autism: a new frontier for autism research. *J. Leukoc. Biol.* *80*, 1–15.
- Ashwood, P., Nguyen, D. V., Hessel, D., Hagerman, R.J., and Tassone, F. (2010). Plasma cytokine profiles in Fragile X subjects: Is there a role for cytokines in the pathogenesis? *Brain. Behav. Immun.* *24*, 898–902.
- Assaf, M., Hyatt, C.J., Wong, C.G., Johnson, M.R., Schultz, R.T., Hendler, T., and Pearlson, G.D. (2013). Mentalizing and motivation neural function during social interactions in autism spectrum disorders. *NeuroImage Clin.* *3*, 321–331.

- Atladóttir, H.Ó., Pedersen, M.G., Thorsen, P., Mortensen, P.B., Deleuran, B., Eaton, W.W., and Parner, E.T. (2009). Association of family history of autoimmune diseases and autism spectrum disorders. *Pediatrics* *124*, 687–694.
- Atladóttir, H.Ó., Thorsen, P., Østergaard, L., Schendel, D.E., Lemcke, S., Abdallah, M., and Parner, E.T. (2010). Maternal infection requiring hospitalization during pregnancy and autism spectrum disorders. *J. Autism Dev. Disord.* *40*, 1423–1430.
- Aubert, P., Oleynikova, E., Rizvi, H., Ndjim, M., Le Berre-Scoul, C., Grohard, P.A., Chevalier, J., Segain, J.P., Le Drean, G., Neunlist, M., et al. (2019). Maternal protein restriction induces gastrointestinal dysfunction and enteric nervous system remodeling in rat offspring. *FASEB J.* *33*, 770–781.
- Bagni, C., and Zukin, R.S. (2019). A Synaptic Perspective of Fragile X Syndrome and Autism Spectrum Disorders. *Neuron* *101*, 1070–1088.
- Baird, G., Charman, T., Baron-Cohen, S., Cox, A., Swettenham, J., Wheelwright, S., and Drew, A. (2000). A screening instrument for autism at 18 months of age: A 6-year follow-up study. *J. Am. Acad. Child Adolesc. Psychiatry* *39*, 694–702.
- Bakker, C.E., and Oostra, B.A. (2003). Understanding fragile X syndrome: Insights from animal models. *Cytogenet. Genome Res.* *100*, 111–123.
- Balaan, C., Corley, M.J., Eulalio, T., Leite-ahyo, K., Alina, P.S., Fang, R., Khadka, V.S., Maunakea, A.K., and Ward, M.A. (2019). Phenotype Relevant To Autism Spectrum Disorder. 137–147.
- Bariselli, S., Tzanoulinou, S., Glangetas, C., Prévost-Solié, C., Pucci, L., Viguié, J., Bezzi, P., O'Connor, E.C., Georges, F., Lüscher, C., et al. (2016). SHANK3 controls maturation of social reward circuits in the VTA. *Nat. Neurosci.* *19*, 926–934.
- Bariselli, S., Hörnberg, H., Prévost-Solié, C., Musardo, S., Hatstatt-Burklé, L., Scheiffele, P., and Bellone, C. (2018). Role of VTA dopamine neurons and neuroligin 3 in sociability traits related to nonfamiliar conspecific interaction. *Nat. Commun.* *9*.
- Becker, J.A., Clesse, D., Spiegelhalter, C., Schwab, Y., Le Merrer, J., and Kieffer, B.L. (2014). Autistic-Like Syndrome in Mu Opioid Receptor Null Mice is Relieved by Facilitated mGluR4 Activity. *Neuropsychopharmacology* *39*, 2049–2060.
- Bejarano-Martín, Á., Canal-Bedia, R., Fernández-Álvarez, C., Cilleros-Martín, M.V., Sánchez-Gómez, M.C., García-Primo, P., Rose-Sweeney, M., Boilson, A., Linertová, R., Roeyers, H., et al. (2019). Early Detection , Diagnosis and Intervention Services for Young Children with Autism Spectrum Disorder in the European Union ( ASDEU ):

Family and Professional Perspectives. *J. Autism Dev. Disord.*

Bellono, N.W., Bayrer, J.R., Leitch, D.B., Castro, J., Zhang, C., O'Donnell, T.A., Brierley, S.M., Ingraham, H.A., and Julius, D. (2017). Enterochromaffin Cells Are Gut Chemosensors that Couple to Sensory Neural Pathways. *Cell* *170*, 185–198.e16.

Belzung, C., and Lemoine, M. (2011). Criteria of validity for animal models of psychiatric disorders: focus on anxiety disorders and depression. *Biol. Mood Anxiety Disord.* *1*, 1–14.

Bender, D.A. (2003). B6\_CHAPTER\_2003\_part\_1\_Encyclopedia of Food Sciences and Nutrition (Second Edition). 462–464.

Benton, D., Williams, C., and Brown, A. (2007). Impact of consuming a milk drink containing a probiotic on mood and cognition. *Eur. J. Clin. Nutr.* *61*, 355–361.

Bercik, P., Park, A.J., Sinclair, D., Khoshdel, A., Lu, J., Huang, X., and Deng, P.A. (2011a). The anxiolytic effect of *Bifidobacterium longum* NCC3001. *Neurogastroenterol. Motil.* *23*, 1132–1139.

Bercik, P., Denou, E., Collins, J., Jackson, W., Lu, J., Jury, J., Deng, Y., Blennerhassett, P., MacRi, J., McCoy, K.D., et al. (2011b). The intestinal microbiota affect central levels of brain-derived neurotropic factor and behavior in mice. *Gastroenterology* *141*, 599–609.

Berry-Kravis, E., Levin, R., Shah, H., Mathur, S., Darnell, J.C., and Ouyang, B. (2015). Cholesterol levels in Fragile X syndrome. *Am. J. Med. Genet. Part A* *167*, 379–384.

Bonaz, B., Bazin, T., and Pellissier, S. (2018). The Vagus Nerve at the Interface of the Microbiota-Gut-Brain Axis. *Front. Neurosci.* *12*.

Borre, Y.E., O'Keeffe, G.W., Clarke, G., Stanton, C., Dinan, T.G., and Cryan, J.F. (2014). Microbiota and neurodevelopmental windows: implications for brain disorders. *Trends Mol. Med.* *20*, 509–518.

Bourgeron, T. (2016). Current knowledge on the genetics of autism and propositions for future research. *Comptes Rendus - Biol.* *339*, 300–307.

Braniste, V., Al-Asmakh, M., Kowal, C., Anuar, F., Abbaspour, A., Tóth, M., Korecka, A., Bakocevic, N., Guan, N.L., Kundu, P., et al. (2014). The gut microbiota influences blood-brain barrier permeability in mice. *Sci. Transl. Med.* *6*, 1–12.

Bravo, J.A., Forsythe, P., Chew, M. V., Escaravage, E., Savignac, H.M., Dinan, T.G., Bienenstock, J., and Cryan, J.F. (2011). Ingestion of *Lactobacillus* strain regulates emotional behavior and central GABA receptor expression in a mouse via the vagus

nerve. *Proc. Natl. Acad. Sci. U. S. A.* *108*, 16050–16055.

Browning, K.N., and Travagli, R.A. (2014). Central nervous system control of gastrointestinal motility and secretion and modulation of gastrointestinal functions. *Compr. Physiol.* *4*, 1339–1368.

Buffington, S.A., Di Prisco, G.V., Auchtung, T.A., Ajami, N.J., Petrosino, J.F., and Costa-Mattioli, M. (2016). Microbial Reconstitution Reverses Maternal Diet-Induced Social and Synaptic Deficits in Offspring. *Cell* *165*, 1762–1775.

Buie, T., Campbell, D.B., Fuchs, G.J., Furuta, G.T., Levy, J., Van De Water, J., Whitaker, A.H., Atkins, D., Bauman, M.L., Beaudet, A.L., et al. (2010). Evaluation, diagnosis, and treatment of gastrointestinal disorders in individuals with ASDs: A consensus report. *Pediatrics* *125*.

Butler, M.G., Fletcher, M., Gale, D.D., Meaney, F.J., McLeod, D.R., Fagan, J., and Carpenter, N.J. (1988). Metacarpophalangeal pattern profile analysis in fragile X syndrome. *Am. J. Med. Genet.* *31*, 767–773.

Butler, M.G., Pratesi, R., Watson, M.S., Breg, W.R., and Singh, D.N. (1993). Anthropometric and craniofacial patterns in mentally retarded males with emphasis on the fragile X syndrome. *Clin. Genet.* *44*, 129–138.

Camilleri, M., Madsen, K., Spiller, R., Van Meerveld, B.G., and Verne, G.N. (2012). Intestinal barrier function in health and gastrointestinal disease. *Neurogastroenterol. Motil.* *24*, 503–512.

Carabotti, M., Scirocco, A., Maselli, M.A., and Severi, C. (2015). The gut-brain axis: Interactions between enteric microbiota, central and enteric nervous systems. *Ann. Gastroenterol.* *28*, 203–209.

Careaga, M., Noyon, T., Basuta, K., Van de Water, J., Tassone, F., Hagerman, R.J., and Ashwood, P. (2014). Group I metabotropic glutamate receptor mediated dynamic immune dysfunction in children with fragile X syndrome. *J. Neuroinflammation* *11*, 1–10.

Carmichael, O., and Lockhart, S. (2012). Neurotrophins and. *Brain Imaging Behav. Neurosci.* 289–320.

Chaidez, V., Hansen, R.L., and Hertz-Picciotto, I. (2014). Gastrointestinal problems in children with autism, developmental delays or typical development. *J. Autism Dev. Disord.* *44*, 1117–1127.

Chen, J., Rao, J.N., Zou, T., Liu, L., Marasa, B.S., Xiao, L., Zeng, X., Turner, D.J., and

- Wang, J.Y. (2007). Polyamines are required for expression of Toll-like receptor 2 modulating intestinal epithelial barrier integrity. *Am. J. Physiol. - Gastrointest. Liver Physiol.* *293*, 568–577.
- Chevallier, C., Kohls, G., Troiani, V., Brodtkin, E.S., and Schultz, R.T. (2012). The social motivation theory of autism. *Trends Cogn. Sci.* *16*, 231–239.
- Cho, I., and Blaser, M.J. (2012). The human microbiome: At the interface of health and disease. *Nat. Rev. Genet.* *13*, 260–270.
- Christensen, D.L., Maenner, M.J., Bilder, D., Constantino, J.N., Daniels, J., Durkin, M.S., Fitzgerald, R.T., Kurzius-Spencer, M., Pettygrove, S.D., Robinson, C., et al. (2019). Prevalence and Characteristics of Autism Spectrum Disorder Among Children Aged 4 Years - Early Autism and Developmental Disabilities Monitoring Network, Seven Sites, United States, 2010, 2012, and 2014. *MMWR. Surveill. Summ.* *68*, 1–19.
- Christensen, J., Grønberg, T.K., Sørensen, M.J., Schendel, D., Parner, E.T., Pedersen, L.H., and , & Vestergaard, M. (2014). Prenatal valproate exposure and risk of autism spectrum disorders and childhood autism. *Arch. Dis. Child. Educ. Pract. Ed.* *99*, 198.
- Chung, H., Pamp, S.J., Hill, J.A., Surana, N.K., Edelman, S.M., Troy, E.B., Reading, N.C., Villablanca, E.J., Wang, S., Mora, J.R., et al. (2012). Gut immune maturation depends on colonization with a host-specific microbiota. *Cell* *149*, 1578–1593.
- Clarke, G., Grenham, S., Scully, P., Fitzgerald, P., Moloney, R.D., Shanahan, F., Dinan, T.G., and Cryan, J.F. (2013). The microbiome-gut-brain axis during early life regulates the hippocampal serotonergic system in a sex-dependent manner. *Mol. Psychiatry* *18*, 666–673.
- Clevers, H.C., and Bevins, C.L. (2013). Paneth Cells: Maestros of the Small Intestinal Crypts. *Annu. Rev. Physiol.* *75*, 289–311.
- Connolly, N., Anixt, J., Manning, P., Ping-I Lin, D., Marsolo, K.A., and Bowers, K. (2016). Maternal metabolic risk factors for autism spectrum disorder—An analysis of electronic medical records and linked birth data. *Autism Res.* *9*, 829–837.
- Coretti, L., Cristiano, C., Florio, E., Scala, G., Lama, A., Keller, S., Cuomo, M., Russo, R., Pero, R., Paciello, O., et al. (2017). Sex-related alterations of gut microbiota composition in the BTBR mouse model of autism spectrum disorder. *Sci. Rep.* *7*, 1–10.
- Cotariu, D., and Zaidman, J.. (1991). Developmental Toxicity of Valproic Acid. *48*, 2–5.
- Crawley, J.N. (2012). Translational animal models of autism and neurodevelopmental

disorders. *Dialogues Clin. Neurosci.* 14, 293–305.

Cremonese-Caira, A., Buirkle, J., Gilbert, R., Nayudu, N., and Faja, S. (2019). Relations between caregiver-report of sleep and executive function problems in children with autism spectrum disorder and attention-deficit/hyperactivity disorder. *Res. Dev. Disabil.* 94, 103464.

Crumevolle-Arias, M., Jaglin, M., Bruneau, A., Vancassel, S., Cardona, A., Daugé, V., Naudon, L., and Rabot, S. (2014). Absence of the gut microbiota enhances anxiety-like behavior and neuroendocrine response to acute stress in rats. *Psychoneuroendocrinology* 42, 207–217.

Cryan, J.F., and Dinan, T.G. (2012). Mind-altering microorganisms: The impact of the gut microbiota on brain and behaviour. *Nat. Rev. Neurosci.* 13, 701–712.

Curran, E.A., O'Neill, S.M., Cryan, J.F., Kenny, L.C., Dinan, T.G., Khashan, A.S., and Kearney, P.M. (2015). Research Review: Birth by caesarean section and development of autism spectrum disorder and attention-deficit/hyperactivity disorder: A systematic review and meta-analysis. *J. Child Psychol. Psychiatry Allied Discip.* 56, 500–508.

D'Eufemia, P., Celli, M., Finocchiaro, R., Pacifico, L., Viozzi, L., Zaccagnini, M., Cardi, E., and Giardini, O. (1996). Abnormal intestinal permeability in children with autism. *Acta Paediatr. Int. J. Paediatr.* 85, 1076–1079.

Dalile, B., Van Oudenhove, L., Vervliet, B., and Verbeke, K. (2019). The role of short-chain fatty acids in microbiota–gut–brain communication. *Nat. Rev. Gastroenterol. Hepatol.* 16, 461–478.

David, L.A., Maurice, C.F., Carmody, R.N., Gootenberg, D.B., Button, J.E., Wolfe, B.E., Ling, A. V., Devlin, A.S., Varma, Y., Fischbach, M.A., et al. (2014). Diet rapidly and reproducibly alters the human gut microbiome. *Nature* 505, 559–563.

Davidovic, L., Tremblay, S., Gravel, M., Koninck, P. De, and Khandjian, E.W.. (2006). Le syndrome de l'X fragile une protéine absente et 1001 ARNm débousolés. 22, 41–46.

Davidovics, Z.H., Michail, S., Nicholson, M.R., Kocielek, L.K., Pai, N., Hansen, R., Schwerd, T., Maspons, A., Shamir, R., Szajewska, H., et al. (2019). Fecal Microbiota Transplantation for Recurrent *Clostridium difficile* Infection and Other Conditions in Children: A Joint Position Paper from the North American Society for Pediatric Gastroenterology, Hepatology, and Nutrition and the European Society for . *J. Pediatr. Gastroenterol. Nutr.* 68, 130–143.

- Davids, J.R., Hagerman, R.J., and Eilert, R.E. (1990). Orthopaedic aspects of fragile-X syndrome. *J. Bone Jt. Surg. - Ser. A* 72, 889–896.
- Desbonnet, L., Clarke, G., Shanahan, F., Dinan, T.G., and Cryan, J.F. (2014). Microbiota is essential for social development in the mouse. *Mol. Psychiatry* 19, 146–148.
- Dewey, K.G., Nommsen-rivers, L.A., Heinig, M.J., and Cohen, R.J. (2003). Risk Factors for Suboptimal Infant Breastfeeding Behavior, Delayed Onset of Lactation, and Excess Neonatal Weight Loss Kathryn. *Pediatrics* 112, 607–619.
- DiSabato, D.J., Quan, N., and Godbout, J.P. (2016). Neuroinflammation: the devil is in the details. *J. Neurochem.* 139, 136–153.
- Doernberg, E., and Hollander, E. (2016). Neurodevelopmental Disorders (ASD and ADHD): DSM-5, ICD-10, and ICD-11. *CNS Spectr.* 21, 295–299.
- Dölen, G., Darvishzadeh, A., Huang, K.W., and Malenka, R.C. (2013). Social reward requires coordinated activity of nucleus accumbens oxytocin and serotonin. *Nature* 501, 179–184.
- Donohoe, D.R., Garge, N., Zhang, X., Sun, W., O’Connell, T.M., Bunker, M.K., and Bultman, S.J. (2011). The microbiome and butyrate regulate energy metabolism and autophagy in the mammalian colon. *Cell Metab.* 13, 517–526.
- Dufour-Rainfray, D., Vourc’h, P., Tourlet, S., Guilloteau, D., Chalon, S., and Andres, C.R. (2011). Fetal exposure to teratogens: Evidence of genes involved in autism. *Neurosci. Biobehav. Rev.* 35, 1254–1265.
- Emond, P., Mavel, S., Aïdoud, N., Nadal-Desbarats, L., Montigny, F., Bonnet-Brilhault, F., Barthélémy, C., Merten, M., Sarda, P., Laumonnier, F., et al. (2013). GC-MS-based urine metabolic profiling of autism spectrum disorders. *Anal. Bioanal. Chem.* 405, 5291–5300.
- Ernst, M., Zametkin, A.J., Matochik, J.A., Pascualvaca, D., and Cohen, R.M. (1997). Low medial prefrontal dopaminergic activity in autistic children [4]. *Lancet* 350, 638.
- Erny, D., De Angelis, A.L.H., Jaitin, D., Wieghofer, P., Staszewski, O., David, E., Keren-Shaul, H., Mhlahoi, T., Jakobshagen, K., Buch, T., et al. (2015). Host microbiota constantly control maturation and function of microglia in the CNS. *Nat. Neurosci.* 18, 965–977.
- Esnafoglu, E., Cirrik, S., Ayyıldız, S.N., Erdil, A., Ertürk, E.Y., Dağlı, A., and Noyan, T. (2017). Increased Serum Zonulin Levels as an Intestinal Permeability Marker in

- Autistic Subjects. *J. Pediatr.* *188*, 240–244.
- Estes, M.L., and McAllister, A.K. (2015). Immune mediators in the brain and peripheral tissues in autism spectrum disorder. *Nat. Rev. Neurosci.* *16*, 469–486.
- Estes, M.L., and McAllister, A.K. (2016). Maternal immune activation: Implications for neuropsychiatric disorders. *Science (80-. )*. *353*, 772–777.
- Evans, K., Evans, R., Royal, J., Esterman, A., and James, S. (2003). Effect of caesarean section on breast milk transfer to the normal term newborn over the first week of life. *Arch Dis Child Fetal Neonatal* *88*, 380–383.
- Farzi, A., Fröhlich, E.E., and Holzer, P. (2018). Gut Microbiota and the Neuroendocrine System. *Neurotherapeutics* *15*, 5–22.
- Fattorusso, A., Di Genova, L., Dell’isola, G.B., Mencaroni, E., and Esposito, S. (2019). Autism spectrum disorders and the gut microbiota. *Nutrients* *11*.
- Felger, J.C., and Lotrich, F.E. (2013). Inflammatory cytokines in depression: Neurobiological mechanisms and therapeutic implications. *Neuroscience* *246*, 199–229.
- Fiorentino, M., Sapone, A., Senger, S., Camhi, S.S., Kadzielski, S.M., Buie, T.M., Kelly, D.L., Cascella, N., and Fasano, A. (2016). Blood-brain barrier and intestinal epithelial barrier alterations in autism spectrum disorders. *Mol. Autism*.
- Fülling, C., Dinan, T.G., and Cryan, J.F. (2019). Gut Microbe to Brain Signaling: What Happens in Vagus.... *Neuron* *101*, 998–1002.
- Fung, T.C., Olson, C.A., and Hsiao, E.Y. (2017). Interactions between the microbiota, immune and nervous systems in health and disease. *Nat. Neurosci.* *20*, 145–155.
- Gabriele, S., Sacco, R., Cerullo, S., Neri, C., Urbani, A., Tripi, G., Malvy, J., Barthelemy, C., Bonnet-Brihault, F., and Persico, A.M. (2014). Urinary p-cresol is elevated in young French children with autism spectrum disorder: A replication study. *Biomarkers* *19*, 463–470.
- Gabriele, S., Sacco, R., Altieri, L., Neri, C., Urbani, A., Bravaccio, C., Riccio, M.P., Iovene, M.R., Bombace, F., Magistris, L. De, et al. (2015). Slow Intestinal Transit Contributes to Elevate Urinary p-Cresol Level in Italian Autistic Children. 1–8.
- Gacias, M., Gaspari, S., Santos, P.M.G., Tamburini, S., Andrade, M., Zhang, F., Shen, N., Tolstikov, V., Kiebish, M.A., Dupree, J.L., et al. (2016). Microbiota-driven transcriptional changes in prefrontal cortex override genetic differences in social behavior. *Elife* *5*, 1–27.
- Gevi, F., Zolla, L., Gabriele, S., and Persico, A.M. (2016). Urinary metabolomics of

young Italian autistic children supports abnormal tryptophan and purine metabolism. *Mol. Autism* 7, 47.

Golubeva, A. V., Joyce, S.A., Moloney, G., Burokas, A., Sherwin, E., Arboleya, S., Flynn, I., Khochanskiy, D., Moya-Pérez, A., Peterson, V., et al. (2017). Microbiota-related Changes in Bile Acid & Tryptophan Metabolism are Associated with Gastrointestinal Dysfunction in a Mouse Model of Autism. *EBioMedicine* 1.

Gorrindo, P., Williams, K.C., Lee, E.B., Walker, L.S., McGrew, S.G., and Levitt, P. (2012). Gastrointestinal dysfunction in autism: Parental report, clinical evaluation, and associated factors. *Autism Res.* 5, 101–108.

Goulet, O., Hojsak, I., Kolacek, S., Pop, T.L., Cokugras, F.C., Zuccotti, G., Pettoello-Mantovani, M., and Fabiano, V. (2019). Paediatricians play a key role in preventing early harmful events that could permanently influence the development of the gut microbiota in childhood. *Acta Paediatr. Int. J. Paediatr.* 108, 1942–1954.

Green, D., Chandler, S., Charman, T., Simonoff, E., and Baird, G. (2016). Brief Report: DSM-5 Sensory Behaviours in Children With and Without an Autism Spectrum Disorder. *J. Autism Dev. Disord.* 46, 3597–3606.

Hagerman, R.J., Van Housen, K., Smith, A.C.M., and McGavran, L. (1984). Consideration of connective tissue dysfunction in the fragile X syndrome. *Am. J. Med. Genet.* 17, 111–121.

Han, W., Tellez, L.A., Perkins, M.H., Perez, I.O., Qu, T., Ferreira, J., Ferreira, T.L., Quinn, D., Liu, Z.W., Gao, X.B., et al. (2018). A Neural Circuit for Gut-Induced Reward. *Cell* 175, 665–678.e23.

Hansen, B.H., Oerbeck, B., Skirbekk, B., Petrovski, B.É., and Kristensen, H. (2018). Neurodevelopmental disorders: prevalence and comorbidity in children referred to mental health services. *Nord. J. Psychiatry* 72, 285–291.

Harrison, C.J., Jack, E.M., Allen, T.D., and Harris, R. (1983). The fragile X: A scanning electron microscope study. *J. Med. Genet.* 20, 280–285.

Hejtz, R.D., Wang, S., Anuar, F., Qian, Y., Björkholm, B., Samuelsson, A., Hibberd, M.L., Forssberg, H., and Pettersson, S. (2011). Normal gut microbiota modulates brain development and behavior. *Proc. Natl. Acad. Sci. U. S. A.* 108, 3047–3052.

Hertz-Picciotto, I., Schmidt, R.J., and Krakowiak, P. (2018). Understanding environmental contributions to autism: Causal concepts and the state of science. *Autism Res.* 11, 554–586.

- Heulens, I., Suttie, M., Postnov, A., De Clerck, N., Perrotta, C.S., Mattina, T., Faravelli, F., Forzano, F., Frank Kooy, R., and Hammond, P. (2013). Craniofacial characteristics of fragile X syndrome in mouse and man. *Eur. J. Hum. Genet.* *21*, 816–823.
- Hinton, V.J., Brown, W.T., Wisniewski, K., and Rudelli, R.D. (1991). Analysis of neocortex in three males with the fragile X syndrome. *Am. J. Med. Genet.* *41*, 289–294.
- Hooper, L. V., Wong, M.H., Thelin, A., Hansson, L., Falk, P.G., and Gordon, J.I. (2001). Molecular analysis of commensal host-microbial relationships in the intestine. *Science* (80- ). *291*, 881–884.
- Hornig, M., Bresnahan, M.A., Che, X., Schultz, A.F., Ukaigwe, J.E., Eddy, M.L., Hirtz, D., Gunnes, N., Lie, K.K., Magnus, P., et al. (2018). Prenatal fever and autism risk. *Mol. Psychiatry* *23*, 759–766.
- Hsiao, E.Y. (2013). Immune dysregulation in autism spectrum disorder. *Int. Rev. Neurobiol.* *113*, 269–302.
- Hsiao, E.Y., McBride, S.W., Hsien, S., Sharon, G., Hyde, E.R., McCue, T., Codelli, J.A., Chow, J., Reisman, S.E., Petrosino, J.F., et al. (2013). Microbiota modulate behavioral and physiological abnormalities associated with neurodevelopmental disorders. *Cell*.
- Huber, K.M., Gallagher, S.M., Warren, S.T., and Bear, M.F. (2002). Altered synaptic plasticity in a mouse model of fragile X mental retardation. *Proc. Natl. Acad. Sci. U. S. A.* *99*, 7746–7750.
- Hung, L.W., Neuner, S., Polepalli, J.S., Beier, K.T., Wright, M., Walsh, J.J., Lewis, E.M., Luo, L., Deisseroth, K., Dölen, G., et al. (2017). Gating of social reward by oxytocin in the ventral tegmental area. *Science* (80- ). 1406–1411.
- Huo, R., Zeng, B., Zeng, L., Cheng, K., Li, B., Luo, Y., Wang, H., Zhou, C., Fang, L., Li, W., et al. (2017). Microbiota Modulate Anxiety-Like Behavior and Endocrine Abnormalities in Hypothalamic-Pituitary-Adrenal Axis. *Front. Cell. Infect. Microbiol.* *7*, 1–9.
- Husted, A.S., Trauelsen, M., Rudenko, O., Hjorth, S.A., and Schwartz, T.W. (2017). GPCR-Mediated Signaling of Metabolites. *Cell Metab.*
- Iglesias-vázquez, L., Riba, G.V.G., Arija, V., and Canals, J. (2020). Composition of gut microbiota in children with autism spectrum disorder: A systematic review and meta-analysis. *Nutrients* *12*, 1–24.
- Inagaki, T., Moschetta, A., Lee, Y.K., Peng, L., Zhao, G., Downes, M., Yu, R.T.,

- Shelton, J.M., Richardson, J.A., Repa, J.J., et al. (2006). Regulation of antibacterial defense in the small intestine by the nuclear bile acid receptor. *Proc. Natl. Acad. Sci. U. S. A.* *103*, 3920–3925.
- Jaglin, M., Rhimi, M., Philippe, C., Pons, N., Bruneau, A., Goustard, B., Daugé, V., Maguin, E., Naudon, L., and Rabot, S. (2018). Indole, a signaling molecule produced by the gut microbiota, negatively impacts emotional behaviors in rats. *Front. Neurosci.* *12*, 1–19.
- Jan, R.K., Rihs, T.A., Kojovic, N., Sperdin, H.F., Franchini, M., Custo, A., Tomescu, M.I., Michel, C.M., and Schaer, M. (2019). Neural Processing of Dynamic Animated Social Interactions in Young Children With Autism Spectrum Disorder: A High-Density Electroencephalography Study. *Front. Psychiatry* *10*, 1–13.
- Jones, M.B., and Szatmari, P. (2002). A risk-factor model of epistatic interaction, focusing on autism. *Am. J. Med. Genet. - Neuropsychiatr. Genet.* *114*, 558–565.
- Jyonouchi, H. (2009). Food allergy and autism spectrum disorders: Is there a link? *Curr. Allergy Asthma Rep.* *9*, 194–201.
- Kang, D.W., Adams, J.B., Gregory, A.C., Borody, T., Chittick, L., Fasano, A., Khoruts, A., Geis, E., Maldonado, J., McDonough-Means, S., et al. (2017). Microbiota Transfer Therapy alters gut ecosystem and improves gastrointestinal and autism symptoms: An open-label study. *Microbiome* *5*, 1–16.
- Kang, D.W., Ilhan, Z.E., Isern, N.G., Hoyt, D.W., Howsmon, D.P., Shaffer, M., Lozupone, C.A., Hahn, J., Adams, J.B., and Krajmalnik-Brown, R. (2018). Differences in fecal microbial metabolites and microbiota of children with autism spectrum disorders. *Anaerobe* *49*, 121–131.
- Kang, D.W., Adams, J.B., Coleman, D.M., Pollard, E.L., Maldonado, J., McDonough-Means, S., Caporaso, J.G., and Krajmalnik-Brown, R. (2019). Long-term benefit of Microbiota Transfer Therapy on autism symptoms and gut microbiota. *Sci. Rep.* *9*, 1–9.
- Kataoka, S., Takuma, K., Hara, Y., Maeda, Y., Ago, Y., and Matsuda, T. (2013). Autism-like behaviours with transient histone hyperacetylation in mice treated prenatally with valproic acid. *Int. J. Neuropsychopharmacol.* *16*, 91–103.
- Khandjian, E., Bardoni, B., Corbin, F., Sittler, A., Giroux, S., Heitz, D., Tremblay, S., Pinset, C., Montarras, D., Rousseau, F., et al. (1998). Novel isoforms of the fragile X related protein FXR1P are expressed during myogenesis. *Hum. Mol. Genet.* *7*, 2121–2128.

- Kidd, S.A., Lachiewicz, A., Barbouth, D., Blitz, R.K., Delahunty, C., McBrien, D., Visootsak, J., and Berry-Kravis, E. (2014). Fragile X syndrome: A review of associated medical problems. *Pediatrics* *134*, 995–1005.
- Kim, S.N., Jo, G.H., Kim, H.A., and Heo, Y. (2016). Aberrant IgG isotype generation in mice with abnormal behaviors. *J. Immunotoxicol.* *13*, 92–96.
- Knoop, K.A., and Newberry, R.D. (2018). Goblet cells: multifaceted players in immunity at mucosal surfaces. *Mucosal Immunol.* *11*, 1551–1557.
- Krishnan, V., Stoppel, D.C., Nong, Y., Johnson, M.A., Nadler, M.J.S., Ozkaynak, E., Teng, B.L., Nagakura, I., Mohammad, F., Silva, M.A., et al. (2017). Autism gene *Ube3a* and seizures impair sociability by repressing VTA *Cbln1*. *Nature* *543*, 507–512.
- Krol, A., and Feng, G. (2018). Windows of opportunity: timing in neurodevelopmental disorders. *Curr. Opin. Neurobiol.* *48*, 59–63.
- Lai, M., Lombardo, M. V., and Baron-Cohen, S. (2013). *Autism.* *6736*.
- Laurence, J.A., and Fatemi, S.H. (2005). Glial fibrillary acidic protein is elevated in superior frontal, parietal and cerebellar cortices of autistic subjects. *Cerebellum* *4*, 206–210.
- Li, Q., and Zhou, J.M. (2016). The microbiota-gut-brain axis and its potential therapeutic role in autism spectrum disorder. *Neuroscience* *324*, 131–139.
- Li, J., Pelletier, M.R., Perez Velazquez, J.L., and Carlen, P.L. (2002). Reduced cortical synaptic plasticity and GluR1 expression associated with fragile X mental retardation protein deficiency. *Mol. Cell. Neurosci.* *19*, 138–151.
- Li, X., Chauhan, A., Sheikh, A.M., Patil, S., Chauhan, V., Li, X.M., Ji, L., Brown, T., and Malik, M. (2009). Elevated immune response in the brain of autistic patients. *J. Neuroimmunol.* *207*, 111–116.
- Lisik, M.Z., Gutmajster, E., and Sieroń, A.L. (2016). Low Levels of HDL in Fragile X Syndrome Patients. *Lipids* *51*, 189–192.
- Liu, F., Li, J., Wu, F., Zheng, H., Peng, Q., and Zhou, H. (2019). Altered composition and function of intestinal microbiota in autism spectrum disorders: a systematic review. *Transl. Psychiatry* *9*.
- Liu, L., Li, L., Min, J., Wang, J., Wu, H., Zeng, Y., Chen, S., and Chu, Z. (2012). Butyrate interferes with the differentiation and function of human monocyte-derived dendritic cells. *Cell. Immunol.* *277*, 66–73.
- Llewellyn-Smith, I.J., Kellett, D.O., Jordan, D., Browning, K.N., and Travaglini, R.A.

(2012). Oxytocin-immunoreactive innervation of identified neurons in the rat dorsal vagal complex. *Neurogastroenterol. Motil.* *24*, 136–146.

Lord, C., and Bishop, S.L. (2015). Recent Advances in Autism Research as Reflected in DSM-5 Criteria for Autism Spectrum Disorder. *Annu. Rev. Clin. Psychol.* *11*, 53–70.

Luchicchi, A., Lecca, S., Melis, M., De Felice, M., Cadeddu, F., Frau, R., Muntoni, A.L., Fadda, P., Devoto, P., and Pistis, M. (2016). Maternal immune activation disrupts dopamine system in the offspring. *Int. J. Neuropsychopharmacol.* *19*, 1–10.

Luczynski, P., Neufeld, K.A.M.V., Oriach, C.S., Clarke, G., Dinan, T.G., and Cryan, J.F. (2016). Growing up in a bubble: Using germ-free animals to assess the influence of the gut microbiota on brain and behavior. *Int. J. Neuropsychopharmacol.* *19*, 1–17.

Lumaban, J.G., and Nelson, D.L. (2015). The Fragile X proteins Fmrp and Fxr2p cooperate to regulate glucose metabolism in mice. *Hum. Mol. Genet.* *24*, 2175–2184.

Luna, R.A., Oezguen, N., Balderas, M., Venkatachalam, A., Runge, J.K., Versalovic, J., Veenstra-VanderWeele, J., Anderson, G.M., Savidge, T., and Williams, K.C. (2017). Distinct Microbiome-Neuroimmune Signatures Correlate With Functional Abdominal Pain in Children With Autism Spectrum Disorder. *Cmgh* *3*, 218–230.

Lund, M.L., Egerod, K.L., Engelstoft, M.S., Dmytriyeva, O., Theodorsson, E., Patel, B.A., and Schwartz, T.W. (2018). Enterochromaffin 5-HT cells – A major target for GLP-1 and gut microbial metabolites. *Mol. Metab.* 70–83.

Mabbott, N.A., Donaldson, D.S., Ohno, H., Williams, I.R., and Mahajan, A. (2013). Microfold (M) cells: Important immunosurveillance posts in the intestinal epithelium. *Mucosal Immunol.* *6*, 666–677.

Macfabe, D.F. (2012). Short-chain fatty acid fermentation products of the gut microbiome: implications in autism spectrum disorders. *Microb. Ecol. Health Dis.* *23*, 1–25.

MacFabe, D.F., Cain, N.E., Boon, F., Ossenkopp, K.P., and Cain, D.P. (2011). Effects of the enteric bacterial metabolic product propionic acid on object-directed behavior, social behavior, cognition, and neuroinflammation in adolescent rats: Relevance to autism spectrum disorder. *Behav. Brain Res.* *217*, 47–54.

De Magistris, L., Familiari, V., Pascotto, A., Sapone, A., Frolli, A., Iardino, P., Carteni, M., De Rosa, M., Francavilla, R., Riegler, G., et al. (2010). Alterations of the intestinal barrier in patients with autism spectrum disorders and in their first-degree relatives. *J. Pediatr. Gastroenterol. Nutr.* *51*, 418–424.

- Masi, A., Quintana, D.S., Glozier, N., Lloyd, A.R., Hickie, I.B., and Guastella, A.J. (2015). Cytokine aberrations in autism spectrum disorder: A systematic review and meta-analysis. *Mol. Psychiatry* 20, 440–446.
- Mazefsky, C.A., Schreiber, D.R., Olino, T.M., and Minshew, N.J. (2014). The association between emotional and behavioral problems and gastrointestinal symptoms among children with high-functioning autism. *Autism* 18, 493–501.
- Mazurek, M.O., Vasa, R.A., Kalb, L.G., Kanne, S.M., Rosenberg, D., Keefer, A., Murray, D.S., Freedman, B., and Lowery, L.A. (2013). Anxiety, sensory over-responsivity, and gastrointestinal problems in children with autism spectrum disorders. *J. Abnorm. Child Psychol.* 41, 165–176.
- McElhanon, B.O., McCracken, C., Karpen, S., and Sharp, W.G. (2014). Gastrointestinal symptoms in autism spectrum disorder: A meta-analysis. *Pediatrics* 133, 872–883.
- Mephram, J.R., Boon, F.H., Foley, K.A., Cain, D.P., MacFabe, D.F., and Ossenkopp, K.P. (2019). Impaired Spatial Cognition in Adult Rats Treated with Multiple Intracerebroventricular (ICV) Infusions of the Enteric Bacterial Metabolite, Propionic Acid, and Return to Baseline After 1 Week of No Treatment: Contribution to a Rodent Model of ASD. *Neurotox. Res.*
- Meyza and Blanchard (2017). The BTBR mouse model of idiopathic autism – current view on mechanisms. *Neurosci. Biobehav. Rev.* 176, 139–148.
- Mientjies, E.J., Nieuwenhuizen, I., Kirkpatrick, L., Zu, T., Hoogeveen-Westerveld, M., Severijnen, L., Rifé, M., Willemsen, R., Nelson, D.L., and Oostra, B.A. (2006). The generation of a conditional Fmr1 knock out mouse model to study Fmrp function in vivo. *Neurobiol. Dis.* 21, 549–555.
- Miles, J.H. (2011). Autism spectrum disorders-A genetics review. *Genet. Med.* 13, 278–294.
- Modabbernia, A., Velthorst, E., and Reichenberg, A. (2017). Environmental risk factors for autism: an evidence-based review of systematic reviews and meta-analyses. *Mol. Autism* 8, 1–16.
- Montalban-Arques, A., Chaparro, M., Gisbert, J.P., and Bernardo, D. (2018). The Innate Immune System in the Gastrointestinal Tract: Role of Intraepithelial Lymphocytes and Lamina Propria Innate Lymphoid Cells in Intestinal Inflammation. *Inflamm. Bowel Dis.* 24, 1649–1659.
- Morales, M., and Margolis, E.B. (2017). Ventral tegmental area: Cellular heterogeneity,

connectivity and behaviour. *Nat. Rev. Neurosci.* 18, 73–85.

Morgan, J.T., Chana, G., Pardo, C.A., Achim, C., Semendeferi, K., Buckwalter, J., Courchesne, E., and Everall, I.P. (2010). Microglial activation and increased microglial density observed in the dorsolateral prefrontal cortex in autism. *Biol. Psychiatry* 68, 368–376.

Mu, Q., Kirby, J., Reilly, C.M., and Luo, X.M. (2017). Leaky gut as a danger signal for autoimmune diseases. *Front. Immunol.* 8, 1–10.

Mundy, P. (2003). Annotation: The neural basis of social impairments in autism: The role of the dorsal medial-frontal cortex and anterior cingulate system. *J. Child Psychol. Psychiatry Allied Discip.* 44, 793–809.

Nagy, N., and Goldstein, A.M. (2017). Enteric nervous system development: A crest cell's journey from neural tube to colon. *Semin. Cell Dev. Biol.* 66, 94–106.

Neufeld, K.M., Kang, N., Bienenstock, J., and Foster, J.A. (2011). Reduced anxiety-like behavior and central neurochemical change in germ-free mice. *Neurogastroenterol. Motil.* 23, 255–265.

Nikolov, R.N., Bearss, K.E., Lettinga, J., Erickson, C., Rodowski, M., Aman, M.G., McCracken, J.T., McDougle, C.J., Tierney, E., Vitiello, B., et al. (2009). Gastrointestinal symptoms in a sample of children with pervasive developmental disorders. *J. Autism Dev. Disord.* 39, 405–413.

Nimchinsky, E.A., Oberlander, A.M., and Svoboda, K. (2001). Abnormal development of dendritic spines in FMR1 knock-out mice. *J. Neurosci.* 21, 5139–5146.

Nogacka, A., Salazar, N., Suárez, M., Milani, C., Arboleya, S., Solís, G., Fernández, N., Alaez, L., Hernández-Barranco, A.M., de los Reyes-Gavilán, C.G., et al. (2017). Impact of intrapartum antimicrobial prophylaxis upon the intestinal microbiota and the prevalence of antibiotic resistance genes in vaginally delivered full-term neonates. *Microbiome* 5, 1–10.

Van Nood, E., Vrieze, A., Nieuwdorp, M., Fuentes, S., Zoetendal, E.G., De Vos, W.M., Visser, C.E., Kuijper, E.J., Bartelsman, J.F.W.M., Tijssen, J.G.P., et al. (2013). Duodenal infusion of donor feces for recurrent *clostridium difficile*. *N. Engl. J. Med.* 368, 407–415.

Ogbonnaya, E.S., Clarke, G., Shanahan, F., Dinan, T.G., Cryan, J.F., and O'Leary, O.F. (2015). Adult Hippocampal Neurogenesis Is Regulated by the Microbiome. *Biol. Psychiatry* 78, e7–e9.

- Ormstad, H., Bryn, V., Verkerk, R., Skjeldal, O.H., Halvorsen, B., Saugstad, O.D., Isaksen, J., and Maes, M. (2018). Serum tryptophan, tryptophan catabolites and brain-derived neurotrophic factor in subgroups of youngsters with autism spectrum disorders. *CNS Neurol. Disord. - Drug Targets* 17, 626–639.
- Ornoy, A., Weinstein-Fudim, L., and Ergaz, Z. (2015). Prenatal factors associated with autism spectrum disorder (ASD). *Reprod. Toxicol.* 56, 155–169.
- Pagnozzi, A.M., Conti, E., Calderoni, S., Fripp, J., and Rose, S.E. (2018). A systematic review of structural MRI biomarkers in autism spectrum disorder: A machine learning perspective. *Int. J. Dev. Neurosci.* 71, 68–82.
- Parracho, H.M.R.T., Bingham, M.O., Gibson, G.R., and McCartney, A.L. (2005). Differences between the gut microflora of children with autistic spectrum disorders and that of healthy children. *J. Med. Microbiol.* 54, 987–991.
- Pascucci, T., Colamartino, M., Fiori, E., Sacco, R., Coviello, A., Ventura, R., Puglisi-Allegra, S., Turriziani, L., and Persico, A.M. (2020). P-cresol alters brain dopamine metabolism and exacerbates autism-like behaviors in the BTBR mouse. *Brain Sci.* 10, 1–16.
- Passmore, I.J., Letertre, M.P.M., Preston, M.D., Bianconi, I., Harrison, A., Nasher, F., Kaur, H., Hong, H.A., Baines, S.D., Cutting, S.M., et al. (2018). Para -cresol production by *Clostridium difficile* affects microbial diversity and membrane integrity of Gram-negative bacteria. *PLoS Pathog* 2018; 14(9): e1007191.
- Pastuła, A., Middelhoff, M., Brandtner, A., Tobiasch, M., Höhl, B., Nuber, A.H., Demir, I.E., Neupert, S., Kollmann, P., Mazzuoli-Weber, G., et al. (2015). Three-Dimensional Gastrointestinal Organoid Culture in Combination with Nerves or Fibroblasts: A Method to Characterize the Gastrointestinal Stem Cell Niche. *Stem Cells Int.*
- Patel, J., Lukkes, J.L., and Shekhar, A. (2018). Overview of genetic models of autism spectrum disorders (Elsevier B.V.).
- Patusco, R., and Ziegler, J. (2018). Role of probiotics in managing gastrointestinal dysfunction in children with autism spectrum disorder: AN update for practitioners. *Adv. Nutr.* 9, 637–650.
- Peça, J., Feliciano, C., Ting, J.T., Wang, W., Wells, M.F., Venkatraman, T.N., Lascola, C.D., Fu, Z., and Feng, G. (2011). Shank3 mutant mice display autistic-like behaviours and striatal dysfunction. *Nature* 472, 437–442.

- Pellissier, L.P., Gandía, J., Laboute, T., Becker, J.A.J., and Le Merrer, J. (2018). M Opioid Receptor, Social Behaviour and Autism Spectrum Disorder: Reward Matters. *Br. J. Pharmacol.* *175*, 2750–2769.
- Penagarikano, O., Mulle, J.G., and Warren, S.T. (2007). The Pathophysiology of Fragile X Syndrome. *Annu. Rev. Genomics Hum. Genet.* *8*, 109–129.
- Persico, A.M., and Napolioni, V. (2013). Urinary p-cresol in autism spectrum disorder. *Neurotoxicol. Teratol.* *36*, 82–90.
- Poutahidis, T., Kearney, S.M., Levkovich, T., Qi, P., Varian, B.J., Lakritz, J.R., Ibrahim, Y.M., Chatzigiagos, A., Alm, E.J., and Erdman, S.E. (2013). Microbial symbionts accelerate wound healing via the neuropeptide hormone oxytocin. *PLoS One* *8*.
- De Preter, V., Geboes, K., Verbrugghe, K., De Vuyst, L., Vanhoutte, T., Huys, G., Swings, J., Pot, B., and Verbeke, K. (2004). The in vivo use of the stable isotope-labelled biomarkers lactose-[<sup>15</sup>N]ureide and [<sup>2</sup>H<sub>4</sub>]tyrosine to assess the effects of pro- and prebiotics on the intestinal flora of healthy human volunteers. *Br. J. Nutr.* *92*, 439–446.
- De Preter, V., Vanhoutte, T., Huys, G., Swings, J., De Vuyst, L., Rutgeerts, P., and Verbeke, K. (2007). Effects of *Lactobacillus casei* Shirota, *Bifidobacterium breve*, and oligofructose-enriched inulin on colonic nitrogen-protein metabolism in healthy humans. *Am. J. Physiol. - Gastrointest. Liver Physiol.* *292*, 358–368.
- Rao, M., and Gershon, M.D. (2016). The bowel and beyond: The enteric nervous system in neurological disorders. *Nat. Rev. Gastroenterol. Hepatol.* *13*(9), 517–528.
- Reigstad, C.S., Salmonson, C.E., Rainey, J.F., Szurszewski, J.H., Linden, D.R., Sonnenburg, J.L., Farrugia, G., and Kashyap, P.C. (2015). Gut microbes promote colonic serotonin production through an effect of short-chain fatty acids on enterochromaffin cells. *FASEB J.* *29*, 1395–1403.
- Robins, A.D.L., and Casagrande, K. (2014). Validation of M-CHAT. *Pediatrics* *133*, 37–45.
- Rogers, T.D., Dickson, P.E., McKimm, E., Heck, D.H., Goldowitz, D., Blaha, C.D., and Mittleman, G. (2013). Reorganization of circuits underlying cerebellar modulation of prefrontal cortical dopamine in mouse models of autism spectrum disorder. *Cerebellum* *12*, 547–556.
- Rothhammer, V., Mascanfroni, I.D., Bunse, L., Takenaka, M.C., Kenison, J.E., Mayo,

- L., Chao, C.C., Patel, B., Yan, R., Blain, M., et al. (2016). Type I interferons and microbial metabolites of tryptophan modulate astrocyte activity and central nervous system inflammation via the aryl hydrocarbon receptor. *Nat. Med.* *22*, 586–597.
- Rutter, M., Caspi, A., and Moffitt, T.E. (2003). Using sex differences in psychopathology to study causal mechanisms: Unifying issues and research strategies. *J. Child Psychol. Psychiatry Allied Discip.* *44*, 1092–1115.
- Rylaarsdam, L., and Guemez-Gamboa, A. (2019). Genetic Causes and Modifiers of Autism Spectrum Disorder. *Front. Cell. Neurosci.* *13*, 1–15.
- Sabbagh-Haddad, A., Haddad, D.S., Michel-Crosato, E., and Arita, E.S. (2016). Fragile X syndrome: Panoramic radiographic evaluation of dental anomalies, dental mineralization stage, and mandibular angle. *J. Appl. Oral Sci.* *24*, 518–523.
- Saghazadeh, A., Ataeinia, B., Keynejad, K., Abdolalizadeh, A., Hirbod-Mobarakeh, A., and Rezaei, N. (2019). Anti-inflammatory cytokines in autism spectrum disorders: A systematic review and meta-analysis. *Cytokine* *123*, 154740.
- Saito, Y., Sato, T., Nomoto, K., and Tsuji, H. (2018). Identification of phenol- and p-cresol-producing intestinal bacteria by using media supplemented with tyrosine and its metabolites. *FEMS Microbiol. Ecol.* *94*, 1–11.
- Sarkar, A., Lehto, S.M., Harty, S., Dinan, T.G., Cryan, J.F., and Burnet, P.W.J. (2016). Psychobiotics and the Manipulation of Bacteria–Gut–Brain Signals. *Trends Neurosci.* *39*, 763–781.
- Sender, R., Fuchs, S., and Milo, R. (2016). Revised Estimates for the Number of Human and Bacteria Cells in the Body. *PLoS Biol.* *14*, 1–14.
- Sgritta, M., Dooling, S.W., Buffington, S.A., Momin, E.N., Francis, M.B., Britton, R.A., and Costa-Mattoli, M. (2019). Mechanisms Underlying Microbial-Mediated Changes in Social Behavior in Mouse Models of Autism Spectrum Disorder. *Neuron* *101*, 246–259.e6.
- Shaaban, S.Y., El Gendy, Y.G., Mehanna, N.S., El-Senousy, W.M., El-Feki, H.S.A., Saad, K., and El-Asheer, O.M. (2018). The role of probiotics in children with autism spectrum disorder: A prospective, open-label study. *Nutr. Neurosci.* *21*, 676–681.
- Shangari, N., Chan, T.S., and O'Brien, P.J. (2005). Sulfation and glucuronidation of phenols: Implications in coenzyme Q metabolism. *Methods Enzymol.* *400*, 342–359.
- Sharkey, K.A., Beck, P.L., and McKay, D.M. (2018). Neuroimmunophysiology of the gut: advances and emerging concepts focusing on the epithelium. *Nat. Rev.*

Gastroenterol. Hepatol.

Sharon, G., Cruz, N.J., Kang, D.W., Gandal, M.J., Wang, B., Kim, Y.M., Zink, E.M., Casey, C.P., Taylor, B.C., Lane, C.J., et al. (2019). Human Gut Microbiota from Autism Spectrum Disorder Promote Behavioral Symptoms in Mice. *Cell* 177, 1600–1618.e17.

Sharp, W.G., Berry, R.C., McCracken, C., Nuhu, N.N., Marvel, E., Saulnier, C.A., Klin, A., Jones, W., and Jaquess, D.L. (2013). Feeding problems and nutrient intake in children with autism spectrum disorders: A meta-analysis and comprehensive review of the literature. *J. Autism Dev. Disord.* 43, 2159–2173.

Sherwin, E., Bordenstein, S.R., Quinn, J.L., Dinan, T.G., and Cryan, J.F. (2019). Microbiota and the social brain. *Science* 366.

da Silva Menezes, J., de Sousa Mucida, D., Cara, D.C., Alvarez-Leite, J.I., Russo, M., Vaz, N.M., and Caetano de Faria, A.M. (2003). Stimulation by food proteins plays a critical role in the maturation of the immune system. *Int. Immunol.* 15, 447–455.

Silverman, J.L., Yang, M., Lord, C., and Crawley, J.N. (2010). Behavioural phenotyping assays for mouse models of autism. *Nat. Rev. Neurosci.* 11, 490–502.

Smith, S.E.P., Li, J., Garbett, K., Mirnics, K., and Patterson, P.H. (2007). Maternal immune activation alters fetal brain development through interleukin-6. *J. Neurosci.* 27, 10695–10702.

Squillace, M., Doderio, L., Federici, M., Migliarini, S., Errico, F., Napolitano, F., Krashia, P., Di Maio, A., Galbusera, A., Bifone, A., et al. (2014). Dysfunctional dopaminergic neurotransmission in asocial BTBR mice. *Transl. Psychiatry* 4, e427-11.

Srikantha, P., and Mohajeri, M.H. (2019). The Possible Role of the Microbiota-Gut-Brain-Axis in Autism Spectrum Disorder. *Int. J. Mol. Sci.* 20, 2115.

Stilling, R.M., Dinan, T.G., and Cryan, J.F. (2014). Microbial genes, brain & behaviour - epigenetic regulation of the gut-brain axis. *Genes, Brain Behav.* 13, 69–86.

Stilling, R.M., van de Wouw, M., Clarke, G., Stanton, C., Dinan, T.G., and Cryan, J.F. (2016). The neuropharmacology of butyrate: The bread and butter of the microbiota-gut-brain axis? *Neurochem. Int.* 99, 110–132.

Stinson, L.F., Payne, M.S., and Keelan, J.A. (2018). A Critical Review of the Bacterial Baptism Hypothesis and the Impact of Cesarean Delivery on the Infant Microbiome. *Front. Med.* 5.

Sudo, N., Chida, Y., Aiba, Y., Sonoda, J., Oyama, N., Yu, X.N., Kubo, C., and Koga, Y. (2004). Postnatal microbial colonization programs the hypothalamic-pituitary-

adrenal system for stress response in mice. *J. Physiol.* 558, 263–275.

Supekar, K., Kochalka, J., Schaer, M., Wakeman, H., Qin, S., Padmanabhan, A., and Menon, V. (2018). Deficits in mesolimbic reward pathway underlie social interaction impairments in children with autism. *Brain* 1–11.

Swann, J.R., Spitzer, S.O., and Diaz Heijtz, R. (2020). Developmental Signatures of Microbiota-Derived Metabolites in the Mouse Brain. *Metabolites* 10, 172.

Tamburini, S., Shen, N., Wu, H.C., and Clemente, J.C. (2016). The microbiome in early life: Implications for health outcomes. *Nat. Med.* 22, 713–722.

Tetreault, N.A., Hakeem, A.Y., Jiang, S., Williams, B.A., Allman, E., Wold, B.J., and Allman, J.M. (2012). Microglia in the cerebral cortex in autism. *J. Autism Dev. Disord.* 42, 2569–2584.

Thaiss, C.A., Zmora, N., Levy, M., and Elinav, E. (2016). The microbiome and innate immunity. *Nature* 535, 65–74.

Thapar, A., Cooper, M., and Rutter, M. (2017). Neurodevelopmental disorders. *The Lancet Psychiatry* 4, 339–346.

De Theije, C.G.M., Wu, J., Da Silva, S.L., Kamphuis, P.J., Garssen, J., Korte, S.M., and Kraneveld, A.D. (2011). Pathways underlying the gut-to-brain connection in autism spectrum disorders as future targets for disease management. *Eur. J. Pharmacol.* 668, 70–80.

De Theije, C.G.M., Koelink, P.J., Korte-Bouws, G.A.H., Lopes da Silva, S., Korte, S.M., Olivier, B., Garssen, J., and Kraneveld, A.D. (2014). Intestinal inflammation in a murine model of autism spectrum disorders. *Brain. Behav. Immun.* 37, 240–247.

Ting, H.-A., and von Moltke, J. (2019). The Immune Function of Tuft Cells at Gut Mucosal Surfaces and Beyond. *J. Immunol.* 202, 1321–1329.

Tomova, A., Husarova, V., Lakatosova, S., Bakos, J., Vlkova, B., Babinska, K., and Ostatnikova, D. (2015). Gastrointestinal microbiota in children with autism in Slovakia. *Physiol. Behav.* 138, 179–187.

De Vadder, F., Grasset, E., Mannerås Holm, L., Karsenty, G., Macpherson, A.J., Olofsson, L.E., and Bäckhed, F. (2018). Gut microbiota regulates maturation of the adult enteric nervous system via enteric serotonin networks. *Proc. Natl. Acad. Sci.* 115(25), 6458–6463.

Veroniki, A.A., Rios, P., Cogo, E., Straus, S.E., Finkelstein, Y., Kealey, R., Reynen, E., Soobiah, C., Thavorn, K., Hutton, B., et al. (2017). Comparative safety of antiepileptic

drugs for neurological development in children exposed during pregnancy and breast feeding: A systematic review and network meta-analysis. *BMJ Open* 7, e017248, 1–12.

Viggiano, D., Ianiro, G., Vanella, G., Bibbò, S., Bruno, G., Simeone, G., and Mele, G. (2015). Gut barrier in health and disease: focus on childhood. *Eur. Rev. Med. Pharmacol. Sci.* 19, 1077–1085.

De Vries, B.B.A., Robinson, H., Stolte-Dijkstra, I., Tjon Pian Gi, C. V., Dijkstra, P.F., Van Doorn, J., Halley, D.J.J., Oostra, B.A., Turner, G., and Niermeijer, M.F. (1995). General overgrowth in the fragile X syndrome: Variability in the phenotypic expression of the FMR1 gene mutation. *J. Med. Genet.* 32, 764–769.

Vuong, H.E., and Hsiao, E.Y. (2017). Emerging Roles for the Gut Microbiome in Autism Spectrum Disorder. *Biol. Psychiatry* 81, 411–423.

Wagner, G.C., Reuhl, K.R., Cheh, M., McRae, P., and Halladay, A.K. (2006). A new neurobehavioral model of autism in mice: Pre- and postnatal exposure to sodium valproate. *J. Autism Dev. Disord.* 36, 779–793.

Wang, G., Huang, S., Wang, Y., Cai, S., Yu, H., Liu, H., Zeng, X., Zhang, G., and Qiao, S. (2019). Bridging intestinal immunity and gut microbiota by metabolites. *Cell. Mol. Life Sci.*

Wang, L., Christophersen, C.T., Sorich, M.J., Gerber, J.P., Angley, M.T., and Conlon, M.A. (2011). Low relative abundances of the mucolytic bacterium *Akkermansia muciniphila* and *Bifidobacterium* spp. in feces of children with autism. *Appl. Environ. Microbiol.* 77, 6718–6721.

Wang, L., Christophersen, C.T., Sorich, M.J., Gerber, J.P., Angley, M.T., and Conlon, M.A. (2012). Elevated fecal short chain fatty acid and ammonia concentrations in children with autism spectrum disorder. *Dig. Dis. Sci.* 57, 2096–2102.

Wang, Y., Tang, S., Xu, S., Weng, S., and Liu, Z. (2016). Maternal body mass index and risk of autism spectrum disorders in offspring: A meta-analysis. *Sci. Rep.* 6, 1–8.

Wikoff, W.R., Anfora, A.T., Liu, J., Schultz, P.G., Lesley, S.A., Peters, E.C., and Siuzdak, G. (2009). Metabolomics analysis reveals large effects of gut microflora on mammalian blood metabolites. *Proc. Natl. Acad. Sci. U. S. A.* 106, 3698–3703.

Wilck, N., Matus, M.G., Kearney, S.M., Olesen, S.W., Forslund, K., Bartolomeus, H., Haase, S., Mahler, A., Balogh, A., Marko, L., et al. (2017). Salt-responsive gut commensal modulates TH17 axis and disease. *Nature* 551, 585–589.

Willemsen, L.E.M., Koetsier, M.A., Van Deventer, S.J.H., and Van Tol, E.A.F. (2003).

Short chain fatty acids stimulate epithelial mucin 2 expression through differential effects on prostaglandin E1 and E2 production by intestinal myofibroblasts. *Gut* 52, 1442–1447.

Williams, B.L., Hornig, M., Buie, T., Bauman, M.L., Cho Paik, M., Wick, I., Bennett, A., Jabado, O., Hirschberg, D.L., and Lipkin, W.I. (2011). Impaired carbohydrate digestion and transport and mucosal dysbiosis in the intestines of children with autism and gastrointestinal disturbances. *PLoS One* 6(9), e24585.

Xiong, X., Liu, D., Wang, Y., Zeng, T., and Peng, Y. (2016). Urinary 3-(3-Hydroxyphenyl)-3-hydroxypropionic Acid, 3-Hydroxyphenylacetic Acid, and 3-Hydroxyhippuric Acid Are Elevated in Children with Autism Spectrum Disorders. *Biomed Res. Int.*

Xu, M., Xu, X., Li, J., and Li, F. (2019). Association between gut microbiota and autism spectrum disorder: A systematic review and meta-analysis. *Front. Psychiatry* 10, 1–11.

Yano, J.M., Yu, K., Donaldson, G.P., Shastri, G.G., Ann, P., Ma, L., Nagler, C.R., Ismagilov, R.F., Mazmanian, S.K., and Hsiao, E.Y. (2015). Indigenous bacteria from the gut microbiota regulate host serotonin biosynthesis. *Cell*. 161, 264-276

Yap, I.K.S., Angley, M., Veselkov, K.A., Holmes, E., Lindon, J.C., and Nicholson, J. (2010). Urinary metabolic phenotyping differentiates children with autism from their unaffected siblings and age-matched controls. *J. Proteome Res.* 9, 2996–3004.

Yip, B.H.K., Leonard, H., Stock, S., Stoltenberg, C., Francis, R.W., Gissler, M., Gross, R., Schendel, D., and Sandin, S. (2017). Caesarean section and risk of autism across gestational age: A multi-national cohort study of 5 million births. *Int. J. Epidemiol.* 46, 429–439.

Zuckerman, L., Rehavi, M., Nachman, R., and Weiner, I. (2003). Immune activation during pregnancy in rats leads to a postpubertal emergence of disrupted latent inhibition, dopaminergic hyperfunction, and altered limbic morphology in the offspring: A novel neurodevelopmental model of schizophrenia. *Neuropsychopharmacology* 28, 1778–1789.